

21039



National Library of Canada

Bibliothèque nationale du Canada

CANADIAN THESES ON MICROFICHE

THÈSES CANADIENNES SUR MICROFICHE

NAME OF AUTHOR/NOM DE L'AUTEUR SHRI PRAKASH RAI

TITLE OF THESIS/TITRE DE LA THÈSE AN INVESTIGATION OF PLANE TURBULENT WALL-WAKES"

UNIVERSITY/UNIVERSITÉ UNIVERSITY OF ALBERTA

DEGREE FOR WHICH THESIS WAS PRESENTED/ GRADE POUR LEQUEL CETTE THÈSE FUT PRÉSENTÉE PH.D.

YEAR THIS DEGREE CONFERRED/ANNÉE D'OBTENTION DE CE DEGRÉ 1974

NAME OF SUPERVISOR/NOM DU DIRECTEUR DE THÈSE Dr. N. RAJARATNAM

Permission is hereby granted to the NATIONAL LIBRARY OF CANADA to microfilm this thesis and to lend or sell copies of the film.

L'autorisation est, par la présente, accordée à la BIBLIOTHÈQUE NATIONALE DU CANADA de microfilmer cette thèse et de prêter ou de vendre des exemplaires du film.

The author reserves other publication rights, and neither the thesis nor extensive extracts from it may be printed or otherwise reproduced without the author's written permission.

L'auteur se réserve les autres droits de publication; ni la thèse ni de longs extraits de celle-ci ne doivent être imprimés ou autrement reproduits sans l'autorisation écrite de l'auteur.

DATED/DATE April 16, '74 SIGNED/SIGNÉ S. Rai

PERMANENT ADDRESS/RÉSIDENCE FIXE 91, NAWABGANJ, VARANASI-1, (U.P.) INDIA

THE UNIVERSITY OF ALBERTA

AN INVESTIGATION OF PLANE TURBULENT
WALL-WAKES

BY



SHRI PRAKASH RAI

A THESIS

SUBMITTED TO THE FACULTY OF GRADUATE STUDIES AND RESEARCH
IN PARTIAL FULFILMENT OF THE REQUIREMENTS FOR THE DEGREE OF
DOCTOR OF PHILOSOPHY

DEPARTMENT OF CIVIL ENGINEERING

EDMONTON, ALBERTA

SPRING, 1974

THE UNIVERSITY OF ALBERTA
FACULTY OF GRADUATE STUDY AND RESEARCH

The undersigned certify that they have read, and recommend to the Faculty of Graduate Studies and Research, for acceptance, a thesis entitled "AN INVESTIGATION OF PLANE TURBULENT WALL-WAKES" submitted by Shri Prakash Rai, in partial fulfilment of the requirements for the degree of Doctor of Philosophy in Hydraulic Engineering.

N. Rajaratnam
.....
N. Rajaratnam Supervisor

T. Blench
.....
T. Blench

D.J. Marsden
.....
D.J. Marsden

A.W. Peterson
.....
A.W. Peterson

John Shaw
.....
J. Shaw

John A. Roberson
.....
J.A. Roberson
External Examiner
Washington State University
Pullman, Washington, U.S.A.

Date... *March 19, '74*

ABSTRACT

On the basis of the two-layer hypothesis, a two-dimensional turbulent wall-wake (with and without pressure gradients) has been investigated. The outer layer was assumed to vary in a manner similar to that of a two-dimensional turbulent plane-wake, and the inner-layer in a manner similar to that of a two-dimensional turbulent boundary layer. The boundary layer type of equation was then analyzed, and suitable relationships for the decay of maximum velocity defect, and the growth of length scales, were established. For each shape and size of obstacle, the velocity profiles were found to be similar beyond a distance of about $25 h$ (h being the height of the obstacle) from the obstacle. The outer layer profile was found to be described well by the classical plane-wake curve, while the inner layer was described by the 'law of the wall'. For zero pressure gradient flows, the distance from the wall, of the point of intersection of the inner and outer layers, was found to be proportional to the half-wake width. The constant of proportionality was found to decrease in the streaming direction for adverse pressure gradient flows. The wall roughness and the Reynolds' number gave indications of the thickening of the inner layer.

Prandtl's mixing length hypothesis was found to give good results for zero pressure gradient flows. Assumption of constant eddy viscosity, based on Gartshore's (1965) analysis, was found to give satisfactory results for wall-wakes with moderately strong pressure gradients. The characteristic Reynolds' number, $u_{1m} b/\nu$, was found to be an important parameter for obtaining the skin friction for adverse pressure gradient flows.

There was an indication of the influence of the coefficient of skin-friction on wake-parameters for the weak adverse pressure gradient flow.

ACKNOWLEDGEMENTS

The author wishes to express his sincere gratitude to Professor N. Rajaratnam for suggesting this topic and giving his thoughtful guidance and advice throughout the course of the study.

The assistance of the Hydraulics Laboratory staff at the University of Alberta, with the fabrication of wind tunnel and some of the instrumentation, is also greatly appreciated.

Thanks are due as well to Mr. Frederick Ziegler and Miss Brenda Lawrence for their valuable assistance with grammatical revisions and the numerous mechanical details involved in the preparation of the thesis.

The author is grateful to the National Research Council of Canada for the support of this project through a grant to Professor Rajaratnam.

TABLE OF CONTENTS

<u>CHAPTER</u>		<u>PAGE</u>
I	INTRODUCTION	1
II	ANALYTICAL CONSIDERATIONS	9
	Introduction	9
	Theoretical Analysis of the Outer-Region	16
	Near-Wake Region	33
	Wall-Wakes with Longitudinal Pressure Gradients	45
III	EXPERIMENTAL ARRANGEMENTS AND MEASUREMENT TECHNIQUES	65
	Introduction	65
	Measurement of Mean Velocity	75
	Measurement of Boundary Shear Stress	77
	Measurement of Turbulence Intensities	87
IV	EXPERIMENTAL RESULTS AND DISCUSSION	109
	Experimental Results for Zero Pressure Gradient Flows	112
	Experimental Results for Adverse Pressure Gradient Flows	155
V	TURBULENCE CHARACTERISTICS OF WALL-WAKES	185
VI	SUMMARY AND CONCLUSIONS	215
	LIST OF REFERENCES	220
	ADDITIONAL REFERENCES	227
	APPENDIX A. MEASURED MEAN-FLOW CHARACTERISTICS	228
	APPENDIX B. MEASURED TURBULENCE CHARACTERISTICS	248

LIST OF TABLES

<u>Table</u>	<u>Page</u>
II-1 Wake-Parameters for Zero Pressure Gradient Flows	38
IV-1 Geometry of the Obstacle and Flow Conditions	110
IV-2 Comparison of Theoretical and Experimental Values of (u_{1m}/U)	171
IV-3 Comparison of Theoretical and Experimental Values of b	177
A.1 Measured Mean Velocity Distribution for Run No. 1	229
A.2 " " " " 2	231
A.3 " " " " 3	233
A.4 " " " " 4	236
A.5 " " " " 5	238
A.6 " " " " 6	240
A.7 " " " " 9	242
A.8 Flow Parameters for Zero Pressure Gradient Flows	244
A.9 Flow Parameters for Adverse Pressure Gradient Flows	246

LIST OF TABLES (Continued)

<u>Table</u>		<u>Page</u>
B.1	Measured Turbulence Characteristics for	
	Run No. 2	249
B.2	" " " "	4 252
B.3	" " " "	6 255
B.4	" " " "	8 258
B.5	" " " "	9 261

LIST OF FIGURES

<u>Figure</u>		<u>Page</u>
2.1	Definition Sketch for Two-Dimensional Wall-Wake	10
2.2	Longitudinal Variation of Wake-Parameters, α and β for Zero Pressure Gradient Flows	40
2.3	Vertical Shift of Logarithmic Profile for Rough Wall	44
2.4	Variation of (U_{lm}/U) with Exponent m	53
3.1	Schematic Representation of Wind-Tunnel	68
3.2	Sand Grain Roughness	73
3.3	Sketch of the Test-Section with Adjustable Wall at the Top	74
3.4	Free Stream Velocity and the Free Stream Turbulence Intensity in the Test-Section of the Wind-Tunnel	76
3.5	Pressure-Shear Ratio for Rough Boundaries (After Hwang and Laursen, 1963)	83
3.6	Details of Hot-Wire Anemometer and Experimental Set-Up	91
3.7	Calibration Curves for X-Probes	106
3.8-a	Schematic Diagram for Calibration of X-Probes	107

LIST OF FIGURES (Continued)

<u>Figure</u>		<u>Page</u>
3.8-b	Comparison of X-Probe and Pitot-Tube Mean Velocity Measurements	107
3.8-c	Comparison of u' - Fluctuations Measured by X-Probe and Single Probe	107
4.1-a	Velocity Distribution in the Region of Separation for Run No. 2	113
4.1-b	Velocity Distribution in the Near-Wake Region for Run No. 2	115
4.1-c	Velocity Distribution in the Far-Wake Region for Run No. 2	116
4.2	Erroneous Computation of u_{lm} and b	120
4.3-a	Velocity Distribution in the Outer- Region for Runs 1, 2 and 3	122
4.3-b	Velocity Distribution in the Outer- Region for Runs 4, 5 and 6	123
4.4-a	Velocity Distribution in the Inner- Region for Runs 1, 2 and 3 (u/u_* vs. $y u_*/v$)	125
4.4-b	Velocity Distribution in the Inner- Region for Runs 4 and 5 (u/u_* vs. $y u_*/v$)	127
4.5	Velocity Distribution in the Inner- Region for Runs 2, 3, 4 and 5 (u/u_* vs. y/b)	129

LIST OF FIGURES (Continued)

<u>Figure</u>		<u>Page</u>
4.6	Velocity Distribution in the Inner- Region for Run No. 6 (Rough Wall)	131
4.7	Growth of Length Scale; (b/h) vs. (x/h)	135
4.8	Growth of Length Scale; (b/hC_{DO}) vs. (x/hC_{DO})	138
4.9	Decay of Velocity Scale	140
4.10	Bed Shear Stress Distribution along the Centre Plane for Runs 1 to 6	142
4.11	Coefficient of Skin Friction along the Centre Plane for Runs 1 to 6	147
4.12	Growth of Boundary Layer Parameters for Runs 2, 4 and 6	154
4.13	Free Stream Velocity Distribution for Runs 7, 8 and 9	157
4.14-a	Velocity Profiles for Run No. 7	159
4.14-b	" " " " 8	160
4.15	Velocity Distribution in the Outer- Region for Runs 7, 8 and 9	162
4.16	Velocity Distribution in the Inner- Region for Runs 7, 8 and 9 $(u/u_*$ vs. $yu_*/v)$	163

LIST OF FIGURES (Continued).

<u>Figure</u>		<u>Page</u>
4.17	Velocity Distribution in the Inner-Region for Runs 7, 8 and 9 (u/u_* vs. y/b)	165
4.18	Distribution of Coefficient of Skin Friction for Runs 7, 8 and 9	168
4.19	Variation of Velocity Scale for Runs 7, 8 and 9	170
4.20	Theoretical Variation of Exponent m for Wall-Wake with Adverse Pressure Gradient Flows	175
4.21	Variation of Length Scale for Runs 7, 8 and 9	178
4.22	Variation of Boundary Layer Parameters for Runs 8 and 9	183
5.1	Intensity of u -component of turbulence for Runs 2, 4 and 6	187
5.2	Intensity of u -component of Turbulence for Runs 8 and 9	189
5.3	Intensity of v -component of Turbulence for Runs 2, 4 and 6	191
5.4	Intensity of v -component of Turbulence for Runs 8 and 9	192

LIST OF FIGURES (Continued)

<u>Figure</u>		<u>Page</u>
5.5	Intensity of w-component of Turbulence for Runs 2, 4 and 6	194
5.6	Intensity of w-component of Turbulence for Runs 8 and 9	195
5.7	Longitudinal Component of Relative Turbulence Intensity for Run No. 2	197
5.8	" " " 4	211
5.9	" " " 6	212
5.10	" " " 8	213
5.11	" " " 9	214
5.12	Distribution of Turbulence Intensity in the Far-Wake Region for Runs 2, 4, 6, 8 and 9	198
5.13	Distribution of Turbulence Shear Stress for Runs 2 and 4	200
5.14	Distribution of Turbulence Shear Stress for Run No. 6 (Rough Wall)	202
5.15	Comparison of Turbulence Shear Stress for Wall-Wakes at Zero Pressure Gradient with (a) Klebanoff's (1954) data for Turbulent Boundary Layer at Zero Pressure Gradient, and (b) Townsend's (1949) data for Wake Behind a Circular Cylinder	203

~~SECRET~~

LIST OF FIGURES (Continued)

<u>Figure</u>		<u>Page</u>
5.16	Variation of Mixing Length for Runs 2, 4 and 6	206
5.17	Shear Stress Distribution for Runs 8 and 9	209

LIST OF SYMBOLS

A, B	Experimentally determined constant
b	Half wake-width
\bar{b}	wake width
B_1	= db/dx
C, C_1 , and C_2, \bar{C}	Experimentally determined constants
C_f	Coefficient of skin friction = $\tau_o / \frac{1}{2} \rho U^2$
C_{fm}	- Do - = $\tau_o / \frac{1}{2} \rho U_{1m}^2$
C_{Do}	Coefficient of Drag = $F_D / \frac{1}{2} \rho U_o^2$
D	Experimentally determined constant
d	Diameter of cylinder
E	Output voltage of D.C. volt-meter
e'	Fluctuating voltage of RMS volt-meter
$\overline{e_A e_B}$	Measured correlation output from correlator
F_D	Drag Force
F_n	= $\int_0^\infty f^n d\lambda$
$f(\lambda)$	= $\frac{U_o - u}{u_{1m}}$
H	Shape Factor δ^*/θ
h	Height of obstacle
I	Electric heating current
k	Height of roughness element

LIST OF SYMBOLS (continued)

k_s	Equivalent sand roughness height
l	Mixing length
m	Experimentally determined exponent
p	Mean pressure
p_o	Static pressure
Δp	= $p - p_o$ pressure difference
R_w	Electric resistance of heated wire
R_e	= $U_o h / \nu$ Reynolds number
R_k	= $u_* k / \nu$ - Do -
R_b	= $U b / \nu$ - Do -
R_θ	= $U \beta / \nu$ - Do -
R_ϵ	= $u_{lm} b / \epsilon$, Eddy viscosity Reynolds number
U	Local free-stream velocity
U_o	Free stream velocity
u	Mean velocity in longitudinal direction
u_*	Shear velocity $(\tau_o / \rho)^{1/2}$
u_{lm}	Maximum velocity defect
$\Delta u / u_*$	Shift of logarithmic profile caused by roughness
u'	Longitudinal component of turbulence fluctuations
$\overline{u'^2}$	r.m.s. value of u'

LIST OF SYMBOLS (continued)

v	Mean velocity normal to wall
v'	Turbulence fluctuations normal to wall
$\sqrt{v'^2}$	r.m.s. value of v'
$\overline{u'v'}$	turbulence shear stress
w'	Turbulence fluctuation in lateral direction
$\sqrt{w'^2}$	r.m.s. value of w'
x	Distance along the wall
x_0	Hypothetical origin of the flow
x_r	Point of reattachment of the flow
y	Distance normal to wall
α	$= u_{lm}/U$, wake parameter
α_p	$= \frac{v}{\rho u_*^3} \frac{dp}{dx}$, Pressure gradient parameter
β	$b/h C_{Do}$, wake parameter
γ	= Intermittency factor
δ	Boundary layer thickness
δ^*	Displacement thickness $\int_0^\infty (1 - \frac{u}{U}) dy$
δ_w	Wake displacement thickness
ϵ	Eddy viscosity
η	$= \alpha\beta$
θ	Momentum thickness $\int_0^\infty \frac{u}{U} (1 - \frac{u}{U}) dy$

LIST OF SYMBOLS (continued)

- ρ Mass density of fluid
- ν Kinematic viscosity of fluid
- λ = y/b
- τ Shear stress
- τ_l Viscous shear stress = $\mu \frac{\partial u}{\partial y}$
- τ_t Turbulent shear stress = $-\rho \overline{u'v'}$
- τ_0 Wall shear stress
- μ Viscosity of fluid

C H A P T E R I

INTRODUCTION

1.1 GENERAL

The occurrence of wakes behind obstacles located on walls, which are called "wall-wakes", is quite frequent in nature. Any protuberance on a wall exposed to a moving stream produces the type of flow associated with a wall-wake. The bed configurations in a channel or stream or the bed materials themselves, if they are large enough, will produce wall-wakes. However, the flow past the obstacle may not always be two-dimensional in nature. Non-tangential injection of fluid through a slot in a wall will produce a flow configuration which is analogous in many respects to a wall-wake.

The size of the obstacle on the wall is of importance mainly in determining the nature of the flow far downstream from the obstacle. For example, if the height of the obstacle is small enough so that it lies within the viscous sub-layer of the boundary layer of the section in which it is located, no appreciable change in flow characteristics will be noted. We may say that the flow will ignore the presence of the obstacle (except, perhaps, in a very small region around it), if the obstacle is submerged in the laminar sublayer of the boundary layer, (Schlichting, 1968). If the obstacle is large enough to protrude out of

the laminar sub-layer, but is still confined within the thickness of the boundary layer, then its presence will be readily felt for quite some distance downstream. An essential feature associated with this case is the earlier transition from laminar to turbulent boundary layer, Liepmann and Fila (1947), Tani and Hama (1953). The flow, once disturbed by the presence of the obstacle, gradually attains the characteristics of a fully-developed turbulent boundary layer as it proceeds downstream from the point of disturbance. The velocity profiles in this region do not exhibit any wake characteristics which can be attributed to the presence of the obstacle. It is only when the obstacle is sufficiently long that it protrudes out of the boundary layer, that we observe a marked change in velocity profiles quite far downstream from the obstacle. In such a case, the wake and wall characteristics of the flow contribute equally in building its structure for long distances downstream from the point of disturbance. It is to this category of flow that we give the name "wall-wake".

Flow past an obstacle that is fully surrounded by fluid differs in several ways from flow past one that is tied to one of the flow boundaries. First of all, the flow in the wake of an isolated obstacle is free to oscillate about the plane of symmetry, whereas such oscillation is wholly prevented in the case of the wall-wake, Roshko (1954, 1955). Further, the presence of the wall

causes considerable reduction (30%-40%) in the form drag of the body (Arie and Rouse, 1956). The striking characteristic of bluff-body flows with no boundary is that, for all Reynolds numbers above a few thousand, the form drag coefficient is approximately constant. From this fact we can deduce that: (1) the separation behavior of the boundary layers formed on the body is determined by body shape alone, and (2) the flow processes in the wake, which determine the base pressure, are dominated by the turbulence generated by the initial shearing between the free stream and the separated flow.

1.2 EXISTING WORKS

Considerable work has been done on the plane turbulent wake. The classical work is that of Schlichting (1930), which is based on Prandtl's mixing length hypothesis. Tollmien (1933) solved the same problem on the basis of von Kármán's hypothesis. Extensive investigations on two and three dimensional plane wake have been carried out since then and some of the important works are listed in additional bibliography. On the other hand, we find very little work done in the field of wall-wakes. Most of the available observations on wall-wakes are primarily concerned with the effect of an obstacle on transition and separation phenomena in the boundary layer. These studies have treated primarily configurations wherein the obstacle is wholly or partially submerged within

the boundary layer. A comprehensive bibliography on this subject can be found in Tani's (1961) work. Experimental investigations on the eddy pattern and drag coefficient for bluff bodies attached to the boundary, have been done by Wieghardt (1953) and Arie and Rouse (1956). Similar work in which the bluff body was immersed in the turbulent boundary layer has been done by Good and Joubert (1968). The effects of fluid injection through the boundary have been examined by Torrence (1967) and Mickley and Davis (1957).

1.3 SCOPE OF PRESENT INVESTIGATION

The present study differs considerably from other investigations in that the obstacle is located almost at the leading edge of the wall. It thus causes a large inviscid disturbance in the on-coming flow while the boundary layer forms downstream from it. The author has not come across any investigation on flows of this type. The only investigation of a flow that bears any resemblance to this type of flow is that of Sforza and Mons (1969). Their studies were mainly concerned with flows past objects of various geometries placed at the leading edge of a flat plate. The experimental results were compared with a mathematical model based on the Oseen linearization for wake-like diffusive flows. Their studies, however, were confined to the region of developing flow ($x/h < 100$), h being the height of the

obstacle and x being the longitudinal distance measured downstream from the obstacle. No measurements of turbulence quantities were made by Sforza and Mons.

In the present experimental program, a simple two-dimensional object placed on a smooth wall was investigated first. Measurements of mean velocity and wall shear stress were made downstream from the obstacle at distances of up to five hundred times its height. The experiment was repeated with obstacles of different shapes and sizes in order to determine whether the shape and size of the obstacle played any significant role in its influence upon the general flow characteristics. In one case the effect of bed roughness downstream from the point of disturbance was also examined.

The study was then extended to wall-wakes with adverse pressure gradients. The application of a moderate pressure gradient can exercise a large influence on the decay of wake-characteristics. Only adverse pressure gradients which would not cause separation of the boundary layer were investigated in the present study.

Another objective of this investigation was to obtain data on turbulence quantities. For this reason, turbulence fluctuations and shear stress were measured for two typical cases of wall-wakes on a smooth, flat wall with zero pressure gradients. An investigation of the effects of wall roughness and adverse pressure gradients on turbulence quantities in a wall-wake comprised the final

section of the experimental program.

1.4 PRESENTATION OF THE STUDY AND RESULTS

The following arrangement has been adopted in presenting the details of the present investigation.

An analytical analysis of the wall-wake, with and without pressure gradient, is presented in Chapter II. The analysis is based upon the assumption that there exists two distinct regions of flow downstream from the obstacle. Boundary layer similarity has been assumed for the flow in the region close to the wall (termed as the "wall-region") and plane wake type flow has been assumed in the region away from the wall (termed as the "outer-region"). Working from the observation that velocity and shear stress profiles are similar, the analysis predicts certain basic relationships for the decay of velocity defect and growth of the half-width of the wake. Dimensional considerations are employed to obtain a number of dimensionless parameters which are useful in the presentation of the experimental results.

In Chapter III details regarding the experimental arrangements and the measurement techniques are discussed. The theory of hot-wire anemometry for turbulence measurements is presented, and certain practical difficulties, which were encountered during the experimental work, are also mentioned.

The measurements of mean turbulent quantities are

7

analyzed in Chapter IV. The effects on the wall-wake of shape and size of the obstacle, wall roughness, and longitudinal adverse pressure gradient, are discussed with reference to the experimental data. The results of mean velocity profiles, wall shear stress, decay of velocity defect, and growth of the half-width of the wake, are presented in convenient forms. Also, comparisons of these results with the theoretical predictions, presented in Chapter II, have been made.

Turbulence measurements for the wall-wake are analyzed in Chapter V. Prandtl's mixing length theory has been tested and found to provide an adequate description for zero pressure gradient flows. Gartshore's (1965) eddy viscosity hypothesis was tested for wall-wakes with adverse pressure gradient flows and was found to give adequate results for moderately strong adverse pressure gradients. The skin friction was found to influence the diffusive behavior of the wall-wake with the weak adverse pressure gradient. Turbulence shear stress and certain other characteristic turbulence parameters were also analyzed, and comparisons with existing measurements for some turbulence parameters are presented.

Conclusions and possible extensions and applications of the present study are discussed in the final chapter - Chapter VI.

Some typical experimental data are tabulated in the appendices, A and B.

This experimental investigation was carried out in the hydraulics laboratory of the University of Alberta, Edmonton, Alberta, Canada, during the period 1970-1972.

CHAPTER II

ANALYTICAL CONSIDERATIONS

2.1 INTRODUCTION

This chapter presents a theoretical analysis of two-dimensional turbulent wall-wakes. Since a purely theoretical solution to this flow phenomenon is not possible, because of the complex nature of turbulent flows, certain approximations have to be made in the basic equations of motion, in order to simplify the problem. The selection of these approximations is of primary importance. The basic concern here is the manner in which a wake-like disturbance develops downstream on a flat plate. Experimental observations on the existence of similarity of flow pattern in the downstream direction, make it easier to choose suitable approximations for the analysis of the above problem.

(In Figure 2.1, a definition sketch of a two-dimensional turbulent wall-wake formed behind an obstacle, (a sharp edged plate resting on a flat plate) is shown. The cartesian coordinate system has been chosen. In Figure 2.1, h is the height of the obstacle placed at the leading edge of the flat plate and x and y are measured along, and normal to, the flat plate.

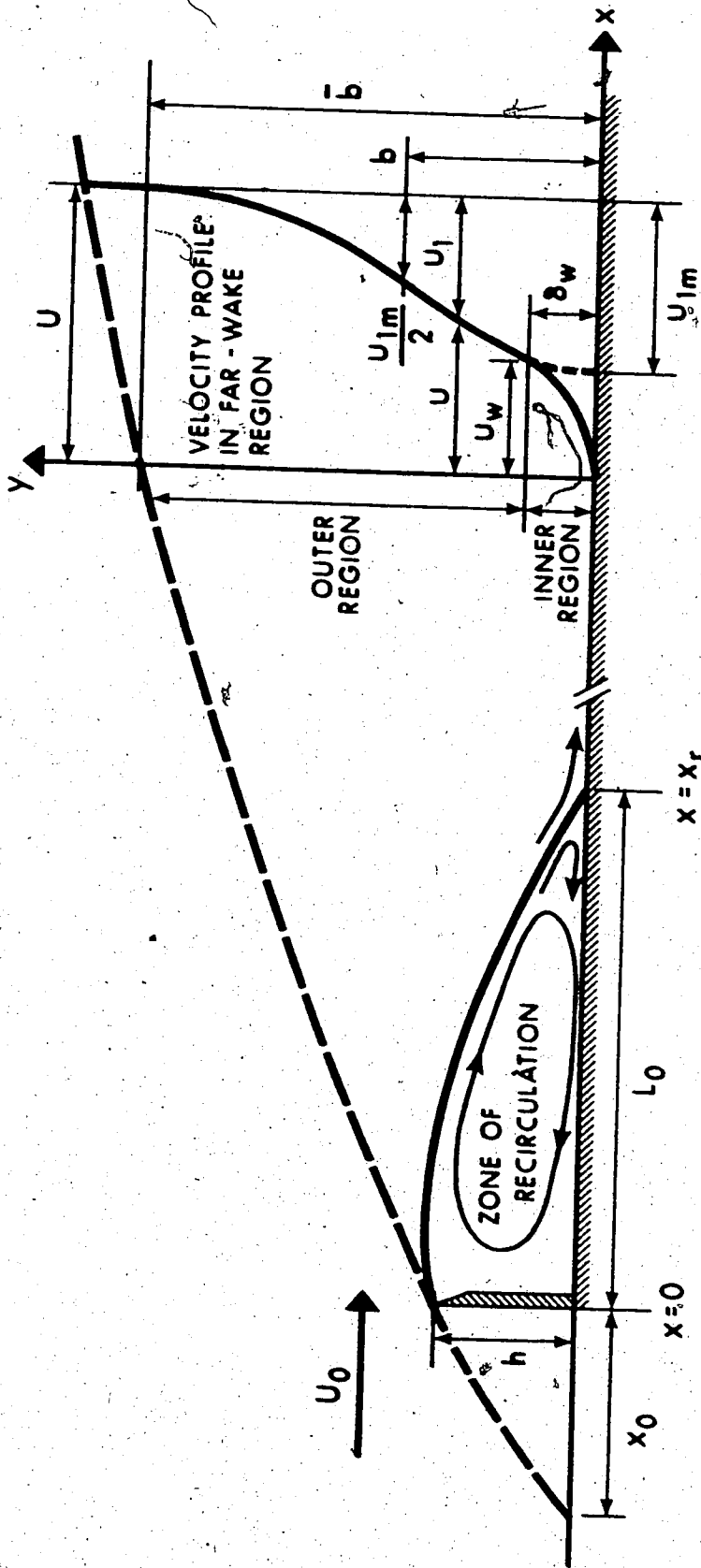


FIGURE 2.1 DEFINITION SKETCH FOR TWO-DIMENSIONAL WALL-WAKES

The wake behind an obstacle on a flat plate is found to be characterized by three regions, namely:

(1) Recirculation region

In this region the effect of vorticity induced by the obstacle is dominant over the effects of viscous and turbulent diffusion. The flow separates at the exposed edge of the obstacle and reattaches downstream on the flat plate. The velocity profiles are characterized by negative velocities (back flow) directly behind the obstacle, and considerably greater than the free stream velocity near the exposed edge of the obstacle.

(ii) Flow Development Region (or Near-Wake Region)

In this region, mixing effects due to the shear layer and the wall infiltrate the flow field. The velocity profiles and shear stress distributions are not similar in this region.

(iii) Far-Wake Region

The flow field in this region has a wake-like character in the area which is away from the wall. The law of similarity (discussed below) for velocity and shear stress distribution holds true in this region. The present investigation has been carried out mainly in this region. It has also been called the "decay-region" for the simple reason that the disturbance to the flow field, created by the obstacle, tends to decay in this region. In the following pages, however, this region is referred to as the "far-wake region".

2.2 SIMILARITY OF FLOW AT HIGH REYNOLDS NUMBERS

In a turbulent flow, suitably defined by boundary conditions, there is a main structure that is independent of the fluid viscosity, provided that it is not too large. In other words, geometrically similar flows are similar at high Reynolds numbers.

The principle of Reynolds number similarity may be stated as follows: In a fully turbulent flow, there exists a region over which the direct action of viscosity on the mean flow is negligible, i.e., the Reynolds stresses are large compared with the mean viscous stresses. Within this region, mean motion and the motion of the energy-containing components of the turbulence, are determined by the boundary conditions of the flow alone. The effect of the fluid viscosity is negligible.

The reasons for the existence of Reynolds number similarity in turbulent flow are to be found in the nature of the transfer and dissipative processes in turbulent motion. Quoting Townsend (1956-a):

"It appears to be a consequence of the non-linear form of the Navier-Stokes equations that an initially smooth distribution of velocity will, in the absence of viscosity, develop velocity discontinuities. In a fluid of finite viscosity, the diffusive action of viscosity tends to smooth out the discontinuities, but except at the immediate neighbourhood of the original discontinuity the resultant velocity distribution remains unchanged. The only effect of a change in the viscosity is to change the spatial extent and the magnitude of the large velocity gradients near the original discontinuity, leaving the

motion between the discontinuities much as it would be with zero viscosity. There is a great deal of evidence, both direct and indirect, for the validity of this principle, and it is fundamental to all turbulent flows."

2.3 SELF-PRESERVATION OF DEVELOPING FLOWS

In a developing flow, the transverse distributions of mean velocity and other mean quantities change as the position in the down-stream direction changes, but the distributions are subject to various restrictions, such as the conservation of momentum and energy. It is often assumed that the mean quantities retain the same functional forms while changing mainly in scale. For a particular flow to be self-preserving, it is necessary that the variation of any mean quantities over any plane, $x = \text{constant}$, should be expressible non-dimensionally through suitable scales of length and velocity, say l_0 and u_0 , as a universal function of (y/l_0) . The scales of length and velocity are functions of x only. The principle of self-preservation asserts that a moving equilibrium is set up in which the conditions at the initiation of the flow are for the most part irrelevant, and the flow in all sections is geometrically similar.

The analysis of the dynamics of self-preserving flows involves only the equation of mean motion, and does not prove that self-preserving flow is possible. It is possible that the other dynamic conditions may prevent the

establishment of self-preserving flow. All available experimental evidence for shear flows indicates, however, that self-preserving flows occur, if a self-preserving form of the equation of mean motion is physically possible.

2.4 THE TWO-DIMENSIONAL FLOW: SELF-PRESERVATION

Townsend (1956-a) has shown that the two-dimensional wake flow can only be self-preserving if the velocity variation across the flow is small, as compared with the free stream velocity. Two-dimensional wake flow satisfies this condition far downstream from the obstacle which produces it. For two-dimensional plane wakes behind circular cylinders, the flow is roughly self-preserving beyond $x/d = 500$ (where d is the diameter of the cylinder), and accurately so beyond $x/d = 1000$. These distances are so large that not many measurements have been made in the range close to self-preservation. Fortunately, the most violent departures from self-preservation occur within one hundred diameters of the cylinder, and so measurements just beyond this limit may be used to infer the nature of the self-preserving range at high Reynolds numbers.

2.5 SIMILARITY ANALYSIS OF TWO-DIMENSIONAL WALL-WAKES

The present analysis of two-dimensional turbulent wall-wakes is based on the assumption that the flow

region, at a distance far downstream from the obstacle, can be divided into two distinct regions: (i) the outer region and (ii) the inner or wall region.

(i) Outer region:

This is the region away from the wall in which inertial forces predominate over the viscous forces, and the effect of the wall on the flow field is negligible. In other words, it is assumed that the flow in this region is not much different from that of a two-dimensional plane wake. Thus, the velocity and shear stress distribution in the outer region should be approximately the same as for that of a two-dimensional plane wake.

(ii) Inner region:

The inner region which is adjacent to the wall is where the effects of the wall predominate. The flow field in this region is completely different from that of a plane wake. Surface conditions of the wall greatly influence the flow in this region. It is reasonable to say that the flow in the inner region of a turbulent wall-wake would behave in a manner similar to the flow in the inner region of a turbulent boundary layer, under the same wall conditions.

There is no distinct line of demarcation separating these two regions and there is a possibility that they may overlap in a given section of the flow region. The wake type and boundary layer type of analyses for the outer and

inner regions, respectively, are presented in the following pages.

2.6 THEORETICAL ANALYSIS OF THE OUTER REGION

The outer region of a turbulent wall-wake can be analyzed with the aid of the assumption that the flow field in this region is not much different than that of a plane turbulent wake. The velocity and shear stress distributions are similar in the far-wake region. This means that they vary from section to section only in magnitude, and if suitable parameters for velocity and length are chosen to non-dimensionalize the data, they will all fall on a single curve. Because of the assumption that the flow in the outer region has a wake-like character, the parameters that would suitably describe the flow in this region should be the same as for that of a plane wake, viz.- the maximum velocity defect and the half width of the wake. Maximum velocity defect is a hypothetical quantity in the case of the wall-wake. In this case it does not reach its plane wake value; rather, it approaches zero because of the presence of a solid boundary (Figure 2.1). In the present analysis, however, we will employ the hypothetical velocity defect, u_{1m} , and the half-width of the wake, b , the ordinate at which the velocity defect is $u_{1m}/2$ (Figure 2.1), as the non-dimensionalizing parameters for velocity and length respectively.

Now, assuming that the flow around the obstacle is independent of the Reynolds number, the similarity principle requires that:

$$\frac{U-u}{u_{1m}} = f(y/b) \quad)$$

$$\text{and} \quad \frac{\tau}{\rho u_{1m}^2} = g(y/b) \quad) \quad (2.1)$$

where u_{1m} and b are functions of x only. U and τ are free stream velocity and shear stress respectively, and f and g denote functional relationships.

The Reynolds equations for the two-dimensional case in the cartesian coordinate system can be written as:

$$u \frac{\partial u}{\partial x} + v \frac{\partial u}{\partial y} = -\frac{1}{\rho} \frac{\partial p}{\partial x} + \nu \left(\frac{\partial^2 u}{\partial x^2} + \frac{\partial^2 u}{\partial y^2} \right) - \left(\frac{\partial \overline{u'^2}}{\partial x} + \frac{\partial \overline{u'v'}}{\partial y} \right)$$

$$u \frac{\partial v}{\partial x} + v \frac{\partial v}{\partial y} = -\frac{1}{\rho} \frac{\partial p}{\partial y} + \nu \left(\frac{\partial^2 v}{\partial x^2} + \frac{\partial^2 v}{\partial y^2} \right) - \left(\frac{\partial \overline{u'v'}}{\partial x} + \frac{\partial \overline{v'^2}}{\partial y} \right) \quad (2.2)$$

and the equation of continuity as:

$$\frac{\partial u}{\partial x} + \frac{\partial v}{\partial y} = 0 \quad (2.3)$$

Where, u and v are the (time) mean velocity components in the x and y directions respectively,
 u' and v' are the fluctuating components of the velocity

p is the mean pressure

ρ is the mass density, and

ν is the kinematic viscosity of the fluid.

2.6.1 BOUNDARY LAYER SIMPLIFICATION OF THE EQUATIONS OF MOTION

A characteristic feature of turbulent wake (as well as jet) is the limited extent of the wake-width in the transverse direction. The pressure across any section can be considered constant. Thus boundary layer type approximations can be applied to the equations of motion.

These approximations are:

- (i) Beyond a certain initial reach from the obstacle, $y \ll x$.
- (ii) The transverse component of velocity, $v \ll u$ in the major portion of the flow field.
- (iii) The fluctuating components are much smaller than the mean components.
- (iv) The velocity gradients in the y direction are much larger than those in the x direction.

A study of the order of magnitude of the equations of motion (Equations 2.2) will lead to the following set of simple equations:

$$u \frac{\partial u}{\partial x} + v \frac{\partial u}{\partial y} = - \frac{1}{\rho} \frac{\partial p}{\partial x} + \nu \frac{\partial^2 u}{\partial y^2} - \frac{\partial \overline{u'v'}}{\partial y} \quad (2.4)$$

and
$$\frac{\partial u}{\partial x} + \frac{\partial v}{\partial y} = 0 \quad (2.5)$$

Combining the second and third terms on the right hand side of equation (2.4), we can rewrite the above equation as:

$$u \frac{\partial u}{\partial x} + v \frac{\partial u}{\partial y} = - \frac{1}{\rho} \frac{\partial p}{\partial x} + \frac{1}{\rho} \frac{\partial \tau}{\partial y} \quad (2.6)$$

where, τ = total shear stress = $\tau_l + \tau_t$

τ_l = viscous shear stress = $\mu \frac{\partial u}{\partial y}$

τ_t = turbulent shear stress = $-\rho u'v'$

2.7 WALL-WAKE WITH ZERO PRESSURE GRADIENT

The equation of motion for the turbulent wall-wake can further be simplified, for the zero pressure gradient case, by substituting $\partial p / \partial x = 0$ in equation (2.6). The final equations then become:

$$u \frac{\partial u}{\partial x} + v \frac{\partial u}{\partial y} = \frac{1}{\rho} \frac{\partial \tau}{\partial y} \quad (2.7)$$

and

$$\frac{\partial u}{\partial x} + \frac{\partial v}{\partial y} = 0$$

2.7.1 MOMENTUM INTEGRAL EQUATION

Integrating equation (2.7) between the limits $y = 0$ and $y = \infty$, we obtain,

$$\int_0^{\infty} u \frac{\partial u}{\partial x} dy + \int_0^{\infty} v \frac{\partial u}{\partial y} dy = \int_0^{\infty} \frac{1}{\rho} \frac{\partial \tau}{\partial y} dy$$

Now,
$$\int_0^{\infty} u \frac{\partial u}{\partial x} dy = \int_0^{\infty} \frac{1}{2} \frac{\partial u^2}{\partial x} dy = \frac{1}{2} \frac{d}{dx} \int_0^{\infty} u^2 dy$$

Integrating the second term on the right hand side of the equation by parts, we obtain

$$(v \cdot u) \Big|_0^{\infty} - \int_0^{\infty} \frac{\partial v}{\partial y} u dy$$

Substituting for v from the equation of continuity, and applying the boundary conditions,

$$u = v = 0 \text{ at } y = 0$$

and
$$u = U = U_0 \text{ at } y = \infty$$

we get,

$$\int_0^{\infty} v \frac{\partial u}{\partial y} dy = -U_0 \int_0^{\infty} \frac{\partial u}{\partial x} dy + \int_0^{\infty} u \frac{\partial u}{\partial x} dy$$

$$= -\frac{d}{dx} \int_0^{\infty} u \cdot U_0 dy + \frac{1}{2} \frac{d}{dx} \int_0^{\infty} u^2 dy$$

Thus, the left hand side becomes

$$\frac{d}{dx} \int_0^{\infty} (u^2 - uU_0) dy$$

where U_0 is the free stream velocity.

The right hand side of the equation is:

$$\int_0^{\infty} \frac{1}{\rho} \frac{\partial \tau}{\partial y} dy = \frac{1}{\rho} (\tau)_0^{\infty} = -\frac{\tau_0}{\rho}$$

by applying the boundary conditions:

$$\tau = 0 \text{ at } y = \infty, \text{ and}$$

$$\tau = \text{wall shear stress, } \tau_0 \text{ at } y = 0$$

We obtain the momentum integral equation in the form

$$\frac{d}{dx} \int_0^{\infty} \rho u (U_0 - u) dy = \tau_0 \quad (2.8)$$

If we assume, as a first approximation, that τ_0 is very small and can be neglected, then equation (2.8) can be reduced to:

$$\frac{d}{dx} \int_0^{\infty} \rho \cdot u \cdot (U_0 - u) dy = 0$$

Integrating both sides of the above equation with respect to x , we get

$$\int_0^{\infty} \rho \cdot u \cdot (U_0 - u) dy = \text{constant} = F_D \quad (2.9)$$

where the constant F_D is identifiable as the drag force.

Substituting equation (2.1) into equation (2.9), we get

$$\int_0^{\infty} U_0 u_{1m} f b d\lambda - \int_0^{\infty} u_{1m}^2 f^2 b d\lambda = \frac{F_D}{\rho}$$

where $\lambda = y/b$

Dividing throughout by U_0^2 in the above equation, and taking the terms which are independent of λ , outside the integral sign, we get:

$$\frac{u_{1m}}{U_0} b \int_0^{\infty} f d\lambda - \left(\frac{u_{1m}}{U_0}\right)^2 b \int_0^{\infty} f^2 d\lambda = \frac{F_D}{\rho U_0^2} \quad (2.10)$$

Equation (2.10) is further reducible in the "far-wake region". If we introduce the fact that $u_{1m} \ll U_0$ in the "far-wake region", so that the term containing $(\frac{u_{1m}}{U_0})^2$ is very small and can be neglected, we get

$$\frac{u_{1m}}{U_0} b \int_0^{\infty} f \, d\lambda = \frac{F_D}{\rho U_0^2}$$

Since the term

$$\int_0^{\infty} f \, d\lambda = F_1$$

is independent of x and is a finite quantity, we can write

$$\left(\frac{u_{1m}}{U_0}\right) b = \frac{F_D}{F_1 \rho U_0^2}$$

The drag force F_D can be written as:

$$F_D = C_{Do} \frac{\rho U_0^2}{2} \cdot h$$

C_{Do} being the drag coefficient.

Thus,

$$\left(\frac{u_{1m}}{U_0}\right) b = \left(\frac{C_{Do}}{2F_1}\right) h$$

or,
$$\left(\frac{u_{1m}}{U_0}\right) \left(\frac{b}{h C_{Do}}\right) = \frac{1}{2F_1} \quad (2.11)$$

In all the turbulent wake (as well as jet) problems, it has been observed that the maximum velocity defect, u_{1m} (or maximum velocity in the case of turbulent jet), and the wake-width, b , vary as some power of x . It is appropriate to assume, therefore, that

$$u_{1m} \propto x^p$$

and, $b \propto x^q$

where p and q are the exponents to be determined.

If we examine equation (2.11) we see that while the left hand side of the equation is proportional to x^{p+q} , the right hand side is independent of x . Thus, for similarity we must have

$$p + q = 0 \quad (2.12)$$

A second equation between p and q can be obtained if we substitute equations (2.1) into equation (2.7) and simplify. We thus obtain:

$$\frac{U_0}{u_{1m}} b' \lambda f' - b \frac{U_0 u_{1m}'}{u_{1m}^2} f + b \frac{u_{1m}'}{u_{1m}} f^2 - b' \lambda f f'$$

$$- b \frac{u_{1m}'}{u_{1m}} f' \int_0^\lambda f \, d\lambda + b' f' \int_0^\lambda \lambda f' \, d\lambda + \frac{\nu}{b u_{1m}} f'' = g' \quad (2.13)$$

where, $b' = \frac{db}{dx}$

$$u'_{lm} = \frac{d}{dx}(u_{lm})$$

$$f' = \frac{df}{d\lambda}$$

$$g' = \frac{dg}{d\lambda}$$

$$f'' = \frac{d^2 f}{d\lambda^2}$$

In equation (2.13) we see that the first two terms on the left hand side are proportional to $(U_0/u_{lm})x^{q-1}$ while the third, fourth, fifth and sixth terms are proportional to x^{q-1} . In the "far-wake region", where $u_{lm} \ll U_0$, these four terms are very small in comparison with the first two terms and, hence, as an approximation we can drop them. Also, the last term on the left hand side, $(\nu/bu_{lm})f''$, is the viscous term and is usually very small, except near the wall. In the outer-region, therefore, we can neglect it. The equation of motion (2.13) in the outer portion of the "far-wake region" can then be approximated to

$$\frac{U_0}{u_{lm}} b' \lambda f' - b \frac{U_0 u'_{lm}}{2 u_{lm}} f = g' \quad (2.14)$$

Since the left hand side of equation (2.14) is proportional to x^{q-p-1} , and the right hand side is independent of x , for similarity we must have

$$q - p - 1 = 0 \quad (2.15)$$

Solving for p and q from equations (2.12) and (2.15) we get

$$\begin{aligned} q &= \frac{1}{2} \\ p &= -\frac{1}{2} \end{aligned} \quad (2.16)$$

$$\begin{aligned} \text{or,} \quad u_{1m} &\propto x^{-1/2} \\ \text{and,} \quad b &\propto x^{1/2} \end{aligned} \quad (2.17)$$

It is to be noted that the exponents p and q are the same as in the case of a plane turbulent wake.

Neglecting the effect of viscosity we could write

$$u_{1m} = f_1(F_D, x, \rho)$$

From dimensional analysis, it can be shown that

$$\frac{u_{1m}}{(F_D/\rho x)^{1/2}} = \text{constant} = \bar{C}_1$$

Substituting for $F_D = h C_{Do} \rho U_o^2/2$, we get

$$\frac{u_{1m}}{U_o} = C_1 (x/hC_{Do})^{-1/2} \quad (2.18)$$

where $C_1 = \frac{\bar{C}_1}{\sqrt{2}} = \text{constant}$

Equations (2.18) and (2.11) indicate that the length scale is $h C_{Do}$.

If we substitute equation (2.18) into equation (2.11), we obtain

$$\frac{b}{hC_{Do}} = C_2 (x/hC_{Do})^{1/2} \quad (2.19)$$

where $C_2 = \frac{1}{2F_1 C_1} = \text{constant}$ (2.20)

Equations (2.18) and (2.19) indicate variation of maximum velocity defect, and of wake width respectively, with reference to x . The coefficients C_1 and C_2 are to be determined experimentally.

2.7.2 EXPRESSION FOR VELOCITY PROFILE IN THE "FAR-WAKE REGION"

The expression for velocity profile in the "far-wake region" can be derived in a manner similar to that

employed by Schlichting (1930) for the turbulent plane-wake. Prandtl's mixing length hypothesis will be employed in this respect.

The shear stress in the outer portion of the "far-wake region" can be approximated by

$$\tau = \tau_t = \rho \ell^2 \left(\frac{\partial u}{\partial y} \right)^2 \quad (2.21)$$

where τ_t = turbulent shear stress = $-\overline{\rho u'v'}$ and ℓ is the mixing length, which is assumed to be proportional to the total width of the wake (Schlichting, 1930). Thus we can write:

$$\ell = kb \quad (2.22)$$

where k is a constant.

If we substitute

$$g' = \frac{d}{d\lambda} (\tau / \rho u_{lm}^2)$$

into equation (2.14) and simplify, we obtain the equation of motion for the "far-wake region", in the following form:

$$U_o \frac{\partial u}{\partial x} = \frac{1}{\rho} \frac{\partial \tau}{\partial y} \quad (2.23)$$

Equation (2.23) is easily solved with the use of equations (2.18), (2.19), (2.21) and (2.22). The following differential equation is then obtained:

$$f + \lambda f' = 4k^2 \frac{C_1}{C_2} f' f'' \quad (2.24)$$

The above differential equation can easily be solved. The left hand side of equation (2.24) can be reduced to

$$\frac{d}{d\lambda} (\lambda f)$$

and the right hand side to

$$2k^2 \frac{C_1}{C_2} \frac{d}{d\lambda} (f'^2)$$

Hence, the differential equation (2.24) reduces to

$$\frac{df}{d\lambda} = \bar{k} \lambda^{1/2} f^{1/2} \quad (2.25)$$

where $\bar{k} = (C_2/2C_1 k^2)^{1/2}$

Solving equation (2.25) we get

$$2f^{1/2} = \frac{2}{3} \bar{k} \lambda^{3/2} + C \quad (2.26)$$

where C is the constant of integration.

For plane turbulent wakes the constant C can be determined by applying the boundary condition

$$\text{at } \lambda = 0, f = 1, \text{ and hence, } C = 2$$

thus
$$f^{1/2} = 1 + \frac{\bar{K}}{3} \lambda^{3/2}$$

The constant \bar{K} can be determined by applying the boundary condition

$$\text{at } \lambda = 1, f = 1/2, \text{ thus } \bar{K}/3 = -0.293$$

Hence,
$$f = (1 - 0.293 \lambda^{3/2})^2 \quad (2.27)$$

Equation (2.27) can be rewritten as

$$\frac{u_o - u}{u_{1m}} = (1 - 0.293 \left\{ \frac{y}{b} \right\}^{3/2})^2 \quad (2.28)$$

It is shown in Chapter IV that the above expression for velocity profile of the turbulent plane-wake describes the flow in the outer region of wall-wake very well.

Besides equation (2.28) there are two empirical equations which describe fairly well the distribution of

velocity defect for the plane-wake. These are:

$$(i) \quad \frac{U_0 - u}{u_{1m}} = e^{-0.693 \left(\frac{Y}{b}\right)^2} \quad (2.29)$$

$$\text{and (ii)} \quad \frac{U_0 - u}{u_{1m}} = \frac{1}{2} \left(1 + \cos \frac{\pi}{2} \frac{Y}{b}\right) \quad (2.30)$$

$$\text{for } 2 \geq \frac{Y}{b} \geq -2$$

In the present analysis, however, Schlichting's equation (equation 2.28) has been employed.

2.7.3 SHEAR STRESS DISTRIBUTION IN THE "FAR-WAKE REGION"

The expression for shear stress in the "far-wake region" can be derived with the help of the mixing-length hypothesis. The shear stress at any point can be written as:

$$\tau = \rho \ell^2 \left(\frac{\partial u}{\partial Y}\right)^2 \quad (2.31)$$

Schlichting experimentally found that the mixing length

$$\ell = 0.18\bar{b}$$

where $\bar{b} = 2.27b$ is the total width of the wake.

Differentiating equation (2.28) with respect to y we obtain:

$$\frac{\partial u}{\partial y} = 0.879 \frac{u_{1m}}{b} \left(\frac{y}{b}\right)^{1/2} (1 - 0.293 \left(\frac{y}{b}\right)^{3/2})$$

Substituting for l and $\frac{\partial u}{\partial y}$ in equation (2.31), we get:

$$\frac{\tau}{\rho u_{1m}^2} = 0.128 \left(\frac{y}{b}\right) \{1 - 0.293 \left(\frac{y}{b}\right)^{3/2}\}^2 \quad (2.32)$$

In summary, the flow characteristics in the far-wake region of a turbulent wake are defined by the following set of equations:

$$\begin{aligned} f = \frac{U_o - u}{u_{1m}} &= (1 - 0.293 \lambda^{3/2})^2 \\ \frac{u_{1m}}{U_o} &= C_1 \left(\frac{x}{h \cdot C_{Do}}\right)^{-1/2} \\ \frac{b}{h \cdot C_{Do}} &= C_2 \left(\frac{x}{h \cdot C_{Do}}\right)^{1/2} \\ g = \frac{\tau}{\rho u_{1m}^2} &= 0.128 \lambda (1 - 0.293 \lambda^{3/2})^2 \end{aligned} \quad (2.33)$$

Where $\lambda = \frac{y}{b}$

The constants C_1 and C_2 were experimentally determined by Schlichting as

$$C_1 = 1.0$$

$$C_2 = 0.25$$

Equations (2.33) have been found to give satisfactory results for turbulent wall-wakes. Some variations in the coefficients C_1 and C_2 have been found, and these will be discussed in Chapter IV.

2.8 "NEAR-WAKE REGION"

We define the "near-wake region" as the region where $u_{1m} \sim U_0$ and hence, we cannot neglect the higher powers of (u_{1m}/U_0) as an approximation. The flow field in the "near-wake region" can be analyzed in the following way:

$$\text{Let, } \int_0^{\infty} f^n d\lambda = F_n$$

$$\frac{u_{1m}}{U_0} = \alpha$$

$$\text{and, } \frac{b}{h \cdot C_{Do}} = \beta$$

Then, we can rewrite equation (2.10) as

$$2\alpha\beta (F_1 - \alpha F_2) = 1 \quad (2.34)$$

2.8.1 ENERGY INTEGRAL EQUATION

We can construct the energy integral equation by multiplying the equation of motion (equation 2.7) by u , and integrating between the limits $y = 0$ and $y = \infty$. After simplification, the result is

$$\frac{d}{dx} \int_0^{\infty} \rho \frac{u}{2} (U_0^2 - u^2) dy = \int_0^{\infty} \tau \frac{\partial u}{\partial y} dy \quad (2.35)$$

If we substitute $u_1 = U_0 - u$ into this equation and evaluate, the left hand side becomes:

$$\frac{\rho}{2} U_0^3 \left(2 F_1 \frac{d}{dx} \alpha \beta - 3 F_2 \frac{d}{dx} \alpha^2 \beta + F_3 \frac{d}{dx} \alpha^3 \beta \right)$$

where, $\bar{x} = \frac{x}{h.C_{Do}}$

and the right hand side of equation (2.35) is

$$\int_0^{\infty} \tau \frac{\partial u}{\partial y} dy = - \int_0^{\infty} \rho u_{1m}^2 g \frac{\partial u_1}{\partial y} dy$$

since, $\frac{\tau}{\rho u_{1m}^2} = g(y/b) = g(\lambda)$

If we substitute for

$$\frac{u_1}{u_{1m}} = f(\lambda)$$

and
$$\frac{\partial u_1}{\partial y} = u_{1mb} \frac{f'}{b}$$

we get,
$$\int_0^{\infty} \tau \frac{\partial u}{\partial y} dy = -\rho u_{1m}^3 \int_0^{\infty} f' \cdot g \cdot d\lambda$$

Since the integral $\int_0^{\infty} f' \cdot g \cdot d\lambda$ is independent of x , we can write this integral as, G_1 (say), then equation (2.35) takes the form:

$$2 F_1 \frac{d}{dx} (\alpha\beta) - 3F_2 \frac{d}{dx} (\alpha^2\beta) + F_3 \frac{d}{dx} (\alpha^3\beta) = -2\alpha^3 G_1 \quad (2.36)$$

The two unknown quantities α and β are solved for by using the two equations (2.34) and (2.36) in the following manner.

Let $\alpha\beta = \eta$

From equation (2.34),

$$\eta = \frac{1}{2(F_1 - \alpha F_2)} \quad (2.37)$$

Substituting for η in equation (2.36), we get

$$2 F_1 \frac{d\eta}{d\bar{x}} - 3 F_2 \left(\alpha \frac{d\eta}{d\bar{x}} + \eta \frac{d\alpha}{d\bar{x}} \right) + F_3 \left(\alpha^2 \frac{d\eta}{d\bar{x}} + 2\alpha\eta \frac{d\alpha}{d\bar{x}} \right) = -2\alpha^3 G_1$$

$$\begin{aligned} \text{or, } \frac{d\eta}{d\bar{x}} (2 F_1 - 3\alpha F_2 + \alpha^2 F_3) \\ = 3 F_2 \eta \frac{d\alpha}{d\bar{x}} - 2 F_3 \alpha \eta \frac{d\alpha}{d\bar{x}} - 2\alpha^3 G_1 \end{aligned} \quad (2.38)$$

Differentiating equation (2.37) with respect to \bar{x} , we get

$$\frac{d\eta}{d\bar{x}} = \frac{1}{2} \frac{F_2}{(F_1 - \alpha F_2)^2} \frac{d\alpha}{d\bar{x}} \quad (2.39)$$

Substituting for $d\eta/d\bar{x}$ in equation (2.38) we get

$$\begin{aligned} \frac{1}{2} (2 F_1 - 3\alpha F_2 + \alpha^2 F_3) \frac{F_2}{(F_1 - \alpha F_2)^2} \frac{d\alpha}{d\bar{x}} \\ = \frac{3 F_2 - 2 F_3 \alpha}{2 (F_1 - \alpha F_2)} \frac{d\alpha}{d\bar{x}} - 2\alpha^3 G_1 \end{aligned}$$

$$\text{or, } \left(\frac{2\alpha F_1 F_3 - \alpha^2 F_2}{2 (F_1 - \alpha F_2)} - \frac{F_2}{2} \right) \frac{d\alpha}{d\bar{x}} = -2\alpha^3 G_1$$

$$\text{or, } \frac{d\alpha}{d\bar{x}} = \frac{4\alpha^3 G_1 (F_1 - \alpha F_2)^2}{(F_1 F_2 - 2\alpha F_1 F_3 + \alpha^2 F_2 F_3)} \quad (2.40)$$

In equation (2.40), the integrals

$$F_1 = \int_0^{\infty} f \, d\lambda$$

$$F_2 = \int_0^{\infty} f^2 \, d\lambda$$

$$F_3 = \int_0^{\infty} f^3 \, d\lambda$$

and $G_1 = \int_0^{\infty} f^4 g \, d\lambda$

are independent of x and can be evaluated numerically, if we substitute for f and g from equation (2.33). Their numerical values have been evaluated as

$$\begin{aligned} F_1 &= 1.02 &) \\ F_2 &= 0.717 &) \\ F_3 &= 0.570 &) \\ G_1 &= -0.044 &) \end{aligned} \quad (2.41)$$

Substituting these values into equation (2.40), we get

$$\frac{d\alpha}{d\bar{x}} = \frac{-0.23\alpha^3(1.422-\alpha)^2}{(1.422-\alpha)^2 - 0.23}$$

or,
$$\frac{d\bar{x}}{d\alpha} = -\frac{4.35}{\alpha^3} + \frac{1}{\alpha^3(1.422-\alpha)^2}$$

Integrating the above expression, we get

$$\bar{x} = \int \left[\frac{d\alpha}{\alpha^3(1.422-\alpha)^2} - 4.35 \right] \frac{d\alpha}{\alpha^3}$$

Solving, we obtain

$$\bar{x} = \frac{1.83}{\alpha^2} - \frac{0.695}{\alpha} + 0.61 + \frac{0.244\alpha}{(1.422-\alpha)} + 1.68 \log\left(\frac{\alpha}{1.422-\alpha}\right) \quad (2.42)$$

From equations (2.42) and (2.37) α ($= \frac{u_{lm}}{U_o}$) and β ($= \frac{b}{hC_{Do}}$), have been computed and are presented in Table II-1.

Table II-1
Variation of Wake-Parameters
for Zero Pressure Gradient Flows

$\alpha = \frac{u_{lm}}{U_o}$	$\beta = \frac{b}{h.C_{Do}}$	$\bar{x} = \frac{x}{h.C_{Do}}$
1.0	1.65	2.96
0.9	1.48	2.92
0.8	1.40	3.10
0.7	1.38	3.57
0.6	1.42	4.48
0.5	1.51	6.23
0.4	1.70	9.73
0.3	2.07	17.70
0.2	2.85	41.57
0.1	5.27	174.80
0.05	10.15	716.30

The wake parameters α and β computed from equations (2.42) and (2.37) are plotted in Figure (2.2). It can be seen that for $\bar{x} > 40$ the variation of α and β can be represented by the relationships of the form:

$$\alpha = \frac{u_{1m}}{U_0} = 1.35 (x/h C_{Do})^{-1/2} \quad (2.43)$$

$$\text{and } \beta = \frac{b}{h C_{Do}} = 0.44 (x/h C_{Do})^{1/2} \quad (2.44)$$

Equations (2.43) and (2.44) indicate that in the far-wake region ($x/h C_{Do} > 40$), the velocity and the length scales for the outer region of the wall-wake follow the one-half power law variation in the longitudinal direction.

It is to be noted that equations (2.43) and (2.44) were obtained without assuming any power-law variation for u_{1m} and b . The variation of u_{1m} and b in the near-wake region can be expressed by its more general form, equations (2.42) and (2.37) (or Figure 2.2).

The coefficients 1.35 and 0.44 in equations (2.43) and (2.44) are different than those obtained experimentally

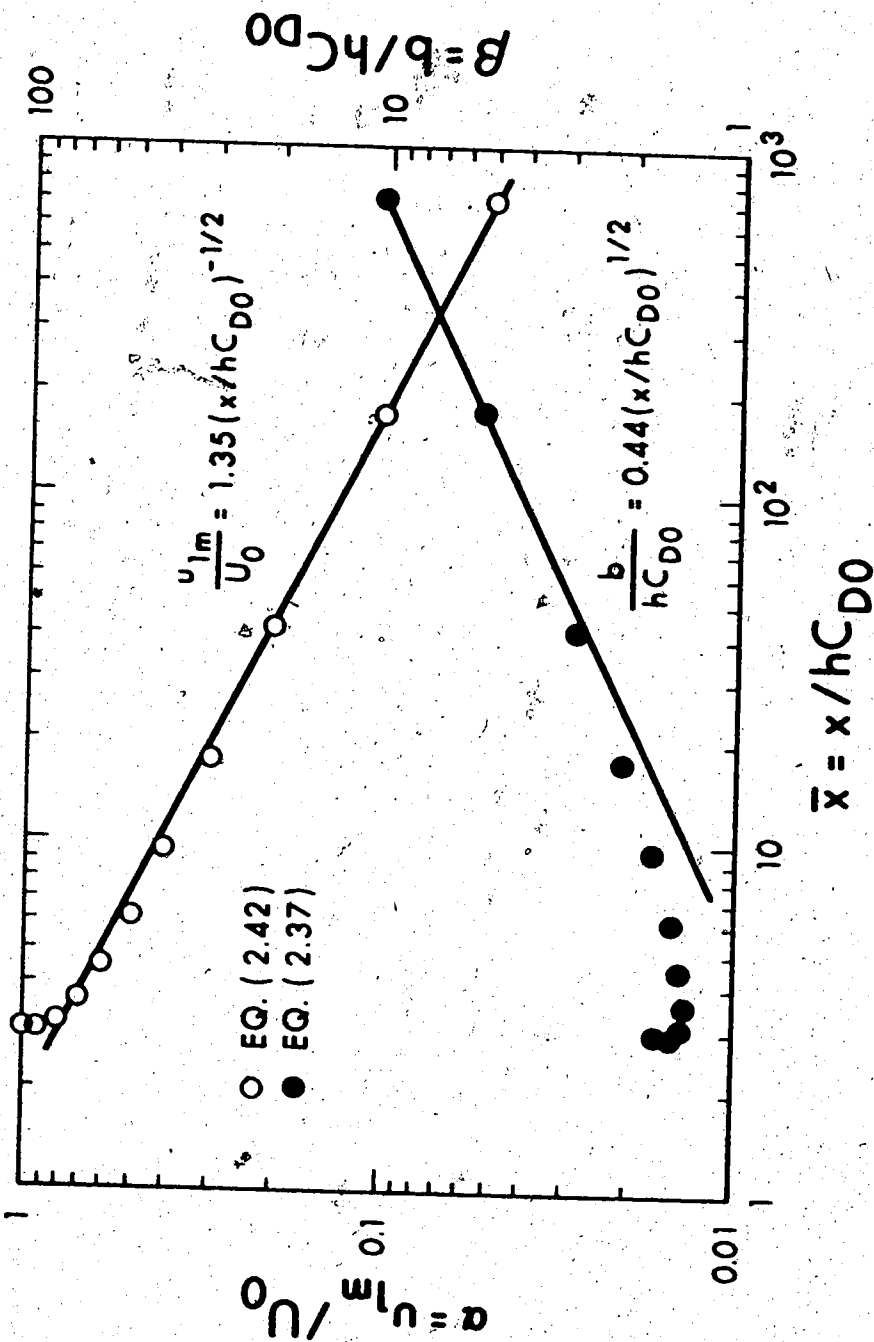


FIGURE 2.2 LONGITUDINAL VARIATION OF WAKE-PARAMETERS FOR ZERO PRESSURE GRADIENT FLOWS

by Schlichting (1930) (viz., 1.00 and 0.25 in equation 2.33), for the plane-wake. The higher values of these coefficients compared to those obtained by Schlichting indicate that the wake width and the centre-line maximum velocity defect for wall-wakes are higher than that for plane-wakes. However, the nature of the variation of b and u_{1m} in the longitudinal direction remains essentially the same as that for a plane-wake.

The experimental verification of equations (2.43) and (2.44) with the present work is discussed in Chapter IV.

2.9 INNER REGION OR WALL-REGION

The flow structure in the inner-region of a wall-wake is different than that in the outer region. The wall characteristics play the predominant role in influencing the flow structure near the wall. It can be suggested that the flow in the inner-region of a wall-wake may not be much different from that in the inner-region of boundary layers. There is a possibility that the "law of

the wall" for the turbulent boundary layer may hold in the inner-region of a turbulent wall-wake as well.

2.9.1 LAW OF THE WALL

The "law of the wall" for the turbulent boundary layer over a smooth surface is of the form

$$\frac{u}{u_*} = f\left(\frac{yu_*}{\nu}\right) \quad (2.45)$$

where $u_* = \sqrt{\frac{\tau_0}{\rho}}$ is the shear velocity.

In the region very close to the wall (viscous sub layer) equation (2.45) takes the linear form

$$\frac{u}{u_*} = \frac{yu_*}{\nu} \quad (2.46)$$

Equation (2.46) has been found to be valid for $\frac{yu_*}{\nu} < 5$. For $\frac{yu_*}{\nu} > 30$ the "law of the wall" takes the form

$$\frac{u}{u_*} = A \log \frac{yu_*}{\nu} + B \quad (2.47)$$

For turbulent boundary layers over a smooth wall with zero pressure gradient, A and B have been found to be universal constants and their values are (Clauser, 1956)

$$A = 5.6$$

$$B = 4.9$$

A comprehensive bibliography on this subject can be found in the work of Runstandler, Kline and Reynolds (1963).

2.9.2 EFFECT OF ROUGHNESS ON THE "LAW OF THE WALL"

It has been observed that the flow structure in the outer region shows the same qualitative features for rough walls as for smooth walls, for turbulent shear flows. It is now well known that the outer flow structure is independent of the surface irregularities. Thus, in the analysis of the wall-wake, the surface roughness can be considered to modify, or change, only the "law of the wall", and not the wake characteristics in the outer-region.

The first extensive study of boundary layer over a rough plate with zero pressure gradient was done by Moore (1951). Hama (1954) developed a relationship between the logarithmic portion of the mean velocity profile and the resistance coefficient, for both smooth and rough surfaces, in the fully developed flow. He proposed that the roughness effect is independent of external flow conditions, and hence is applicable, for a given roughness, to pipe flows, to open channel flows, or to flows over a flat plate. Comprehensive literature on this topic is available in the Stanford report by Liu, Kline and Johnston (1966).

Clauser (1956) and Hama (1954) have also demonstrated that an equation of the following form may be used to describe the mean velocity distribution in the inner

region of rough turbulent flow, in a constant pressure field.

$$\frac{u}{u_*} = A \log \frac{yu_*}{\nu} + B - \frac{\Delta u}{u_*} \quad (2.48)$$

where $\frac{\Delta u}{u_*}$ is a function of the roughness Reynolds number, $R_k = \frac{ku_*}{\nu}$, and this term shifts the plot vertically but does not change the slopes (Figure 2.3).

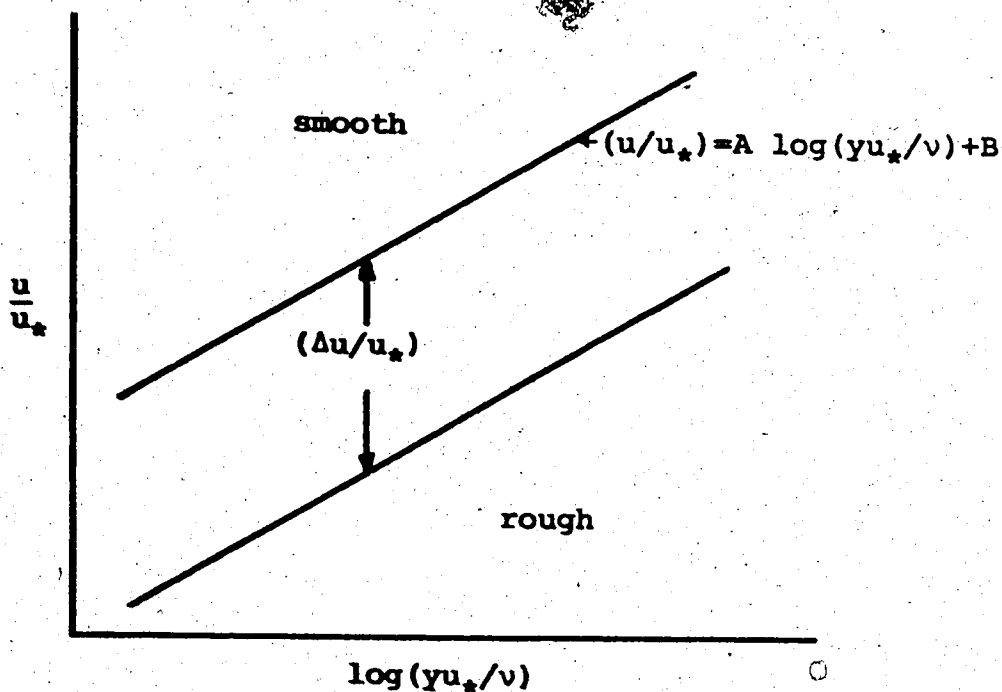


Figure 2.3 Vertical Shift of Logarithmic Profile for Rough Wall

For the smooth wall $\Delta u/u_* = 0$. For roughness Reynolds numbers, $\frac{ku_*}{\nu} > 70$, k being the height of the roughness elements, an equation of the type

$$\frac{\Delta u}{u_*} = 5.6 \log \frac{ku_*}{\nu} + D \quad (2.49)$$

has been found to be valid, where D is a constant which is dependent upon the shape and distribution of the roughness elements. For rough turbulent flow, the value of $D = -3.3$ for sand roughness (Hama, 1954). The equation of velocity distribution in the inner region of rough turbulent flow then becomes

$$\frac{u}{u_*} = 5.6 \log \frac{y}{k} + 8.2 \quad (2.50)$$

The presentation of rough wall data is seriously complicated by the fact that the origin $y = 0$ is undefined, because of the presence of the roughness elements. The criteria and method for the determination of "effective" origin are discussed in Chapter III.

2.10 WALL-WAKES WITH LONGITUDINAL PRESSURE GRADIENTS

2.10.1 INTRODUCTION

The two-layer hypothesis for the wall-wake with zero pressure gradient, proposed in section 2.5, can be extended to the analysis of wall-wakes with pressure gradients. We assume that the outer region of the wall-wake will behave in a manner similar to that of a two-dimensional plane wake with pressure gradients, and the inner region will behave like a two-dimensional turbulent

boundary layer with pressure gradients. We also assume that the law of similarity for the flow field holds true in the far-wake region, for moderate pressure gradients.

2.10.2 EQUATIONS OF MOTION

The equation of motion (if second order terms are omitted) and the equation of continuity, for two-dimensional flows with pressure gradient, are respectively:

$$u \frac{\partial u}{\partial x} + v \frac{\partial u}{\partial y} = -\frac{1}{\rho} \frac{\partial p}{\partial x} + \frac{1}{\rho} \frac{\partial \tau}{\partial y} \quad (2.51)$$

and
$$\frac{\partial u}{\partial x} + \frac{\partial v}{\partial y} = 0 \quad (2.52)$$

Applying the Bernoulli condition

$$\frac{1}{\rho} \frac{\partial p}{\partial x} = -U \frac{dU}{dx} \quad (2.53)$$

where U is the local free stream velocity, we can rewrite equation (2.51) in the following manner:

$$u \frac{\partial u}{\partial x} + v \frac{\partial u}{\partial y} = U \frac{dU}{dx} + \frac{1}{\rho} \frac{\partial \tau}{\partial y} \quad (2.54)$$

For self-preserving (self-similar) flows, in the far-wake region (section 2.6), we can write

$$\frac{U-u}{u_{1m}} = f_1 (y/b) = f_1 (\lambda) \quad (2.55)$$

$$\frac{\tau}{\rho u_{1m}^2} = g_1 (y/b) = g_1 (\lambda) \quad (2.56)$$

Where u_{1m} and b are defined in Figure (2.1) and functions f_1 and g_1 are independent of x .

Substituting equation (2.55) into the equation of continuity (2.52), we get the cross-stream velocity, v , as

$$v = bu'_{1m} \int_0^\lambda f_1 d\lambda - b'u_{1m} \int_0^\lambda \lambda f_1' d\lambda - b\lambda \frac{dU}{dx} \quad (2.57)$$

where $u'_{1m} = \frac{du_{1m}}{dx}$

$$b' = \frac{db}{dx}$$

$$f_1' = df_1/d\lambda$$

Substituting equations (2.55), (2.56) and (2.57) into the equation of motion (2.54) and simplifying, we get

$$-\frac{dg_1}{d\lambda} = -g_1' = b \frac{u'_{1m}}{u_{1m}} (f_1' F_1(\lambda) - f_1^2) - b' \left(\frac{U}{u_{1m}} \lambda f_1' - F_1(\lambda) f_1' \right) +$$

$$\frac{bUu'_{1m}}{2u_{1m}} (f_1) - \frac{b}{u_{1m}} \frac{dU}{dx} (\lambda f_1' - f_1) \quad (2.58)$$

where $F_1(\lambda) = \int_0^\lambda f_1 d\lambda$

An examination of the above equation will reveal that while the left hand side is independent of x , the

terms outside the brackets on the right hand side are functions of x . Therefore, for similarity of flow, the following conditions must be satisfied:

$$b \frac{u'_{1m}}{u_{1m}} = \text{constant}$$

$$U/u_{1m} = \text{constant}$$

$$b' = \text{constant}$$

and $\frac{b}{u_{1m}} \frac{dU}{dx} = \text{constant}$

The above four conditions could easily be simplified to give the following expressions:

$$\frac{db}{dx} = \text{constant} \quad)$$

$$\frac{u_{1m}}{U} = \text{constant} \quad)$$

and $\frac{b}{u_{1m}} \frac{du_{1m}}{dx} = \text{constant} \quad)$

(2.59)

Thus we find that the half wake-width varies linearly with x .

or, $ba(x+x_0)$

where x_0 is a constant which (when the origin of coordinates for x has been chosen) identifies the position of the hypothetical origin of the flow.

Substituting the expression for b , into the third expression of equations (2.59), we get

$$\frac{du_{lm}}{u_{lm}} \propto \frac{dx}{(x+x_0)}$$

Integrating both sides of the above expression and simplifying, we obtain

$$u_{lm} \propto (x+x_0)^m$$

and hence, $U \propto (x+x_0)^m$

It is to be noted here that the above relationship is true for any pressure gradient. However, the exponent m is not arbitrary, it depends on the pressure gradient. It is shown elsewhere that m depends on the factor u_{lm}/U . The exponent m will be negative for adverse pressure gradients and positive for favourable pressure gradients.

A second solution is $b = \text{constant}$ with u_{lm} and U both being proportional to $e^{\text{constant}(x+x_0)}$.

These results were first derived by Rotta (1953), and later discussed by Townsend (1956-b) for flows with small velocity defects.

2.10.3 MOMENTUM INTEGRAL EQUATION

The momentum integral equation can be obtained by integrating equation (2.54) between the limits $y = 0$ and $y = \infty$ thus

$$\int_0^{\infty} u \frac{\partial u}{\partial x} dy + \int_0^{\infty} v \frac{\partial u}{\partial y} dy = \int_0^{\infty} U \frac{dU}{dx} dy + \frac{1}{\rho} \int_0^{\infty} \frac{\partial \tau}{\partial y} dy \quad (2.60)$$

Applying the boundary conditions

$$\text{at } y = 0; \tau = \tau_0; u = 0$$

$$\text{and at } y = \infty; \tau = 0; u = U$$

and simplifying and rearranging the terms, we obtain the momentum integral equation as:

$$\frac{d}{dx} \int_0^{\infty} \rho u (U-u) dy + \rho \frac{dU}{dx} \int_0^{\infty} (U-u) dy = \tau_0 \quad (2.61)$$

For a plane-wake $\tau_0 = 0$ and $u = U - u_{1m} f_1$ and equation (2.61) reduces to:

$$\frac{d}{dx} (u_{1m} U b F_1) - \frac{d}{dx} (u_{1m}^2 b F_2) + \frac{dU}{dx} u_{1m} b F_1 = 0 \quad (2.62)$$

where $F_1 = \int_0^{\infty} f_1 d\lambda$

and $F_2 = \int_0^{\infty} f_1^2 d\lambda$

Available data on plane-wakes with pressure gradients (Hill et. al, 1963; Gartshore, 1965; Newman, 1967) indicate that f_1 has the same functional form as for plane-wakes with zero pressure gradient, provided we replace U_0 by U .

Thus,
$$\frac{U-u}{u_{1m}} = f_1(\lambda) = (1-0.293\lambda^{3/2})^2$$

with
$$F_1 = 1.02, F_2 = 0.717 \text{ (equation 2.41)}$$

If we substitute for

$$b = B_1 (x + x_0)$$

$$u_{1m} = B_2 (x + x_0)^m$$

$$\text{and } U = B_3 (x + x_0)^m$$

where B_1 , B_2 and B_3 are dimensional constants of proportionality and will vary with pressure gradient, equation (2.62) can be written as:

$$\frac{d}{dx} (B_1 B_2 B_3 F_1 \{x + x_0\}^{2m+1}) - \frac{d}{dx} (B_1 B_2^2 F_2 \{x + x_0\}^{2m+1}) = 0$$

$$m B_1 B_2 B_3 F_1 (x + x_0)^{2m} = 0$$

Since B_1, B_2, B_3, F_1 and F_2 are independent of x , we can write

$$(2m+1) \cdot B_1 B_2 B_3 F_1 (x+x_0)^{2m} - (2m+1) B_1 B_2^2 F_2 (x+x_0)^{2m} + m B_1 B_2 B_3 F_1 (x+x_0)^{2m} = 0$$

$$\text{or, } B_1 B_2 B_3 (3m+1) F_1 = B_1 B_2^2 F_2 (2m+1)$$

$$\text{or, } \frac{B_2}{B_3} = \frac{u_{1m}}{U} = \frac{F_1}{F_2} \frac{(3m+1)}{(2m+1)} \quad (2.63)$$

If we substitute for F_1 (=1.02) and F_2 (=0.717), we obtain the expression for u_{1m}/U as

$$\frac{u_{1m}}{U} = 1.42 \left(\frac{3m+1}{2m+1} \right) \quad (2.64)$$

The above expression shows the dependence of the ratio of velocities u_{1m}/U on the exponent m , and hence on the pressure gradient. To enable a more clear understanding, equation (2.64) is plotted in Figure (2.4).

The following characteristic features of equation (2.64) can be observed from Figure (2.4).

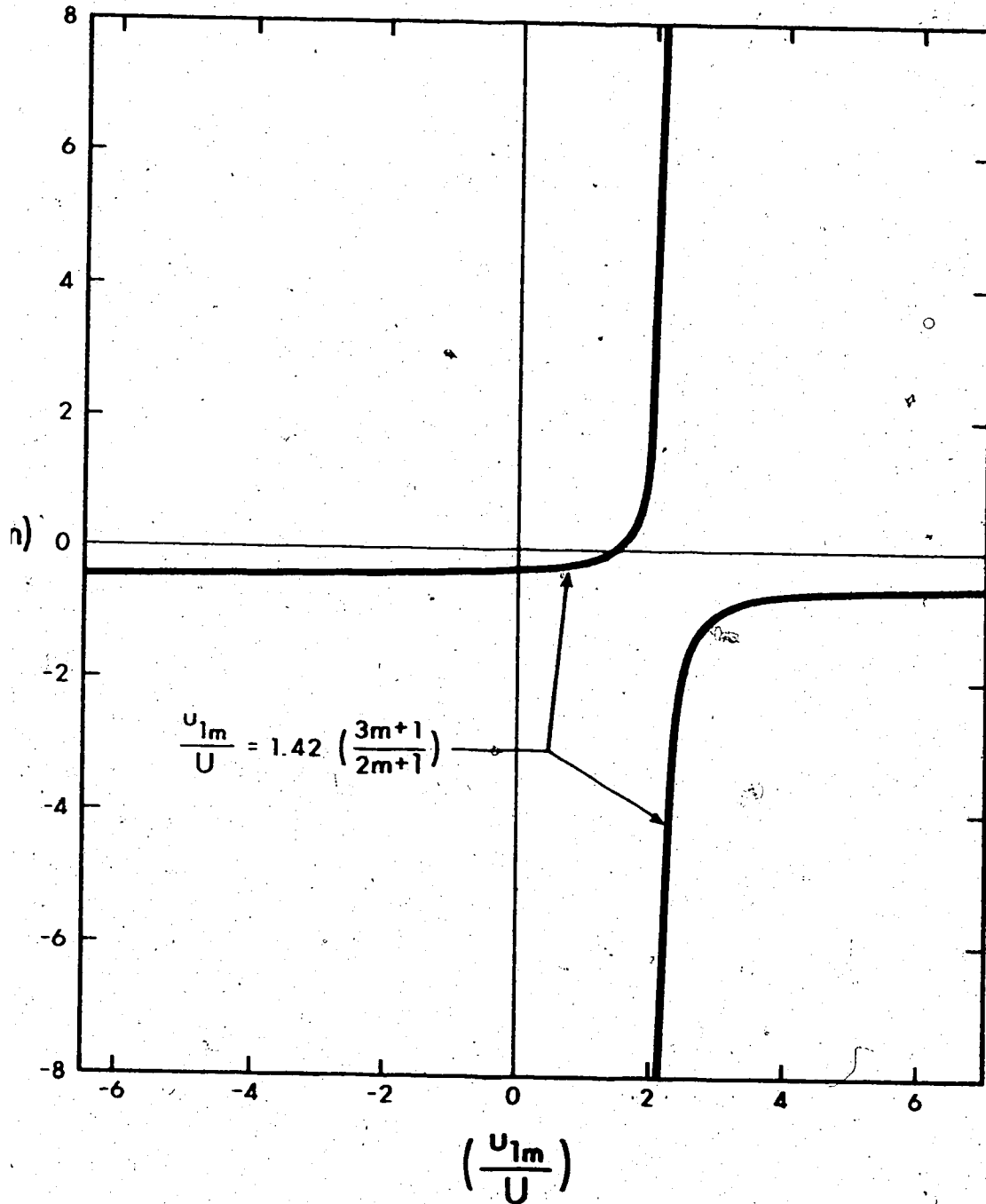


FIGURE 2.4 VARIATION OF (u_{1m}/U) WITH EXPONENT m

- (i) $m \rightarrow \pm \infty$; $(u_{1m}/U) \rightarrow 2.13$
- (ii) $m = 0$; $(u_{1m}/U) = 1.42$
- (iii) $m = -0.185$; $(u_{1m}/U) = 1$
- (iv) $m = -1/3$; $(u_{1m}/U) = 0$
- (v) $m = -1/2$; $(u_{1m}/U) \rightarrow \pm \infty$

If $1 > (u_{1m}/U) > 0$, the solution represents a self-preserving wake in an adverse pressure gradient with m between $-1/3$ and -0.185 . For large values of m , back flow occurs.

Patel and Newman (1961) obtained the same expression for jets and wall jets in a moving stream and classified them as follows:

- (i) m between $-1/3$ and $-1/2$: jet flow
- (ii) m between $-1/3$ and -0.185 : wake flow
- (iii) $-\frac{1}{2} > m > -0.185$: back flow

Equation (2.64) helps in determining only one of the unknowns (u_{1m}). To determine the other unknown, b (or B_1), we require one more equation. Various methods which are available differ in terms of the choice of the second equation. However, they all have important shortcomings with the possible exception of Gartshore's (1965) method. A brief discussion of Abramovich's (1963) and Gartshore's methods follows.

2.10.4 ABRAMOVICH'S (1963) METHOD

Abramovich's equation is derived from the consideration of a mixing layer in constant pressure. It is reasonable to assume that the spatial rate of growth of the mixing layer will depend on the level of turbulence in this layer, which in turn depends on u_{1m} .

$$\text{Thus } \frac{db}{dx} = B_1 = F(u_{1m}/U)$$

For a wake or jet type flow in constant pressure, it can be shown that

$$F(u_{1m}/U) = F\left(\frac{u_{1m}}{U-u_{1m}/2}\right)$$

Expanding as a polynomial, this may be written as

$$\frac{db}{dx} = A_0 + A_1 \left(\frac{u_{1m}}{U-u_{1m}/2}\right) + A_2 \frac{u_{1m}^2}{(U-u_{1m}/2)^2} + \dots$$

If $u_{1m} = 0$, no mixing occurs, $db/dx = 0$ and thus $A_0 = 0$.

Abramovich, following Prandtl, chooses only the first term A_1 in the above expansion, on the ground that the rate of spread is proportional to cross-stream turbulence v' , which in turn depends on u_{1m} .

For jet flows in zero pressure gradient, the coefficient A_1 was found to be 0.052.

For small deficit wakes ($u_{1m} \ll U$) in zero pressure gradient, the coefficient A_1 can be obtained with the help of equations (2.43) and (2.44) which gives $A_1 = 0.163$.

In pressure gradients we continue to assume

$$\frac{db}{dx} = 0.163 \frac{u_{1m}}{U - u_{1m}/2} \quad (2.65)$$

we can rewrite equation (2.65) as

$$\frac{db}{dx} = 0.163 \frac{(u_{1m}/U)}{1 - \frac{1}{2}(u_{1m}/U)}$$

If we substitute for (u_{1m}/U) from Equation (2.64), we get

$$\frac{db}{dx} = 1.78 \left(\frac{3m+1}{2.23-m} \right) \quad (2.66)$$

Both these equations (2.65 and 2.66) have been found to predict higher values and their limitations are discussed in Chapter IV.

2.10.5 GARTSHORE'S (1965) METHOD

The most sophisticated method currently available for shear flows with pressure gradients is that of Gartshore. It permits the eddy viscosity Reynolds number

$$R_{\epsilon} = \frac{u_{lm} b}{\epsilon}$$

(where ϵ is eddy viscosity), to vary both in the downstream direction of a particular flow and from one flow to another. This variation is related to $(\partial u/\partial x)/(\partial u/\partial y)$ at $y = b$. This theory is therefore not subject to the limitations of other theories, which have assumed that R_{ϵ} is constant (Hill et. al, 1963), or that the mixing length is proportional to the width of the flow. An approach similar to Gartshore's was suggested independently by Bradbury (1963). Both are based on Townsend's (1956-a) large eddy equilibrium hypothesis.

An expression for R_{ϵ} can be obtained by applying the equation of vorticity to two similar fields of

turbulence, which are characterized by a length scale L_B , and a vorticity scale ω_B , both of which are positive quantities.

On the basis of Townsend's assumption that the typical lifetime of a large eddy is proportional to $1/|\partial u/\partial y|$, Gartshore derived (for small $\partial u/\partial x$);

$$L_B^2 \propto (1 + \text{constant} \left| \frac{\partial u/\partial x}{\partial u/\partial y} \right|) \quad (2.67)$$

The above equation was derived from the assumption of the initial existence of identical large eddies, in fields which are themselves not identical, but merely similar. The theory is again restricted to small $\frac{\partial u/\partial x}{\partial u/\partial y}$.

On the basis of the energy equation for large eddies, which are superimposed on a mean flow with scales u_{1m} and b , one is able to deduce that

$$\frac{1}{R_c} \propto \frac{L_B^2}{b^2}$$

Combining the above expression with equation (2.67) we obtain

$$\frac{1}{R_{\epsilon}} = \frac{1}{R_{\epsilon_0}} \left(1 + \text{constant} \left| \frac{\partial u / \partial x}{\partial u / \partial y} \right| \right)$$

where R_{ϵ_0} is the value of R_{ϵ} at $\partial u / \partial x = 0$.

For small perturbation wakes the above expression reduces to

$$\frac{1}{R_{\epsilon}} = 0.077 (1 - 9.1 \left| \frac{\partial u / \partial x}{\partial u / \partial y} \right|) \quad (2.68)$$

Gartshore applies the above theory specifically for the purpose of obtaining the shearing stress at $y = b$, and then states the half momentum integral equation between the limits $y = 0$ and $y = b$, to obtain the solution for shear flows with pressure gradients. He uses the Runge-Kutta technique to obtain the solution for equations (2.67) and (2.68).

In the following pages, equation (2.68) has been used to obtain a second equation to solve for the other unknown B_1 . If we substitute the expression for shear

stress, τ , in equation (2.68) and then evaluate the equation at $\lambda = 1$ ($y = b$), we have

$$\frac{\tau}{\rho} = \epsilon \frac{\partial u}{\partial y} = \frac{u_{1m} b}{R_\epsilon} \frac{\partial u}{\partial y} = - \frac{u_{1m}^2}{R_\epsilon} f_1'$$

or,

$$\frac{\tau}{\rho u_{1m}^2} = g_1(\lambda) = \frac{-f_1'}{R_\epsilon} \quad (2.69)$$

We can rewrite equation (2.58) as:

$$-g_1' = \frac{d}{d\lambda} (f_1'/R_\epsilon) = mB_1 \{f_1' F_1(\lambda) - f_1^2\} + mB_1 \frac{U}{u_{1m}}$$

$$(2f_1 - \lambda f_1') + B_1 F_1(\lambda) f_1' - B_1 \frac{U}{u_{1m}} \lambda f_1' \quad (2.70)$$

where

$$F_1(\lambda) = \int_0^\lambda f_1' d\lambda$$

We can obtain an expression for R_ϵ from equation (2.68) by substituting for $\partial u/\partial x$ and $\partial u/\partial z$. It then takes the following form:

$$\frac{1}{R_\epsilon} = 0.077 (1 - 9.1 B_1 \left| \frac{mf_1}{f_1'} - \lambda - m \frac{U}{u_{1m}} \frac{1}{f_1'} \right|) \quad (2.71)$$

The left hand side of equation (2.70) is, therefore,

$$\begin{aligned} \frac{d}{d\lambda} (f_1'/R_\epsilon) &= 0.077 \frac{d}{d\lambda} (f_1' - 9.1 B_1 \left| mf_1' - \lambda f_1'' - m \frac{U}{u_{1m}} \right|) \\ &= 0.077 (f_1'' - 9.1 B_1 \left| mf_1'' - \{\lambda f_1''' + f_1''\} \right|) \end{aligned}$$

This expression can be evaluated for $\lambda = 1$, noting that

$$f_1(1) = 1/2; \quad f_1'(1) = -0.622; \quad f_1''(1) = 0.076; \quad \text{and}$$

$$F_1(1) = 0.787$$

we thus obtain

$$g_1'(1) = -0.077 (0.076 - 5.65 B_1 \{0.88 - m\}) \quad (2.72)$$

Similarly we can evaluate the right hand side of equation (2.70) for $\lambda = 1$, and we get

$$\text{R.H.S.} = 1.622 B_1 \left(\{m + 0.383\} \frac{U}{u_{1m}} - 0.455 \{m + 0.622\} \right)$$

If we substitute for $\frac{u_{1m}}{U} = 1.42 \left(\frac{3m+1}{2m+1} \right)$ (equation 2.64) and simplify, we get

$$\begin{aligned} \text{R.H.S.} &= \frac{3B_1}{(3m+1)} (0.02m^2 - 0.04m - 0.008) \\ &= 0.06B_1 \left(\frac{\{m-2.185\} \{m+0.185\}}{3m+1} \right) \end{aligned}$$

Equating the left and right hand sides of equation (2.70) we obtain

$$0.077 (0.076 - 5.65 B_1 \{0.88-m\}) =$$

$$0.06 B_1 \left(\frac{\{m-2.185\} \{m+0.185\}}{3m+1} \right)$$

solving we get

$$B_1 = \frac{0.0047(3m+1)}{(0.28+0.48m-m^2)} \quad (2.73)$$

This equation can be approximated to:

$$B_1 = \left(\frac{0.013}{0.81-m} \right) \quad (2.74)$$

Thus the flow characteristics for self-preserving wakes in pressure gradients are defined by the following set of equations:

$$b = B_1 (x + x_0)$$

$$u_{1m} \text{ and } U \propto (x + x_0)^m$$

$$-0.185 > m > -1/3$$

$$\frac{u_{1m}}{U} = 1.42 \left(\frac{3m+1}{2m+1} \right)$$

$$B_1 = \left(\frac{0.013}{0.81-m} \right)$$

$$\frac{\tau}{\rho u_{1m}^2} = \frac{0.88}{R_\epsilon} \lambda^{1/2} (1 - 0.293 \lambda^{3/2})$$

$$\text{and } \frac{1}{R_\epsilon} = 0.077 (1 - 9.1 B_1 \left| \frac{mf_1}{f_1} \right|^{-\lambda-m} \frac{U}{u_{1m}} \cdot \frac{1}{f_1})$$

The foregoing analysis is for two-dimensional plane wakes with pressure gradients. It is assumed that the outer layer of the wall-wake behaves in a manner similar to that of a plane-wake. Verification and discussion of equations (2.75), with reference to the experimental results, are presented in Chapter IV.

We continue to assume that the law of the wall holds true in the near region of the wall-wake, with pressure gradients. This assumption is valid only for moderate adverse pressure gradients. Its validity for the adverse pressure gradient tested is discussed in Chapter IV.

CHAPTER III

EXPERIMENTAL ARRANGEMENTS AND MEASUREMENT TECHNIQUES

3.1 INTRODUCTION

This chapter describes the experimental arrangements and the measurement techniques adopted in the present study. In order to obtain a satisfactory analysis of the present study, measurements of the following flow parameters were made: mean velocity in the longitudinal direction of the flow, wall shear stress, components of turbulence fluctuations in longitudinal and lateral directions, and turbulent shear stress across the flow.

The choice between an open-channel and a wind-tunnel, to carry out the experimental program, was based upon which arrangement would serve as the easiest and most economical to work with.

After some preliminary measurements in an open channel, it was found that the water in the Hydraulics Laboratory was not clean enough to carry out turbulence measurements with a hot-film probe, and a few hot-film probes were destroyed in the process. It was therefore decided to construct an open circuit wind-tunnel to carry out this experimental program.

Mean velocity and turbulence were measured with a

hot-wire and a DISA 55D01 constant-temperature anemometer unit. Mean velocities were further checked by a Pitot static tube. In the following sections, details of the wind-tunnel and the measurement techniques used are described.

3.2 DESIGN REQUIREMENTS FOR WIND TUNNEL

The main requirement of a wind tunnel is that it must provide a translational uniform rectilinear air flow. The fulfillment of this requirement is very difficult. To a first approximation linearity and flow uniformity are provided by the geometry of the tunnel walls and by its internal constructional elements.

The velocity distribution should vary as little as possible over the length of the test section and the static pressure should be constant. The deviation of flow velocity from the mean value should be within $\pm 0.75\%$, while flow direction in the horizontal or vertical plane should not deviate from the axial direction by more than $\pm 0.25^\circ$, Garlin and Slezinger, (1966). Usually in low speed tunnels, the static pressure varies linearly along the test section.

An even more difficult problem involved in the use of wind tunnels is the maintenance of low initial turbulence in the test section of the tunnel. A high level of turbulence or vorticity affects test results in that it changes the flow pattern by causing premature transition

from laminar to turbulent flow in the boundary layer. Strong turbulence also presents other problems such as causing the transition layer to be displaced forwardly along the body which causes changes in the frictional resistance, etc. Thus, an increase in turbulence is, to a certain degree, analogous to an increase in the Reynolds number.

Turbulence in the wind tunnel can be reduced by providing a high contraction ratio at the entrance and by using a number of fine mesh turbulence-reducing screens in the settling chamber. For an extremely low turbulence tunnel, a contraction ratio as high as 25:1 has been used. A moderately low turbulence wind tunnel usually has a turbulence intensity in the range of 0.5% to 1.0%.

The wind tunnel used for this investigation was designed with two objectives in mind: (1) The test-section had to be long enough to allow measurements to be taken at distances far downstream from the position of the obstacle, i.e., sufficiently downstream that the structure of the flow in the far-wake region could be fully established, and (2) the turbulence level in the free stream had to be moderately low without providing a high contraction ratio. A schematic representation of the wind tunnel is shown in Figure 3.1.

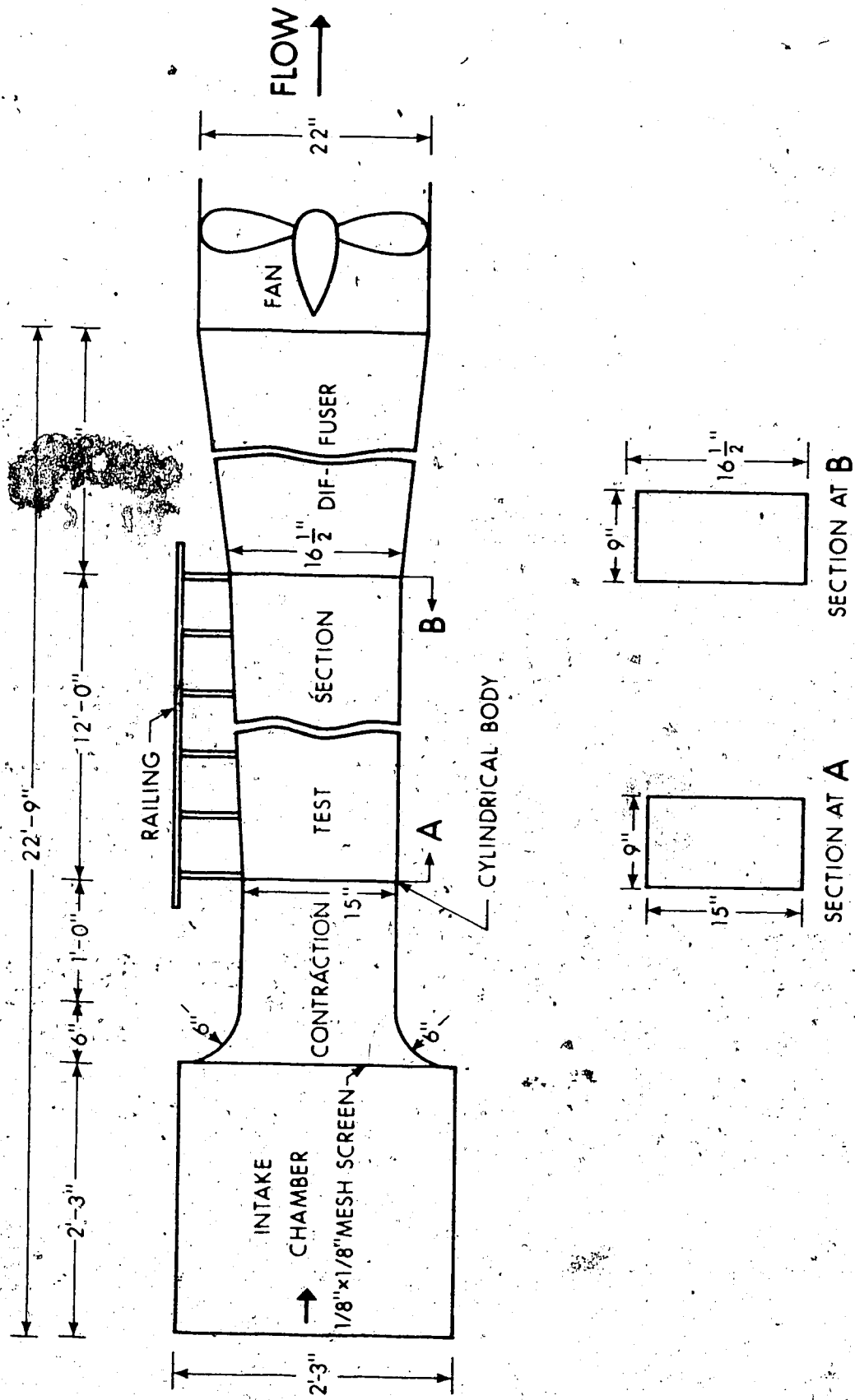


FIGURE 3.1 SCHEMATIC REPRESENTATION OF WIND-TUNNEL

3.2.1 INTAKE CHAMBER

An intake chamber was attached to the entrance section of the wind tunnel in order to cut down the turbulence of the entering air stream and to make it as dust-free as possible. The sides of the intake chamber were made of 1/8 inch x 1/8 inch mesh screen, 27 inches long, thus giving it the shape of a cubical box. To cut down the entrance of dust particles, the box was wrapped with an oil-impregnated fibreglass first and then with medical gauze. This arrangement caused a 5% reduction in the static pressure.

3.2.2 CONTRACTION

The wind tunnel contraction was made of #22 gauge galvanized sheet metal. The top and the bottom each had a radius of 6 inches and the sides had a radius of 9 inches. To obtain a uniform velocity in the test section, the contraction was followed by one foot of uniform cross-section, 15 inches x 19 inches. The overall contraction in the cross-section was 5.4:1.○

3.2.3 TEST SECTION

The test section was made of 3/4 inch plywood with the front wall being made of a 1/2 inch transparent p.v.c. sheet. This transparent front wall was divided into three 4-foot long removable doors, which allowed access to the

interior of the test section.

For smooth wall studies, an 1/8 inch p.v.c. sheet was attached to the floor of the wind tunnel and all cylindrical bodies studied were placed at the leading edge of this p.v.c. sheet, in a vertical plane, normal to the flow direction. Since all the measurements were to be made in a vertical plane, in the central region of the test section, a rectangular, rather than a square, cross-section was decided upon. The entrance of the 12 feet long test section was 15 inches high, 9 inches wide.

It seemed desirable that the test section should have a longitudinal expansion to allow for development of the boundary layer thickness on its wall. With boundary layer measurements, it is customary to give longitudinal expansion in accordance with the growth of the displacement thickness on the wall. In this case, however, because of the presence of the obstacle at the leading edge, the flow region underwent a further constriction. The longitudinal expansion required, therefore, was more than the one that accorded with the displacement thickness. Further, the shape and size of the obstacles were factors to be taken into consideration in providing the longitudinal expansion. To account for all these factors, an adjustable wall or vents in various sections of the wall would have been necessary. However, it was not the aim of this study to provide an exact longitudinal expansion for each and

every case. Rather, a constant longitudinal expansion of 1.1% was provided on the upper wall, and it was found that the free stream velocity in the central region was within 2% of its average value for all obstacles tested.

Railings were placed on top of the test section for a probe traverse, and an one-inch wide slot, through which probes and probe support were introduced, was cut along the middle of the top wall of the test section. This slot was sealed by means of adhesive tape once the probe was introduced.

3.2.4 DIFFUSER

The diffuser was 7 feet long and made of a 3/4-inch plywood sheet. It was transitioned from a rectangular cross-section of 16 1/2 inch x 9 inch to a circular cross-section of 22 inches in diameter.

3.2.5 FAN

A 21-inch direct-drive, duct-mounted fan, with a 1 1/2 H.P. electric motor, was used. It produced an average velocity of 96.0 feet per second in the test section.

3.3 ROUGHNESS TYPE

A continuous strip of #36 aluminum oxide wet-or-dry cloth, manufactured by 3M Company, was glued to the floor

of the wind tunnel to study the effect of roughness on the wall-wake. The grains of this cloth were very angular and are shown in Figure 3.2. The grain size ranged from 0.38 mm. to 0.70 mm., with a median size of 0.56 mm. (0.00183 feet). This was taken as the nominal roughness height, k .

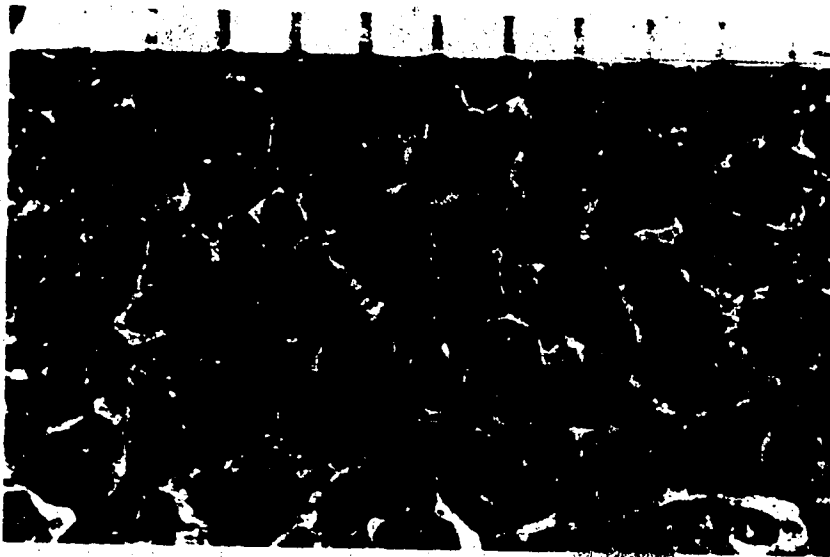
While measuring bed shear on rough boundaries, Hollingshead (1972) found that the equivalent sand grain roughness for this particular cloth, is 3.3 times the nominal height, (i.e., $k_s = 0.0061$ feet). The high k_s/k ratio resulted because the grains were very angular, and many had their long axis, which was about twice the sieve size, oriented normal to the boundary.

3.4 APPLICATION OF ADVERSE PRESSURE GRADIENT

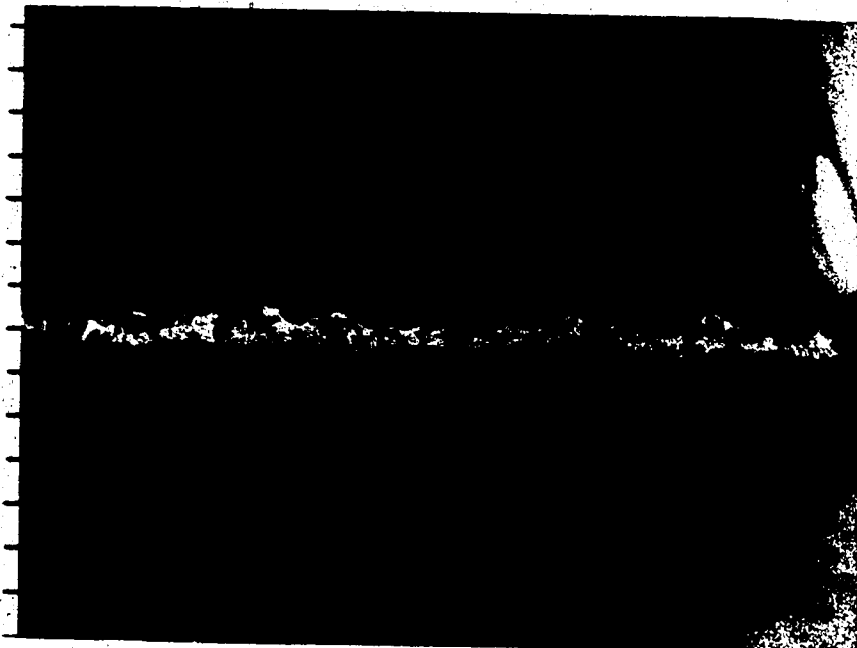
A false top, which could be adjusted to any desired height at the entrance end of the test section, to apply an arbitrary adverse pressure gradient, was fixed to the test section. The contraction at the entrance of the wind tunnel was suitably transitioned so as to join the adjustable end of this wall. The details of the three adverse pressure gradient cases studied are shown in Figure 3.3.

3.5 MEAN VELOCITY AND THE FREE STREAM TURBULENCE IN THE WIND TUNNEL

The free stream velocity, U , and the turbulence

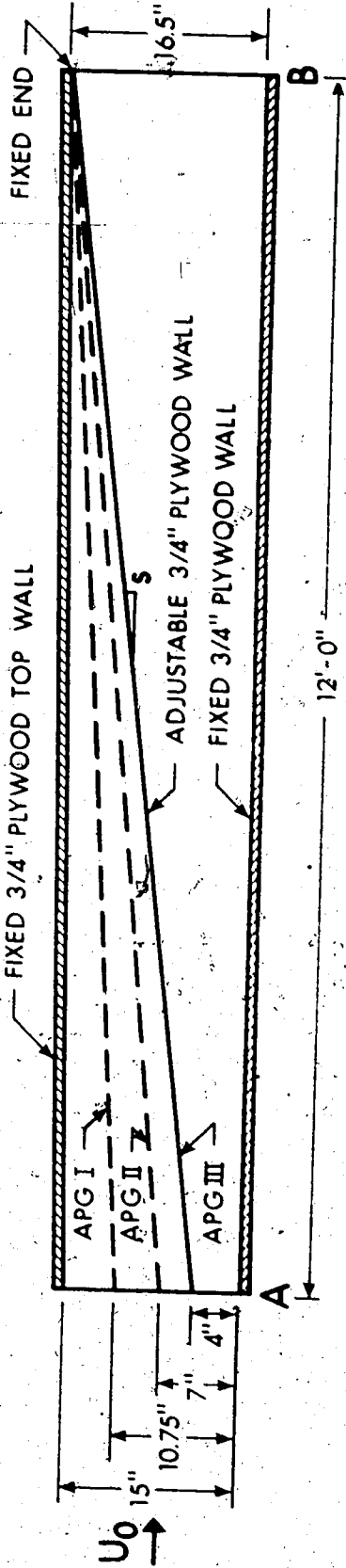


PLAN VIEW SCALE IN MILLIMETERS



SECTION SCALE IN MILLIMETERS

FIGURE 3.2 SAND GRAIN ROUGHNESS



APG	X - sec, AT A	X - sec, AT B	SLOPE, s	U_0 (ft/sec)
I	10.75" x 9"	16.5" x 9"	1:25	107.0
II	7" x 9"	16.5" x 9"	1:15	121.0
III	4" x 9"	16.5" x 9"	1:11.5	145.0

FIGURE 3.3 SKETCH OF THE TEST-SECTION WITH ADJUSTABLE WALL, AT THE TOP

$$\text{intensity } T = \frac{(1/3 \{ \overline{u'^2} + \overline{v'^2} + \overline{w'^2} \})^{1/2}}{U} \times 100$$

through the test section of the wind tunnel, are plotted in Figure 3.4. The average free stream velocity was taken as 96.0 ft./sec. There was only a slight variation in this velocity in the major portion of the test section. The turbulence intensity in the test section was a little high, 0.72%, but no further means of reducing the turbulence was applied.

3.6 MEASUREMENT OF MEAN VELOCITY

The mean velocity in the flow field was measured with a flattened total head tube, with an external thickness of 0.024 inch (0.002 ft.) and width of 1/8 inch in conjunction with a static tube of 0.1 inch diameter. The static tube had four holes, with diameters of 0.016 inch, spaced at 90 degree intervals around the tube, at approximately 8 diameters from the leading edge. The space between the total head and static tubes was 1/2 inch. Careful calibration of the total head tube, under low turbulence conditions in the free stream, showed no appreciable error when compared with large diameter tube measurements. The total head and static tubes were connected to a very sensitive inclined manometer on which mean velocities as low as 3 ft./sec. could be measured with suitable accuracy.

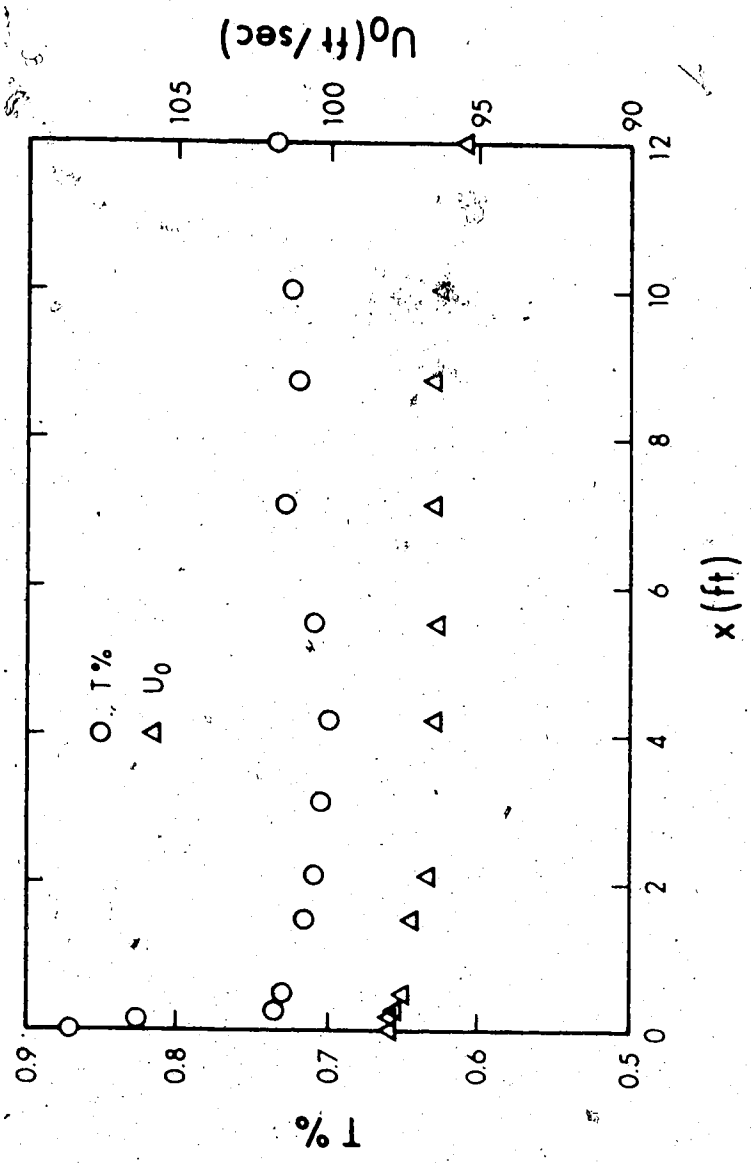


FIGURE 3.4 FREE STREAM VELOCITY AND FREE STREAM TURBULENCE INTENSITY IN THE TEST-SECTION OF THE WIND-TUNNEL

In all cases, the probe was mounted on a traversing mechanism that could be oriented to the nearest 1/1000 of a foot in the vertical direction.

Corrections for turbulence fluctuations, viscous effect, displacement of the effective center, and angle of attack, were thought to be small enough to make their application to the present measurements unnecessary.

3.7 MEASUREMENT OF BOUNDARY SHEAR STRESS

Measurements of boundary shear were carried out with a Preston tube. Slope of velocity profiles near the wall were also used in determining the boundary shear. However, this was done only to check the relative discrepancy between the two methods. This discrepancy was found to be 10%-15%. The value of boundary shear, τ_0 , measured by the Preston tube was adopted for most of the cases, although an error of up to 10% in τ_0 could be expected in some cases. Following is a brief discussion of the Preston tube technique.

3.7.1 PRESTON TUBE

A Preston tube is a total head tube, resting on a surface facing the flow. This convenient method of measuring skin friction was first introduced by J. H. Preston (1954) and is based mainly on similarity considerations and the fact that a law of the wall is valid near the

surface. This law of the wall is commonly expressed as:

$$\frac{u}{u_*} = f\left(\frac{yu_*}{\nu}\right) \quad (3.1)$$

Instead of considering the mean velocity at a point close to the wall, we may consider in the dimensional analysis the difference between the pressure recorded by a total head tube resting on the wall and the local static pressure. If we call this pressure difference Δp , and call the diameter of the total head tube d , then the analysis shows that:

$$\frac{\Delta p}{\tau_0} = g\left(\frac{u_* d}{\nu}\right)$$

or, alternatively,

$$\frac{\tau_0 d^2}{\rho \nu} = g_1\left(\frac{\Delta p d^2}{\rho \nu}\right)$$

where ρ and ν are mass density and kinematic viscosity of the fluid respectively.

Either of these expressions gives us a means of determining skin friction.

For a total head tube of a given geometry, either of the functions (g or g_1), can be simply and accurately determined by experiment. The total head tubes used by Preston were of circular section with a ratio of internal to external diameter of 0.6. The calibration curve

representing the function g_1 , was determined from measurements with four total head tubes of different diameters in a 2-inch pipe.

At the time Preston proposed his method, there was a considerable body of evidence to indicate that the function f (equation 3.1), defining the law of the wall, was universal for fully-developed turbulent flow in pipes and in channels. But only the experiments of Ludwig and Tillman (1950) show directly that it applies also in the wall region of the turbulent boundary layer.

The principle of the method has since been confirmed by numerous investigators for pipe, channel, and boundary layer flows. A comprehensive bibliography on the subject can be found in the work of Patel (1965).

The most accurate and reliable calibration equation for the Preston tube was experimentally obtained by Patel (1965) in the form:

$$y^* = 0.8287 - 0.1381 x^* + 0.1437 x^{*2} - 0.0060 x^{*3}$$

$$\text{for } 2.9 < x^* < 5.6 \quad (3.2)$$

$$\text{Where } y^* = \log_{10} \left(\frac{\tau_0 d^2}{4\rho v^2} \right) = \log_{10} \left(\frac{1}{4} \left\{ \frac{u_* d}{v} \right\}^2 \right)$$

$$\text{and } x^* = \log_{10} \left(\frac{\Delta p d^2}{4\rho v^2} \right)$$

The calibration equation for the range

$$0 < x^* < 2.9$$

was represented by the straight line

$$y^* = \frac{1}{2} x^* + 0.037 \quad (3.3)$$

and for $5.6 \leq x^* < 7.6$ by the expression

$$x^* = y^* + 2 \log_{10} (1.95 y^* + 4.10) \quad (3.4)$$

From these calibration equations, Patel determined the constants $A = 5.5$ and $B = 5.45$ for the logarithmic law of the wall, for the turbulent boundary layer, expressed in the form

$$\frac{u}{u^*} = A \log_{10} \frac{yu^*}{v} + B$$

3.7.2 PRESTON TUBE IN PRESSURE GRADIENTS

Equations 3.2 to 3.4 were derived for zero pressure gradient flows. For a very strong pressure gradient, however, it is certain that the law of the wall, in its usual form, must break down and the Preston tube calibration would be expected to change. The modified form of the law of the wall for turbulent flow with pressure gradient can be written as:

$$\frac{u}{u_*} = F \left(\frac{yu_*}{v}, \alpha_p \right) \quad (3.5)$$

where $\alpha_p = \frac{v}{\rho u_*^3} \frac{dp}{dx}$ is the pressure gradient parameter, which measures the severity of the pressure gradient

as it affects the flow in the wall region.

It is now an established fact that with the application of an adverse pressure gradient, the region of application of the law of the wall is reduced, and at some particular high value of α_p , there is no region left for which the law of the wall is valid. However, for small values of α_p , deviation from the law of the wall is small. The Preston tube would therefore only incur a small error which would depend on its diameter and the value of α_p .

After examining the available experimental data, Patel (1965) suggested the following limitations for Preston tubes recording τ_0 within the prescribed error range. For adverse pressure gradients:

$$\text{maximum error 6\%: } 0 < \alpha_p < 0.015, \frac{u_* d}{\nu} \leq 250.$$

for favorable pressure gradients:

maximum error 6%:

$$0 > \alpha_p > -0.007, \frac{u_* d}{\nu} \leq 200, \frac{d\alpha_p}{dx} < 0$$

He emphasized the point that these limiting conditions are purely empirical in nature and give only a rough guide to the use of Preston tubes. The additional restriction of $d\alpha_p/dx < 0$, in favorable pressure gradients, has been imposed to ensure that the flow is sufficiently far from the commencement of laminar reversion. In severe pressure gradients the Preston tube was found to over-estimate the skin friction.

3.7.3 PRESTON TUBE ON ROUGH BOUNDARIES

If the boundary is uniformly rough, like a bed of spherical marbles, or similar to Nikuradse's sand roughness with k representing the roughness height, for a Preston tube of external diameter d placed on it; it can be shown that:

$$\frac{\Delta p d^2}{4\rho v^2} = F_2 \left(\frac{\tau_0 d^2}{4\rho v^2 k}, \frac{d}{k} \right) \quad (3.6)$$

for rough turbulent flow, equation 3.6 becomes:

$$\frac{\Delta p}{\tau_0} = F_3 (d/k) \quad (3.7)$$

Equation 3.7 was suggested by Preston himself. Hwang and Laursen (1963) attempted to evaluate it both analytically and experimentally, and for developed rough wall flow they obtained the equation:

$$\frac{\Delta p}{\tau_0} = 16.53 \left(\left\{ \log \frac{30h}{k_s} \right\}^2 - \log \frac{30h}{k_s} \left\{ 0.25 \left(\frac{a}{h} \right)^2 + 0.0833 \left(\frac{a}{h} \right)^4 \right\} + \left\{ 0.25 \left(\frac{a}{h} \right)^2 + 0.1146 \left(\frac{a}{h} \right)^4 \right\} \right) \quad (3.8)$$

where h = height of the center of stagnation tube from zero datum

a = inner radius of stagnation tube

k_s = equivalent sand roughness

The above equation is shown in Figure 3.5 in a modified form.

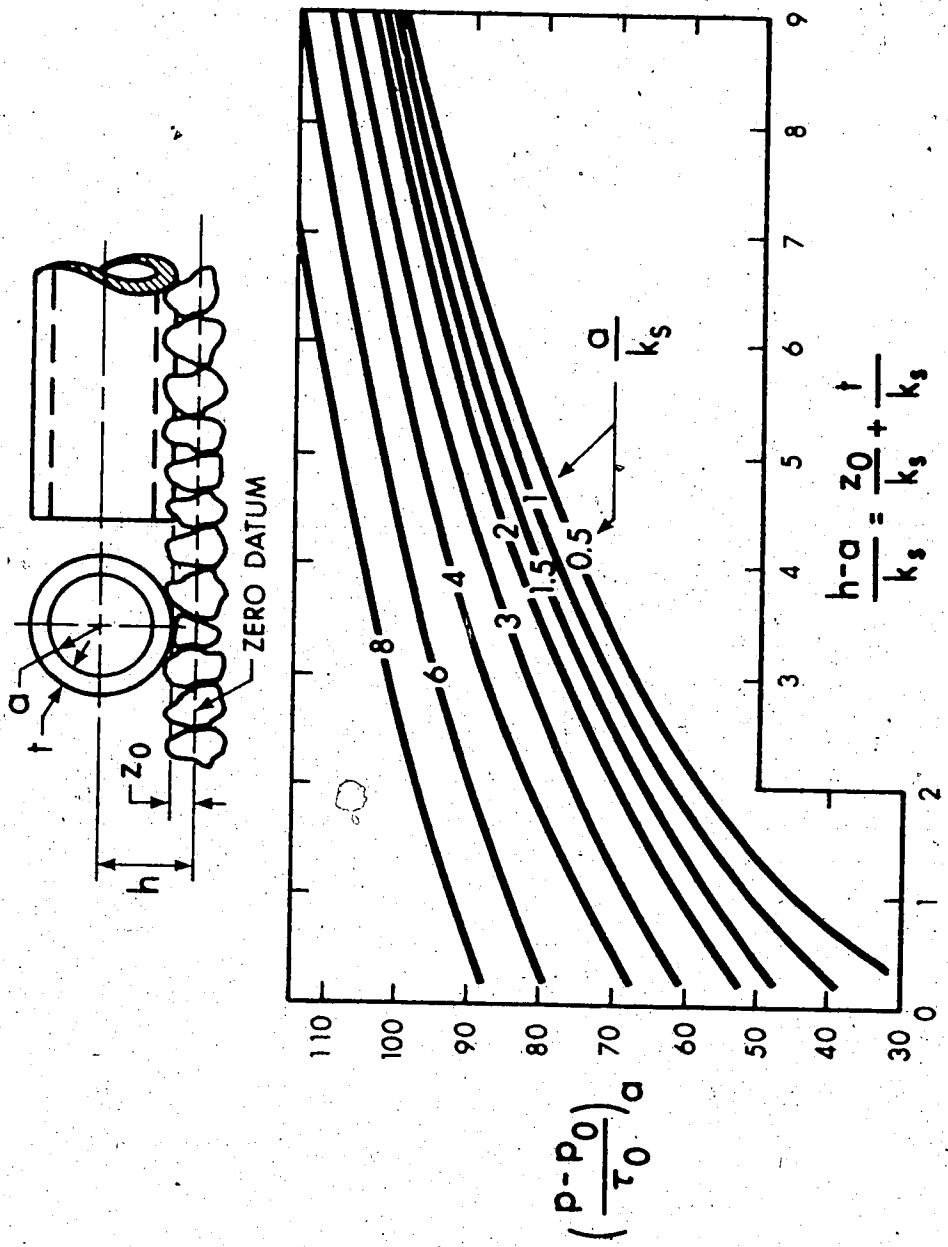


FIGURE 3.5 PRESSURE-SHEAR RATIO FOR ROUGH BOUNDARIES (AFTER HWANG AND LAURSEN, 1963)

Hollingshead (1972) has carried out an investigation in this field and an extensive discussion of this subject can be found in his work.

3.7.4 VELOCITY PROFILE METHOD

For a two-dimensional turbulent boundary layer, the shear stress near the wall can be assumed to be very nearly constant. Working from this assumption, the velocity profile in the vicinity of a rough wall is given by:

$$\frac{u}{u_*} = 5.75 \log \frac{y}{k_s} + B_s \quad (3.9)$$

where B_s is a function of the roughness Reynolds number $(u_* k_s / \nu)$.

The above equation can be rewritten as

$$u_* = (\tau_o / \rho)^{1/2} = \frac{1}{5.75} \left\{ \frac{u_2 - u_1}{\log(y_2 / y_1)} \right\} \quad (3.10)$$

where u_1 and u_2 are mean velocities at ordinates y_1 and y_2 respectively.

This is a convenient expression for boundary shear computation since a knowledge of k_s and B_s is not necessary. To use this method, however, it is necessary to know the correct datum from which y is to be measured. This datum selection is generally made by trial and error, with the datum being changed until a plot of u versus $\log y$ becomes a straight line.

3.7.5 APPLICATION OF PRESTON TUBE TECHNIQUE IN THE PRESENT STUDY

The plot of velocity profiles (Figures 4.4, 4.16; Chapter IV), in the inner region of the wall-wake, with and without pressure gradients, indicates the validity of the law of the wall for wall-wake flows. The Preston tube technique was therefore adopted to measure the boundary shear stress.

Two types of stagnation tubes were used to measure τ_o . Tube one had a flattened rectangular cross-section, of external thickness 0.024 inch and width 0.10 inch. The second tube was circular in cross-section, having an outside diameter of 0.11 inch and an inside diameter of 0.085 inch. The external thickness of the flattened tube was used for parameter d , in computing the value of τ_o , from equation 3.2. The discrepancy between the values of τ_o , computed by the two tubes, was found to be within the limits of experimental error.

For the rough boundary, a circular total head tube was used to determine boundary shear stress. The nominal roughness, k , of the rough boundary, was 0.00183 feet and the equivalent roughness, k_s , was 0.0061 feet. The zero datum of the rough boundary, (z_o in Figure 3.5), was found by the graphical method described in section 3.7.4, to be approximately half the nominal roughness, (0.0009 feet).

Hwang and Laursen's equation (Figure 3.5) was used to compute the value of τ_o , with $(h-a)/k_s = 0.32$, and $a/k_s =$

0.58. From Figure 3.5 we obtain:

$$\frac{p-p_0}{\tau_0} \approx 31.0 \quad (3.11)$$

This expression was used to determine the value of τ_0 for the rough wall. Wall shear stress for the rough wall was also computed by the slope of the velocity profile method. The discrepancy between the two values of τ_0 was found to be large for reason explained in Section 4.2.4. The values of boundary shear obtained from velocity profile method was found to give better results, and were adopted.

For adverse pressure gradient flows, the flattened tube with the calibration equation (3.2) was used to determine τ_0 . In the investigation the maximum values of α_p and $u_* d/v$ were found to be within the limits proposed by Patel and hence the Preston tube measurements were used without any correction.

To obtain an idea of the order of magnitude of the error, in the measured value of τ_0 , the boundary shear stress was also computed by the velocity profile method. The discrepancy between the values of τ_0 determined by these two methods was found to be 10%-15% for adverse pressure gradient flows and 3% to 6% for zero pressure gradient flows. However, the boundary shear stress computed by the slope of velocity profile methods was found to be inconsistent for some runs. Hence, the Preston tube measurements for τ_0 were adopted for all the runs except

for rough wall (run number 6). No correction for turbulence and flow displacement, caused by the probe geometry, was applied to the measured value of Δp ($=p-p_0$). It was assumed that the combined error in τ_0 , thus determined, was not large enough to cause any appreciable discrepancy in the analysis of the flow.

Figures 4.4 and 4.16 (Chapter IV) indicate the justification for this assumption.

3.8 MEASUREMENT OF TURBULENCE INTENSITIES

The hot-wire anemometer is the instrument most widely used for fluctuation measurements. At the present time, other techniques of turbulence measurement (viz. optical technique, Doppler technique, etc.), are still in the developing stages. The laser Doppler technique, in which instantaneous velocity is deduced from the Doppler frequency shift of light, scattered from particles moving within the fluid, is being investigated by many groups of researchers. Its advantage over the hot-wire method is that there is no solid sensing element in the flow whereas hot-wire probes and their supports may be large enough to disturb the flow, while the wire itself is small and very delicate. A brief discussion of other techniques of turbulence measurement can be found in Bradshaw (1971). In the present investigation the hot-wire technique was used to measure turbulence. A description of the principle of

of the hot-wire anemometer is given below.

3.8.1 HOT-WIRE ANEMOMETRY

The principle of hot-wire anemometry is based on the relation between the rate of heat loss from a heated body, and the velocity of fluid flow in which it is immersed. The first systematic work on this relationship was done by King (1914). He found that the rate of heat loss, Q , from a cylinder of diameter d , and length l , immersed in a fluid of temperature T_f , could be represented by the equation:

$$Q = k_f \cdot l \left[1 + \left(\frac{2\pi\rho C_p u \cdot d}{k_f} \right)^{1/2} \right] (T_w - T_f) \quad (3.12)$$

where k_f = thermal conductivity of the fluid

c_p = specific heat of fluid at constant pressure

ρ = fluid density

u = fluid velocity

T_w = Temperature of the cylinder

The fluid is assumed to be flowing in a direction perpendicular to the axis of the cylinder. In non-dimensional form, this expression can be written as:

$$N_u = A + B \sqrt{R_e} \quad (3.13)$$

where $N_u = \frac{Q/l}{\pi k_f (T_w - T_f)} =$ Nusselt number

$R_e = (ud/\nu) =$ Reynolds number and A and B are constants.

However, the basic assumptions of King's theory are not entirely valid, and in practice the heat transfer is of a more complex nature. Experiments carried out by Collis and Williams (1959) show that the equation:

$$N_u = \left(\frac{T_m}{T_f} \right)^{0.17} (0.24 + 0.56 R_e^{0.45}) \quad (3.14)$$

$$\text{where } T_m = (T_w + T_f) / 2$$

will give the best results for hot-wires operated in air at Reynolds number in the range $0.02 < R_e < 44$.

The above expressions are for cylinders of large aspect ratio (l/d), for which the heat transfer can be considered two-dimensional. For hot-wires with aspect ratios of the order of 200, which are commonly used, the effect of heat conduction to the support becomes significant. Direct calibration is therefore necessary.

3.8.2 HOT-WIRE ANEMOMETERS

A hot-wire anemometer consists of a fine, electrically heated wire, stretched across the ends of two prongs. When exposed to an air stream the wire loses heat by convection, with the result that its temperature (and therefore electrical resistance) varies with the velocity and current of the air stream in accordance with King's law. The instrument can be used in two ways. One method is to heat the wire with a constant current and then determine the velocity by measurement of resistance. This method is

known as the "constant current method". With the other method, the wire is maintained at a constant temperature, and therefore constant resistance, and the velocity is determined from the measured value of the current. This method is known as the "constant temperature method". Either one can be used for low frequency velocity fluctuations, but the latter is generally used, because with it we can obtain increased accuracy for high frequency fluctuations. In the present study a DISA type 55D01 constant-temperature anemometer unit was used. This unit is a commercially available item (DISA Elektronik A/S, Herlev, Denmark). Its principle of operation is shown by a block diagram in Figure 3.6-a.

For conditions of thermal equilibrium, the rate of heat loss, Q , from the hot-wire, must be equal to the heating power generated by the electric current, that is, it must be equal to $(I^2 R_w)$, where I is the probe current and R_w is the operating resistance of the wire. For a hot-wire operated at a specific over-heating ratio, in a specific fluid, at a specific temperature, the quantity

$$\left(\frac{Q}{T_w - T_f} \right) \propto \left(\frac{I^2 R_w}{R_w - R_f} \right)$$

where R_f is the resistance of the wire at fluid temperature. Comparing the above expression with equation 3.14 we can say that:

$$\frac{I^2 R_w}{R_w - R_f} = A_1 (T_f) + B_1 u^{0.45} \quad (3.15)$$

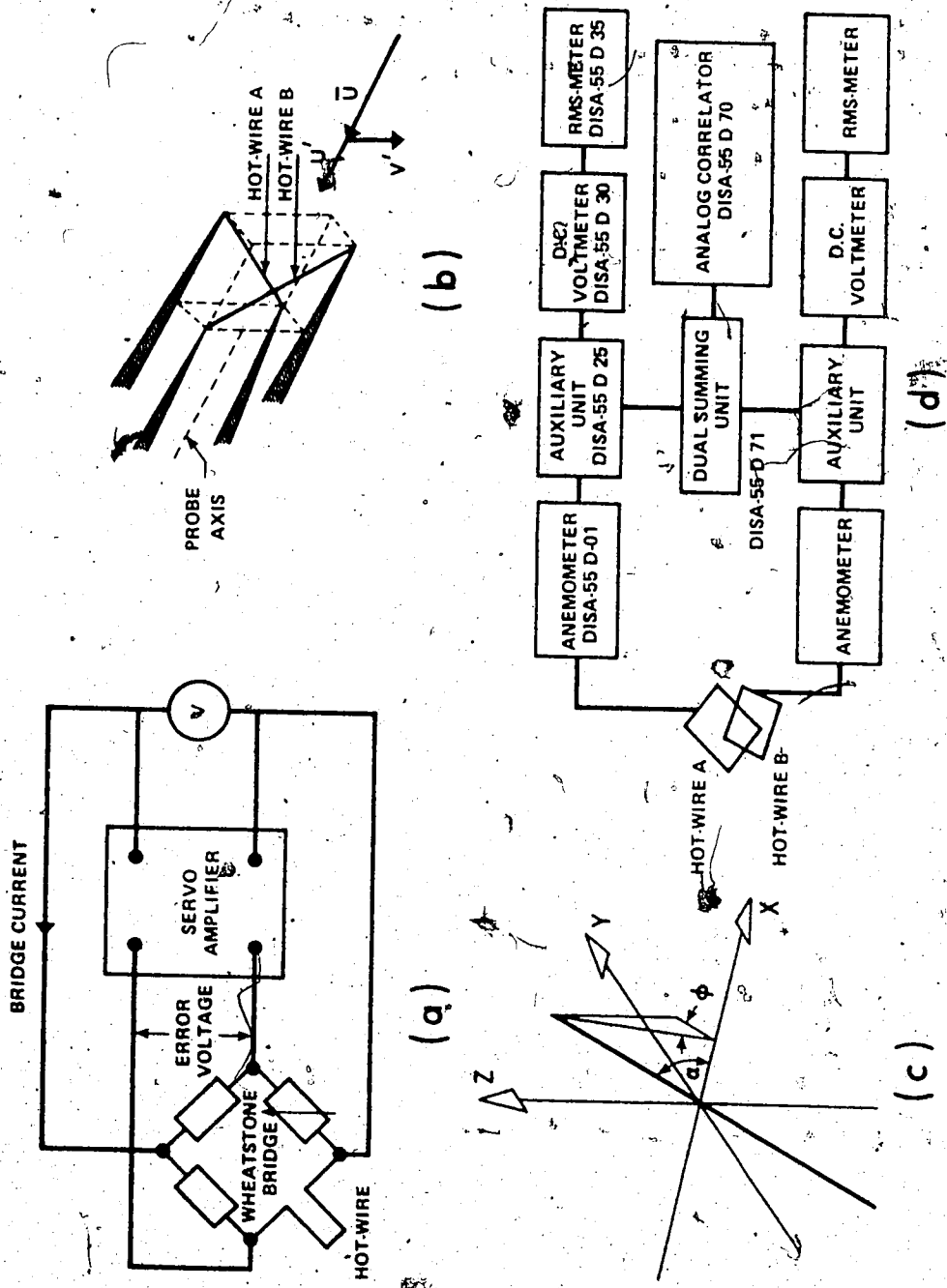


FIGURE 3.6 DETAILS OF HOT-WIRE ANEMOMETER AND EXPERIMENTAL SET UP

to a fair approximation, for a given wire, where A_1 is a function of T_f , but B_1 is not. Equation 3.15 can be written in a general form as:

$$\frac{R_w}{R_w - R_f} I^2 = A_1 + B_1 u^n \quad (3.16)$$

where constants A_1 , B_1 , and n are chosen so they best fit the calibration data within a selected velocity interval.

The output of the anemometer is a bridge voltage, E , and the squared voltage, E^2 , is proportional to the heat loss of the wire at the velocity in question. Thus, equation 3.16 in terms of the bridge voltage E , of the anemometer can be written as:

$$E^2 = A_1 + B_1 u^n$$

the constant of proportionality being absorbed in A_1 and B_1 . Thus if E_0 is the bridge voltage at zero velocity, the above equation can be written as

$$E^2 = E_0^2 + B_1 u^n \quad (3.17)$$

The empirical equations 3.15 or 3.17 representing heat loss and velocity can be used for the evaluation of velocity fluctuations from anemometer measurements. However, in order to describe the hot-wire response to fluctuating flow, a term which takes into account the thermal inertia of the wire must be added to the right hand side of equation 3.15 or 3.17. Assuming a uniform temperature distribution along the wire, we then obtain the following heat balance equation:

$$\frac{R_w}{R_w - R_f} I^2 = A_1 + B_1 u^n + \frac{C}{R_w - R_f} \frac{dR}{dt} \quad (3.18)$$

where $C = \frac{C_w}{\alpha R_f}$ is the modified heat capacity of the wire.

C_w = specific heat of wire

α = temperature coefficient of resistance (referring to the temperature of the fluid)

The thermal inertia of the wire influences its frequency response in a constant current mode of operation. This is especially true when the wire is exposed to a sudden change in the velocity, or when the velocity fluctuations are large. A constant temperature mode of operation is thus preferable to a constant current operation under such circumstances, as the constant temperature system minimizes the effect of probe thermal inertia by keeping the wire at a constant temperature (resistance), and using the heating current as a measure of heat transfer, and hence also of velocity.

3.8.3 CONSTANT TEMPERATURE OPERATION

The constant temperature mode of operation was first proposed by Kennelly et. al. as early as 1909. However, this principle requires a sophisticated and well-designed electronic system, as explained by the aid of the block diagram in Figure 3.6-a.

The wheatstone bridge is in exact balance at a

certain bridge voltage, which is supplied by the servo amplifier. A slight change of the probe resistance, due to a change in the convective cooling of the wire, produces a small unbalanced voltage. This voltage, after having undergone considerable amplification, is then used to adjust the bridge voltage, and hence probe current, in such a way that the bridge will be kept balanced and the wire resistance kept constant. Thus the temperature variations of the hot-wire remain extremely small, and it can be shown (Andersen, 1966) that the upper frequency limit is increased by a factor of:

$$G = 2aR_w s$$

where $a = \frac{R_w - R_f}{R_w}$ is the over-heating ratio and s is the amplifier transconductance.

Because of the constant temperature of the wire, the constants A_1 and B_1 in equation 3.16 are indeed constant, that is, independent of the turbulence fluctuations. Thus the constant temperature method is the most expedient when measurements in turbulent flows of great relative intensity are to be made. A detailed description of the constant temperature operation of the hot-wire anemometer can be found in Hinze (1959) and Bradshaw (1971).

3.8.4 MEASUREMENTS OF FLOW FLUCTUATIONS

Beginning with the simple case of one-dimensional

flow, we can measure the fluctuating component of flow velocity with a hot-wire mounted perpendicular to the flow direction, using the calibration curve $E = f(u)$ (equation 3.17). In actual measurements, the slope dE/du of the calibration curve, $E = f(u)$, determines the sensitivity of the output voltage to changes in velocity if these are less than about 10-20% of u .

This can be shown as follows:

$$E = f(u)$$

$$\text{Therefore, } dE = \frac{df}{du} du$$

or, for small fluctuations,

$$e' = \frac{df}{du} u'$$

where e' is the fluctuation in voltage and u' the fluctuation of velocity. The quantity e' ($=dE$) is usually measured as the r.m.s. value of the fluctuating voltage, $= \sqrt{(e'^2)}$, on an r.m.s. voltmeter connected to the hot-wire anemometer. The corresponding r.m.s. value of the fluctuating component of the velocity, $= \sqrt{(u'^2)}$, can be found directly from the equation 3.19, if we know the slope dE/du of the calibration curve. If the amplitude of the calibration curve is large, as compared to the mean velocity, it may be necessary to correct for the distortion caused by the non-linear response of the hot-wire. However, this difficulty can be overcome by means of a linearizer.

3.8.5 MEASUREMENTS OF CROSS COMPONENTS AND CORRELATION

A wire perpendicular to the mean flow direction will be sensitive to instantaneous velocity fluctuations in this direction only as long as the velocity fluctuations in the transverse directions are small. If the wire forms an angle of 45 degrees to the mean flow, it will display equal sensitivity to either of the two fluctuating velocity components in the plane formed by the direction of mean flow and the wire axis. Thus two wires placed at an angle of 45 degrees with respect to the mean velocity, (Figure 3.6-b) will generate output signals proportional to the sum $(u'+v')$ and the difference $(u'-v')$ of the two fluctuating components.

Such a configuration of the hot-wire of the X-probe is very useful in the measurements of Reynolds stresses. In the following section, the mode of operation of an X-probe in the measurement of turbulent quantities is discussed.

3.8.6 THE X-PROBE IN A PLANE FLOW FIELD

The simplest form of X-probe consists of two hot-wires attached to the prongs of the supports so as to be located, as nearly as possible, in the same plane. This plane will be referred to as the "probe plane". In the probe plane they form a cross. The wires are connected to separate

anemometers. The turbulence components are separated by means of a correlator. In many cases the probe is placed in the flow field in such a way that the mean flow velocity vector is located in the probe plane, thus both wires being in this plane are exposed to the flow at the same angle. Consequently, in this position, only one longitudinal component of mean flow velocity is present so it is usually the position in which the probe is calibrated. If deviation from the flow direction occurs, or cannot be avoided in subsequent measurements, the transversal components of mean velocity will occur, affecting measurements of both the longitudinal mean velocity component and the turbulence component. In the following discussion, it is assumed that both wires of the X-probe are inclined at an angle of 45 degrees to the mean flow direction, and that the probe plane is parallel to the direction of the mean flow.

Since it is very difficult to find an X-probe which has hot-wires with identical calibration curves, let us assume that the calibration curves for hot-wires A and B of the X-probe (Figure 3.6-b) are:

$$\begin{aligned} E_A^2 &= E_{O_A}^2 + B_A u_{w_A}^{n_A} \\ \text{and } E_B^2 &= E_{O_B}^2 + B_B u_{w_B}^{n_B} \end{aligned} \quad (3.20)$$

where $E_{A,B}$ = bridge voltages for the two hot-wires,

$E_{O_{A,B}}$, $B_{A,B}$, and $n_{A,B}$ are constants which are independent of flow velocity and can be determined by calibration of the hot-wires, and $u_{w_{A,B}}$ is the flow velocity acting in a direction perpendicular to the axis of hot-wires.

For two-dimensional turbulent flows, we may write the instantaneous velocities in longitudinal and transverse directions as:

$$u = \bar{u} + u'$$

$$v = \bar{v} + v'$$

designating the time averages of the components as \bar{u} , \bar{v} , and the instantaneous values of the turbulent fluctuations as u' and v' .

The component of velocity perpendicular to the hot-wire axis can, therefore, be written as:

$$u_{w_A} = u \sin 45^\circ - v \cos 45^\circ = \frac{1}{\sqrt{2}} (u - v) \quad (3.21)$$

$$u_{w_B} = u \sin 45^\circ + v \cos 45^\circ = \frac{1}{\sqrt{2}} (u + v)$$

3.8.7 DETERMINING MEAN VELOCITY WITH THE X-PROBE

Applying the rule of averages to equations 3.21, we can write:

$$\bar{u}_{w_A} = \frac{1}{\sqrt{2}} (\bar{u} - \bar{v})$$

$$\bar{u}_{w_B} = \frac{1}{\sqrt{2}} (\bar{u} + \bar{v}) \quad (3.22)$$

Hence
$$\bar{u} = \frac{1}{\sqrt{2}} (\bar{u}_{w_A} + \bar{u}_{w_B})$$

and
$$\bar{v} = \frac{1}{\sqrt{2}} (\bar{u}_{w_B} - \bar{u}_{w_A}) \quad (3.22)$$

Substituting the values of \bar{u}_{w_A} and \bar{u}_{w_B} from calibration equations 3.20, we can write the mean components of velocities in the longitudinal and transverse directions as:

$$\bar{u} = \frac{1}{\sqrt{2}} \{ (\bar{E}_A^2 - E_{O_A}^2) / B_A \}^{1/n_A} + \frac{1}{\sqrt{2}} \{ (\bar{E}_B^2 - E_{O_B}^2) / B_B \}^{1/n_B} \quad (3.23)$$

and
$$\bar{v} = \frac{1}{\sqrt{2}} \{ (\bar{E}_B^2 - E_{O_B}^2) / B_B \}^{1/n_B} - \frac{1}{\sqrt{2}} \{ (\bar{E}_A^2 - E_{O_A}^2) / B_A \}^{1/n_A} \quad (3.24)$$

where \bar{E}_A^2 and \bar{E}_B^2 are the mean squared output voltages and can be measured on a D.C. voltmeter connected to the anemometer.

In equations 3.23 and 3.24, all the terms on the right hand side of the equations are known and hence \bar{u} and \bar{v} can easily be calculated.

3.8.8 DETERMINING TURBULENCE INTENSITY AND SHEAR STRESS

The turbulence fluctuations are computed by measuring voltage fluctuations in the anemometer circuits. Differentiating the analytical expression of the calibration curve of a hot-wire (equation 3.20), we get:

$$dE = \frac{\bar{E}^2 - E_O^2}{2\bar{E}} \cdot n \cdot \frac{du_w}{\bar{u}_w}$$

dE is then the voltage fluctuation, e' , caused by the velocity fluctuation $du_w (=u'_w)$, at \bar{u}'_w . The voltage fluctuations for the wires A and B, therefore, will become:

$$e'_A = \frac{E_A^2 - E_{O_A}^2}{2\bar{E}_A} \cdot n_A \frac{u'_{wA}}{\bar{u}_{wA}} \quad)$$

$$\text{and } e'_B = \frac{E_B^2 - E_{O_B}^2}{2\bar{E}_B} \cdot n_B \frac{u'_{wB}}{\bar{u}_{wB}} \quad) \quad (3.25)$$

The velocity fluctuations normal to the two wires in accordance with equations 3.21, will be:

$$u'_{wA} = \frac{1}{\sqrt{2}} (u' - v')$$

$$\text{and } u'_{wB} = \frac{1}{\sqrt{2}} (u' + v')$$

$$\text{or, } u' = \frac{1}{\sqrt{2}} (u'_{wA} + u'_{wB}) \quad)$$

$$\text{and } v' = \frac{1}{\sqrt{2}} (u'_{wB} - u'_{wA}) \quad) \quad (3.26)$$

Substituting the values of u'_{wA} , u'_{wB} from equations 3.25, and \bar{u}_{wA} , \bar{u}_{wB} from equations 3.20, into equations 3.26 and simplifying, we obtain the following expressions for u' and v'

$$u' = \frac{1}{\sqrt{2}} (H_A e'_A + H_B e'_B) \quad)$$

$$v' = \frac{1}{\sqrt{2}} (H_B e'_B - H_A e'_A) \quad) \quad (3.27)$$

where
$$H_A = \frac{2\bar{E}_A}{n_A(\bar{E}_A - E_{O_A}^2)} \{ (\bar{E}_A^2 - E_{O_A}^2) / B_A \}^{1/n_A}$$

$$H_B = \frac{2\bar{E}_B}{n_B(\bar{E}_B - E_{O_B}^2)} \{ (\bar{E}_B^2 - E_{O_B}^2) / B_B \}^{1/n_B}$$
(3.28)

Squaring and taking the time average of equations 3.27 results in

$$\overline{u'^2} = \frac{1}{2} (H_A^2 \overline{e'_A{}^2} + H_B^2 \overline{e'_B{}^2} + 2H_A H_B \overline{e'_A e'_B})$$

$$\overline{v'^2} = \frac{1}{2} (H_A^2 \overline{e'_A{}^2} + H_B^2 \overline{e'_B{}^2} - 2H_A H_B \overline{e'_A e'_B})$$
(3.29)

similarly, multiplying u' and v' in equations 3.27, and taking the time average, gives us the turbulent shear stress term as:

$$\overline{u'v'} = \frac{1}{2} (H_B^2 \overline{e'_B{}^2} - H_A^2 \overline{e'_A{}^2})$$
(3.30)

The quantities $\overline{e'_A{}^2}$, $\overline{e'_B{}^2}$ can be measured directly on an r.m.s. voltmeter connected to the anemometer. The correlation factor, $\overline{e'_A e'_B}$, between the fluctuating components of voltage, can be measured directly on an analog correlator, also connected to the anemometer.

The third component of the turbulence fluctuations, w' , can be measured by rotating the X-probe 90 degrees in the vertical plane. For two-dimensional turbulent flow it can be shown that:

$$\overline{w'^2} = \left\{ \frac{1}{2} + (\overline{v}/\overline{u})^2 \right\} \left\{ H_A^2 \overline{e'^2} + H_B^2 \overline{e'^2} - 2H_A H_B \overline{e'_A e'_B} \right\} \quad (3.31)$$

Numerical calculations of $\overline{u'^2}$, $\overline{v'^2}$, $\overline{w'^2}$ and $\overline{u'v'}$ from equations 3.29, 3.31 and 3.30 can easily be performed with a calculator or computer.

3.8.9. INFLUENCE OF INACCURACIES OF THE ANGLE OF ATTACK

An experimental investigation of the error in measurements with an X-probe, caused by inaccurate angles of attack, was carried out by Klatt (1969). Error can be caused by an inaccuracy in the angle of attack in the probe plane (angle α in Figure 3.6-c), and/or by an inaccuracy in the angle between the probe plane and the mean flow direction (angle ϕ in Figure 3.6-c). However, the error caused by inaccuracies in the angle of attack compared to that assumed in the foregoing analysis, was very small. Klatt's investigation led to the decision that the X-probe can be used in oblique operation at angles of up to $\pm 25^\circ$ in the probe plane without causing an error of more than 1% in mean velocities \overline{u} and \overline{v} . On the other hand, the angle ϕ should not be greater than 5° so as to limit the error in \overline{u} and \overline{v} to less than 1%.

When determining turbulence quantities, measured values of adequate accuracy can only be expected for u' ,

and for low-level isotropic turbulence at angles not greater than 20-25°. For transverse components of velocity fluctuation, the oblique angle of attack should be restricted to below 10° to give adequate results.

It should be noted here that the influence of inaccurate angles of attack on the measured value of flow velocities and turbulent fluctuations will also depend on the turbulence level and its structure. Very near the wall, therefore, the error in measured values of turbulent fluctuations, and the error in the mean velocities, would be quite significant. The maximum fluctuation in a boundary layer occurs at, or near, $\frac{yu_*}{\nu} = 12$. Hence, measurements taken around this region are liable to be faulty and should be corrected. In the present study, however, all the measurements were taken well above this region, and no corrections were applied to the measured values. In addition, the ratio \bar{v}/\bar{u} never exceeded 0.1 in the regions where measurements were performed. This further reduced the error.

Equations 3.29, 3.30 and 3.31, therefore, were used to directly determine turbulent fluctuations.

3.9 ARRANGEMENT FOR MEASUREMENT OF MEAN VELOCITIES AND TURBULENT QUANTITIES BY X-PROBE

The arrangement for the measurements of mean velocity and turbulent fluctuations by an X-probe is shown in

the block diagram of Figure 3.6-d. The mean voltage drops, $E_{A,B}$, across each hot-wire, were measured with DISA 55D30 D.C. voltmeters and the r.m.s. values of the voltage fluctuations, $e_{A,B}^2$, by DISA type 55D35 R.M.S. voltmeters. The correlation factor, $\frac{e_A e_B}{E_A E_B}$, was measured directly by a DISA type 55D70 Analog correlator, through a DISA type 55D71 Dual summing unit.

All operations were performed at a 1:20 bridge ratio and at a probe over heating ratio of 0.8. The upper frequency limit of the anemometer was 600-800 kHz and the lower frequency limit 28Hz.

3.9.1 X-PROBES

A DISA type 55A32 X-probe was used to measure \bar{u} , \bar{v} , $\sqrt{u'^2}$, $\sqrt{v'^2}$ and $\overline{u'v'}$. A DISA type 55A39 X-probe was used to measure $\sqrt{w'^2}$ instead of rotating the first X-probe 90 degrees in the vertical plane. The wires of both X-probes were of 5 micron diameter platinum-coated tungsten with an effective length of approximately 1 m.m. The aspect ratios of the wires were 200.

3.10 CALIBRATION OF X-PROBES

Calibration curves for the X-probes were determined by passing compressed air through a 3-inch diameter pipe, fitted with a heating element and a 0.92 inch diameter nozzle, at the outlet. The heating element was connected

to a rheostat, R (Figure 3.8-a), which was adjustable to allow maintenance of a constant temperature of 70° F at the outlet. The mean outlet velocity was found by measuring the pressure drop across the nozzle. During calibration, the X-probes were placed 1/4 inch from the nozzle, with the axis of the probe on the axis of the nozzle. The effective cooling velocity, u_w of both the wires, for DISA type 55A32 X-probe, was assumed to be (assuming a 45° inclination) $u_w = 0.707u$, while for DISA type 55A39 X-probe, u_w was equal to u . The calibration curves for both probes are plotted in Figure 3.7. The following calibration equations for the X-probes were found:

1. DISA type 55A32 X-probe

$$\begin{aligned} \text{wire A: } E_A^2 &= 8.8 + 1.62 u_w^{0.45} \\ \text{wire B: } E_B^2 &= 8.95 + 1.57 u_w^{0.46} \end{aligned} \quad (3.32)$$

2. DISA type 55A39 X-probe

$$\begin{aligned} \text{wire A: } E_A^2 &= 8.85 + 0.94 u_w^{0.49} \\ \text{wire B: } E_B^2 &= 8.3 + u_w^{0.49} \end{aligned} \quad (3.33)$$

It is to be noted that for DISA type 55A32 X-probe, $u_w = 0.707 u$, hence the coefficients 1.62 and 1.57 for wires A and B will reduce to 1.15 and 1.11 respectively for the mean flow velocity u .

A comparison of mean velocity profiles, measured by the X-probe and by the flattened Pitot-tube of diameter

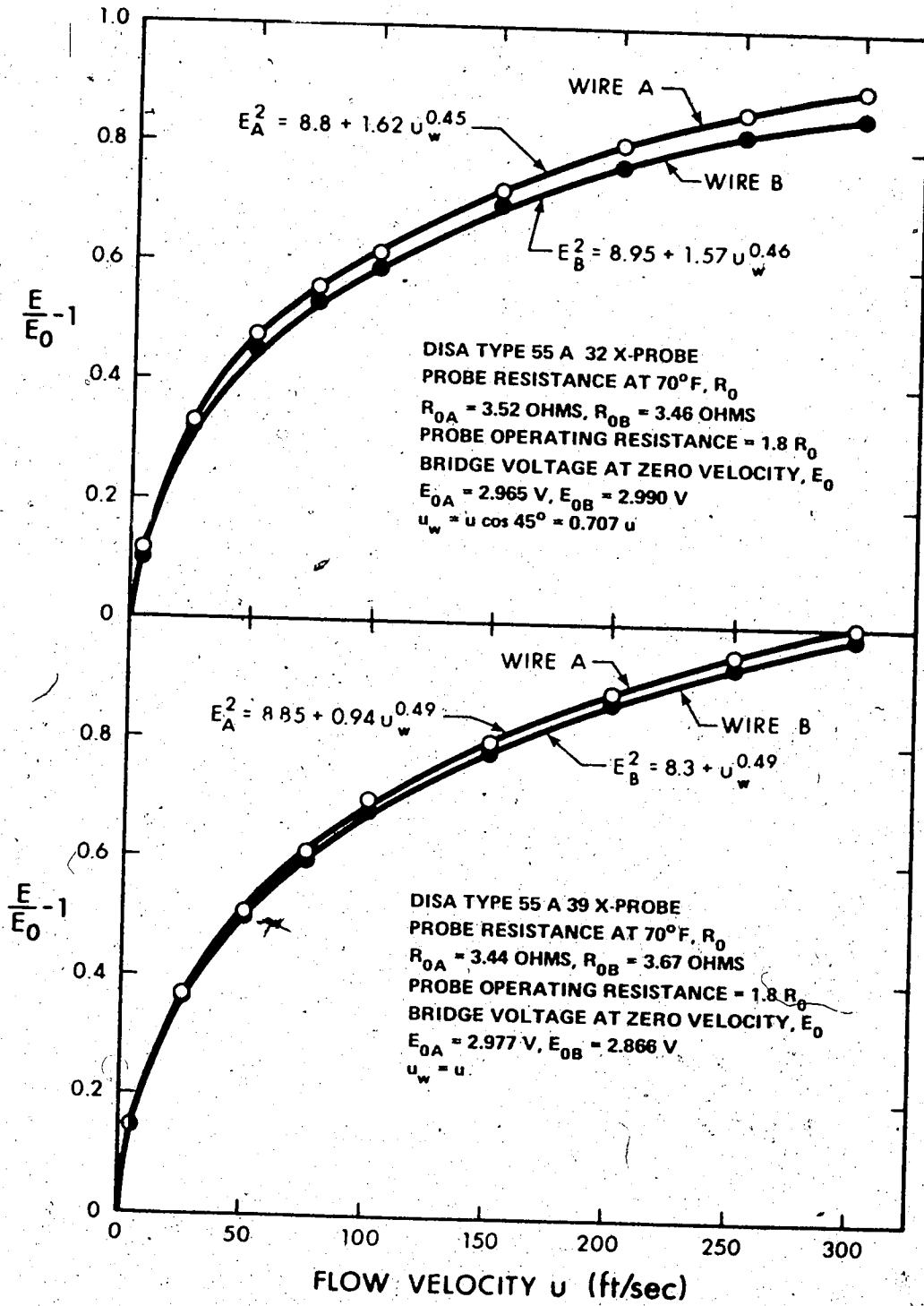


FIGURE 3.7 CALIBRATION CURVES FOR X-PROBES

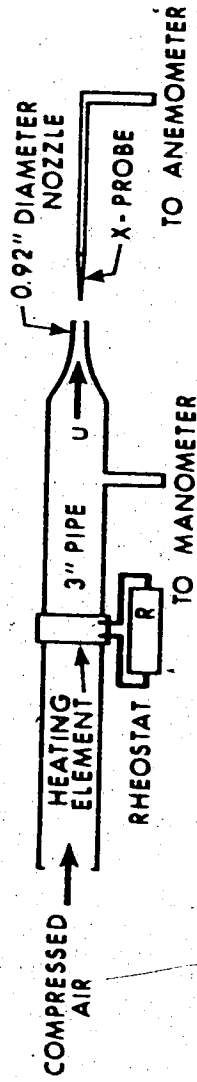


FIGURE 3.8-a SCHEMATIC DIAGRAM FOR CALIBRATION OF X-PROBES

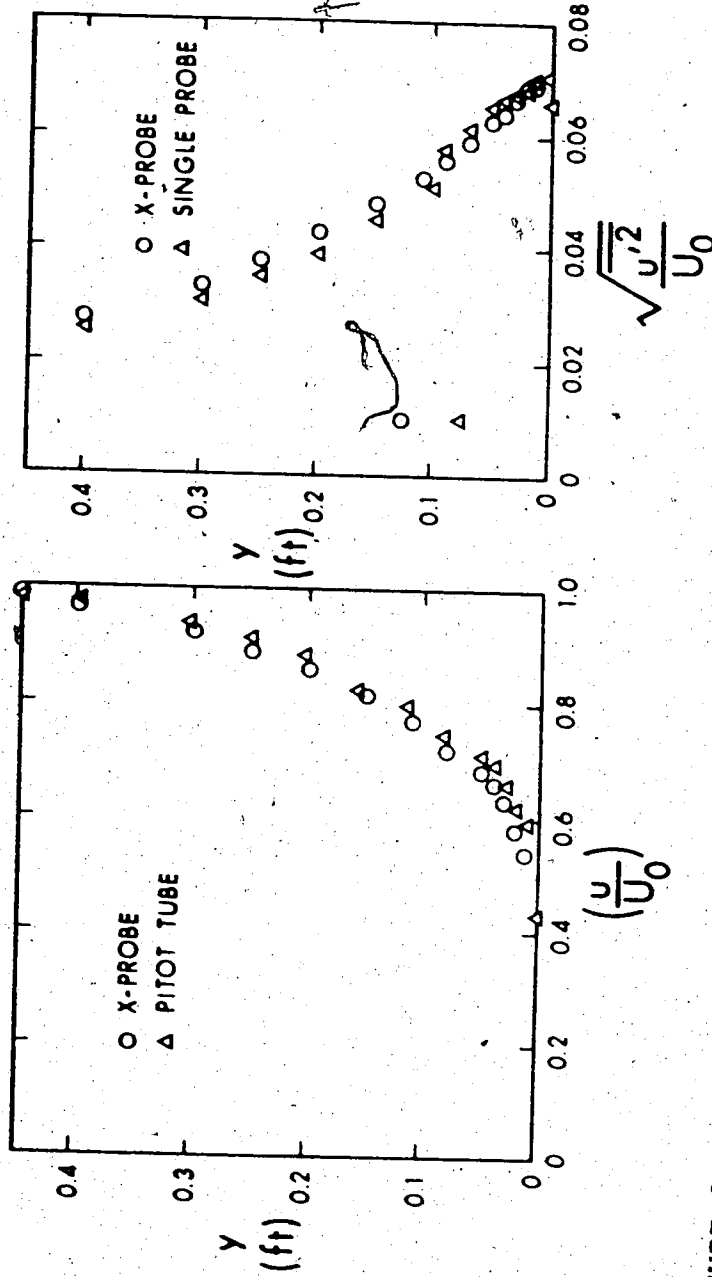


FIGURE 3.8-b COMPARISON OF X-PROBE AND PITOT-TUBE MEAN VELOCITY MEASUREMENTS

FIGURE 3.8-c COMPARISON OF u'-FLUCTUATIONS MEASURED BY X-PROBE AND SINGLE PROBE

.002 feet, is plotted in Figure 3.8-b. The maximum discrepancy between the two measurements was found to be less than 5% except in the vicinity of the wall where it was somewhat higher. This occurred because the measured values of mean velocities obtained with both instruments needed to be corrected for the high level of turbulence present near the wall. The Pitot tube measurements were adopted for the analysis of the mean velocity.

3.10.1 CHECK OF VELOCITY FLUCTUATION MEASUREMENTS

The longitudinal component of velocity fluctuations, u' , measured by the X-probe, was checked against that measured by a single-wire probe, (DISA type 55A22), of which the standard calibration curve was supplied by the DISA company. The measured values of $\sqrt{u'^2}/U_0$, from the single wire and the X-probe, are plotted in Figure 3.8-c. The maximum discrepancy was found to be less than 7%. It was assumed that the errors in measurement of v' and w' fluctuations were of the same order of magnitude as that of u' .

CHAPTER IV

EXPERIMENTAL RESULTS AND DISCUSSION

4.1 EXPERIMENTS

Two sets of experiments were carried out for the present investigation. The first series of six experiments was carried out with zero pressure gradient flows, and the second series, of three experiments, with longitudinal adverse pressure gradients. All but one run (run number 6) had a smooth bottom wall, and the cylindrical obstacle was placed at the leading edge of the wall. The significant details of these two groups of experiments are given in Table IV-1.

The centre line mean velocity field was measured by a flattened total head tube of external thickness 0.024 inches. The turbulent fluctuations and turbulent shear stress were measured by means of a constant temperature hot-wire anemometer. The turbulent quantities were measured for five cases: three zero pressure gradient flows, including the rough wall (runs number 2, 4 and 6), and two adverse pressure gradient flows (runs number 8 and number 9). The boundary shear along the centre line was explored by the same flattened total head tube, used as a Preston tube, for all runs except run number 6 (the

TABLE IV-1: GEOMETRY OF THE OBSTACLE AND FLOW CONDITIONS

Run No.	Shape	Height h (in.)	Free Stream Velocity U ₀ (ft/sec)	$R_e = \frac{U_0 \cdot h}{\nu}$	Pressure Gradient	Wall Condition	Turbulence Characteristics Measured	Series No.
1	Semi-circular cylinder	0.25	40.0	5,200	zero	smooth	none	I
2	semi-circular cylinder	0.25	96.0	12,500	zero	smooth	$\sqrt{u'^2}, \sqrt{v'^2}, \sqrt{w'^2}, \overline{u'v'}$	I
3	sharp-edged plate	0.25	96.0	12,500	zero	smooth	none	I
4	sharp-edged plate	0.50	96.0	25,000	zero	smooth	$\sqrt{u'^2}, \sqrt{v'^2}, \sqrt{w'^2}, \overline{u'v'}$	I
5	sharp-edged plate	0.75	96.0	37,500	zero	smooth	none	I
6	sharp-edged plate	0.50	96.0	25,000	zero	rough	$\sqrt{u'^2}, \sqrt{v'^2}, \sqrt{w'^2}, \overline{u'v'}$	I
7	sharp-edged plate	0.50	107.0	28,000	I	smooth	none	II
8	sharp-edged plate	0.50	121.0	31,500	II	smooth	$\sqrt{u'^2}, \sqrt{v'^2}, \sqrt{w'^2}, \overline{u'v'}$	II
9	sharp-edged plate	0.25	145.0	18,850	III	smooth	$\sqrt{u'^2}, \sqrt{v'^2}, \sqrt{w'^2}, \overline{u'v'}$	II

rough wall). A circular total head tube with an outside diameter of 0.11 inches and an inside diameter of 0.085 inches, was used to measure the boundary shear for run number 6. The reason for using a circular tube for the rough wall case was that it permitted the application of Hwang and Laursen's (1963) calibration equations (Fig. 3.5 - Chapter III) for determining τ_0 .

The free stream velocity for all the runs, except run number 1, in series I, was 96.0 ft./sec. For run number 1 it was 40.0 ft./sec. This run has been referred as the low Reynolds number case.

For the first two runs, a semi-circular cylinder of 1/4 inch radius was used as the obstacle. Sharp-edged plates with heights varying from 1/4 inch to 3/4 inch were used as the obstacles for the rest of the runs.

The mildest longitudinal adverse pressure gradient applied was denoted as APG-I (run number 7), and the strongest as APG-III (run number 9). APG-II (run number 8) was between these two.

The lowest and highest values of the free-stream Reynolds numbers, $(U_0 h/\nu)$, were 5200 and 37,500, respectively.

4.2 EXPERIMENTAL RESULTS FOR SERIES I (ZERO PRESSURE GRADIENT FLOWS)

A typical velocity distribution in the centre-plane for run number 2 is plotted in Figure 4.1(a-c). In this case, unlike that of a wall-jet, it is hard to differentiate between the wake-like and boundary layer-like characteristics from these plots of velocity profile. Therefore, to determine the velocity scale, u_{1m} , and the length scale, b , for the wake profile, some indirect method has to be used. Such a method is discussed in the next section.

In Figure 4.1(a) the velocity distribution in the region immediately behind the obstacle is plotted, ($x/h = 3$ to 12). This is the region of recirculation. The flow separates from the obstacle and re-attaches downstream, at a certain distance which is dependent upon the shape of the obstacle and the free-stream Reynolds number. For this particular case the point of re-attachment was at approximately $x/h = 11.5$. Since the purpose of the present study was to investigate the flow structure at long distances from the obstacle (far-wake region), extensive measurements were not made in the region of recirculation. The characteristic feature of the recirculation region is the formation of a standing eddy, and the reversal of flow near the boundary. This can be observed in Figure 4.1(a).

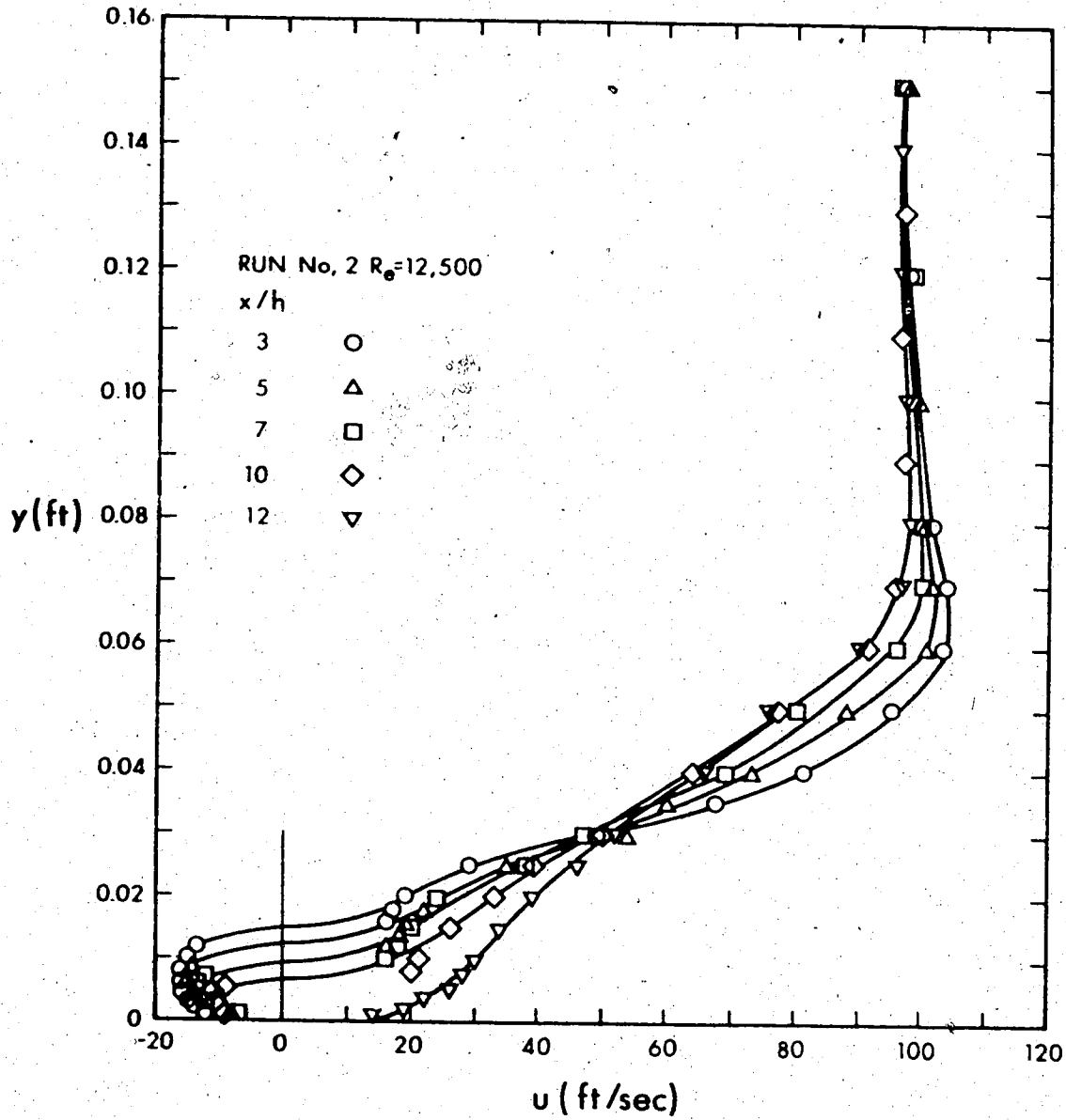


FIGURE 4.1-a VELOCITY DISTRIBUTION IN THE REGION OF SEPARATION FOR RUN NUMBER 2

Figure 4.1(b) shows the velocity distribution in the near wake region, ($x/h = 16$ to 75). A point of inflexion can be observed on the plots for the $x/h = 25$, 50 and 75 . On the other two profiles, ($x/h = 16$ and 20), it is not distinguishable. The point of inflexion can be used as a rough guide in determining the point at which the velocity profiles begin to change from wake-like flow to boundary layer-type flow.

Velocity distribution in the far-wake region, ($x/h = 100$ to 500), is plotted in Figure 4.1(c). The point of inflexion on the velocity profiles is not clearly marked in this region. However, one may notice that the velocity profiles near the boundary fall on a single curve (shown by a chained line). Unlike a plane-wake, the velocity for a wall-wake will approach zero at the wall instead of attaining the maximum velocity defect, u_{lm} . If $y = \delta_w$ (Figure 4.1-c), is the point at which the velocity profile deviates from its wake-like character, then an analysis of the velocity in the wall region can be made by assuming that

$$(u/u_w) = f(y/\delta_w) \quad (4.1)$$

where $u = u_w$ at $y = \delta_w$.

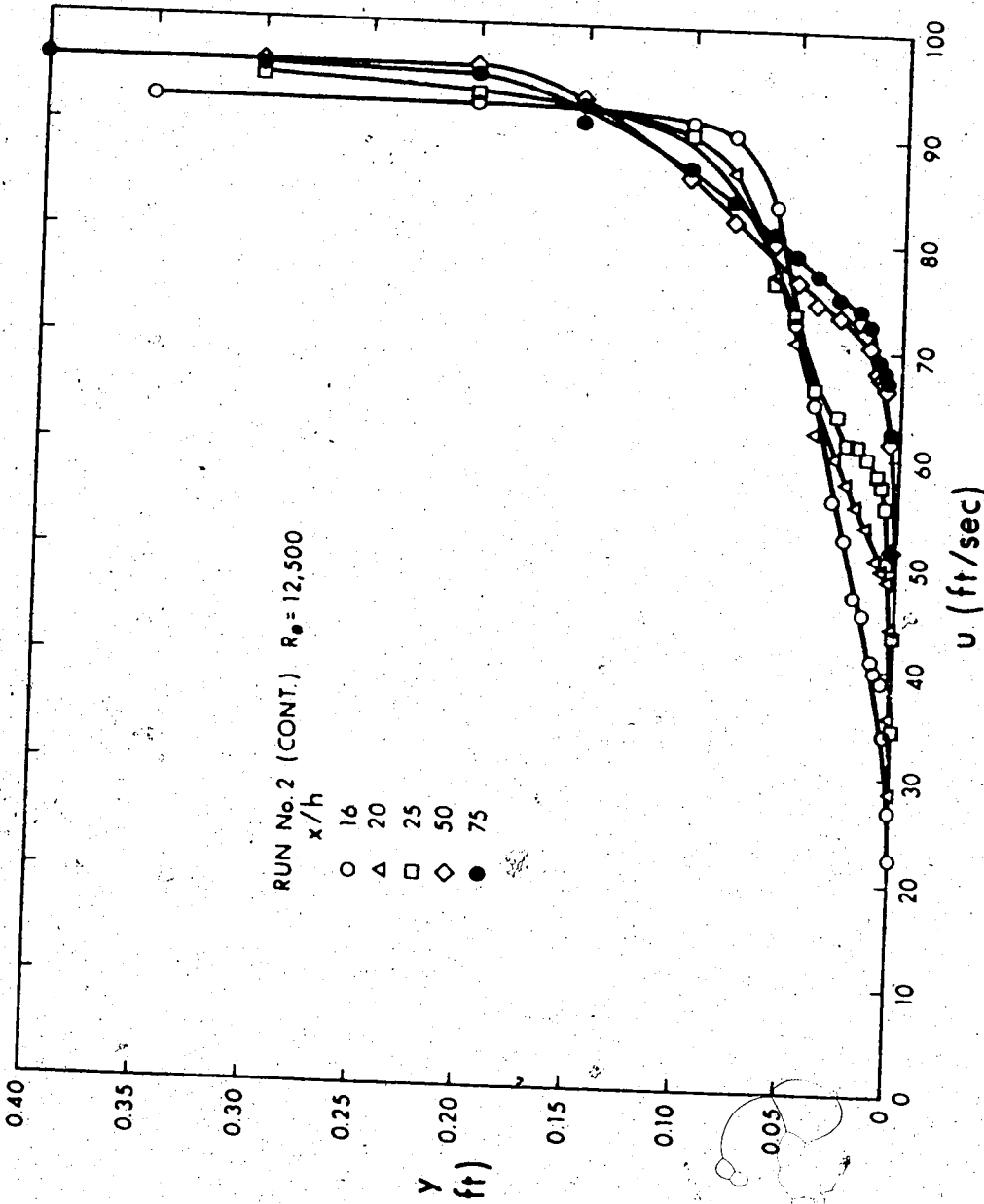


FIGURE 4.1-b VELOCITY DISTRIBUTION IN THE NEAR-WAKE REGION FOR RUN NUMBER 2

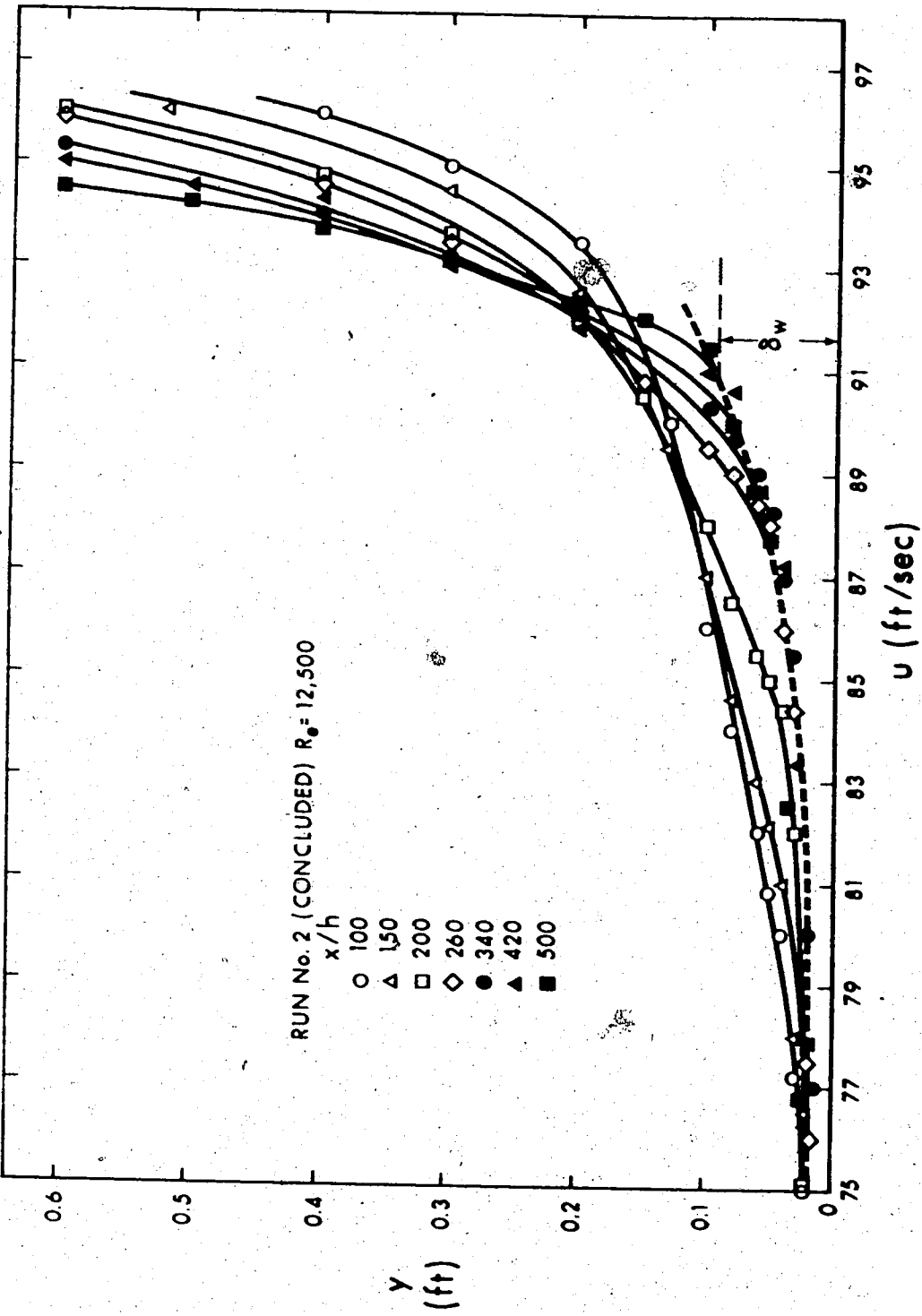


FIGURE 4.1-1-C VELOCITY DISTRIBUTION IN THE FAR-WAKE REGION FOR RUN NUMBER 2

This analysis is similar to that of the wall-region of a wall-jet. In the case of the wall-wake, this type of analysis involves the practical difficulty of determining the point $y = \delta_w$, which varies in the longitudinal direction x . The distance, δ_w , can be visualized as being the distance by which the outer layer of the wall-wake is displaced from the boundary. In boundary layer terminology, one can call this distance the "wake-displacement thickness". The possibility of correlations between δ_w , and the half-wake width, b , and between the characteristic boundary layer thicknesses, δ^* and θ , and δ_w , may also be suggested. The velocity profiles for the other runs were not plotted. It was considered more expedient to display them in tabular form. They are shown in Tables A-1 to A-6 (Appendix A).

4.2.1 DETERMINATION OF u_{1m} and b

The velocity and length scales, u_{1m} and b , for the outer region of the wall-wake, cannot be determined directly from the velocity profile plots so an indirect method has to be used.

Assuming that the velocity profile in the outer region of the wall-wake is described by the equation

$$\frac{U_o - u}{u_{1m}} = (1 - 0.293 \left\{ \frac{y}{b} \right\}^{3/2})^2$$

where u_1 and u_2 are the measured velocities at ordinates y_1 and y_2 respectively, we can write:

$$\frac{U_o - u_1}{u_{1m}} = (1 - 0.293 \left\{ \frac{y_1}{b} \right\}^{3/2})^2 \quad (4.2)$$

$$\text{and } \frac{U_o - u_2}{u_{1m}} = (1 - 0.293 \left\{ \frac{y_2}{b} \right\}^{3/2})^2 \quad (4.3)$$

Dividing equation (4.2) by equation (4.3) and taking the square-root, we obtain:

$$\left\{ \frac{(U_o - u_1)}{(U_o - u_2)} \right\}^{1/2} = \frac{3.41 - (y_1/b)^{3/2}}{3.41 - (y_2/b)^{3/2}}$$

solving, we obtain:

$$b = \left\{ (k_1 y_2^{3/2} - y_1^{3/2}) / 3.41(k_1 - 1) \right\}^{2/3} \quad (4.4)$$

where $k_1 = \left\{ \frac{(U_o - u_1)}{(U_o - u_2)} \right\}^{1/2}$

In equation (4.4) we know y_1 , y_2 and k_1 , hence b can be easily determined. Once we determine b , u_{1m} can be determined by either equation (4.2) or (4.3). It should be noted that $u_1(y_1)$ and $u_2(y_2)$ should be chosen such that they fall in the outer-region, otherwise the calculated value of u_{1m} and b will be incorrect. One should be careful in the selection of points, $u_1(y_1)$, and $u_2(y_2)$, for the computation of u_{1m} and b . A large error in u_{1m} can result from a faulty selection. This can be explained by means of Figure 4.2. Let us assume that A (u_1, y_1), and B (u_2, y_2), are two typical experimental points, selected for the computation of u_{1m} and b . As can be seen in the figure, a large error in the computed value of u_{1m} will be produced by fitting the erroneous wake profile (plotted as a chained line) to these points; even though the relative error in A and B is small.

It was found that the best result can be obtained by selecting A and B from the middle one-third region of the velocity profile. The values so computed must be checked by at least one more set of points. The velocity and length scales so computed are tabulated in Table A-7 (Appendix A).

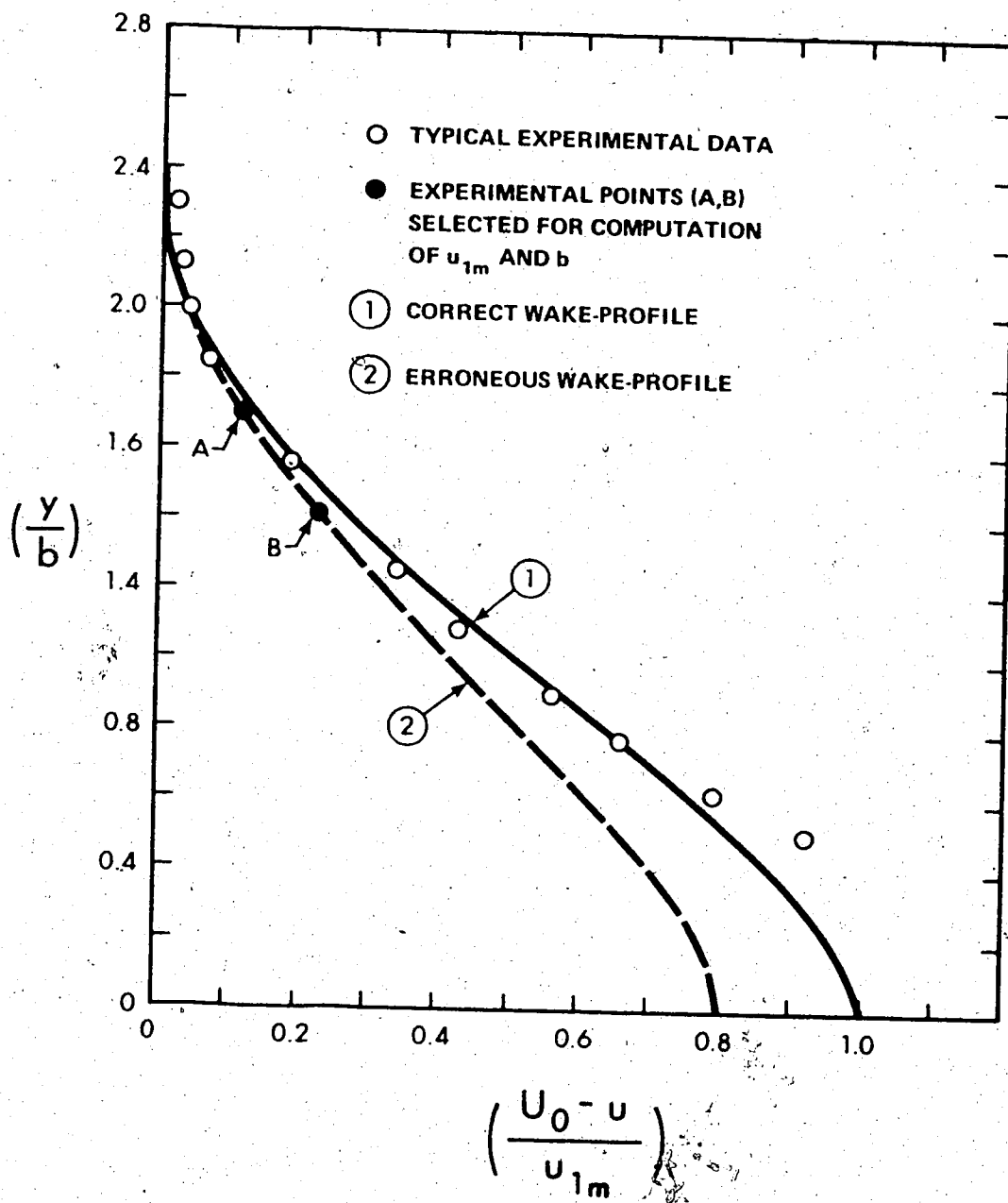


FIGURE 4.2 ERRONEOUS COMPUTATION OF u_{1m} AND b

4.2.2 VELOCITY DISTRIBUTION IN THE OUTER REGION

For all runs in Series I, the velocity profiles in the center-plane were checked for similarity, by plotting the non-dimensional velocity defect $(u_0 - u)/u_{1m}$, against $\lambda = y/b$. The plots are shown in Figure 4.3(a,b). It can be observed that the velocity profiles attain similarity within a short length ($x/h = 25$) after the flow reattaches to the wall. The point of reattachment ($x = x_r$, Figure 2.1) for the six runs, was found to range from approximately 11 to 14 times the height of the obstacle. A fairly close agreement with the wake-profile (equation 2.28), can be seen for all six runs.

For run number 1 ($R_e = 5,200$), the deviation from the wake-profile can be seen to start at approximately $y/b = 0.3$, whereas for runs 2, 3 and 4 the value is slightly higher, ($y/b=0.4$). For runs 5 and 6 this value is higher still, ($y/b=0.6$). If we recognize the fact that the Reynolds number is largest for run number 5 (37,500), and smallest for run number 1 (5,200), and also that the wall is rough in run number 6, then these plots indicate that: high Reynolds number, as well as the wall roughness, tend to decrease the extent of the outer-region. Conversely, the inner-region of the wall-wake has a tendency to increase with the Reynolds number and the wall roughness. A definite conclusion regarding this observation cannot be drawn, because of the scatter of the data.

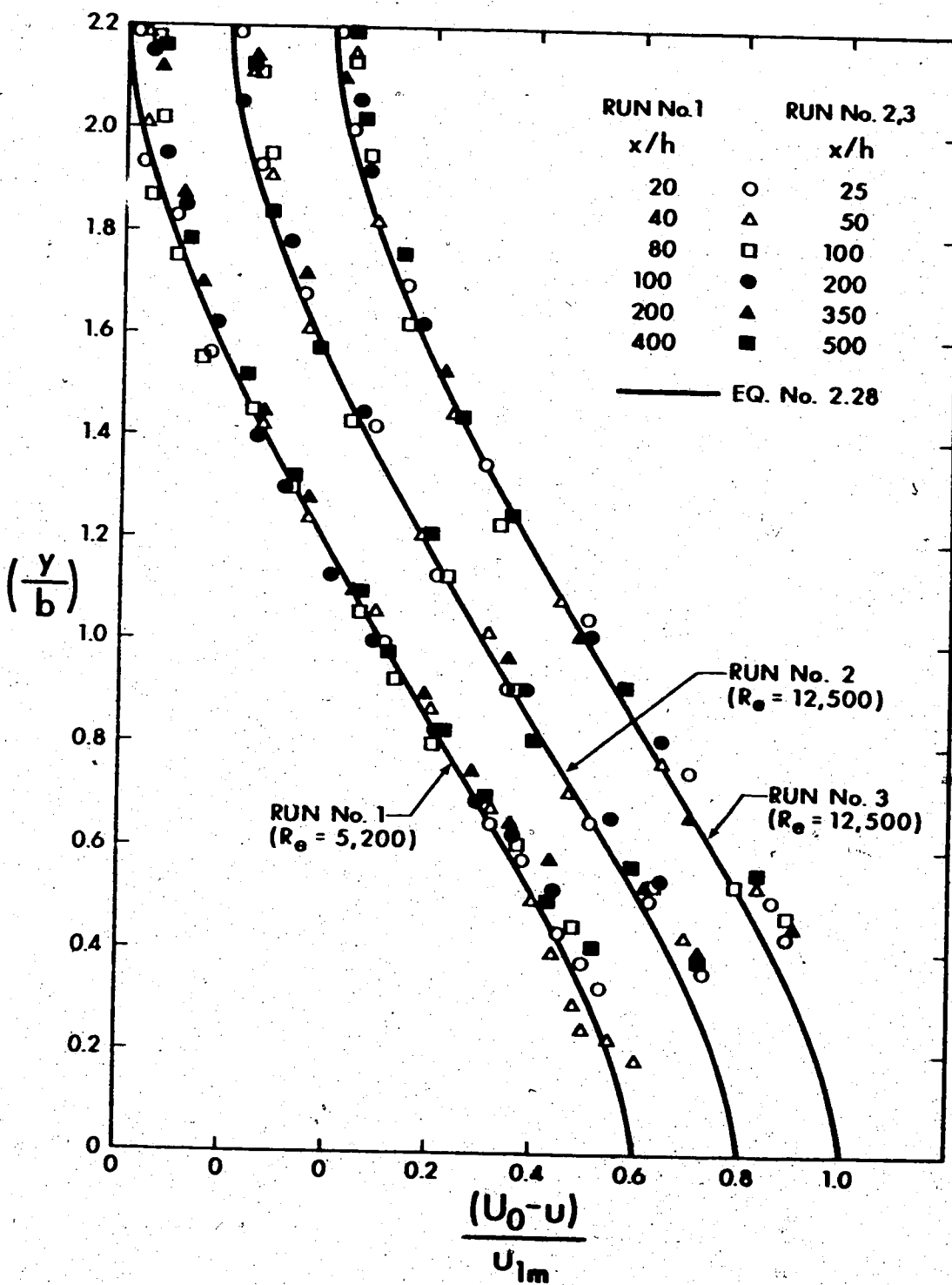


FIGURE 4.3-a VELOCITY DISTRIBUTION IN THE OUTER-REGION FOR RUNS 1,2,AND 3

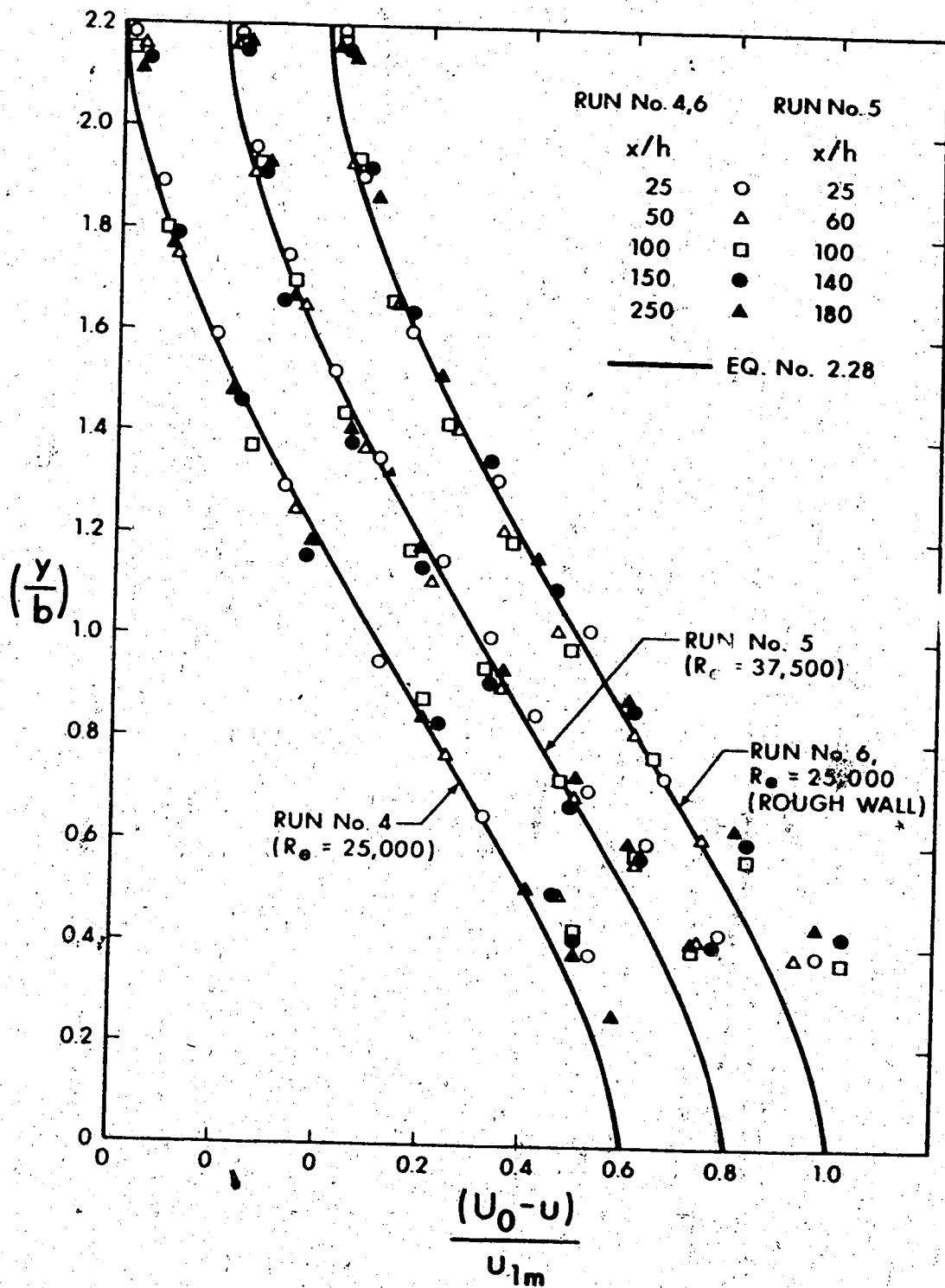


FIGURE 4.3-b. VELOCITY DISTRIBUTION IN THE OUTER-REGION FOR RUNS 4, 5 AND 6

However, it would seem logical that there would be a faster growth of the boundary layer under these situations.

If $y = \delta_w$ is the point of deviation of the velocity profiles from the wake-profile, then the above observation indicates that the ratio δ_w/b remains constant in the far-wake region, for any particular flow and wall characteristics. Reynolds number and wall roughness may affect the ratio only by a scale factor.

4.2.3 VELOCITY DISTRIBUTION IN THE INNER REGION (SMOOTH WALL)

Velocity distributions in the "inner region", for the first five runs, are plotted in Figures 4.4 (a, b). The shear velocity, u_* , for all runs has been computed by the Preston-tube technique described in Chapter III. It may be seen that the law of the wall:

$$\frac{u}{u_*} = A \log \frac{yu_*}{\nu} + B$$

holds true in the inner region, for all five runs. For run number 1 (low Reynolds number case), the data becomes too scattered beyond $yu_*/\nu = 400$, and the "law of the wall" does not seem to be valid beyond this point. This indicates that the inner region is smaller for this run.

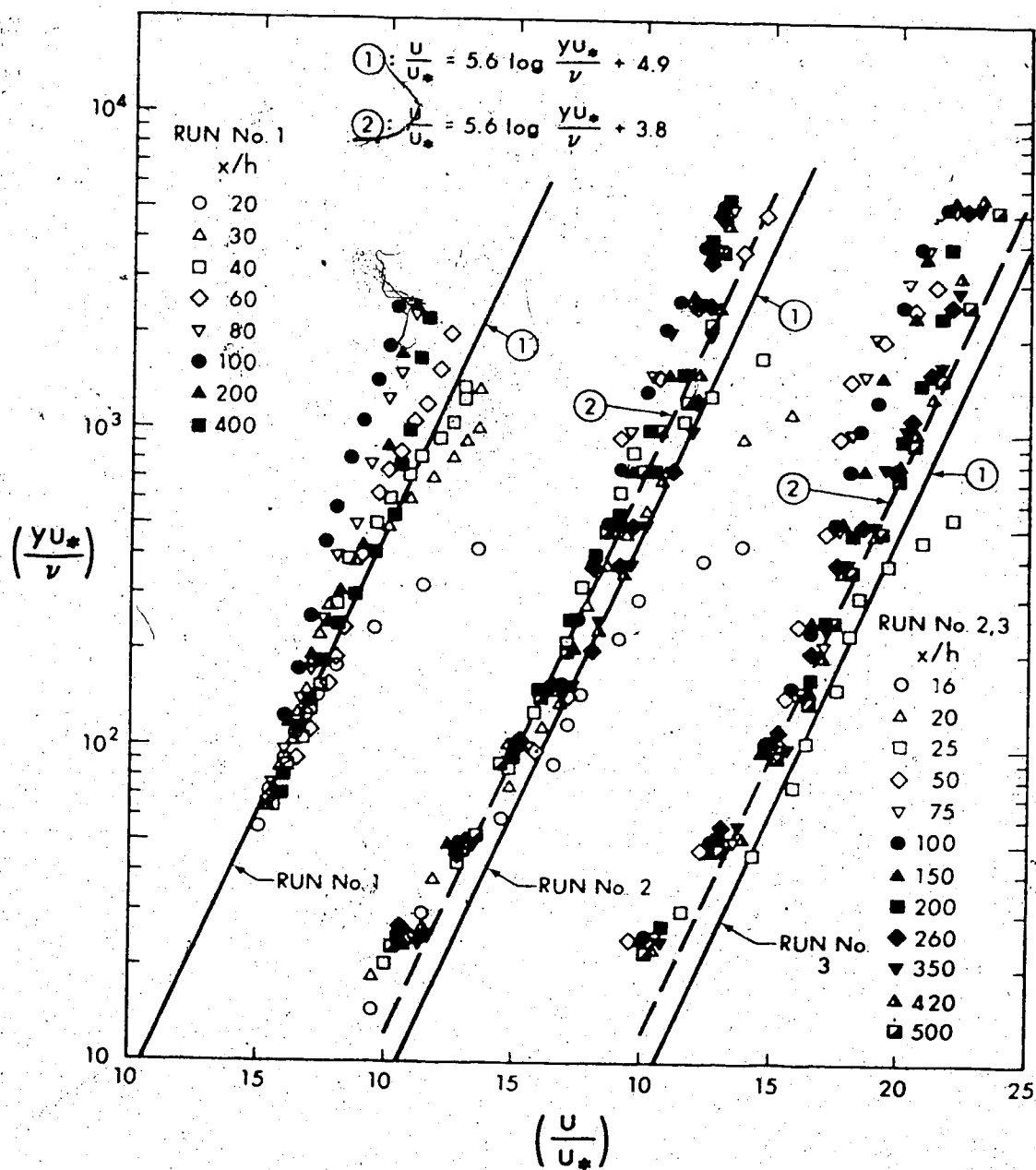


FIGURE 4.4-a VELOCITY DISTRIBUTION IN THE INNER-REGION FOR RUNS 1, 2 AND 3

For runs 2, 3, 4 and 5, the logarithmic form of velocity distribution is seen to be valid for yu_*/ν up to 1000 to 2000. This indicates that the "law of the wall" is valid over a larger region for high Reynolds numbers. In other words, we can say that the "inner-region" of a two-dimensional turbulent wall-wake increases with the free-stream Reynolds number. The effect of the free-stream Reynolds number on the "law of the wall" in turbulent boundary layers is already well known (Runstandler, Kline, Reynolds, 1963). However, it was found that the experimental data fall slightly away for most runs from the equation describing the law of the wall in the turbulent boundary layer, viz.

$$\frac{u}{u_*} = 5.6 \log \frac{yu_*}{\nu} + 4.9 \quad (4.5)$$

Equation (4.5) is shown as a solid line (marked (1)), in Figures 4.4(a,b).

A better approximation for describing the velocity profile in the inner region was found to be

$$\frac{u}{u_*} = 5.6 \log \frac{yu_*}{\nu} + 3.8 \quad (4.6)$$

and is shown as a chained line (marked (2)) in Figures 4.4(a,b). The discrepancy which appears can be attributed,

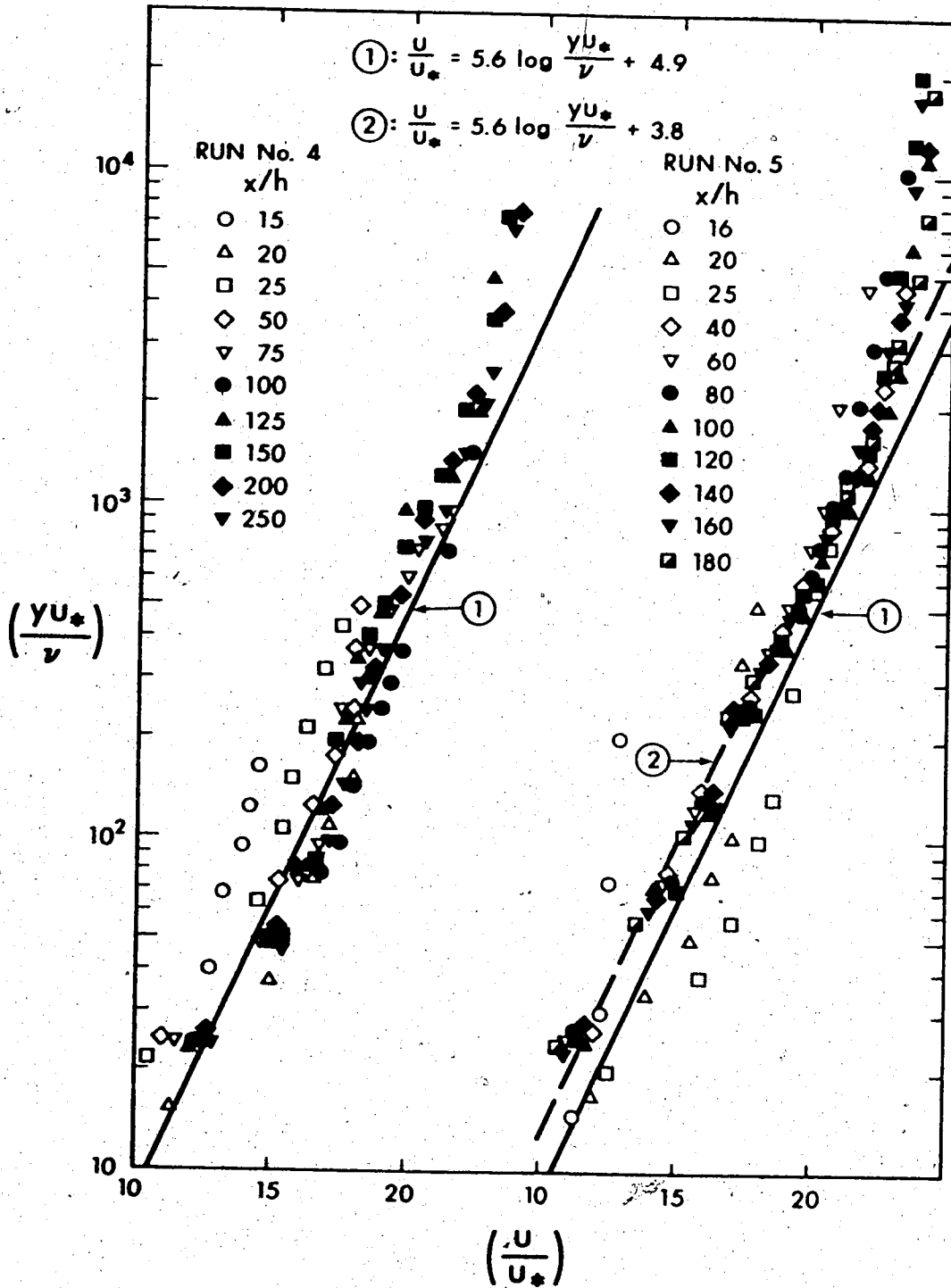


FIGURE 4.4-b VELOCITY DISTRIBUTION IN THE INNER-REGION FOR RUNS 4 AND 5

at least partly, to the error in the Preston tube measurements of u_* . Since the slope of the logarithmic profiles remains unchanged, it seems that the Preston tube measured values of u_* are consistently higher than the actual values. This may be because no corrections for turbulence and probe geometry have been applied to the Preston tube measurements.

The large deviation (in all five runs) of the experimental points from the "law of the wall", in the region $x/h \leq 25$, indicates that the flow in the wall-region has not developed to fully turbulent flow. As we move further downstream, the data begin to fall on a single line (equation 4.6), indicating the validity of the law of the wall in the inner region.

It was not possible to take measurements in the region of $yu_*/\nu < 25$, with the instruments available. However, it is understood that the velocity profile in the region close to the wall is of the form:

$$\frac{u}{u_*} = \frac{yu_*}{\nu} \quad (4.8)$$

Velocity profiles in the inner region, for runs 2, 3, 4 and 5, are plotted in terms of (y/b) , in Figure (4.5). It has been found that a power law, of the form:

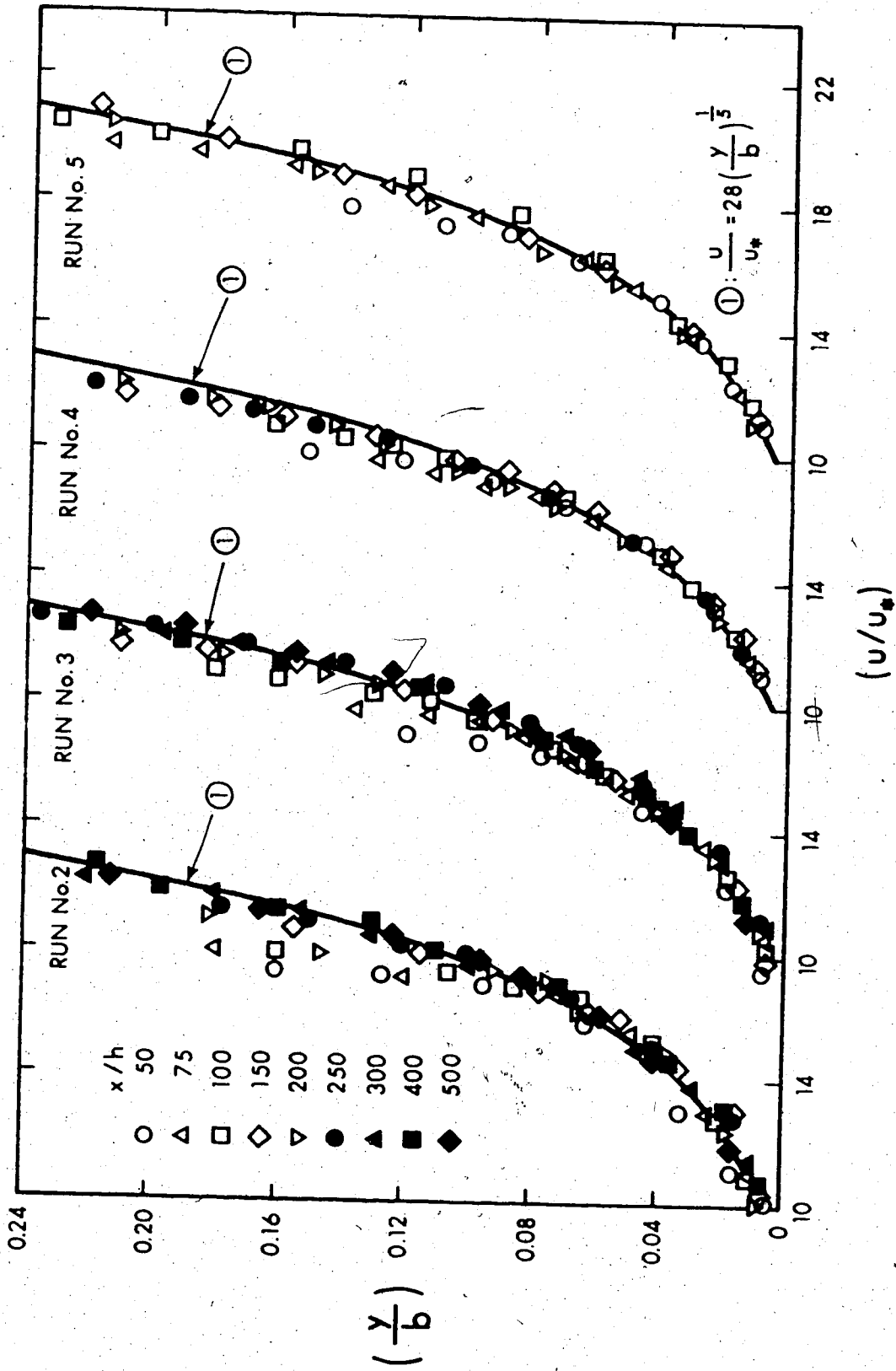


FIGURE 4.5 VELOCITY DISTRIBUTION IN THE INNER-REGION FOR RUNS 2, 3, 4 AND 5

$$\frac{u}{u_*} = 28 \left(\frac{y}{b}\right)^{1/5} \quad (4.9),$$

describes the velocity profile, in the far-wake region, very well for all four runs. It can be seen that the region over which equation (4.9) holds, increases as x/h increases. If $y = \delta_w$ is the point at which the velocity profile deviates from equation (4.9) and adheres to the wake profile, and if $u = u_w$ at $y = \delta_w$, then from equation (4.9) we may derive:

$$\frac{u}{u_w} = \left(\frac{y}{\delta_w}\right)^{1/5} \quad (4.10).$$

Equation (4.10) represents the velocity profile in the inner-region of the wall-wake, with zero pressure gradient. However, u_w and δ_w are yet to be evaluated.

4.2.4. VELOCITY DISTRIBUTION IN THE INNER-REGION FOR THE ROUGH WALL-WAKE

Velocity distribution in the inner region for run number 6 (the rough wall case) is shown in Figure (4.6), where u/u_* is plotted against (y/k_s) , k_s being the equivalent sand roughness height. The value of k_s for the type of roughness used was found to be equal to 0.0061 feet. The effective datum was found to be 0.0009 feet below the

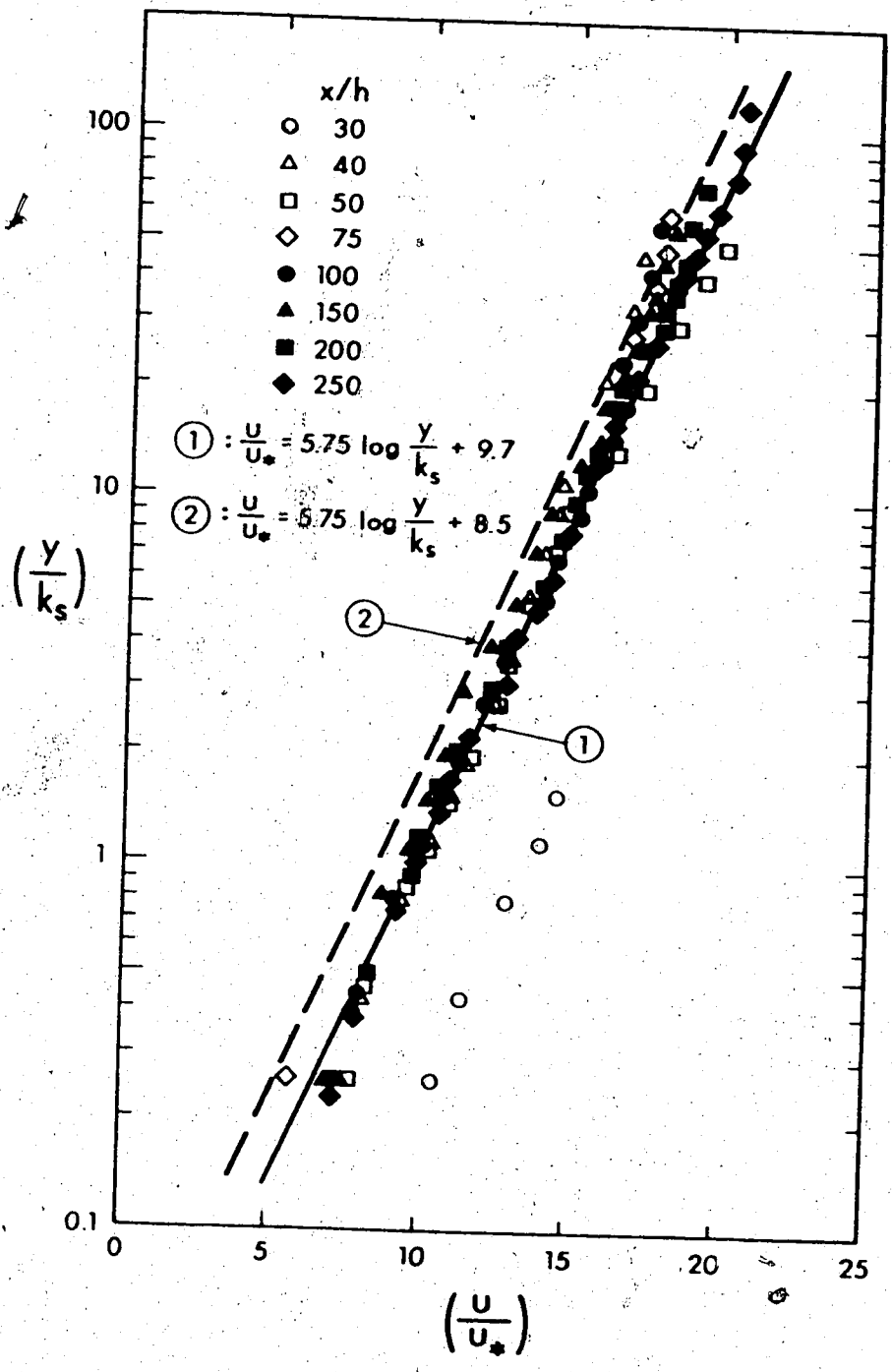


FIGURE 4.6 VELOCITY DISTRIBUTION IN THE INNER-REGION FOR RUN NUMBER 6 (ROUGH WALL)

crest of the protruberances, by using the method described in section 3.7.4 (Chapter III).

The shear velocity, u_* , was computed from the slope of the logarithmic profile, which was assumed to be of the form:

$$\frac{u}{u_*} = 5.75 \log \frac{y}{k_s} + 8.5 \quad (4.11).$$

$$\text{Thus, } u_* = \frac{1}{5.75} \frac{u_1 - u_2}{\log(y_1/y_2)},$$

where u_1 and u_2 are mean velocities at ordinates y_1 and y_2 , respectively. Shear velocity was also computed by using Hwang and Laursen's equation (equation 3.8), but it was found that u_* , thus computed, was not consistent. For some profiles, u_* computed by equation (3.8) was too low, and for others too high, as compared to the values computed by using the slope of the logarithmic profile. Thus the values of u_* determined by the slope of the logarithmic profile were adopted.

The plot in Figure (4.6) indicates that u_* , thus determined, is fairly accurate, as all the data for $x/h \geq 40$ fall on a single line, without much scatter. One can conclude that the flow in the inner regions becomes rough turbulent flow beyond $x/h \geq 40$. Further, it may be

noticed that even though u_* was computed from equation (4.11), this equation (marked (1) in Figure 4.6) does not represent the best-fit-line for the experimental points in the plot. This could be due to the fact that the k_s value adopted for the type of roughness used, may not be correct. The correct k_s value can be computed from the equation of the best-fit-line, given by:

$$\frac{u}{u_*} = 5.75 \log \frac{y}{k_s} + 9.7 \quad (4.12)$$

If $(k_s)_c$ is the correct value of k_s , then for rough turbulent flow we must have:

$$\frac{u}{u_*} = 5.75 \log \frac{y}{(k_s)_c} + 8.5 \quad (4.13)$$

Subtracting one from the other, we obtain:

$$5.75 \log \frac{k}{(k_s)_c} = 1.2$$

Since the value of k_s adopted was 0.0061 feet, we obtain

$$(k_s)_c = 0.0038 \text{ feet.}$$

The change in the equivalent sand roughness height, for the rough strip used in this experiment, resulted from the fact that the aluminum oxide cloth used for the roughness study was the same as that used by Hollingshead, (1972). The value of k_s determined by Hollingshead was 0.0061 feet (section 3.3, Chapter III). The cloth he used was subsequently used in water for a long period of time, before being used for the present study. Hence its k_s value is likely to decrease.

From Figures (4.4) and (4.6), it can be concluded that the logarithmic velocity profile holds true for flow in the inner region of the wall-wake, for smooth as well as rough surfaces. The region over which the logarithmic law is valid is larger for a rough surface than for a smooth one, under the same flow conditions. It is likely that the grain size and the roughness pattern will further influence the region of validity of the logarithmic profile.

4.2.5 GROWTH OF LENGTH SCALE

The length scale, b , nondimensionalized by the height of the obstacle, h , is plotted against x/h in Figure (4.7), and is tabulated in Table A-7 (Appendix A). In this plot the drag coefficient, C_{Do} , has not been taken into account. This plot was, in fact, used to compute C_{Do} for some of the obstacles, for which the determination of C_{Do} by other means was difficult. It can be seen that

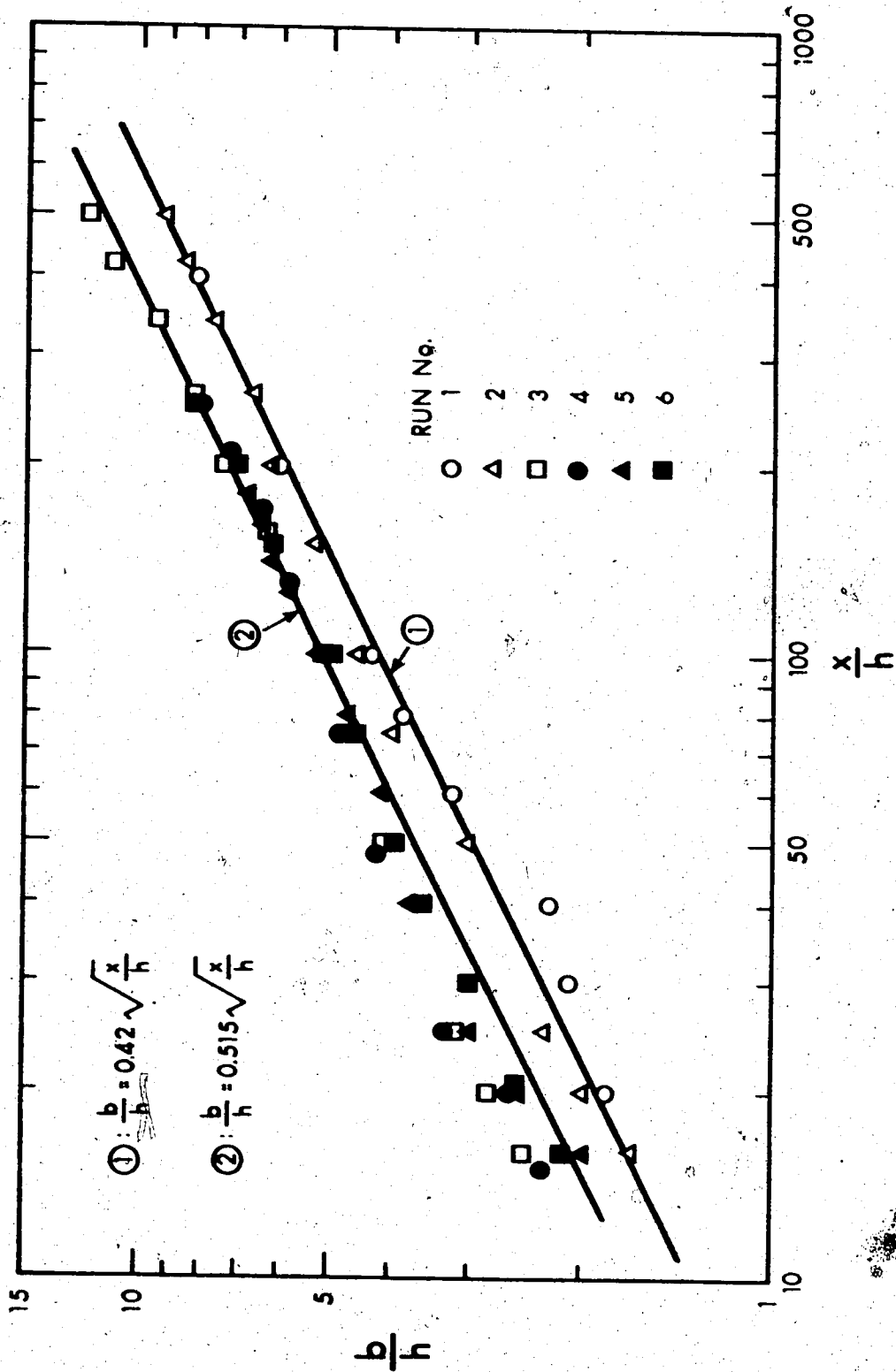


FIGURE 4.7 GROWTH OF LENGTH SCALE; (b/h) VS. (x/h)

the length scale varies with the square-root of the distance from the obstacle, as was predicted by the theory. Further, the experimental points fall on two separate lines. The data for runs number 1 and number 2 (semi-circular cylinders) indicate that for these two runs the half-wake width, b , is less than that for a sharp-edged plate (runs 3, 4, 5 and 6). This is obvious because the coefficient of drag for a semi-circular cylinder resting on a floor is less than that for a sharp-edged plate resting on a floor. If we take $C_{Do} = 1.25$ for a sharp-edged plate resting on a wall (Hoerner, 1965), then C_{Do} for a semi-circular cylinder resting on the wall can be computed as follows. We have the equations of line (1) and line (2), in figure (4.7), as:

$$\text{line (1): } b/h = 0.42 (x/h)^{1/2}$$

$$\text{line (2): } b/h = 0.515 (x/h)^{1/2}$$

If the equation for the growth of the length scale is of the form:

$$b/hC_{Do} = C_2 (x/hC_{Do})^{1/2}$$

$$\text{then, } b/h = C_2 (x C_{Do}/h)^{1/2}$$

For line (2), the value of $C_{Do} = 1.25$

Therefore, $C_2 = 0.46$

Therefore, C_{Do} for line (1), (runs number 1 and number 2), is

$$C_{Do} = 0.84$$

The computed value of $C_{Do} = 0.84$ has been adopted for runs number 1 and number 2 in the plot of $(b/h.C_{Do})$ versus $(x/h.C_{Do})$, in Figure (4.8). It is to be noted that run number 1 (low Reynolds number case), and run number 2 (high Reynolds number case), are at different Reynolds numbers for the same obstacles (semi-circular cylinder), and the value of C_{Do} might be different for both of them. But, since line (2) in Figure (4.6) is the mean line for runs number 1 and number 2, the value of 0.84 for C_{Do} is, in fact, the mean drag coefficient for the two cases. The experimental points for line (1) in Figure (4.7) indicate that the difference between the actual values of C_{Do} (for run number 1 and run number 2) and the mean value of 0.84, is not appreciable.

From Figure (4.8) it was found that the growth of the length scale could be described by the equation:

$$b/h C_{Do} = 0.46 (x/h C_{Do})^{1/2} \quad (4.14)$$

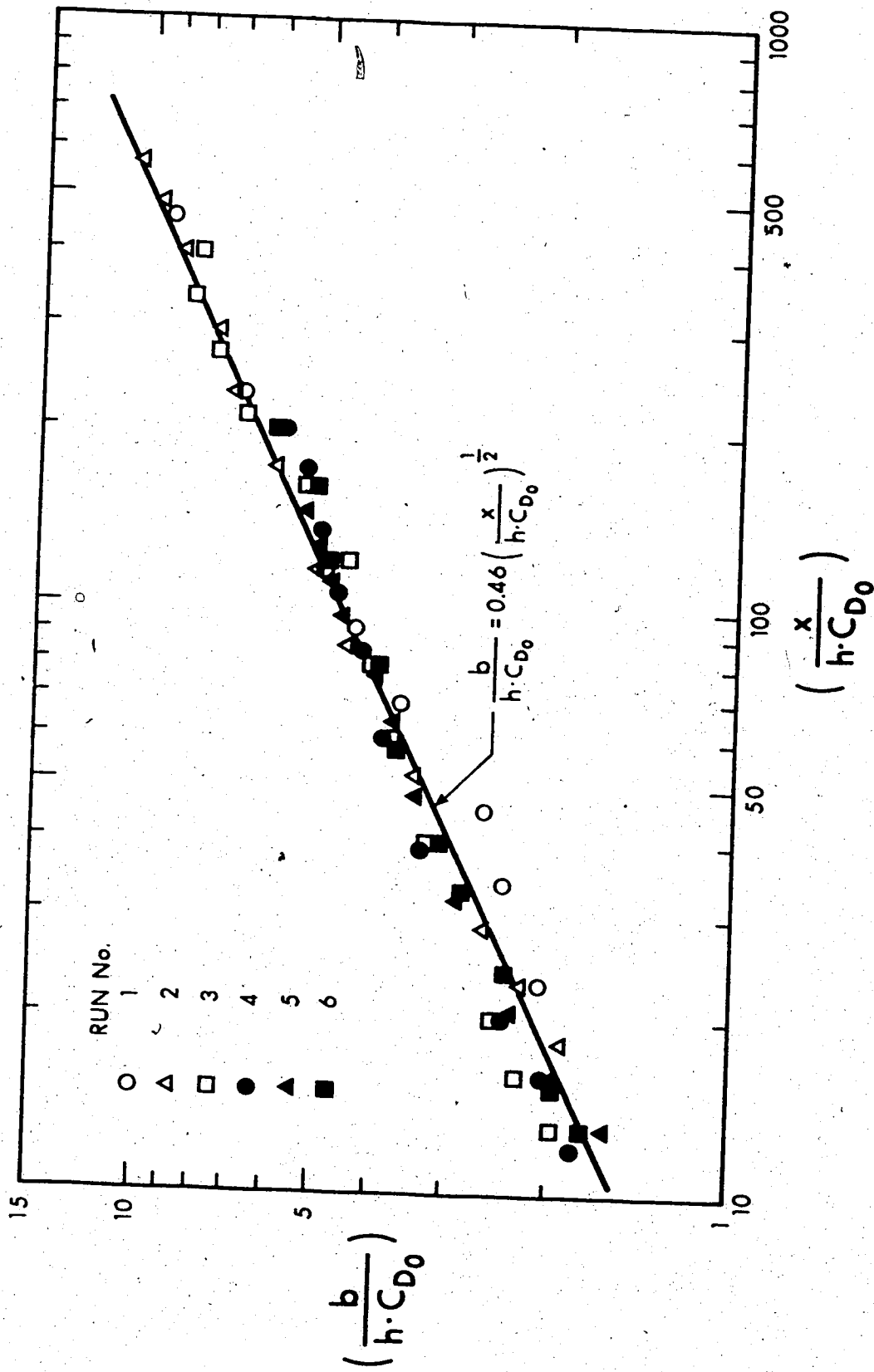


FIGURE 4.8 GROWTH OF LENGTH SCALE; (b/hC_{D0}) VS. (x/hC_{D0})

There is only a slight change in the coefficient $C_2 (= 0.46)$ from the theoretical equation (equation 2.44), derived earlier, for the growth of half-wake-width.

It may also be noticed that the half-wake-width for the case of the rough wall (run number 6) increases in the same way as for the smooth wall. This confirms our hypothesis, that wall-characteristics will not affect the wake-characteristics of a turbulent wall-wake to any appreciable extent.

To determine the virtual origin of the growth of the wake, $(b/h C_{Do})$ was plotted against $(x/h C_{Do})^{1/2}$. The virtual origin was found to lie at $(x/h C_{Do}) = -4$. Since this value is not of much significance in the "far-wake region", its effect was ignored.

4.2.6 DECAY OF VELOCITY DEFECT SCALE

In Figure (4.9), a plot of u_{lm}/U_0 versus $(x/h C_{Do})$ is shown. It was found that the centre line velocity defect decays in the manner described by:

$$\frac{u_{lm}}{U_0} = 1.3 (x/h C_{Do})^{-1/2} \quad (4.15)$$

for $(x/h C_{Do}) > 30$.

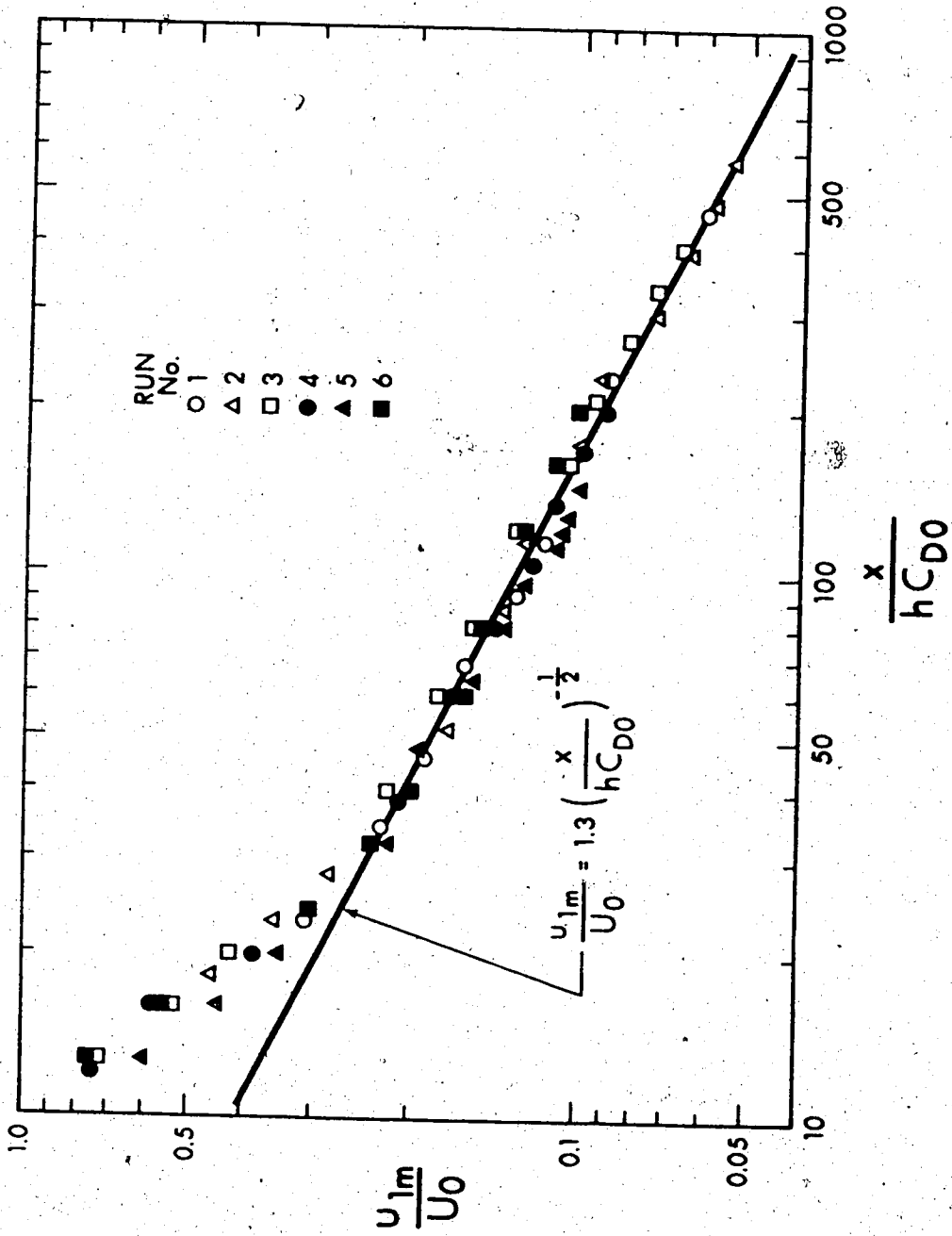


FIGURE 4.9 DECAY OF VELOCITY SCALE

Thus, the inverse square-root law for the decay of velocity defect, as predicted by the theory, holds true (equation 2.33). The discrepancy between the measured value of the coefficient, C_2 ($=1.3$), and the one predicted by theory ($C_2 = 1.35$, equation 2.43), is very small.

This deviation of coefficients C_1 and C_2 from their theoretical values may be the result of one or more of the following factors:

- (i) Errors in experimental measurements.
- (ii) Error in the adopted value for C_{Do} .
- (iii) In the theoretical computations of these coefficients, it was assumed that the velocity profiles follow equation (2.28) right up to the boundary, which is not true.

However, since the deviation is very small, no attempt was made to compute the corrected values of the coefficients C_1 and C_2 .

Once again we find that the roughness of the wall does not affect the decay of the velocity scale.

4.2.7 DISTRIBUTION OF BED SHEAR STRESS, τ_o

A plot of $\tau_o / \frac{1}{2} \rho u_{1m}^2$ versus $x/h C_{Do}$, is shown in Figure (4.10), on a log-log scale. It was found that $\tau_o / \frac{1}{2} \rho u_{1m}^2 = C_{fm}$, increases linearly, in the far-wake region, with $x/h C_{Do}$, in the manner described by the

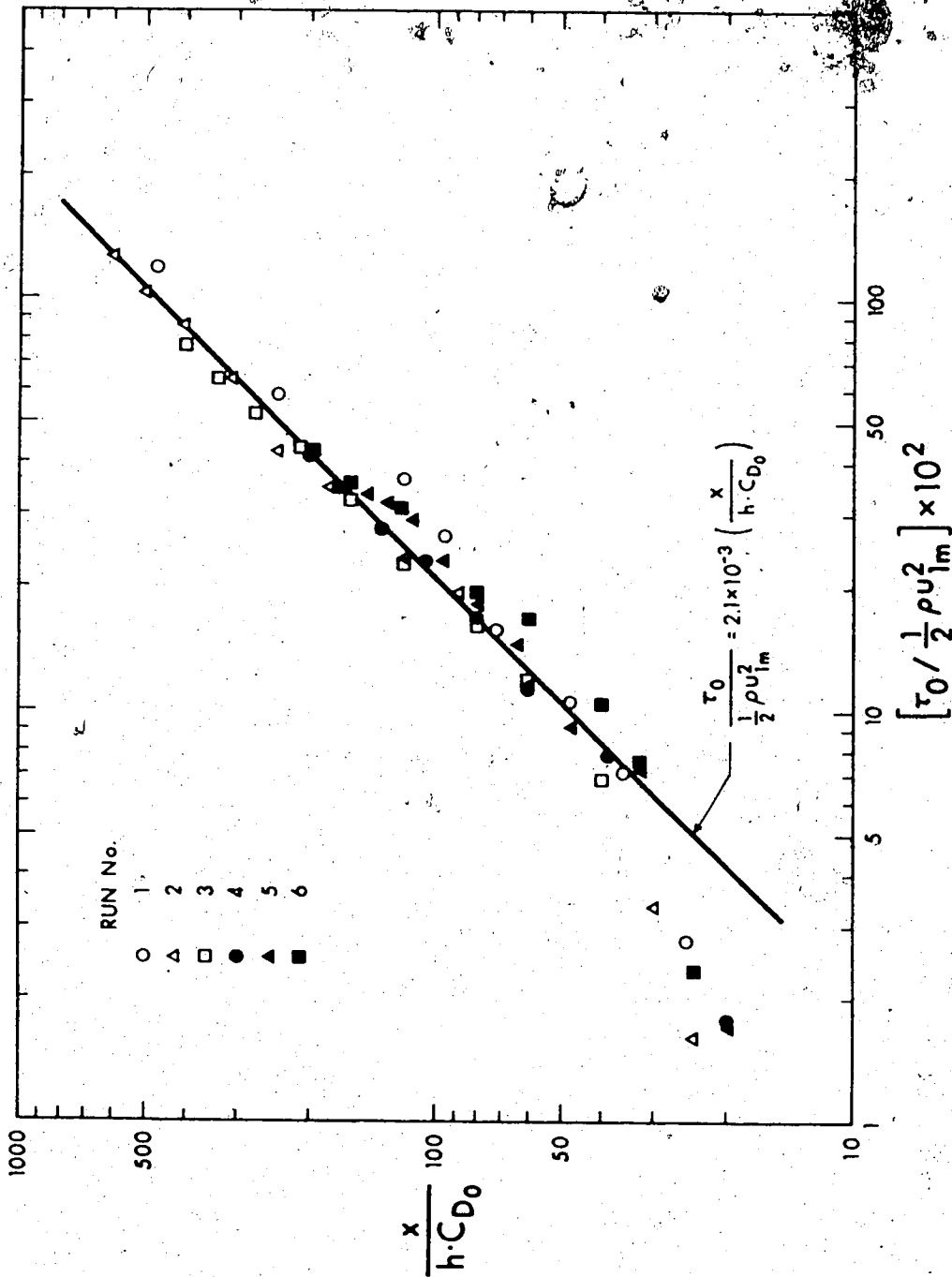


FIGURE 4.10. BED SHEAR STRESS DISTRIBUTION ALONG THE CENTER PLANE

equation:

$$\frac{\tau_0}{\frac{1}{2}\rho u_{1m}^2} = 2.1 \times 10^{-3} \left(\frac{x}{h \cdot C_{Do}} \right) \quad (4.16)$$

The above equation can be seen to approximate the distribution of C_{fm} closely, except for runs number 1 and number 6, for which the discrepancy is a little high. The influence of the Reynolds number on the distribution of C_{fm} does not indicate any definite pattern. A conclusive statement on the Reynolds number effect, therefore, cannot be made. For rough wall flow (run number 6), the value of C_{fm} can be seen to be larger than for smooth wall flow, in the range $x/h \cdot C_{Do} \leq 120$. Since only one case of roughness was tested, it would be premature to draw a definite conclusion regarding the effect of roughness on C_{fm} . However, it would seem logical that there would be a higher value of C_{fm} for rough flow than for smooth flow. This can also be explained from equation (4.16), which can be written in its general form as:

$$C_{fm} = \frac{\tau_0}{\frac{1}{2}\rho u_{1m}^2} \propto (x/h \cdot C_{Do})^{-3}$$

Since u_{1m} was found to be independent of wall roughness, and τ_0 has a higher value for rough wall flow than

for smooth wall flow, C_{fm} will be higher for the rough wall case.

It can be concluded from the plot of C_{fm} versus $(x/h C_{Do})$, that C_{fm} is proportional to $(x/h C_{Do})$. A relationship of this nature can be obtained by considering the velocity profiles of the inner and outer regions at their point of intersection, $(y = \delta_w)$. The wake profile at $y = \delta_w$, $(u = u_w)$, can be written as:

$$\frac{U_o - u_w}{u_{lm}} = (1 - 0.293 \left\{ \frac{\delta_w}{b} \right\}^{3/2})^2,$$

and the wall profile, from the 1/5th power profile (equation 4.9), can be written as:

$$\frac{u_w}{u_*} \propto \left(\frac{\delta_w}{b} \right)^{1/5}.$$

The experimental plots of velocity profile indicate that (δ_w/b) is independent of x , or in general we can say that:

$$\frac{\delta_w}{b} = A(R_e, b/k_s),$$

where A is a constant which is dependent upon the Reynolds number R_e , and roughness characteristic of the wall b/k_s .

Equating the two profiles at $y = \delta_w$, we obtain:

$$\frac{u_*}{u_{lm}} \propto A_1(R_e, y/k_s) \cdot \frac{U_o}{u_{lm}}$$

If we substitute for $C_{fm} = (2u_*/u_{lm})^2$, and

$\frac{u_{lm}}{U_o} \propto (x/h.C_{Do})^{-1/2}$, we obtain:

$$C_{fm} \propto A_1(R_e, y/k_s) \left(\frac{x}{h.C_{Do}}\right)$$

The above expression is the same as equation (4.16), if we recognize that:

$$A_1(R_e, y/k_s) = 2.1 \times 10^{-3}$$

It is to be noted, however, that A_1 will depend on (y/k_s) , and possibly on R_e , and its experimentally obtained value of 2.1×10^{-3} gives only its order of magnitude.

Explanation of the behavior of τ_o will be facilitated by making a plot of $\tau_o / \frac{1}{2}\rho U_o^2 (=C_f)$ versus $(x/h.C_{Do})$.

If we divide both sides of equation (4.16) by U_o^2 , we get:

$$\frac{\tau_o}{\frac{1}{2}\rho U_o^2} = 2.1 \times 10^{-3} \left(\frac{x}{h \cdot C_{Do}} \right) \cdot \left(\frac{u_{1m}}{U_o} \right)^2$$

If we substitute for $\left(\frac{u_{1m}}{U_o} \right)^2$, from equation (4.15), which is:

$$\frac{u_{1m}}{U_o} = 1.3 (x/hC_{Do})^{-1/2},$$

we obtain:

$$C_f = \frac{\tau_o}{\frac{1}{2}\rho U_o^2} = 3.55 \times 10^{-3} \quad (4.17).$$

Thus, we find that the coefficient of skin friction, C_f , becomes independent of $x/h \cdot C_{Do}$, and remains constant in the down-stream direction.

A plot of C_f versus x/hC_{Do} is shown in Figure (4.11). It may be seen that in the "far-wake region", ($x/hC_{Do} > 30$), the coefficient of skin friction attains constancy for all six runs. The value of C_f for runs 2, 3, 4 and 5 is very nearly equal to 0.0035, as was computed in equation (4.17). For runs number 1 and number 6, the value of C_f is approximately equal to 0.0042. This constancy of the

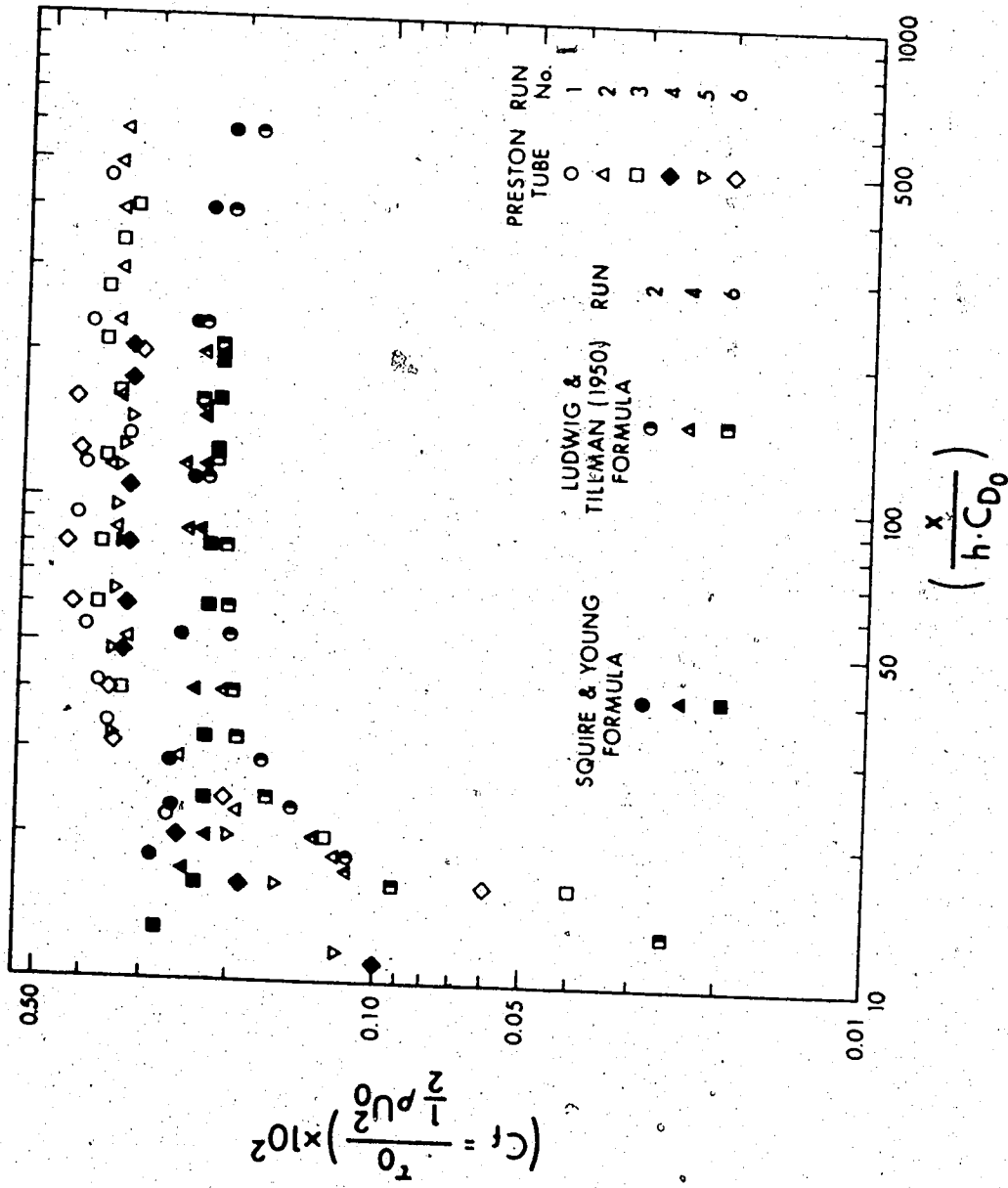


FIGURE 4.11 COEFFICIENT OF SKIN FRICTION ALONG THE CENTER PLANE

coefficient of skin friction, for the wall-wake on a smooth boundary, is a significant departure from the case of a fully-developed turbulent boundary layer on a smooth wall. In the latter case, the coefficient of skin friction decreases in the longitudinal direction.

To check the above observation, the coefficients of skin friction were also computed by the Squire and Young (Schlichting, 1968) formula, given by:

$$C_f = \frac{0.0576}{(\log\{4.075R_\theta\})^2} \quad (4.18)$$

and the Ludwig and Tillman (1950) formula:

$$C_f = \frac{0.246}{10^{0.678H} R_\theta^{0.268}} \quad (4.19)$$

where θ is the momentum thickness, defined earlier, $H = \delta^*/\theta$ is the shape parameter, and

$$R_\theta = \frac{U_o \theta}{\nu}$$

In both the equations, measured values of θ and H are used to compute C_f . The computed values of C_f from both these equations are plotted in the same figure,

(Figure 4.11). It is seen that the coefficients of skin friction, as computed from the Squire and Young and the Ludwig and Tillman formulae, show generally the same behavior as the measured values of C_f , except that their magnitudes are considerably less than the measured values. This indicates that the coefficients 0.0576 and 0.246, in equations (4.18) and (4.19) respectively, are less than the ones obtained experimentally. One reason for this might be that the nature of the "inner region" of a turbulent wall-wake is disturbed by the presence of the obstacle at the leading edge of the plate. Such a disturbance could cause a modification in the coefficients in equations (4.18) and (4.19). Error in the Preston tube measurements may also be a factor.

From the plot in Figure 4.11, it was found that if the coefficients in equations (4.18) and (4.19) are increased to 0.092 and 0.393 respectively, then the measured and the computed values of C_f fall on a single mean curve. However, a large discrepancy between the experimental data and that computed by the Squire and Young formula, can be observed in the near-wake region ($x/hC_{D0} < 30$). This is because the Squire and Young formula is valid only for a fully-developed turbulent boundary layer, while in the case of a wall-wake, the skin friction is zero at the point of reattachment, and increases as we

move downstream from this point. It is only beyond a certain distance downstream from the point of reattachment that the skin friction attains the value associated with fully-developed flow. The Ludwig and Tillman equation, on the other hand, can be seen to show the same trend as the experimental data. Thus, an appropriate equation for the coefficient of skin friction could be of the form:

$$C_f = \frac{0.393}{10^{0.678H} R_\theta^{0.268}} \quad (4.20)$$

There was no other experimental data found to confirm the validity of the above equation. It should be noted that the above equation is the same as the Ludwig and Tillman equation (equation 4.19), excepting that the coefficient 0.246 in equation (4.19) is replaced by 0.393.

4.2.8 VARIATION OF WAKE DISPLACEMENT THICKNESS, δ_w

An expression for the wake displacement thickness, δ_w , can be obtained by equating the velocity, u_w , obtained from the wake profile with that obtained from the inner profile, at $y = \delta_w$.

From wake profile we have:

$$\frac{U_0 - u_w}{u_{1m}} = (1 - 0.293 \left\{ \frac{\delta_w}{b} \right\}^{3/2})^2 \quad (4.21),$$

and from the inner profile, (equation 4.10):

$$\frac{u_w}{u_*} = 28 \left(\frac{\delta_w}{b}\right)^{1/5} \quad (4.22)$$

Substituting equation (4.22) into equation (4.21) we get:

$$\frac{U_o}{u_{1m}} - 28 \left(\frac{\delta_w}{b}\right)^{1/5} \frac{u_*}{u_{1m}} = (1 - 0.293 \left(\frac{\delta_w}{b}\right)^{3/2})^2$$

An approximate solution for (δ_w/b) can be obtained from the above equation, if we assume that $\delta_w \ll b$, so that the right hand side of the equation is approximately equal to 1.

$$\text{Thus: } 28 \left(\frac{\delta_w}{b}\right)^{1/5} = \frac{U_o - u_{1m}}{u_*}$$

$$\text{or } 28 \left(\frac{\delta_w}{b}\right)^{1/5} = \frac{U_o}{u_*} \left(1 - \frac{u_{1m}}{U_o}\right)$$

In the far-wake region we can assume $u_{1m} \ll U_o$, and hence:

$$28 \left(\frac{\delta_w}{b}\right)^{1/5} = \frac{U_o}{u_*} = \left(\frac{2}{C_f}\right)^{1/2}$$

If we substitute for $C_f = 3.55 \times 10^{-3}$, from equation (4.17), and simplify, we obtain:

$$\frac{\delta_w}{b} = 0.44 \quad (4.23)$$

Thus in the far-wake region, the ratio, (δ_w/b) , becomes independent of x .

Variation of δ_w in the longitudinal direction can be derived by substituting equation (4.14) for b . We thus obtain:

$$\frac{\delta_w}{hC_{Do}} = 0.2 \left(\frac{x}{hC_{Do}} \right)^{1/2} \quad (4.24)$$

Thus the point at which the inner and outer regions of the wall-wake (with zero pressure gradient) meet, increases longitudinally as $x^{1/2}$. It was not possible to verify experimentally equation (4.24), because of the difficulty of determining δ_w from the velocity profiles. An examination of the velocity profiles plotted in Figures 4.3(a, b), however, confirms the validity of equation (4.23).

4.2.9 GROWTH OF BOUNDARY LAYER PARAMETERS.

Boundary layer parameters, as defined by:

$$\text{displacement thickness, } \delta^* = \int_0^{\infty} \left(1 - \frac{u}{U_0}\right) dy,$$

$$\text{momentum thickness, } \theta = \int_0^{\infty} \frac{u}{U_0} \left(1 - \frac{u}{U_0}\right) dy, \text{ and}$$

$$\text{shape parameter, } \lambda_H = \frac{\delta^*}{\theta},$$

are plotted in Figure 4.12 for runs numbers 2, 4 and 6. These parameters have been computed by integrating the measured velocity profiles. For a turbulent boundary layer on a smooth flat plate, at zero pressure gradient, assuming a 1/7th power law for the velocity profile, i.e.

$$\frac{u}{U_0} = (y/\delta)^{1/7} \quad (4.25),$$

where δ is the boundary layer thickness, we can easily derive expressions for these parameters. They are of the following form:

$$\frac{\delta^*}{x} = 0.0462 \left(\frac{U_0 x}{\nu}\right)^{-1/5} \quad (4.26),$$

$$\frac{\theta}{x} = 0.036 \left(\frac{U_0 x}{\nu}\right)^{-1/5} \quad (4.27),$$

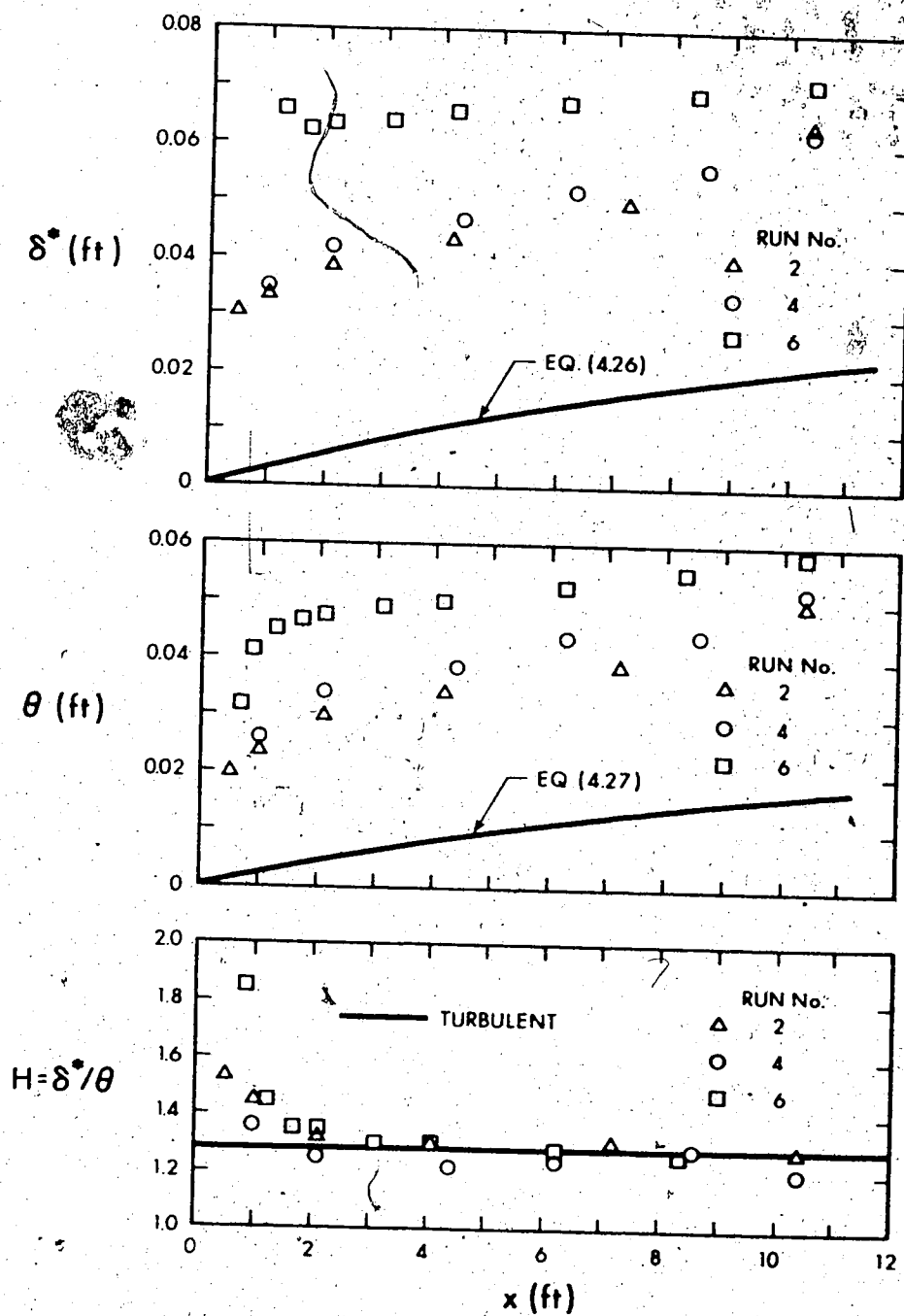


FIGURE 4.12 GROWTH OF BOUNDARY LAYER PARAMETERS FOR RUNS 2, 4 AND 6

and
$$H = \frac{\delta^*}{\theta} = 1.285 \quad (4.28).$$

Equations (4.26), (4.27) and (4.28) are plotted in Figure (4.12) along with the experimental data. It can be observed that the measured values of δ^* and θ , for the wall-wake, are much higher than the corresponding values for the turbulent boundary layer, on a smooth plate. This is obvious because the momentum loss and the displacement effect are much higher in the case of a wall-wake, due to the presence of the obstacle at the leading edge. For run number 6 (rough wall), the values of δ^* and θ are even higher than for runs numbers 2 and 4. This is because the roughness of the wall creates a further increase in the momentum and displacement thicknesses. This fact is well established for the case of turbulent boundary layers on rough walls. (Liu, et al, 1966.)

In the plot of shape parameter, H , we see that the experimental data attain the value of 1.285 (for turbulent flow) in the far-wake region.

4.3 EXPERIMENTAL RESULTS FOR WALL-WAKES WITH ADVERSE PRESSURE GRADIENTS

Three cases (runs numbers 7, 8 and 9) of wall-wakes with adverse pressure gradients were investigated for the present study. They are classified as APG-I, APG-II and

APG-III, in Series II of Table IV-1. APG-I was the weakest pressure gradient, and APG-III, the strongest.

The pressure gradient flow was created by attaching a false roof to the entire length of the test-section in the wind tunnel. The plate was fixed on the downstream end of the test-section, and at the upstream end it was adjustable to any desired height (Figure 3.3). For APG-I, the opening at the upstream end was 10.75 inches, and for APG-III, it was 4 inches. Further details are shown in Figure (3.3). The entrance section for the three runs was not the same, consequently the entrance velocity, U_0 , was different for each run. The maximum value of U_0 was 145 feet per second, for APG-III, and the minimum, 107 feet per second, for APG-I. For APG-II, the value of U_0 was 121 feet per second.

4.3.1 FREE STREAM VELOCITY DISTRIBUTION

The free stream velocity distributions for the three runs are plotted in Figure (4.13). The solid lines fitted empirically to the experimental data were found to be described by the following equations:

$$\text{APG-I} \quad : \quad \frac{U}{U_0} = (x + 0.2)^{-0.115} \quad (4.29)$$

$$\text{APG-II} \quad : \quad \frac{U}{U_0} = 1.02 (x + 0.2)^{-0.215} \quad (4.30)$$

$$\text{APG-III} \quad : \quad \frac{U}{U_0} = 1.015 (x + 0.9)^{-0.31} \quad (4.31)$$

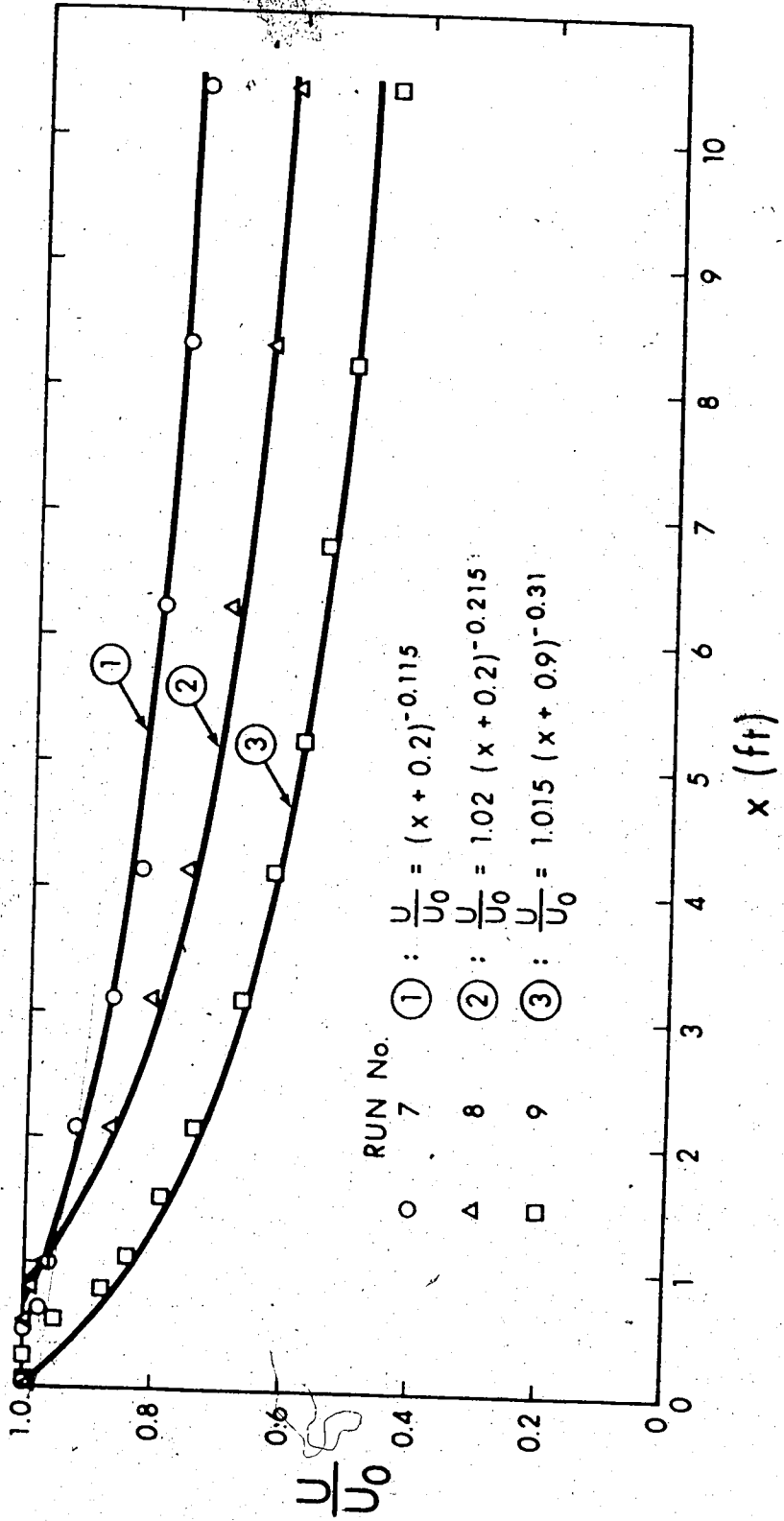


FIGURE 4.13 FREE STREAM VELOCITY DISTRIBUTION FOR RUNS 7, 8 AND 9

These equations indicate that for all practical cases the external pressure gradient can always be expressed by an exponential equation of the form, (Wyganski and Fiedler, 1968):

$$\frac{U}{U_0} = x^m (1 + C_1 x^{-m} + C_2 x^{-m-1} + \dots)$$

These equations satisfy the criteria necessary for self similar flows with pressure gradients, viz.:

$$U \propto (x + x_0)^m$$

The values of the exponent m , for the three runs, are therefore equal to -0.115, -0.215 and -0.31, respectively.

4.3.2 MEAN VELOCITY DISTRIBUTION FOR WALL-WAKES WITH ADVERSE PRESSURE GRADIENTS

The mean velocity profiles for runs number 7 and 8 are plotted in Figures (4.14 a,b). The velocity profile data for run number 9 is tabulated in Appendix A.

In order to verify the wake-like character of the velocity profiles in the outer-region, non-dimensional plots of $(U-u)/u_{1m}$ versus y/b have been shown in Figures (4.15). It can be noticed that the velocity profiles

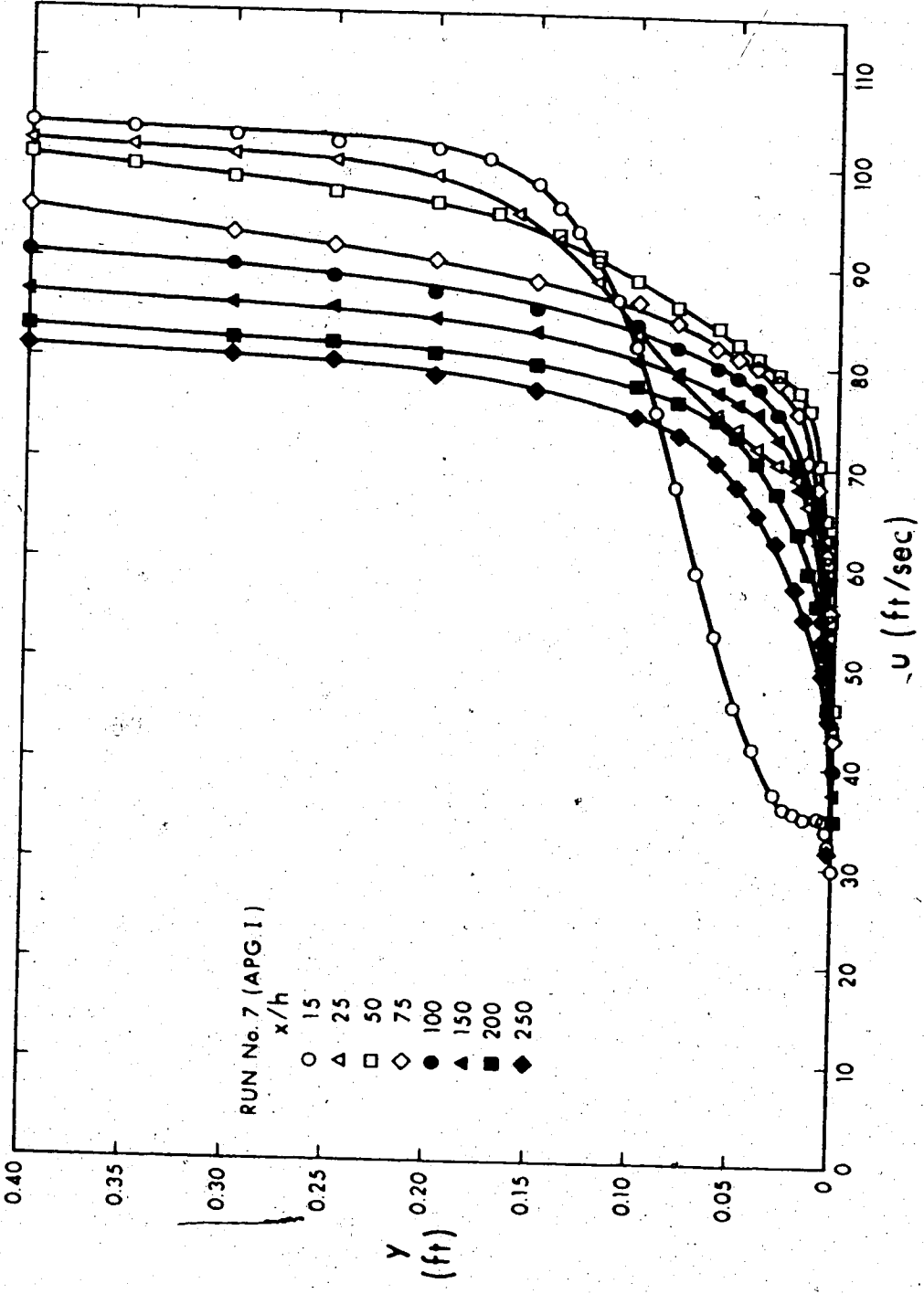


FIGURE 4.14-a VELOCITY PROFILES FOR RUN NUMBER 7

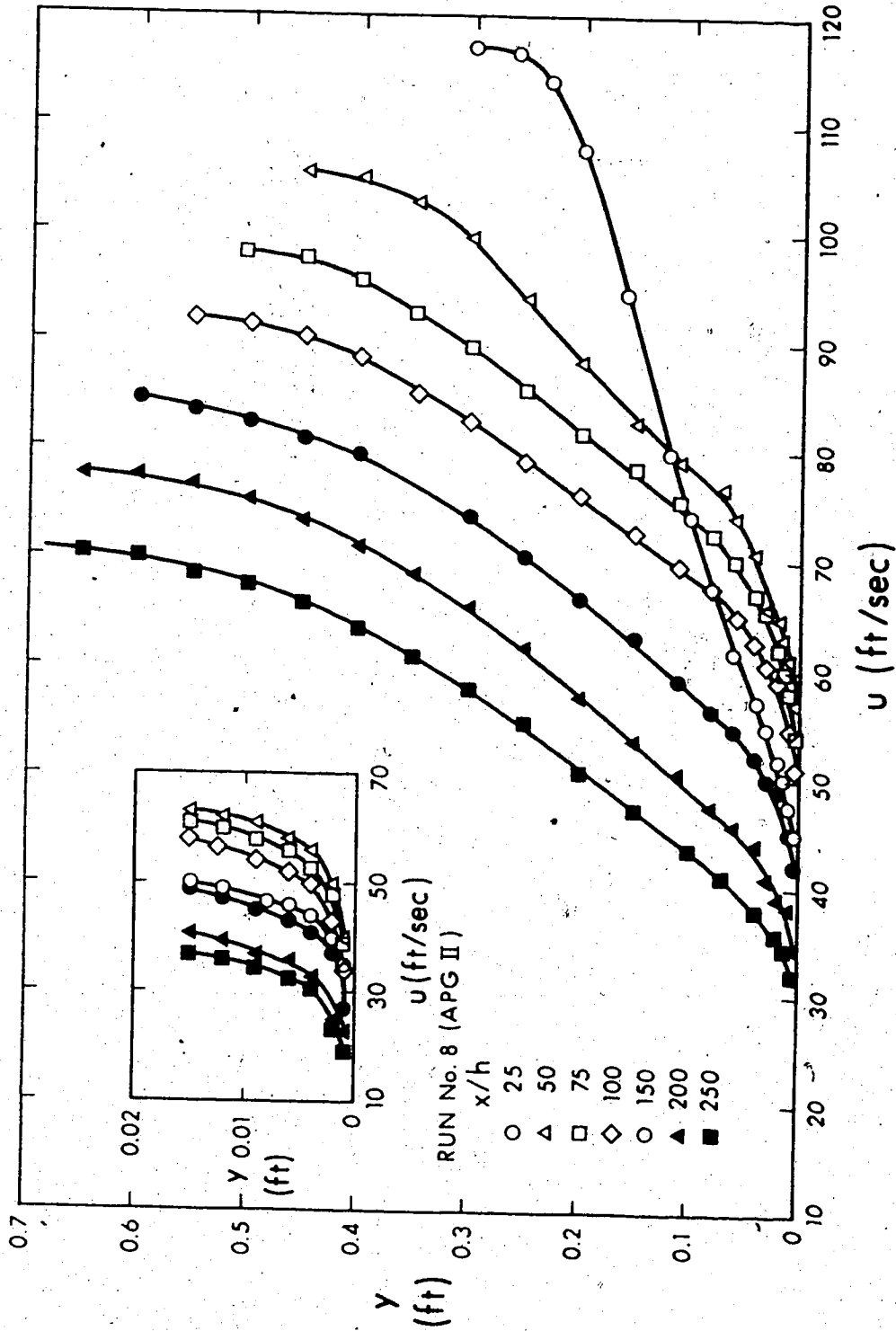


FIGURE 4.14-b VELOCITY PROFILES FOR RUN NUMBER 8 .

for all three runs agree well with the plane wake profile:

$$\frac{U-u}{u_{1m}} = (1 - 0.293 \left\{ \frac{y}{b} \right\}^{3/2})^2$$

in the far-wake region ($x/h \geq 50$).

The scatter of the data near the wall once again makes it difficult to locate exactly the level at which the velocity profile starts shifting from the wake profile to the boundary layer profile. An approximate value of the point of deviation seems to be somewhere around $y/b = 0.50$ or below for the three runs.

4.3.3 VELOCITY DISTRIBUTION IN THE INNER-REGION OF WALL-WAKES WITH ADVERSE PRESSURE GRADIENTS

In the inner-region of the wall-wakes with adverse pressure gradients, velocity profiles were again tested for the "law of the wall". Figure (4.16) indicates that the logarithmic law holds for all three pressure gradient runs. The scatter of the data is not much greater than normally expected in this type of plot. The best-fit-line for APG-I was found to be of the form:

$$\frac{u}{u_*} = 5.6 \log \frac{yu_*}{\nu} + 7.4 \quad (4.32),$$

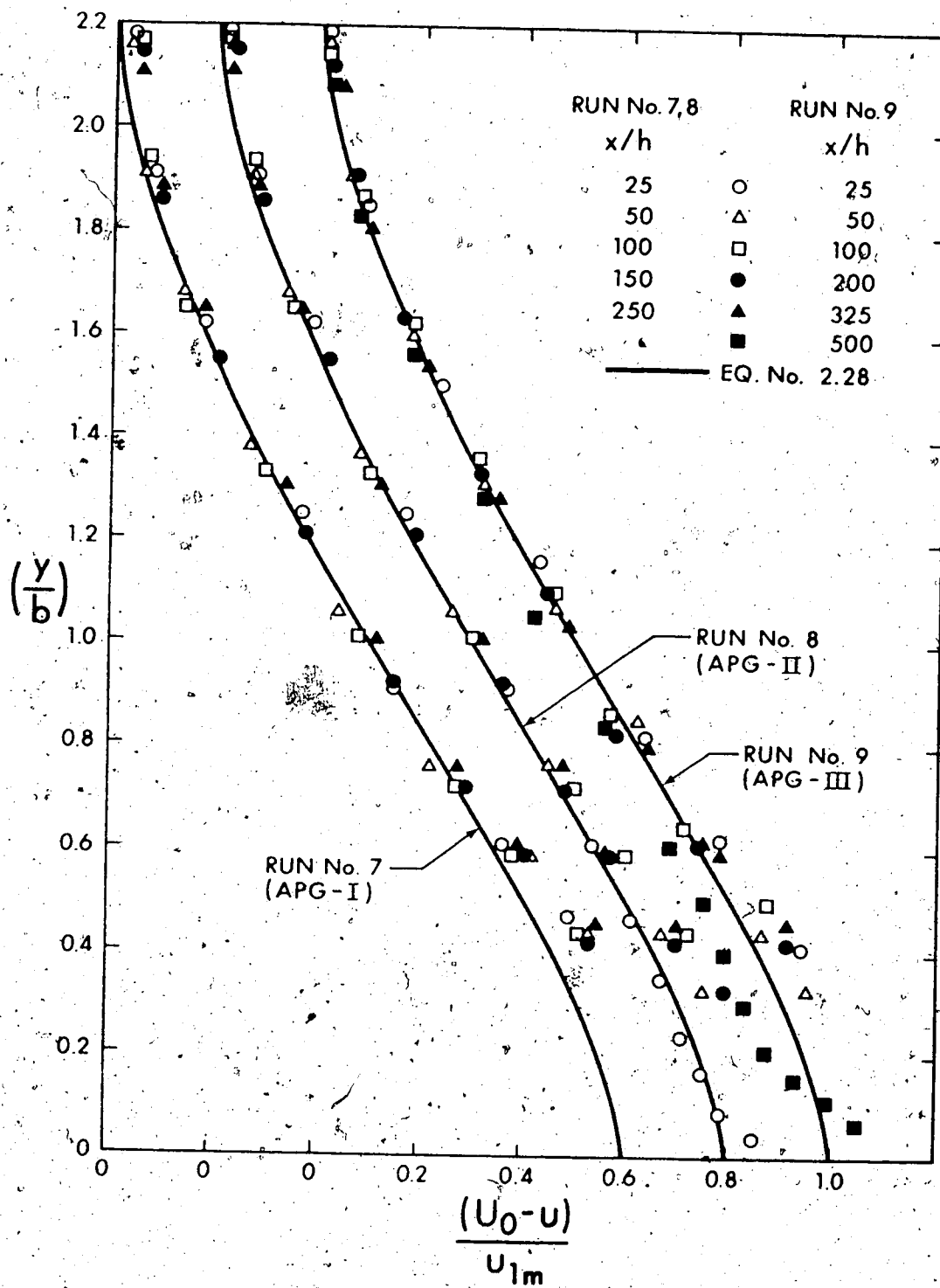


FIGURE 4.15 VELOCITY DISTRIBUTION IN THE OUTER-REGION FOR RUNS 7, 8 AND 9

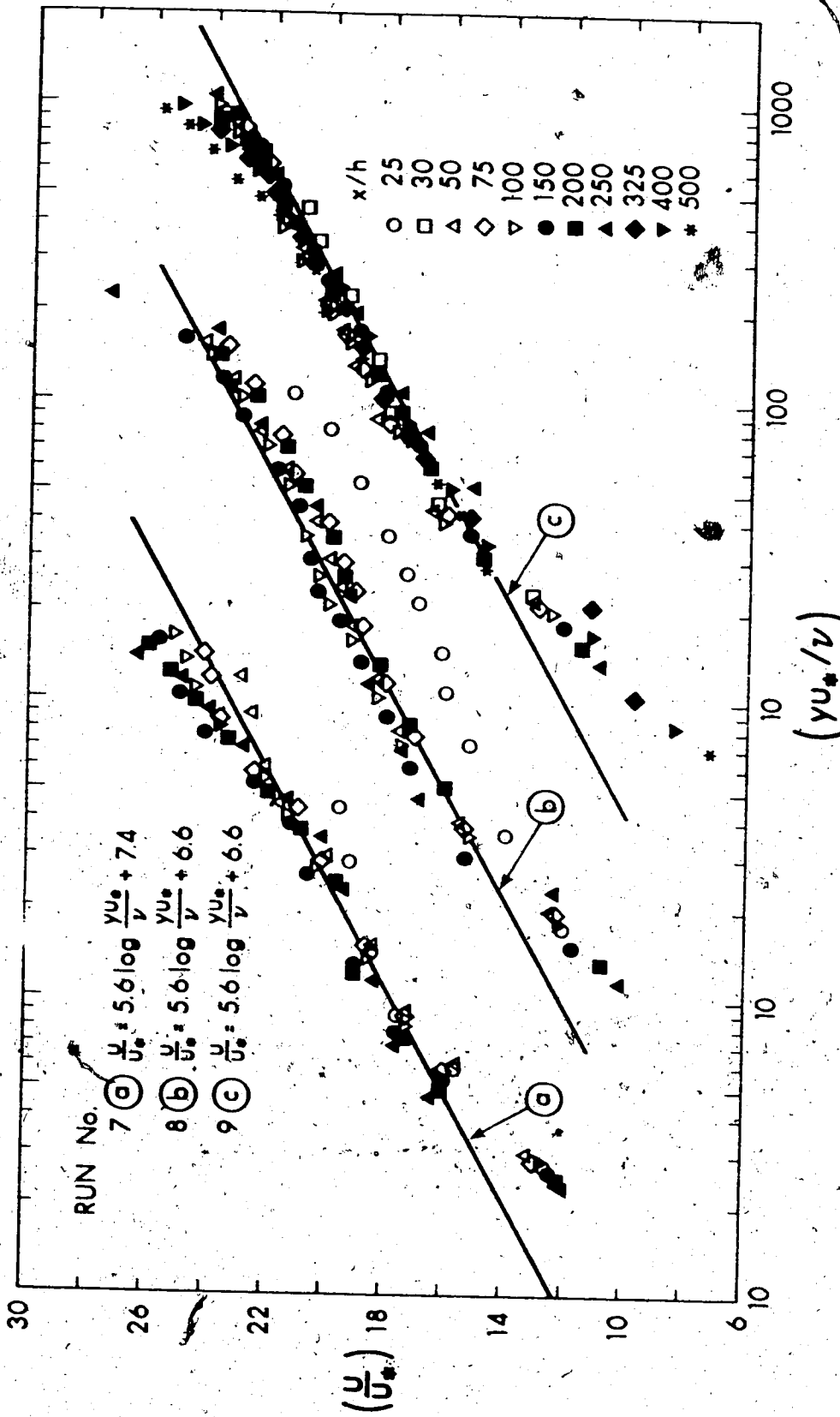


FIGURE 4.16 VELOCITY DISTRIBUTION IN THE INNER-REGION FOR RUNS 7, 8 AND 9

and for APG-II and APG-III, it was of the form:

$$\frac{u}{u_*} = 5.6 \log \frac{yu_*}{\nu} + 6.6 \quad (4.33)$$

These plots confirm the validity of the two-layer hypothesis for wall-wakes with adverse pressure gradients. At very strong adverse pressure gradients, however, the logarithmic profiles may not hold near the wall. For such flows the boundary layer might separate, while the wake profile in the outer region may still hold.

Velocity profiles in the inner region are again plotted, in terms of (u/u_*) versus (y/b) , in Figure (4.17). It can be seen that a logarithmic relationship of the form:

$$\frac{u}{u_*} = 5.6 \log \frac{y}{b} + B_1 \quad (4.34)$$

holds for all three runs. For zero pressure gradient flows the relationship was in the form of a power law, (Figure 4.5). In equation (4.34), B_1 was found to be 26.0 for the best-fit-lines for APG-I and APG-II, and 26.5 for APG-III.

If we compare equation (4.34), (assuming $B_1 = 26.0$), with equation (4.33), we obtain:

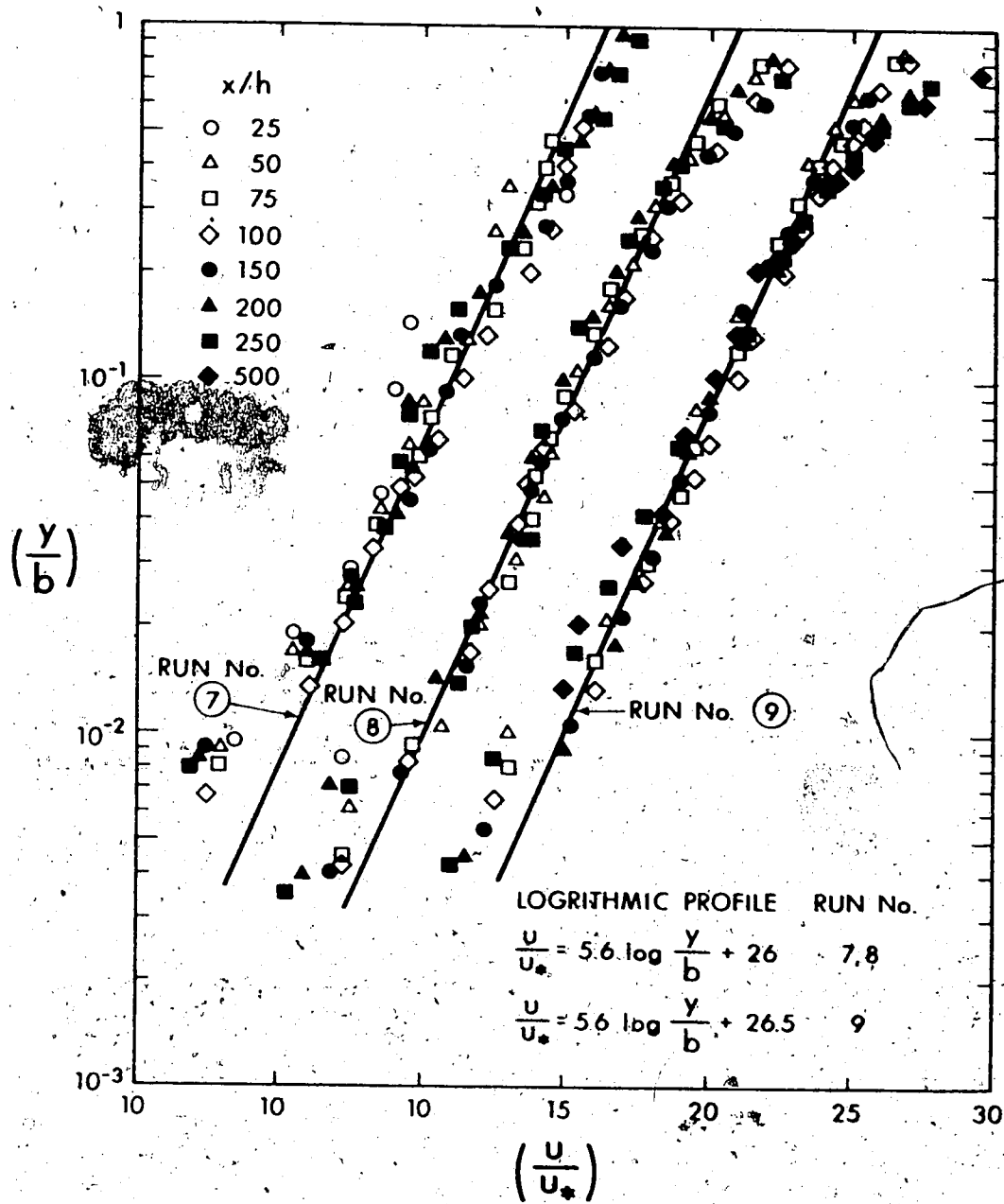


FIGURE 4.17 VELOCITY DISTRIBUTION IN THE INNER-REGION FOR RUNS 7,8 AND 9

$$5.6 \log \frac{bu^*}{\nu} = 19.4,$$

$$\text{or } \frac{bu^*}{\nu} = 10^{3.46} \quad (4.35).$$

In equation (4.35), the factor ν/u_* can be considered as the length scale for the wall-region. Thus we can see that the ratio of the length scale for the outer region, b , to the length scale for the wall region, (ν/u_*) , remains constant for wall-wakes with adverse pressure gradients. Equation (4.35) has been used in determining the expression for the local coefficient of skin friction, $C_f (= \tau_o / \frac{1}{2}\rho U^2)$.

4.3.4 DISTRIBUTION OF BOUNDARY SHEAR STRESS

An expression for the coefficient of skin friction can be obtained if we divide both sides of equation (4.35) by the factor $(Ub/\nu = R_b)$. We obtain:

$$\frac{u^*}{U} = \frac{10^{3.46}}{R_b}$$

$$\text{or } \left(\frac{C_f}{2}\right)^{1/2} = \frac{10^{3.46}}{R_b} \quad (4.36),$$

$$\text{where } C_f = 2 \left(\frac{u^*}{U}\right)^2 = \frac{\tau_o}{\frac{1}{2}\rho U^2}.$$

Squaring equation (4.36), and simplifying, we obtain:

$$C_f = \frac{16.6 \times 10^6}{R_b^2} \quad (4.37)$$

In the above equation, the Reynolds number,

$$R_b = \frac{U b}{\nu}$$

If we substitute for $U \propto (x+x_0)^m$, and $b \propto (x+x_0)$, we obtain:

$$C_f \propto \frac{1}{(x+x_0)^{2(m+1)}} \quad (4.38)$$

The constant of proportionality in the above equation will depend on some appropriate pressure gradient parameter, (or the exponent m).

Equation (4.37), for the skin friction coefficient, C_f , is plotted in Figure (4.18), along with the experiment data for the three pressure gradient runs. It may be seen that the skin frictions for APG-II and APG-III are satisfactorily represented by equation (4.37). For weak pressure gradient flow, (APG-I), the skin friction seems to be independent of R_b , and is more or less constant in the downstream direction.

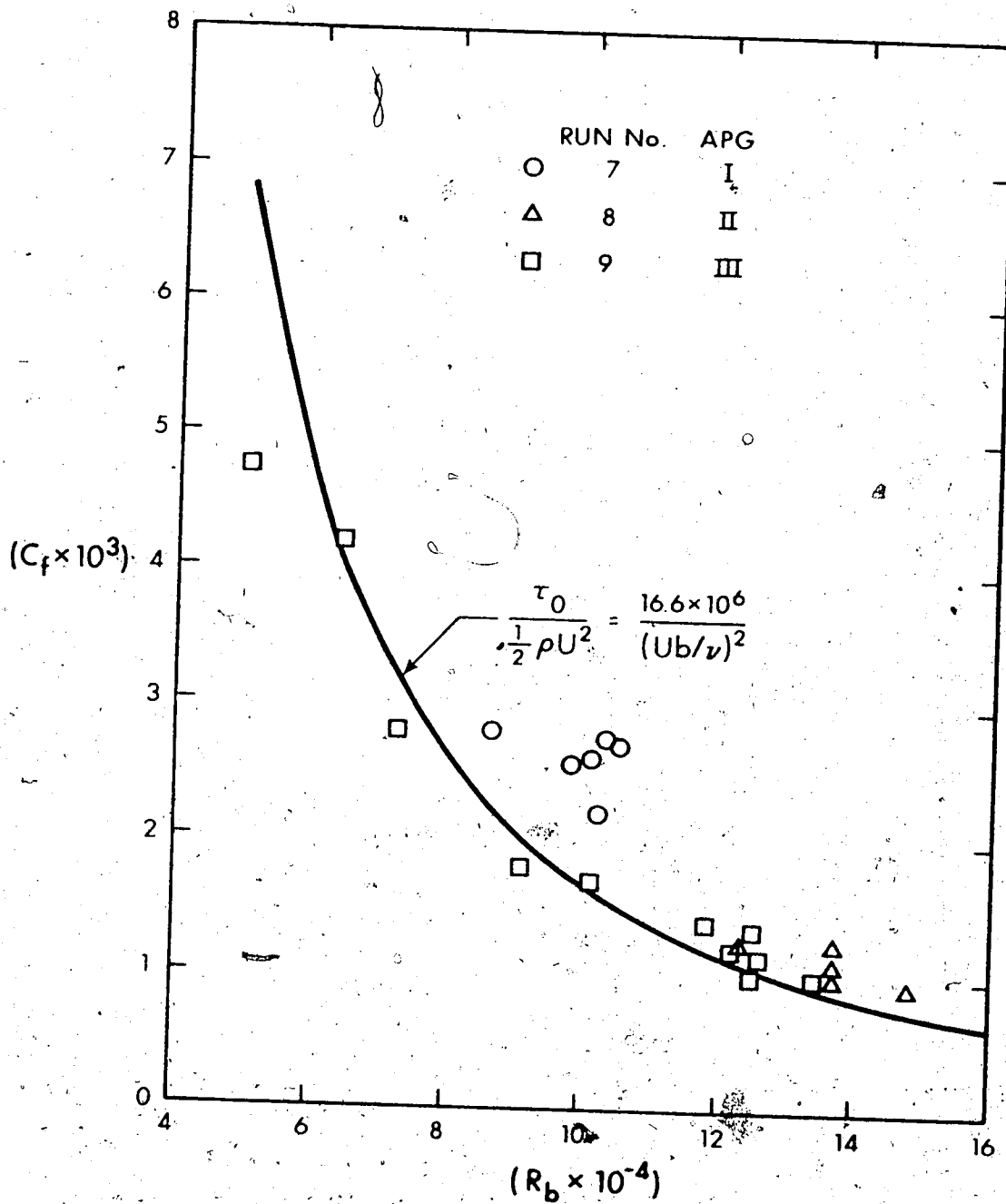


FIGURE 4.18 DISTRIBUTION OF COEFFICIENT OF SKIN FRICTION FOR RUNS 7, 8 AND 9

A single curve for the variation of skin friction indicates that equation (4.37) is independent of any pressure gradient parameter. It seems that the Reynolds number, R_b , could be an important parameter in defining certain flow characteristics for wall-wakes with pressure gradients, especially if the pressure gradient is strong.

4.3.5 VARIATION OF VELOCITY SCALE

Figure (4.19) shows the variation of the non-dimensionalized velocity scale, (u_{1m}/U) , in the longitudinal direction. In the far-wake region, the ratio u_{1m}/U does attain a constant value (shown by the chained line), as predicted by the theory. However, there is a discrepancy between the (u_{1m}/U) value predicted by equation (2.64):

$$\frac{u_{1m}}{U} = 1.42 \left(\frac{3m+1}{2m+1} \right) \quad (2.64),$$

and the one experimentally observed. The ratios of (u_{1m}/U) , experimentally obtained in the far-wake region for the three runs, and the ones predicted by equation (2.64), are tabulated as follows:

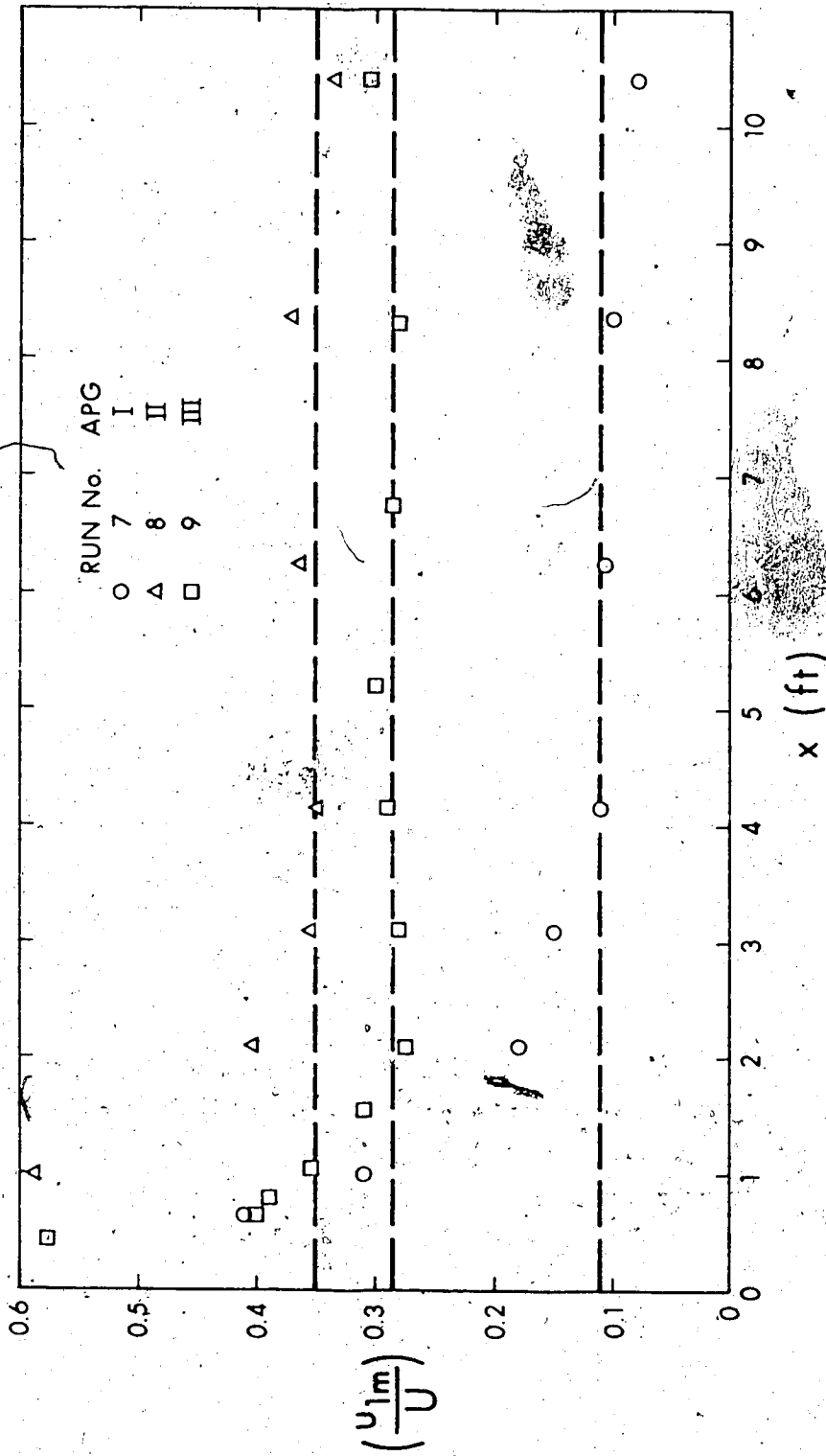


FIGURE 4.19 VARIATION OF VELOCITY SCALE FOR RUNS 7, 8 AND 9

TABLE IV-2
COMPARISON OF THEORETICAL
AND EXPERIMENTAL VALUES
of (u_{1m}/U)

Run No.	APG	m	(u_{1m}/U) (Experiment)	(u_{1m}/U) (Eq. 2.64)
7	I	-0.115	0.110	1.070
8	II	-0.215	0.350	0.835
9	III	-0.310	0.285	0.261

It can be observed that the discrepancy between the two values of (u_{1m}/U) is greater for weak pressure gradient flows (where the exponent $-m$ is small), than for strong pressure gradient flows. For APG-I, equation (2.64) predicts a value of $(u_{1m}/U) > 1$, which is obvious because equation (2.64) gives the limiting values of m as -0.185 and $-1/3$, for self-preserving flows, whereas the exponent m for APG-I is -0.115 , which is beyond the limits of self-preserving flow. However, a constant ratio of (u_{1m}/U) for APG-I, in the far-wake region, and the similarity of the velocity profiles (Figure 4.15, 4.16), indicate that the flow was self preserving for APG-I.

For APG-II, the discrepancy between the two values of (u_{1m}/U) is still too large to be considered as experimental error. A possible reason for the discrepancy could be an error in the coefficient 1.42, in equation

(2.64). This coefficient was obtained as the ratio (F_1/F_2) , in equation (2.63). The numerical values of parameters F_1 and F_2 were evaluated by considering a plane-wake profile, (equation 2.41). For a wall-wake, the values of F_1 and F_2 will be different than the ones given by the plane-wake profile, because of the change in velocity profile near the wall.

For APG-III, the discrepancy between the two values of u_{1m}/U is the smallest. In fact, we can say, in this case, that equation (2.64) agrees fairly well with the experimental data.

The above observations, from Figure (4.19), reveal that the plane-wake analysis of the outer-layer of a turbulent wall-wake predicts values for u_{1m}/U which correspond reasonably well with the experimentally obtained values, for moderately strong adverse pressure gradient flows. For weak adverse pressure gradient flows the predictions are far from the experimental observation. A possible reason for this could be the negligence of the coefficient of skin friction in the momentum integral equation (2.61). If we write the momentum integral equation (equation 2.61) in its complete form, it is:

$$\frac{d}{dx} (u_{1m} U b F_1) - \frac{d}{dx} (u_{1m}^2 b F_2) + \frac{dU}{dx} u_{1m} b F_1 = \frac{\tau_0}{\rho}$$

If we apply the conditions described by equation (2.59), and simplify, we obtain:

$$B_1 B_2 B_3 F_1 (3m+1) (x+x_0)^{2m} - B_1 B_2^2 F_2 (2m+1) (x+x_0)^{2m} = \frac{\tau_0}{\rho}$$

Dividing throughout by $U^2 (= B_3^2 \{x+x_0\}^{2m})$, we get:

$$B_1 (B_2/B_3) F_1 (3m+1) - B_1 (B_2/B_3)^2 F_2 (2m+1) = \frac{\tau_0}{\rho U^2} = \frac{C_f}{2} \quad (4.39).$$

Substituting for $B_2/B_3 = u_{1m}/U$, we obtain:

$$\frac{u_{1m}}{U} \{ (3m+1) F_1 - \{2m+1\} \frac{u_{1m}}{U} F_2 \} = \frac{C_f}{2} \quad (4.40).$$

It is to be noted that equation (4.40) will take the same form as equation (2.63), if we assume that $C_f = 0$. In terms of exponent m , the above equation can be written as:

$$m = \frac{\{C_f/2B_1(u_{1m}/U)\} + (u_{1m}/U) F_2 - F_1}{3F_1 - 2(u_{1m}/U) F_2} \quad (4.41).$$

An examination of the foregoing expression reveals that as $(u_{1m}/U) \rightarrow 0$, the numerator of equation (4.41) tends to infinity, and hence $m \rightarrow \infty$. This is in contrast to the situation for a plane-wake case, in which $m = -1/3$ at $(u_{1m}/U) = 0$. Equation (4.41) is plotted in Figure (4.20), for different values of C_f , assuming Abramovich's expression for B_1 ($=db/dx$), given by equation (2.65):

$$B_1 = \frac{db}{dx} = 0.175 \frac{u_{1m}/U}{1 - \frac{1}{2}(u_{1m}/U)}$$

The values of F_1 ($=1.02$) and F_2 ($=0.717$) were assumed to be the same as for a plane wake.

Figure (4.20) shows that for each value of m , we obtain two values of (u_{1m}/U) ; one is small and the other is large. It seems that for a wall-wake, the smaller value of (u_{1m}/U) gives the right solution at weak pressure gradients. It may also be noticed that the discrepancy between the wall-wake equation (equation 4.41), and the plane-wake equation (equation 2.64), is not large on the right hand side of Figure (4.20). Either of the two equations may be used for the determination of (u_{1m}/U) , for strong adverse pressure gradient flows.

To determine (u_{1m}/U) from Figure (4.20), we must know the skin friction, C_f . For adverse pressure gradient

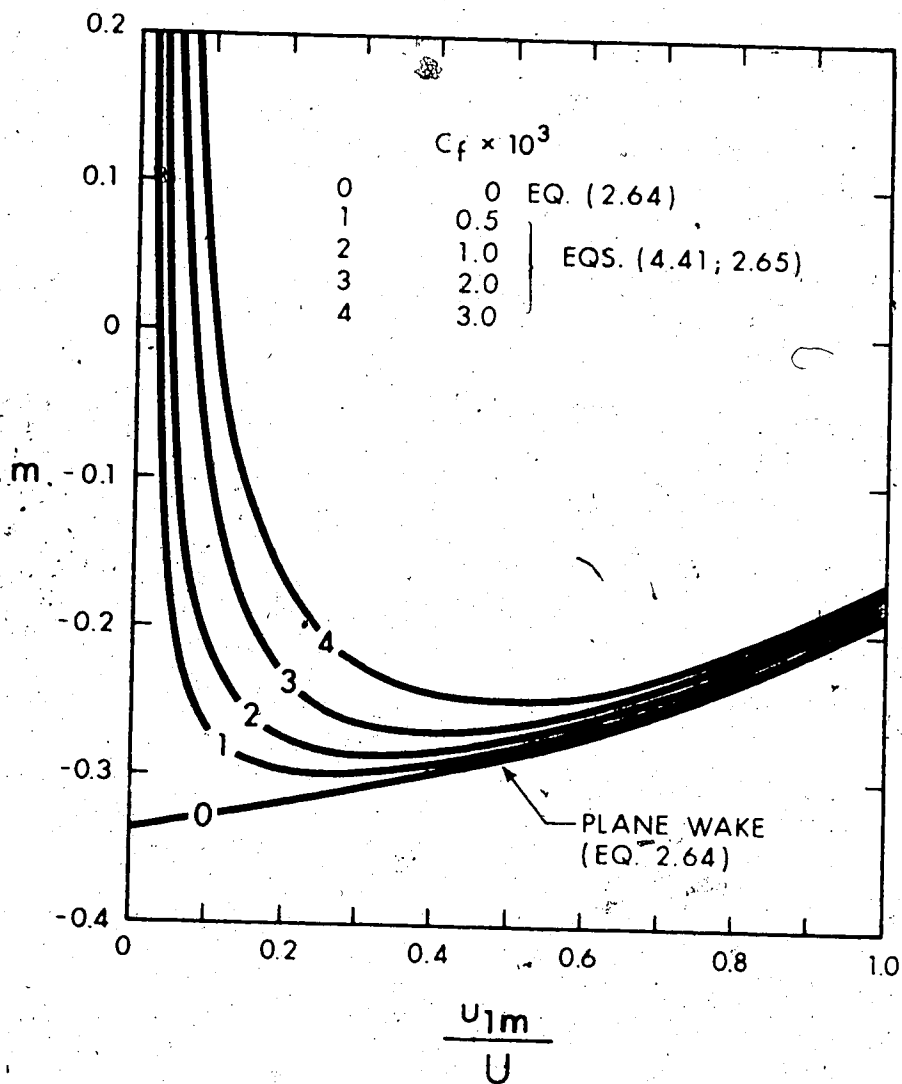


FIGURE 4.20 THEORETICAL VARIATION OF EXPONENT m FOR WALL-WAKE WITH ADVERSE PRESSURE GRADIENT FLOWS

flows, the coefficient of skin friction usually decreases in the downstream direction. This has been observed in Figure (4.18) for two strong pressure gradient flows. The same plot also indicates that C_f is more or less constant for APG-I. More measurements on weak adverse pressure gradient flows are necessary before a definite statement can be made on whether the skin friction remains constant for wall-wake flows. For the present case, the value of C_f for APG-I may be taken as 2.5×10^{-3} . For this value of C_f , and with $m = -0.115$, we obtain $(u_{1m}/U) = 0.12$. This value is in excellent agreement with the experimental value of 0.11.

The large discrepancy between the experimental and the predicted values for u_{1m}/U , (Table IV-2), for APG-II, still cannot be explained. Figure (4.20) does not help much in predicting the value of u_{1m}/U , because of the fact that the skin friction is not constant. Figure (4.20), (equation 4.41), would be of great help if it were possible to obtain an expression for C_f in terms of the exponent m (or some other suitable pressure gradient parameter). For this, however, more measurements are necessary in a varied range of adverse pressure gradient flows. An important revelation obtained from equation (4.41) is that the backflow predicted by the plane-wake equation for $-m < 0.185$, does not hold for the case of the wall-wake. On

the contrary, the ratio (u_{1m}/U) for the wall-wake reduces considerably for weak adverse pressure gradient flows.

4.3.6 VARIATION OF LENGTH SCALE

Figure (4.21) shows the variation of length scale, b , in the longitudinal direction. A linear variation of the length scale with x in the far-wake region, can be observed for all three pressure gradient flows. Such a variation in the length scale was predicted by theory for self-preserving wake flows with pressure gradient. The slopes, $db/dx (=B_1)$, for the three runs were determined, and a comparison with those obtained by Abramovich's equations (equations 2.65, 2.66), and by Gartshore's equation (equation 2.74), is shown in the following table.

TABLE IV-3: COMPARISON OF THEORETICAL AND EXPERIMENTAL VALUES OF b

Run No.	APG	m	B_1 (eq. 2.65)	B_1 (eq. 2.66)	B_1 (eq. 2.74)	B_1 (expt.)
I	-0.115		0.0186	0.500	0.0140	0.0045
S	II	-0.215	0.0690	0.230	0.0127	0.0135
9	III	-0.310	0.0530	0.035	0.0116	0.0130

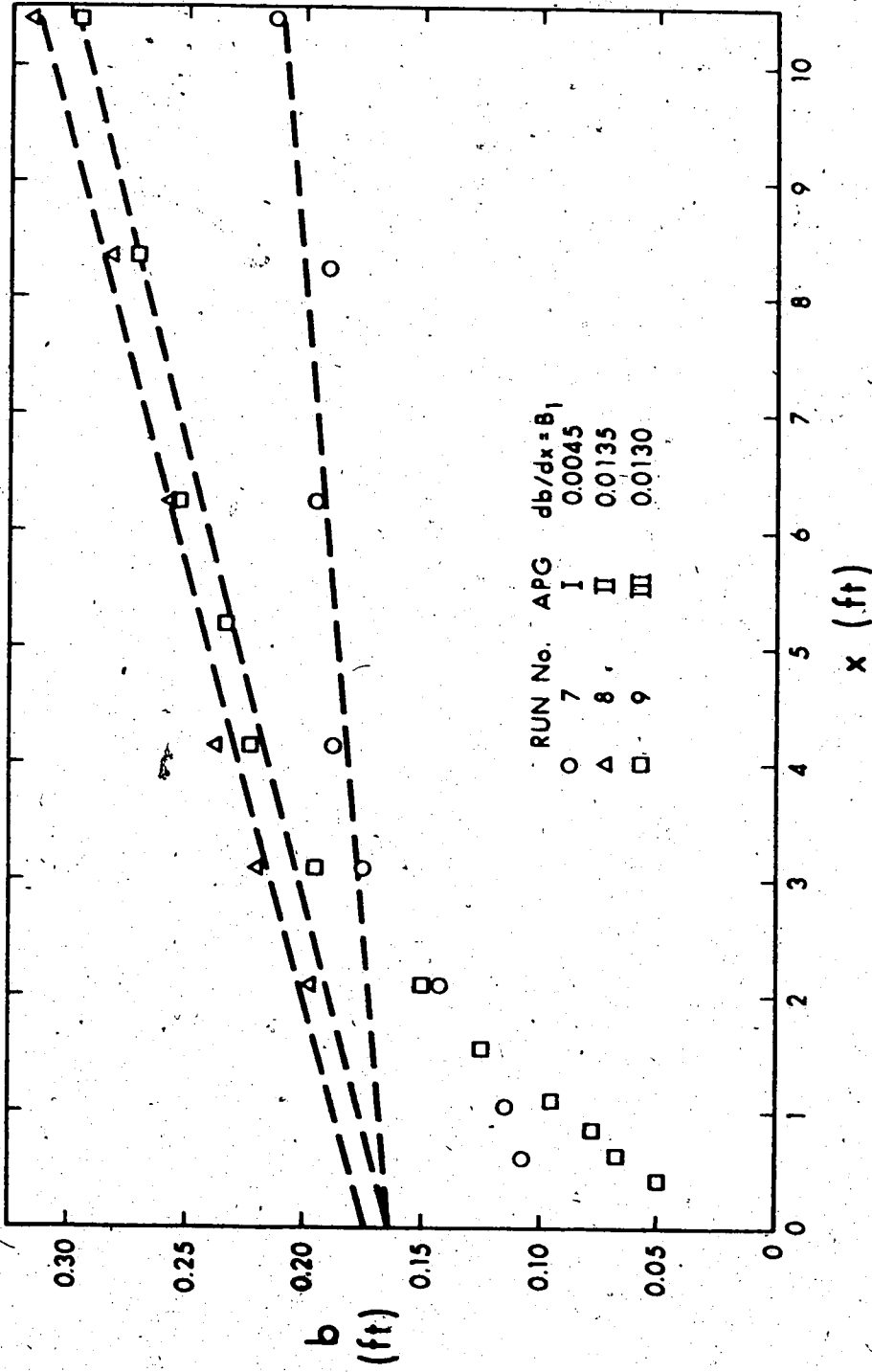


FIGURE 4.21 VARIATION OF LENGTH SCALE FOR RUNS 7, 8 AND 9

It may be seen that the coefficient B_1 , obtained from Gartshore's equation, (2.74), gives the most satisfactory result for APG-II and APG-III. For APG-I, the discrepancy is very large. In using Abramovich's equation, (2.65), measured values of (u_{1m}/U) were used, whereas theoretical values of (u_{1m}/U) , given by equation 2.64, were used in equation (2.66). Both these equations, (2.65 and 2.66), can be seen to predict much higher values of B_1 than the ones experimentally obtained. It is to be noted that the coefficient 0.163, in equation (2.65), was obtained by assuming the boundary condition for zero pressure gradient flow in the polynomial for db/dx . It is therefore not illogical that there would be error in the estimate of B_1 with the use of this equation.

4.3.7 VARIATION OF WAKE-DISPLACEMENT THICKNESS, δ_w

An expression for wake-displacement thickness, δ_w , can be obtained by equating the wake profile:

$$\frac{U-u}{u_{1m}} = (1 - 0.293 \left\{ \frac{y}{b} \right\}^{3/2})^2 \quad (4.42),$$

and the wall profile, (equation 4.34):

$$\frac{u}{u_*} = 5.6 \log \frac{y}{b} + 26 \quad (4.34),$$

at $y = \delta_w$; $u = u_w$, which gives:

$$(1 - 0.293 \left\{ \frac{\delta_w}{b} \right\}^{3/2})^2 = \frac{U}{u_{1m}} - \frac{u_*}{u_{1m}} (5.6 \log \frac{\delta_w}{b} + 26) \quad (4.43).$$

Equation (4.43) is too complicated to solve for δ_w . An approximate solution for δ_w can be obtained if we assume that the shear stress at $y = \delta_w$, as derived from the two profiles, is equal. Thus the slopes, $\partial u / \partial y$ at $y = \delta_w$, must be equal for the two profiles.

Differentiating equations (4.42) and (4.34), with respect to y , and equating $(\partial u / \partial y)$ at $y = \delta_w$, we obtain:

$$\frac{2.44 u_*}{\delta_w} = 0.88 \left[\frac{u_{1m}}{b} \left(\frac{\delta_w}{b} \right)^{1/2} \left\{ 1 - 0.293 \left(\frac{\delta_w}{b} \right)^{3/2} \right\} \right]$$

$$\text{or, } \frac{u_*}{u_{1m}} = 0.36 \left[\left(\frac{\delta_w}{b} \right)^{3/2} - 0.293 \left(\frac{\delta_w}{b} \right)^3 \right] \quad (4.44)$$

If $(\delta_w/b) < 1$, so that the second term on the right hand side is small enough to neglect, in comparison to the first term, we can write:

$$\frac{u_*}{u_{1m}} = 0.36 \left(\frac{\delta_w}{b} \right)^{3/2} \quad (4.45)$$

Equation (4.45) indicates that the factor (δ_w/b) will vary with the ratio (u_*/u_{1m}) . It is to be noted that both the shear velocity u_* and the velocity defect u_{1m} depend on the pressure gradient in the same manner. In adverse pressure gradient flows both velocities decrease in the downstream direction.

If we substitute for u_* from equation (4.35), into equation (4.45) and simplify, we obtain:

$$\left(\frac{\delta_w}{b}\right)^{3/2} \approx \frac{0.8 \times 10^4}{(bu_{1m}/\nu)} \quad (4.46)$$

In the above equation the factor (bu_{1m}/ν) is proportional to the Reynolds number $R_b (=Ub/\nu)$ because u_{1m} is proportional to U . If we consider the fact that

$$b \propto (x+x_0)$$

$$\text{and } u_{1m} \propto (x+x_0)^m,$$

then from the above equation we obtain:

$$\frac{\delta_w}{b} \propto (x+x_0)^{-2(m+1)/3} \quad (4.47)$$

This expression indicates that δ_w^* will decrease as we move in the downstream direction from the obstacle. This means that the outer region will grow, and the inner region will diminish, in the down-stream direction. The constant of proportionality in the above equation will depend on the pressure gradient. Experimental verification of equations (4.47) and (4.46) was not possible, because of the scatter of the data for the two velocity profile plots in Figures (4.15 and 4.17).

4.3.8 VARIATION OF BOUNDARY LAYER PARAMETERS

Boundary layer displacement thickness, δ^* , momentum thickness, θ , and the shape parameter, H , as derived from integration of the velocity profiles, are plotted in Figure (4.22). The boundary layer parameters decrease at first and then steadily increase. The high values of δ^* and θ , near the obstacle, are indicative of high order of turbulence present in this region.

The strong adverse pressure gradient, (APG-III), has increased all three parameters, with the greatest difference being that for δ^* .

The increase in θ , even though the skin friction decreased in going from APG-II to APG-III, is explained by the fact that $d\theta/dx$, in the Kármán momentum equation:

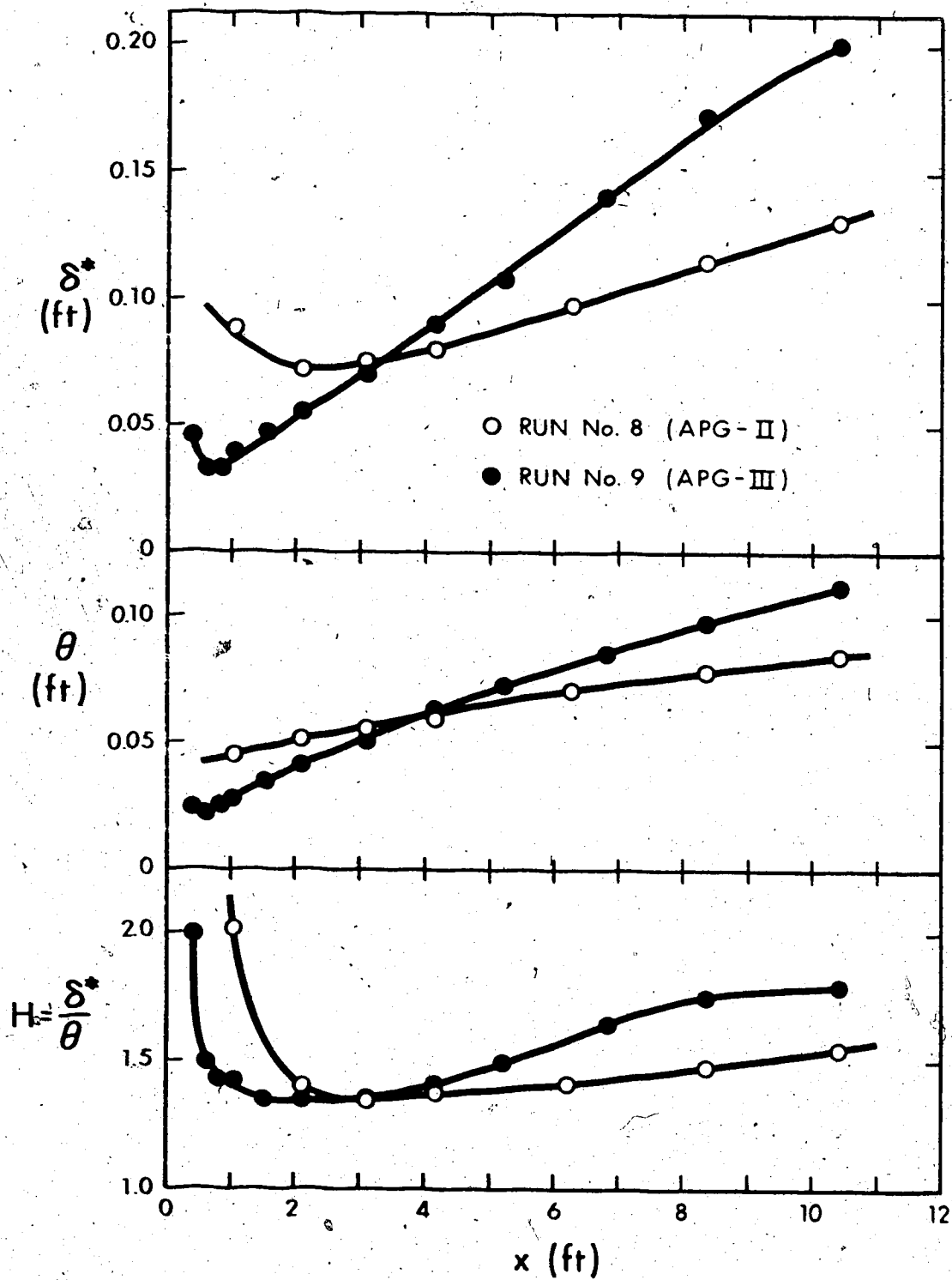


FIGURE 4.22. VARIATION OF BOUNDARY LAYER PARAMETERS FOR RUNS 8 AND 9

$$\frac{d\theta}{dx} = \frac{\theta}{2\rho U^2} \cdot \frac{dp}{dx} \left(\frac{\delta^*}{2\theta} + 1 \right) + \frac{\tau_0}{\rho U^2}$$

is controlled largely by the first term.

CHAPTER V

TURBULENCE CHARACTERISTICS OF WALL-WAKE

5.1 INTRODUCTION

This chapter presents the experimental analysis of the turbulence characteristics of the wall-wake. Many results of measurements on turbulence intensities in boundary layers as well as in plane-wakes have been published, yet no such results are available for wall-wakes. Because of the lack of such material, it becomes a very difficult task to make any very conclusive statements about the structure of turbulence in a wall-wake. In the following pages an attempt has been made to explain the behaviour of some of the turbulence characteristics of wall-wakes.

Since the aim of the present study was to give a qualitative analysis of the turbulence characteristics, only five experiments were selected for turbulence measurement. Three of these were from Series I (runs number 2, 4 and 6 - rough surface), and two from Series II (APG II and APG III). The average free stream velocity for zero pressure gradient flows was 96.0 ft./sec., and the free stream turbulence was 0.72 per cent. The diameter of the X-probe used prohibited the taking of measurements at distances any closer to the wall than 0.012 feet.

Since it was not possible to apply all the corrections needed for the hot-wire measurements, none were applied. The results presented here, however, will give an understanding of the development of turbulence characteristics from one section to the other.

The measured values of turbulence quantities for the five runs are tabulated in Appendix B.

5.2 TURBULENCE INTENSITIES

Measured values of the u-component of turbulence intensity, with respect to the free stream velocity U_0 , for zero pressure gradient flows (runs number 2, 4 and 6), are plotted in Figure 5.1. The nature of the distribution of the longitudinal component of turbulence intensity is essentially the same for all three runs. A high level of turbulence in the near wake region ($x/h = 25, 50$) results from the disturbance to the flow caused by the obstacle. Since the near wake region is the region of intense turbulence, it is expected to have a much higher level of turbulence than the far-wake region. The maxima can be seen to occur at about the half-wake width ($y/h = 1$) in the near wake region. Since the turbulent boundary layer is not fully developed in this region, the turbulence intensity gradually decreases as we move towards the wall, instead of attaining its maximum value. At $x/h = 100$ the curve is more flattened and the

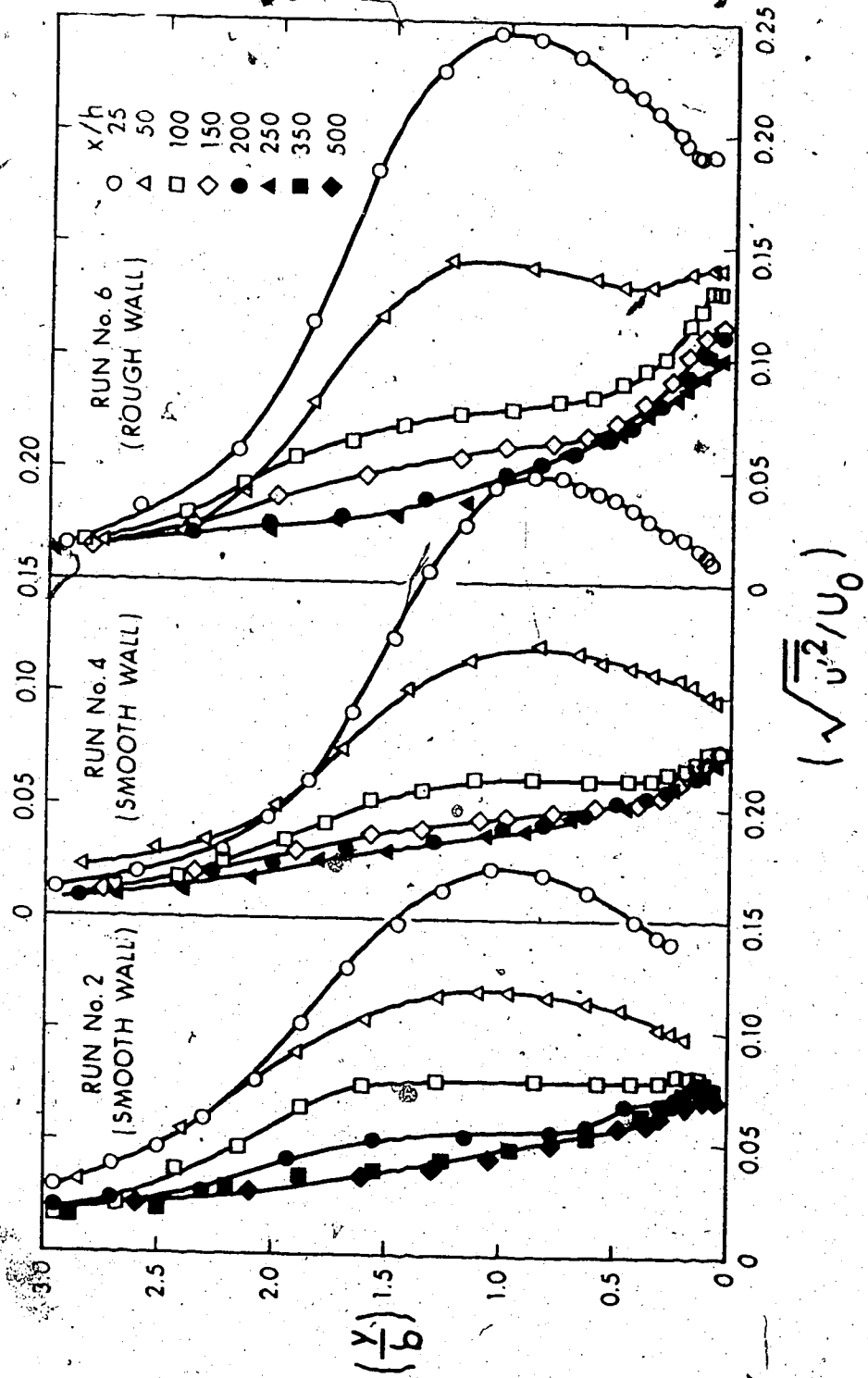


FIGURE 5.1 INTENSITY OF u-COMPONENT OF TURBULENCE FOR RUNS 2, 4 AND 6

turbulence intensity is practically constant in the central region of the flow. The maximum occurs very near the wall, indicating that the turbulence structure in the wall region is fully established. Similarity in the profiles is not observable in the outer region since U_0 (instead of u_{lm}) has been used as the velocity scale.

The only noticeable effect of the height and shape of the obstacle appears in the relative magnitude of turbulence intensity in the near wake region (runs number 2 and 4), whereas the roughness of the wall, in run number 6, causes a higher level of turbulence throughout the flow region. The maximum intensity of turbulence in the far-wake region of the rough wall flow can be seen to be approximately 50% higher than that of the smooth wall flow.

Figure 5.2 shows plots of the longitudinal component of turbulence intensity for two adverse pressure gradient flows. Application of adverse pressure gradient affects the turbulence quantities in the following ways (Scottron, 1967).

- (i) There is a rapid thickening of the boundary layer and an earlier transition from laminar to turbulent flow.
- (ii) A reduction in wall shear stress occurs, producing a reduction in the turbulence level near the wall.

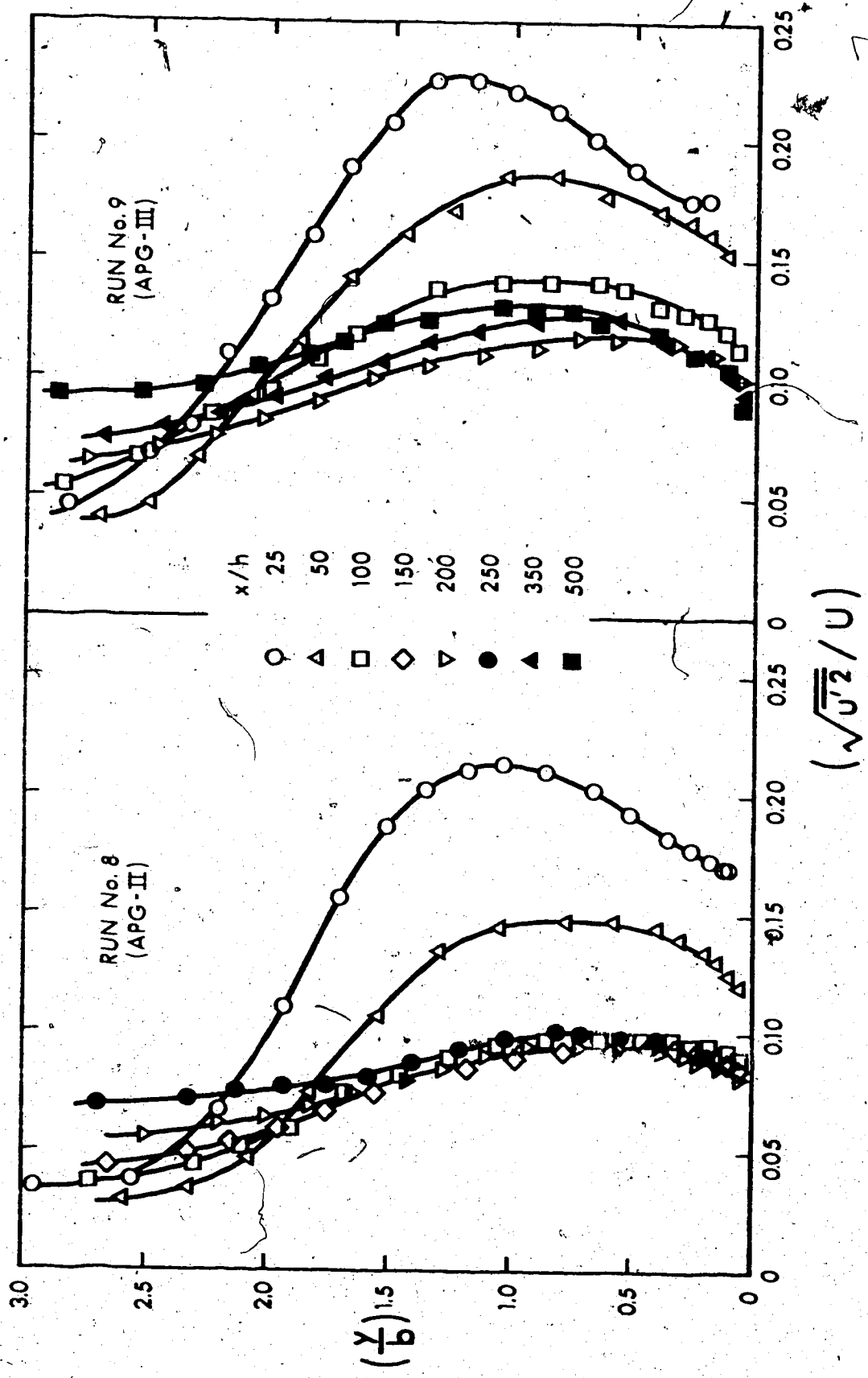


FIGURE 5.2 INTENSITY OF u-COMPONENT OF TURBULENCE FOR RUNS 8 AND 9

- (iii) A general increase in the turbulence level of the whole region is noted. This effect seems to override the other effects (such as wall shear stress variation).
- (iv) There is a high level of turbulence at distances well away from the wall.

The drop in wall shear stress which results from the application of adverse pressure gradient reduces the turbulence intensity near the wall. However, the influence of continued pressure rise and upstream generated turbulence, serve to produce a higher intensity of turbulence well away from the wall.

A high level of turbulence in the near-wake region can again be observed, for both adverse pressure gradient flows, in Figure (5.2). For the weak pressure gradient flow (APG II), a complete similarity in profile, from very near the wall up to $y/b=1.5$, can be observed for $x/h > 100$. Beyond this point, ($y/b > 1.5$), the intensity of turbulence tends to increase in the downstream direction. The intensity of turbulence in the outer region thus grows because of the application of adverse pressure gradient. The strong adverse pressure gradient flow, (APG III), exhibits essentially the same features, except that the intensity of turbulence starts increasing at much smaller values of y/b (≈ 0.4). It can be concluded that the application of adverse pressure gradient prohibits the diffusive

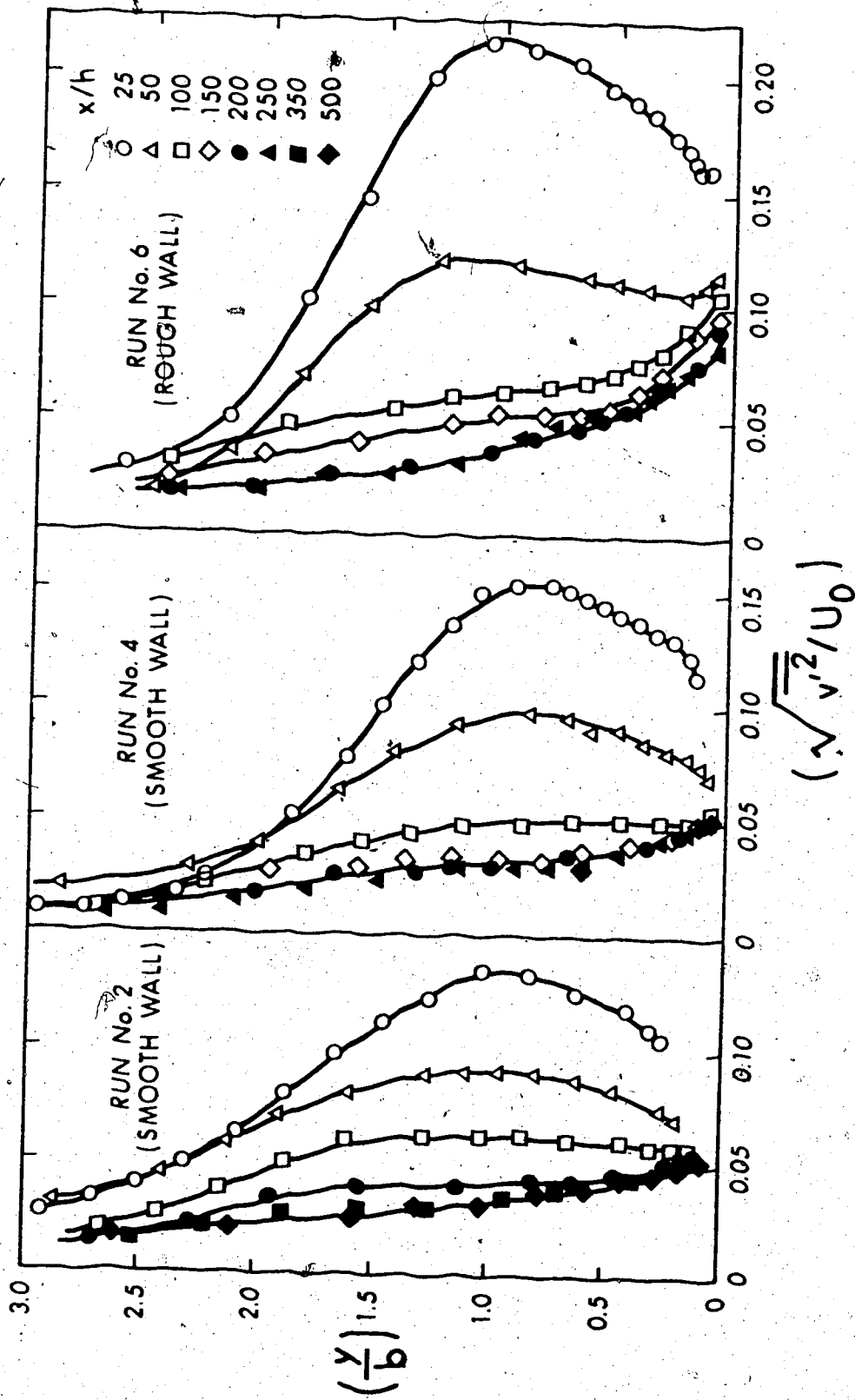


FIGURE 5.3 INTENSITY OF v-COMPONENT OF TURBULENCE FOR RUNS 2, 4 AND 6

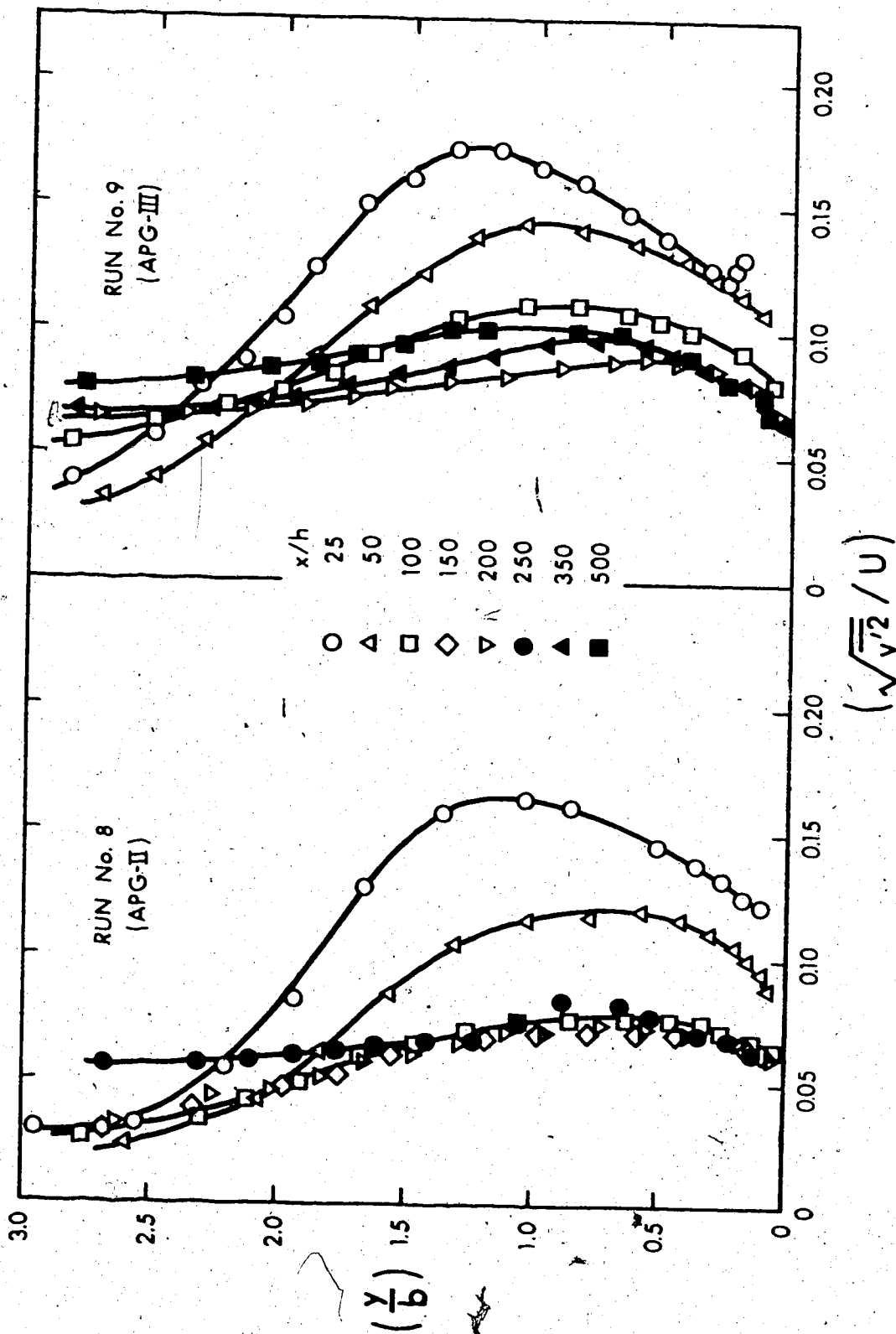


FIGURE 5.4 INTENSITY OF V-COMPONENT OF TURBULENCE FOR RUNS 8 AND 9

behaviour of the wake and, in fact, increases the turbulence level (in the outer region of the flow) in the downstream direction. The effect of the wall on the intensity of turbulence seems to diminish with a strong adverse pressure gradient. A steeper gradient of profile near the wall, and a generally higher magnitude of turbulence intensity, can also be observed for the strong adverse pressure gradient flow. The outward movement of wall-generated turbulence, which is due to the adverse pressure gradient, is clearly noticeable, as the turbulence intensities attain their maximum value at points away from the wall.

The v and w components of turbulence intensity are plotted in Figures (5.3 to 5.6). The behaviour of the transverse components can be seen to be essentially the same as that of the u -component, except that their magnitudes are smaller than that of the longitudinal component (anisotropy). The degree of anisotropy increases as we move towards the wall, for all the cases. For all five runs, the u -component of the intensity of turbulence was found to be the largest, and the w -component the smallest.

In Figures 5.7, 5.8 and 5.9 (the latter two figures are shown at the end of the chapter), the u -components of turbulence intensity, relative to the local mean velocity, \bar{u} , for zero pressure gradient flows, are plotted. These

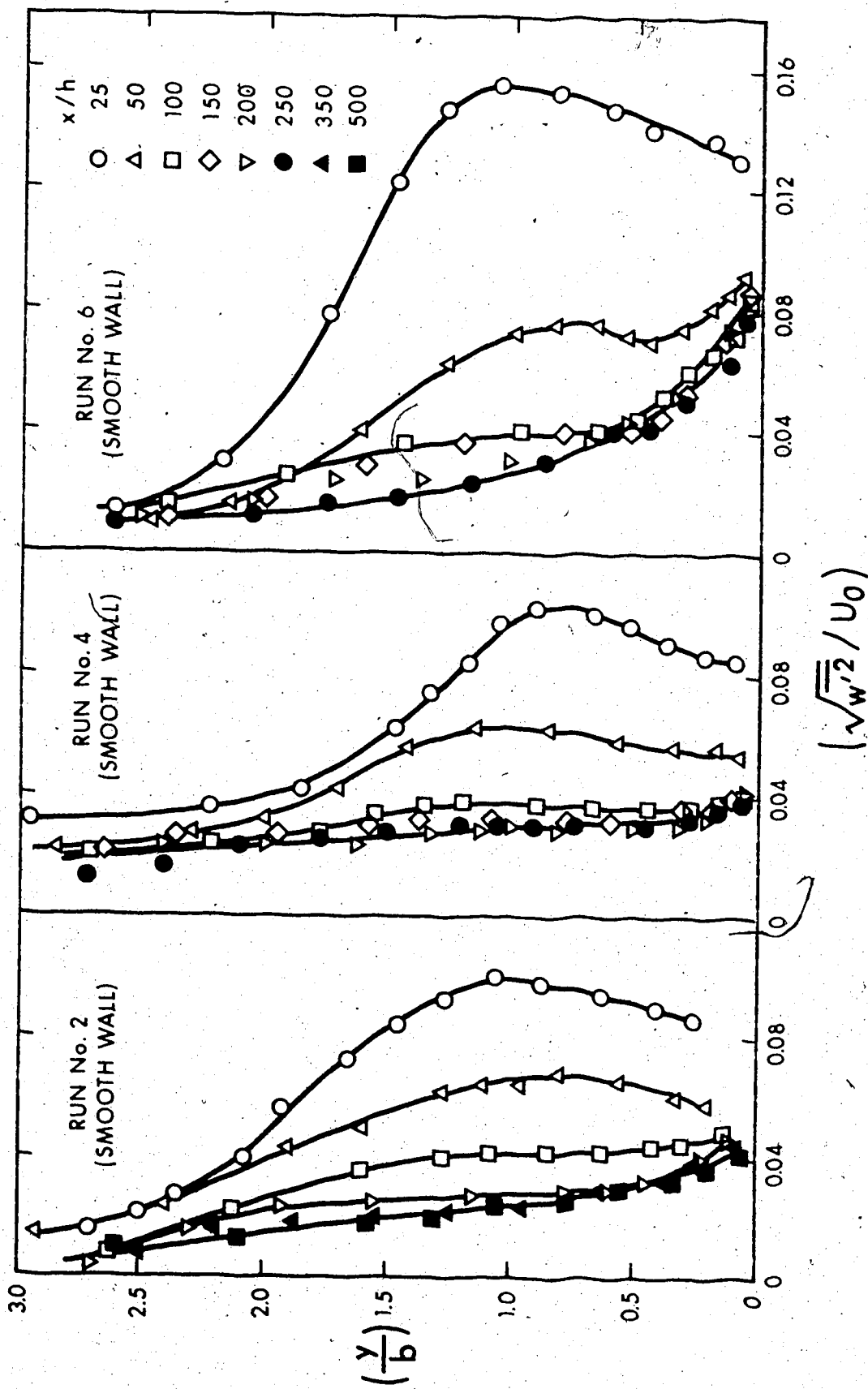


FIGURE 5.5 INTENSITY OF w-COMPONENT OF TURBULENCE FOR RUNS 2,4 AND 6

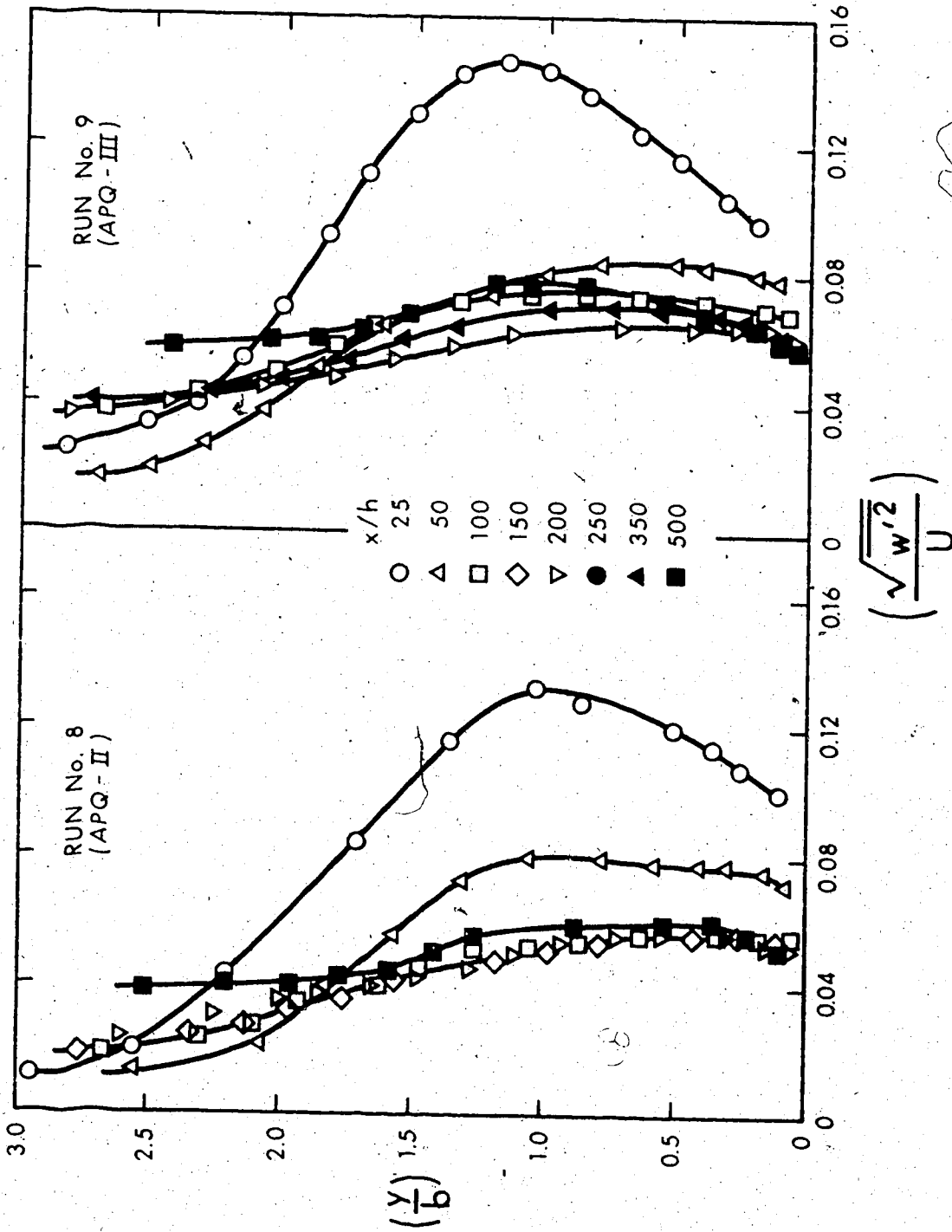


FIGURE 5.6 INTENSITY OF w-COMPONENT OF TURBULENCE FOR RUNS 8 AND 9

profiles are compared with $\sqrt{u'^2}/U_0$ profiles in the same plot. The general trend of both profiles is the same in the outer region. Near the wall the relative intensity $\sqrt{u'^2}/\bar{u}$ can be seen to increase rapidly, especially in the far-wake region. These plots indicate that the mean velocity, \bar{u} , near the wall, decreases at a faster rate than the root mean square value of the turbulence fluctuation, $\sqrt{u'^2}$. The difference between the two profiles seems to remain constant in the downstream direction.

For adverse pressure gradient flows, (Figures 5.10 and 5.11, shown at the end of the chapter), this difference can be seen to increase in the downstream direction. This indicates that, in the case of adverse pressure gradient, mean velocity near the wall decreases in the downstream direction at a faster rate than the turbulent fluctuations decrease. The stronger the pressure gradient, the more pronounced the effect, as can be observed in Figure (5.11).

The three components of relative turbulence intensity, and the total turbulence intensity,

$$T = (\{\overline{u'^2} + \overline{v'^2} + \overline{w'^2}\}/3)^{1/2}/U$$

in the far-wake region, are plotted (for all five runs) in Figure (5.12), for the sake of comparison. The profiles at the last station for each run (viz. at $x/h = 250$ for

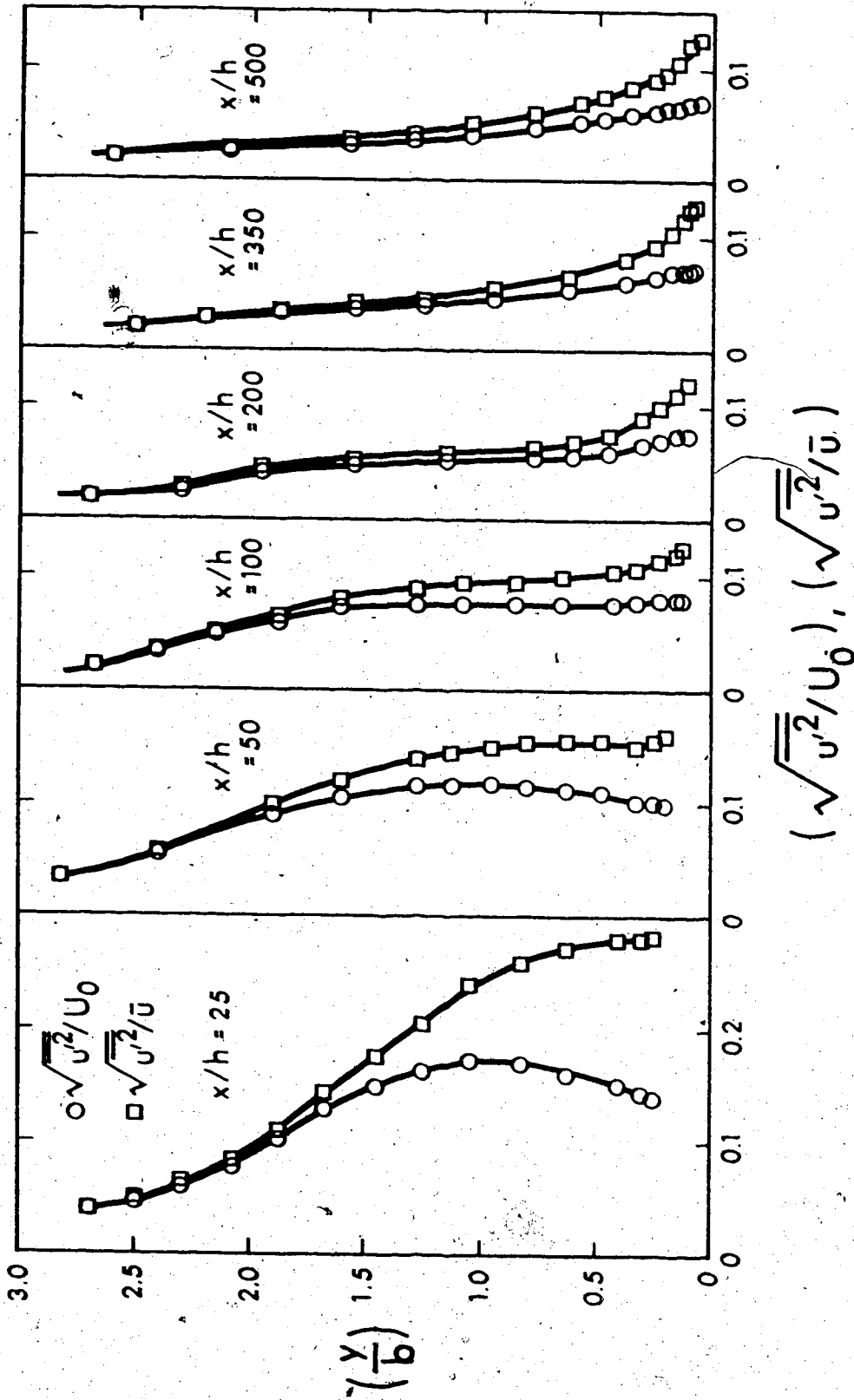


FIGURE 5.7 LONGITUDINAL COMPONENT OF RELATIVE TURBULENCE INTENSITY FOR RUN NUMBER 2

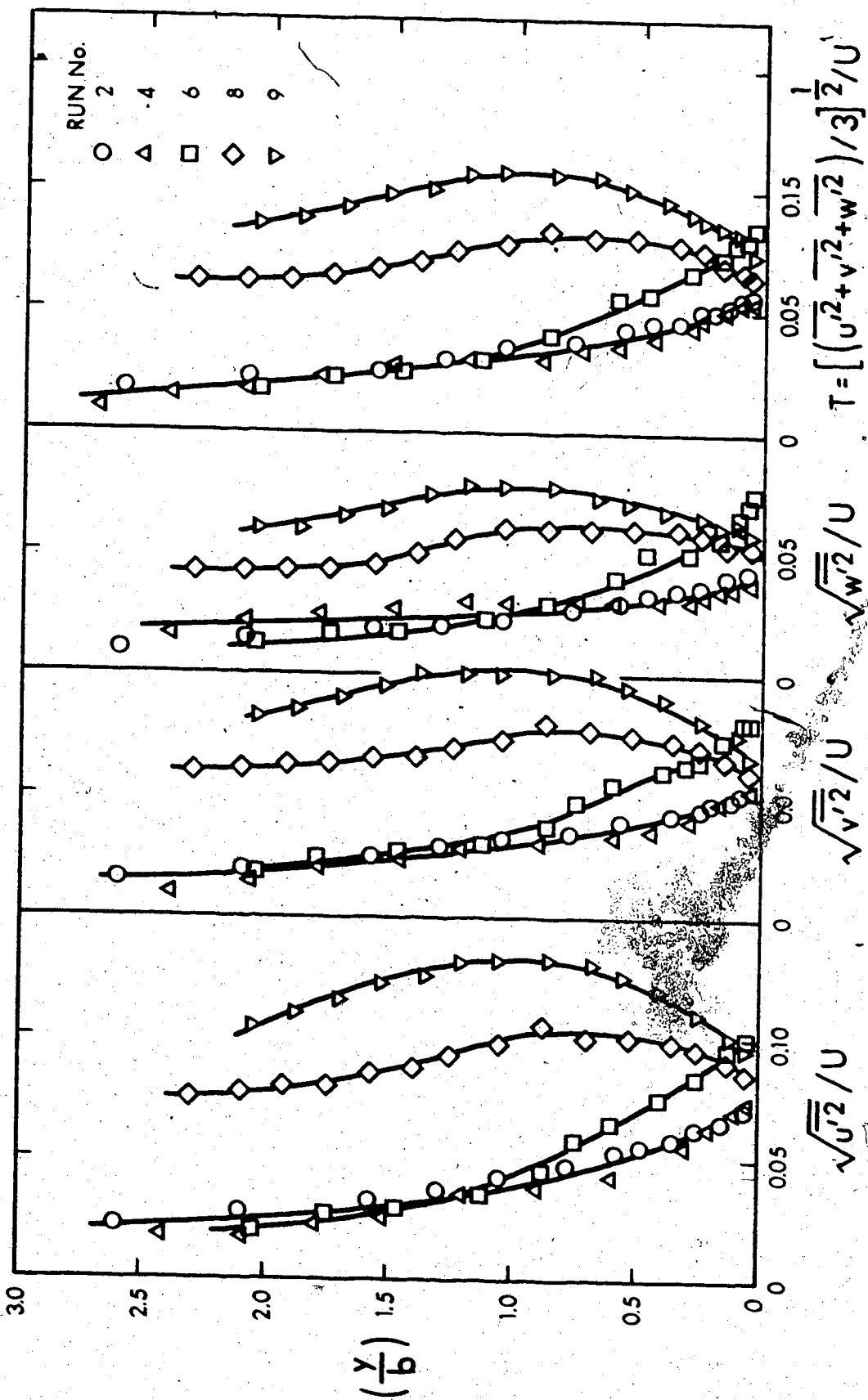


FIGURE 5.12 DISTRIBUTION OF TURBULENCE INTENSITY IN THE FAR-WAKE REGION FOR RUNS 2, 4, 6, 8 AND 9

runs 4, 6 and 8 and at $x/h = 500$ for runs 2 and 9), are in fact compared in this plot.

For runs 2 and 4 (smooth wall with zero pressure gradient), it can be observed that the three components of turbulence intensity for one run are very nearly equal to the corresponding components in the other run. This indicates that the size of the obstacle does not influence the turbulence intensity in the far-wake region. The influence of wall roughness and the adverse pressure gradients can be clearly observed in these plots. Another distinct feature is the similarity of the profiles of the three components of turbulence intensity in the far-wake region.

5.3 SHEAR STRESS DISTRIBUTIONS FOR ZERO PRESSURE GRADIENT FLOWS

The distributions of turbulence shear stress

$$\frac{\tau_t}{\rho U_0^2} = \frac{\overline{u'v'}}{U_0^2}$$

are shown in Figure (5.13), for smooth wall with zero pressure gradient flows. In the near wake region the maximum shear stress can be seen to occur away from the wall. For $x/h \approx 150$, the similarity in profiles can clearly be observed with the maxima occurring very near the wall. A constant shear layer, close to the wall, can also be noticed in the far wake region.

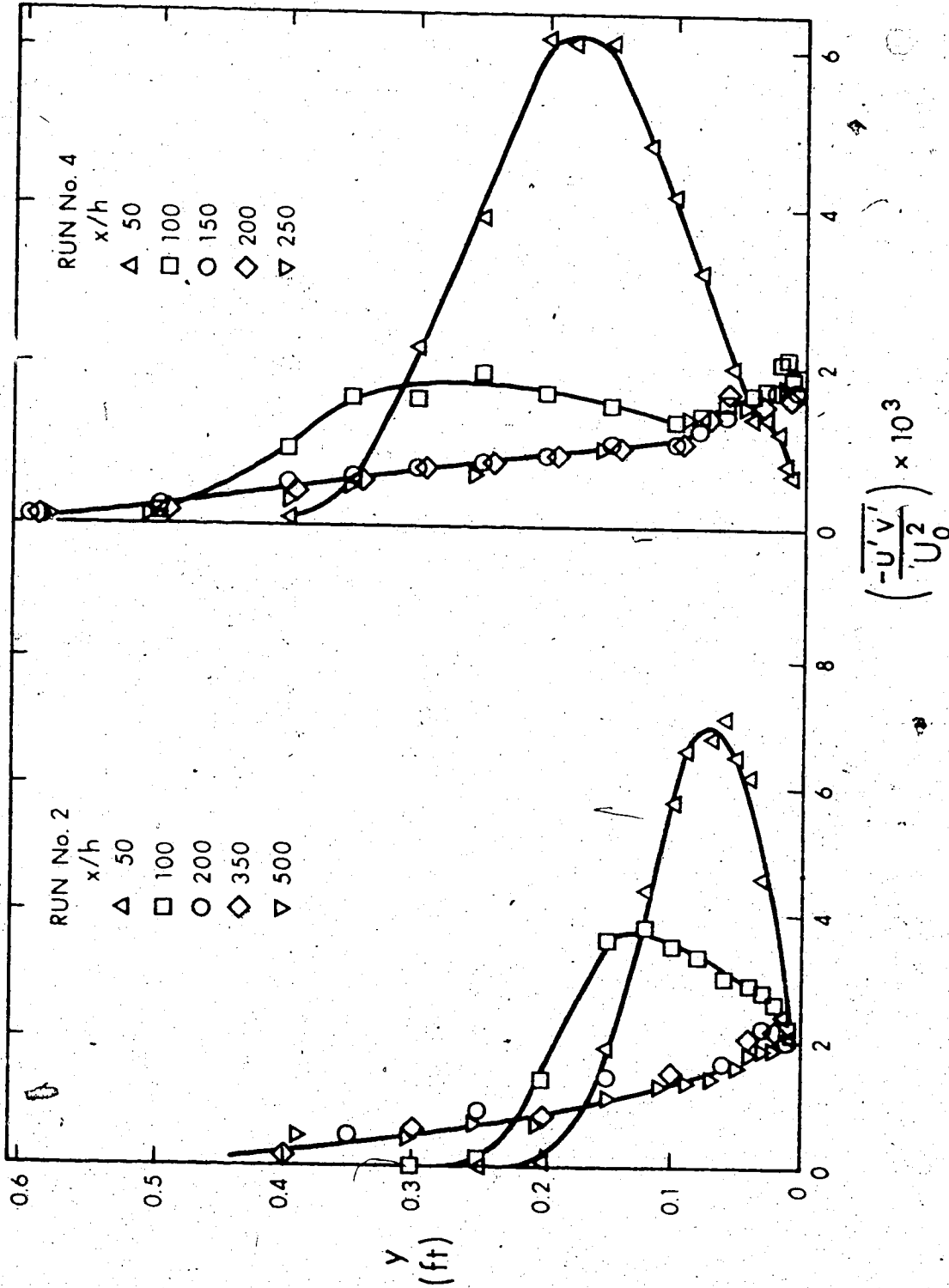


FIGURE 5.13 DISTRIBUTION OF TURBULENCE SHEAR STRESS FOR RUNS 2 AND 4

Higher values of turbulence shear stress near the wall, which occur because of the roughness of the wall, are distinctly noticeable in Figure (5.14). Another distinct feature is the smaller constant shear layer near the wall. The shear stress seems to decrease rapidly as we move away from the wall. A possible reason for the small region of constant shear layer near the wall could be the presence of larger magnitudes of normal Reynolds stresses in this area.

In Figure (5.15), turbulence shear stresses in the far wake region, for zero pressure gradient flows, are shown. Figure (5.15-a) shows the plot of $\tau/\tau_0 = -\overline{u'v'}/u_*^2$ against y/b . Klebanoff's (1954) data for the turbulent boundary layer on a smooth wall is also shown for comparison. His data was reduced to the y/b scale, on the assumption that the total wake-width $B (=2.27b)$ was approximately equal to the boundary layer thickness δ . It can be seen that the discrepancy between the boundary layer shear stress and that of the wall-wake is small in the area close to the wall. In the central and outer regions of the wall-wake, however, this discrepancy is large. This indicates that the shear velocity, u_* , is not the proper velocity scale for the outer region.

In Figure (5.15-b), the plot of $\tau/\rho u_{im}^2 = -\overline{u'v'}/u_{im}^2$ against y/b is shown. Townsend's (1949) data for the plane-wake behind a circular cylinder is also shown for

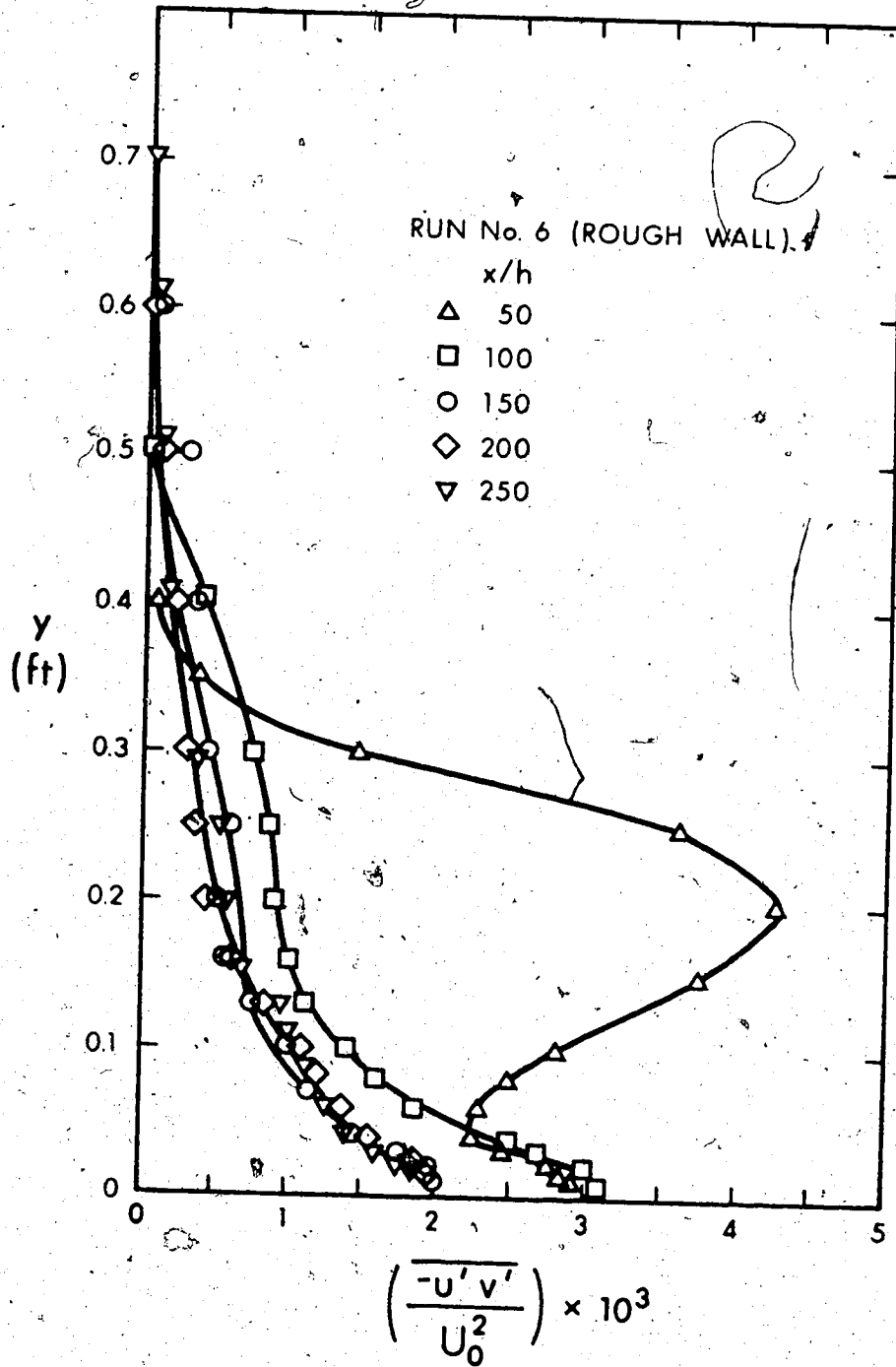


FIGURE 5.14. DISTRIBUTION OF TURBULENCE SHEAR STRESS FOR RUN NUMBER 6 (ROUGH WALL)

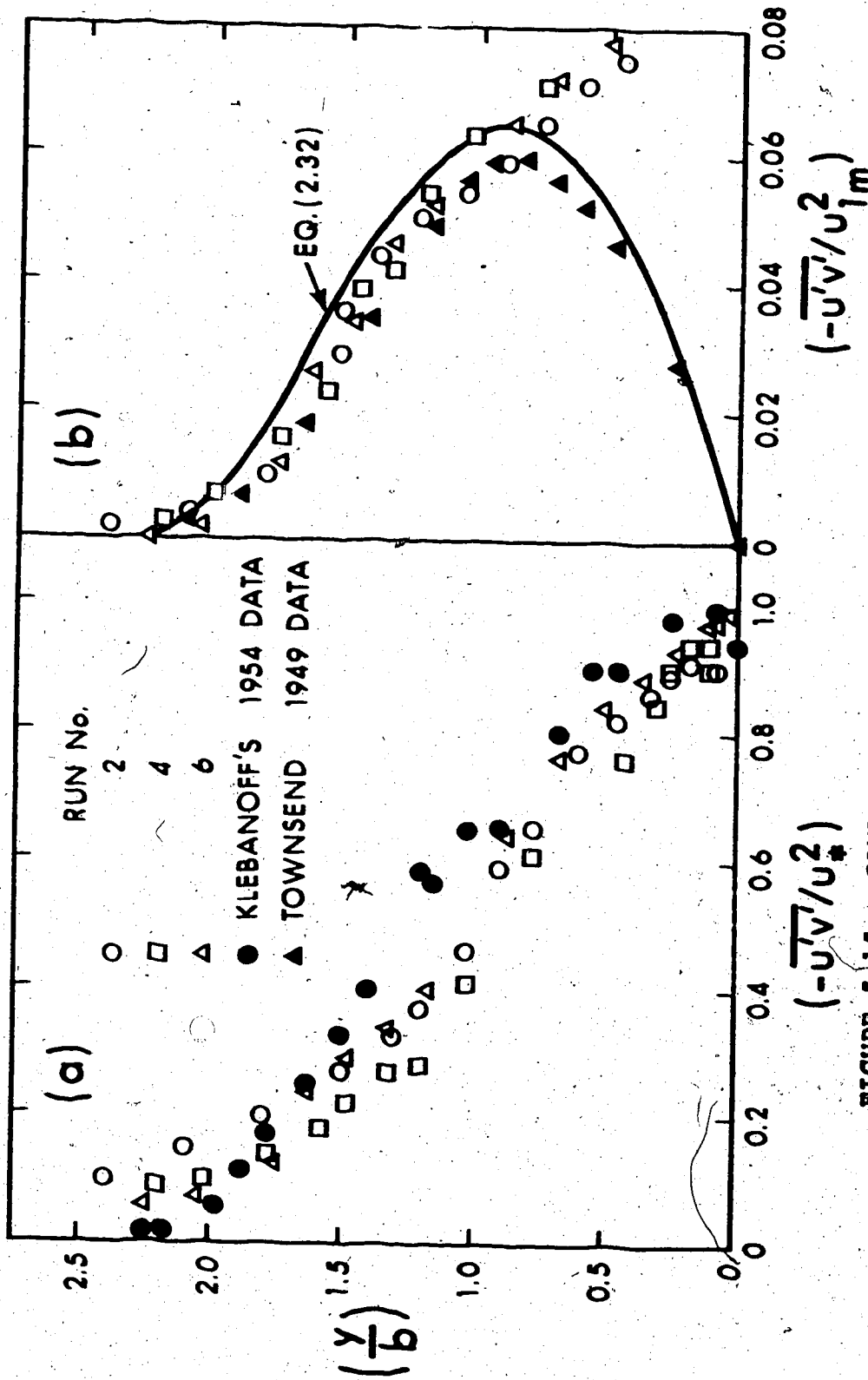


FIGURE 5.15 COMPARISON OF TURBULENCE SHEAR STRESS FOR WALL-WAKES AT ZERO PRESSURE GRADIENT WITH (a) KLEBANOFF'S (1954) DATA FOR TURBULENT BOUNDARY LAYER AT ZERO PRESSURE GRADIENT AND (b) TOWNSEND'S (1949) DATA FOR WAKE BEHIND A CIRCULAR CYLINDER

comparison. The discrepancy between the wall-wake data and that of the plane wake can be seen to be very small in the outer region. The assumption that there is similarity between the shear stress distributions in the outer region is, therefore, justified.

The equation (2.32),

$$\frac{\tau}{\rho u_{1m}^2} = 0.128 \frac{y}{b} (1 - 0.293 \left\{ \frac{y}{b} \right\}^{3/2})^2 \quad (2.32)$$

obtained in Chapter II, is also shown in the same figure. It can be noticed that the equation, (2.32), estimates a slightly higher value for $\tau/\rho u_{1m}^2$ than that which was experimentally obtained. This may be due to one or more of the following factors:

- (i) The hot-wire measurements for $\overline{u'v'}$ may be slightly erroneous,
- (ii) There may be error in the computation of u_{1m} , and
- (iii) The coefficient for the expression of mixing length (viz. $l = 0.407b$ - Schlichting, 1930), used in deriving equation (2.32), may not be absolutely correct.

A modified coefficient for the mixing length has been obtained, using the experimental data. This is discussed in the following pages.

The influence of the wall on the shear stress distribution can readily be noticed in the inner region. The

shear stress across the wall-wake starts deviating from that across the plane-wake profile at about $y/b = 0.75$. The effect of roughness is not clearly noticeable.

5.4 MIXING LENGTH FOR WALL-WAKE WITH ZERO PRESSURE GRADIENT FLOWS

According to Prandtl's mixing length hypothesis, the expression for turbulent shear stress can be written as:

$$\tau_t = -\rho \overline{u'v'} = \rho \ell^2 \left| \frac{d\bar{u}}{dy} \right| \frac{d\bar{u}}{dy} \quad (5.1)$$

In the outer region of wall-wake, the velocity profile can be represented by:

$$\frac{U_0 - \bar{u}}{u_{1m}} = (1 - 0.293 \left\{ \frac{y}{b} \right\}^{3/2})^2$$

Differentiating the above equation with respect to y , and substituting into equation (5.1), we obtain

$$-\frac{\overline{u'v'}}{u_{1m}^2} = 0.79 \frac{\ell^2}{b^2} \frac{y}{b} (1 - 0.293 \left\{ \frac{y}{b} \right\}^{3/2})^2 \quad (5.2)$$

The mixing length, ℓ , was evaluated from the above expression, for measured values of $-\overline{u'v'}/u_{1m}^2$, and the average value for the three runs was found to be

$$\ell = 0.38b, \text{ for } (y/b) \geq 0.7 \quad (5.3)$$

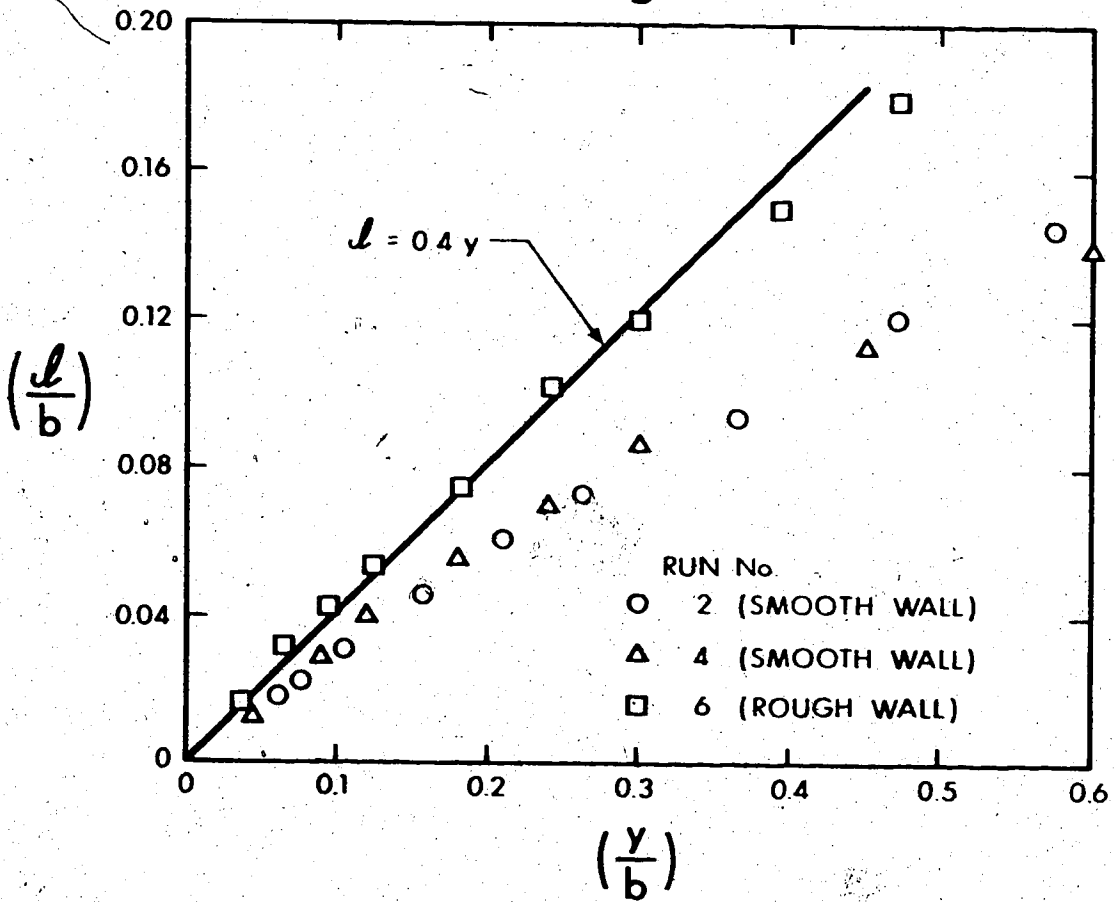
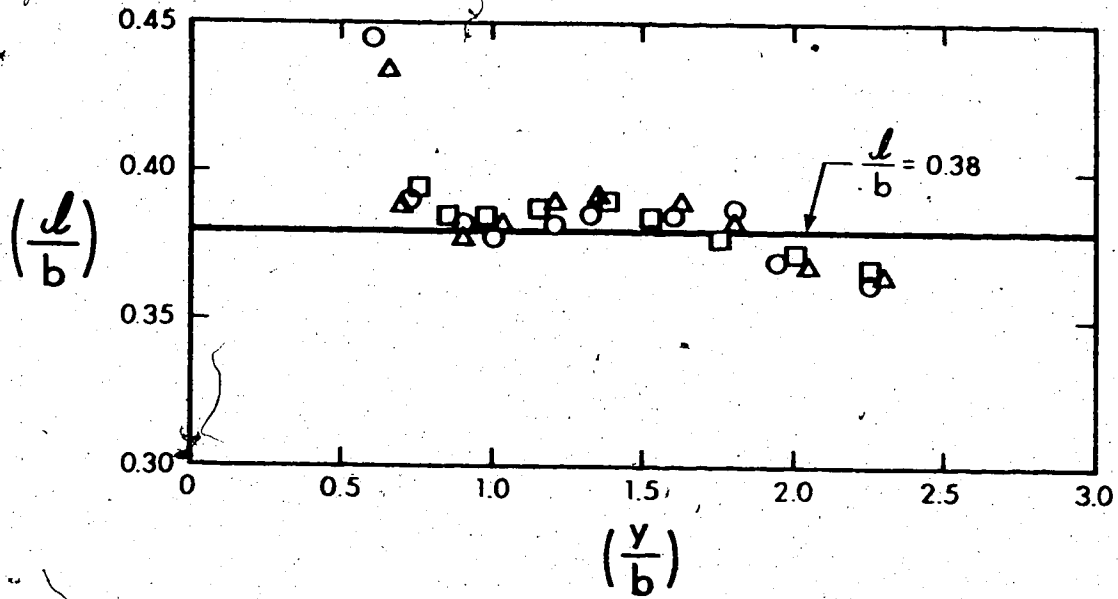


FIGURE 5.16 VARIATION OF MIXING LENGTHS FOR RUNS 2, 4 AND 6

In the inner region, the mixing length was similarly evaluated by assuming the logarithmic velocity profile. The data is compared with the turbulent boundary layer equation for the mixing length:

$$l = 0.4y \quad (5.4)$$

The agreement in the inner region, ($\frac{y}{b} \leq 0.1$), of the wall-region, is seen to be satisfactory for both rough and smooth wall flows. For $y/b > 0.1$, the smooth wall data can be seen to depart significantly from equation (5.4). This discrepancy can be attributed to an error in the measurements of both $-\overline{u'v'}$ and u_* .

The above plot indicates that the mixing length, at any section in the wall region, varies linearly with y in the inner region, and bears a constant ratio with the half wake width in the outer region, thus justifying the assumption of the two layer hypotheses.

5.5 SHEAR STRESS DISTRIBUTION FOR ADVERSE PRESSURE GRADIENT RUNS

The expression for shear stress distribution across the flow was derived in Chapter I, (equation (2.69, (2.75), in the form:

$$\frac{\tau}{\rho u_{lm}^2} = \frac{0.88}{R_\epsilon} \lambda^{1/2} (1 - 0.293\lambda^{3/2}) \quad (5.5)$$

$$\text{where } \frac{1}{R_\epsilon} = \frac{\epsilon}{u_{1m} b} = 0.077 \left(1 - 9.1 B_1 \left| \frac{mf_1}{f_1'} - \lambda - m \frac{U}{u_{1m}} \frac{1}{f_1'} \right| \right) \quad (5.6)$$

and ϵ is the eddy viscosity.

If we assume that ϵ varies only in the x direction and remains constant across the flow, then we can determine a simple expression for R_ϵ from the above equation, by evaluating the equation at

$$\lambda = 1; f_1(1) = 1/2, f_1'(1) = -0.622$$

If we also substitute for B_1 from equation (2.73), and for (u_{1m}/U) from equation (2.64), and simplify, we obtain

$$\frac{1}{R_\epsilon} = 0.08 \left(\frac{0.78-m}{0.92-m} \right) \quad (5.7)$$

The expression for shear stress thus becomes:

$$\frac{\tau}{\rho u_{1m}^2} = 0.0704 \left(\frac{0.78-m}{0.92-m} \right) \lambda^{1/2} \{1 - 0.293 \lambda^{3/2}\} \quad (5.8)$$

Equation (5.8), along with measured values of $(-\overline{u'v'}/u_{1m}^2)$ for the two adverse pressure gradient flows, are plotted in Figure (5.17). In using equation (5.8), the experimental values of m were used. For APG-II, $m = -0.215$ and for APG-III, $m = -0.310$.

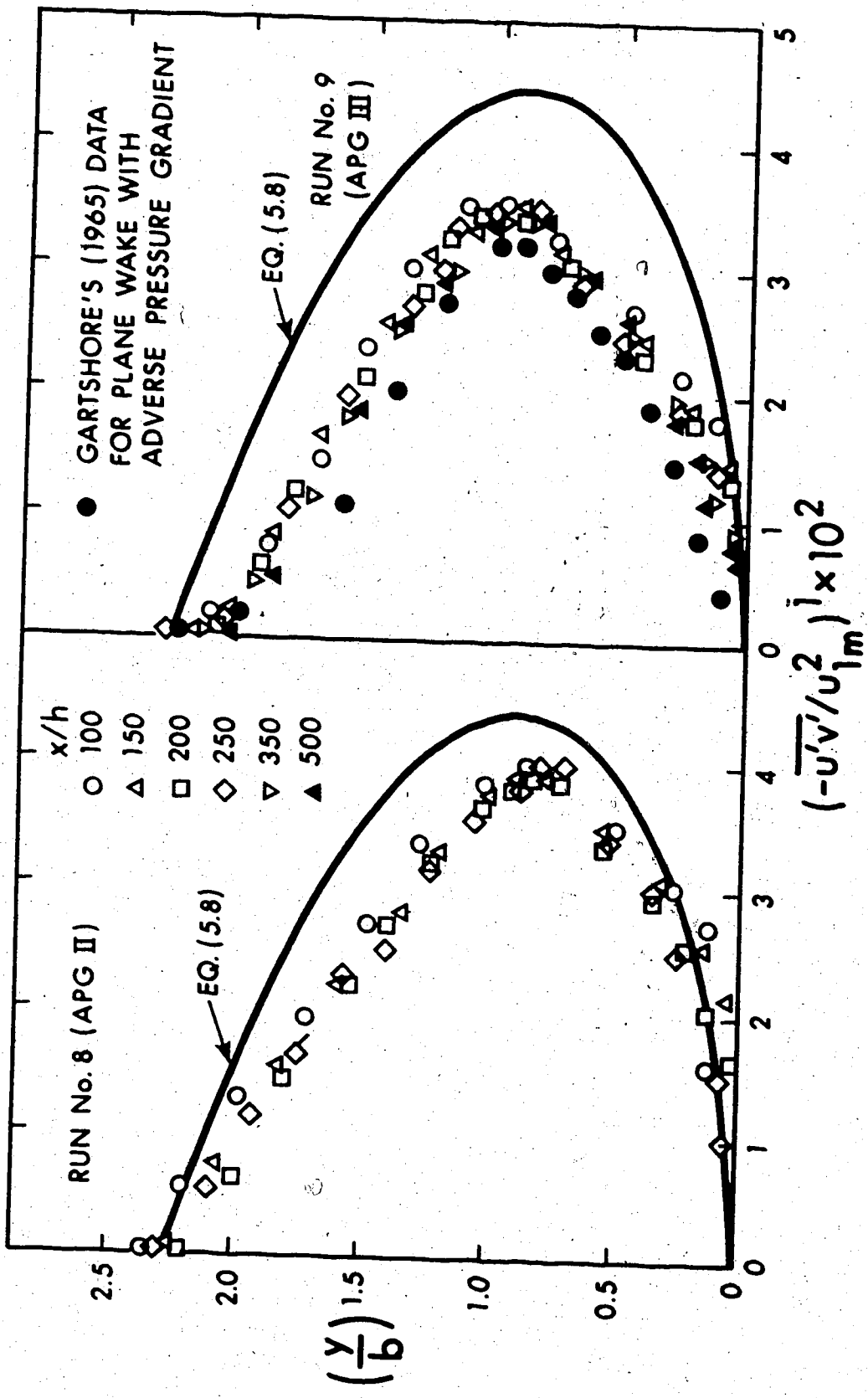


FIGURE 5.17 SHEAR STRESS DISTRIBUTION FOR RUNS 8 AND 9

Similarity in shear stress distribution can be noted. However, equation (5.8) can be seen to estimate values which are higher than the experimentally obtained values, by a factor of about 15% for APG-II and 25% for APG-III. Gartshore's (1965) plane-wake measurements for pressure gradient "B" ($m = -0.3125$, $u_{lm}/U = 0.239$), are also shown in the plot. The agreement between the two results is very close, the slight discrepancy being caused by the fact that a higher level of turbulence was present in the wind tunnel for the present study.

The measurements of shear stress are seen to differ from equation (5.8) only by a scaling factor. This will simply modify the coefficient 0.08 in the equation for R_ϵ (equation 5.7). The main equation for the shear stress (equation 2.75) will, as a matter of fact, remain unchanged. Thus the assumption of constant eddy viscosity across the flow is basically justified. Wygnanski and Fiedler (1968) suggested that the expression for eddy viscosity (equation 2.68) should be corrected for the intermittency factor γ . A high value of ϵ in the present study can be attributed to this factor.

Because of the lack of measurements of other turbulence quantities, it is not possible at this stage to analyze the turbulent structure of the wall-wake. Such a study is therefore recommended for future investigation.

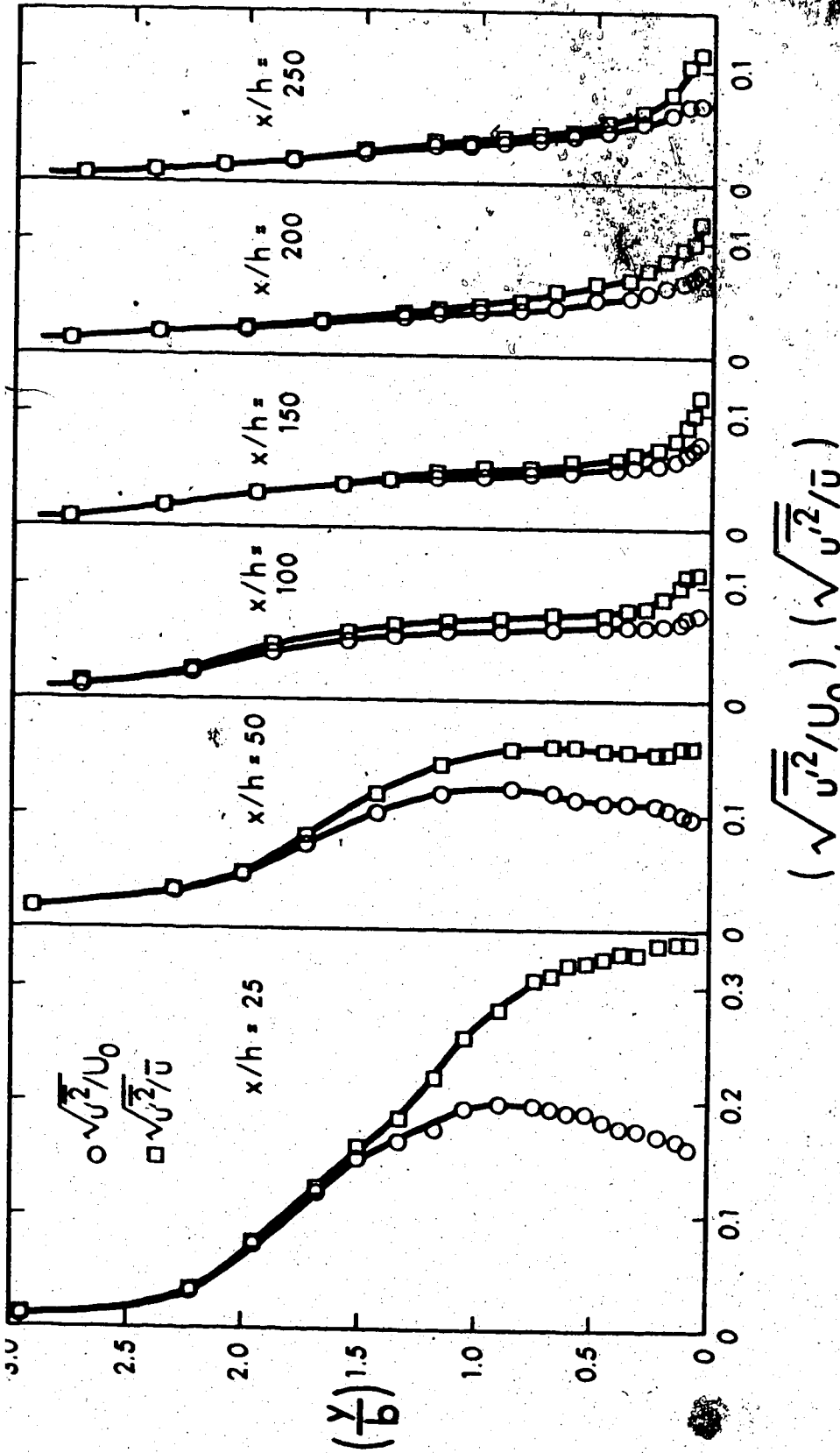


FIGURE 5.8 LONGITUDINAL COMPONENT OF RELATIVE TURBULENCE INTENSITY FOR RUN NUMBER 4

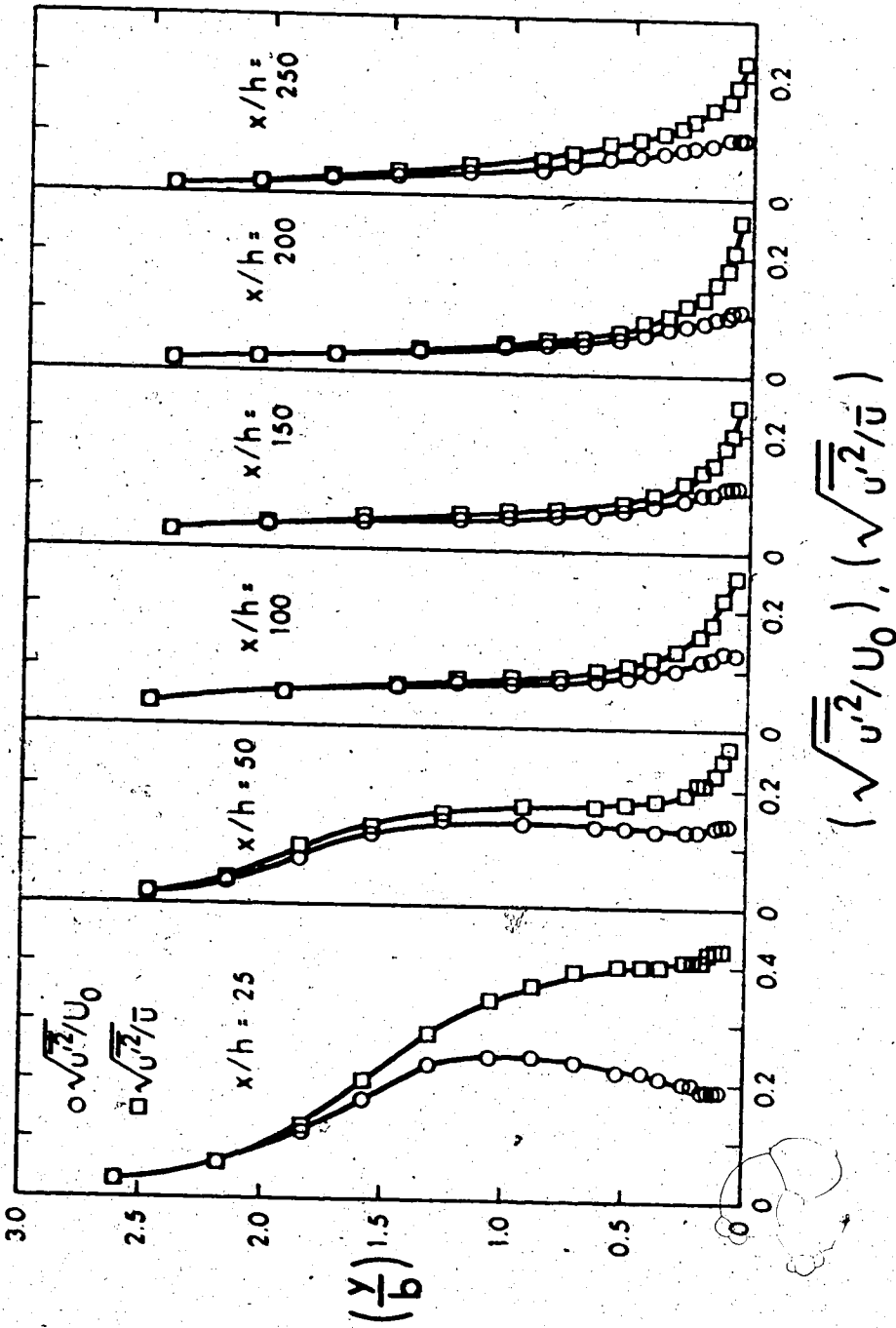


FIGURE 5.9 LONGITUDINAL COMPONENT OF RELATIVE TURBULENCE INTENSITY FOR RUN NUMBER 6

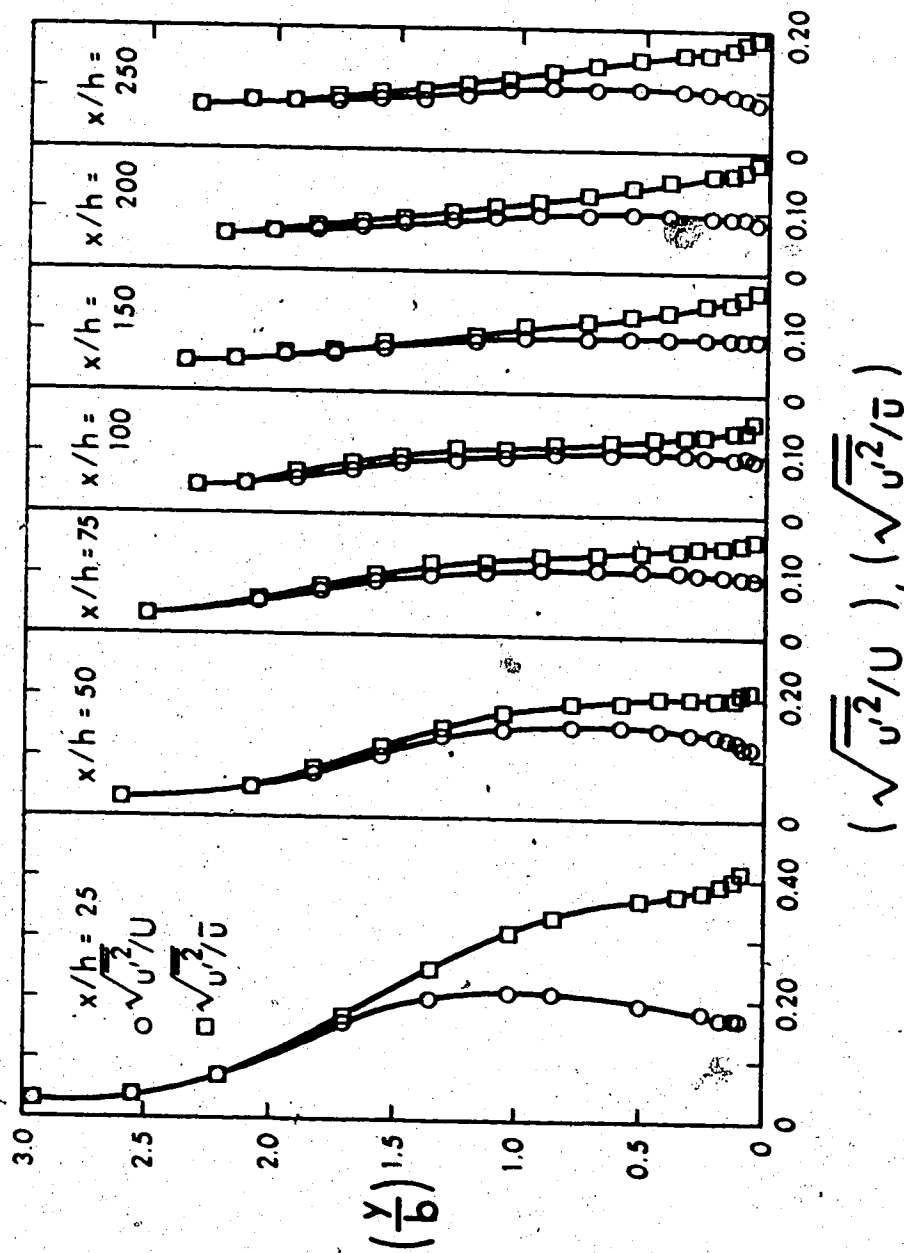


FIGURE 5.10 LONGITUDINAL COMPONENT OF RELATIVE TURBULENCE FOR RUN NUMBER 8

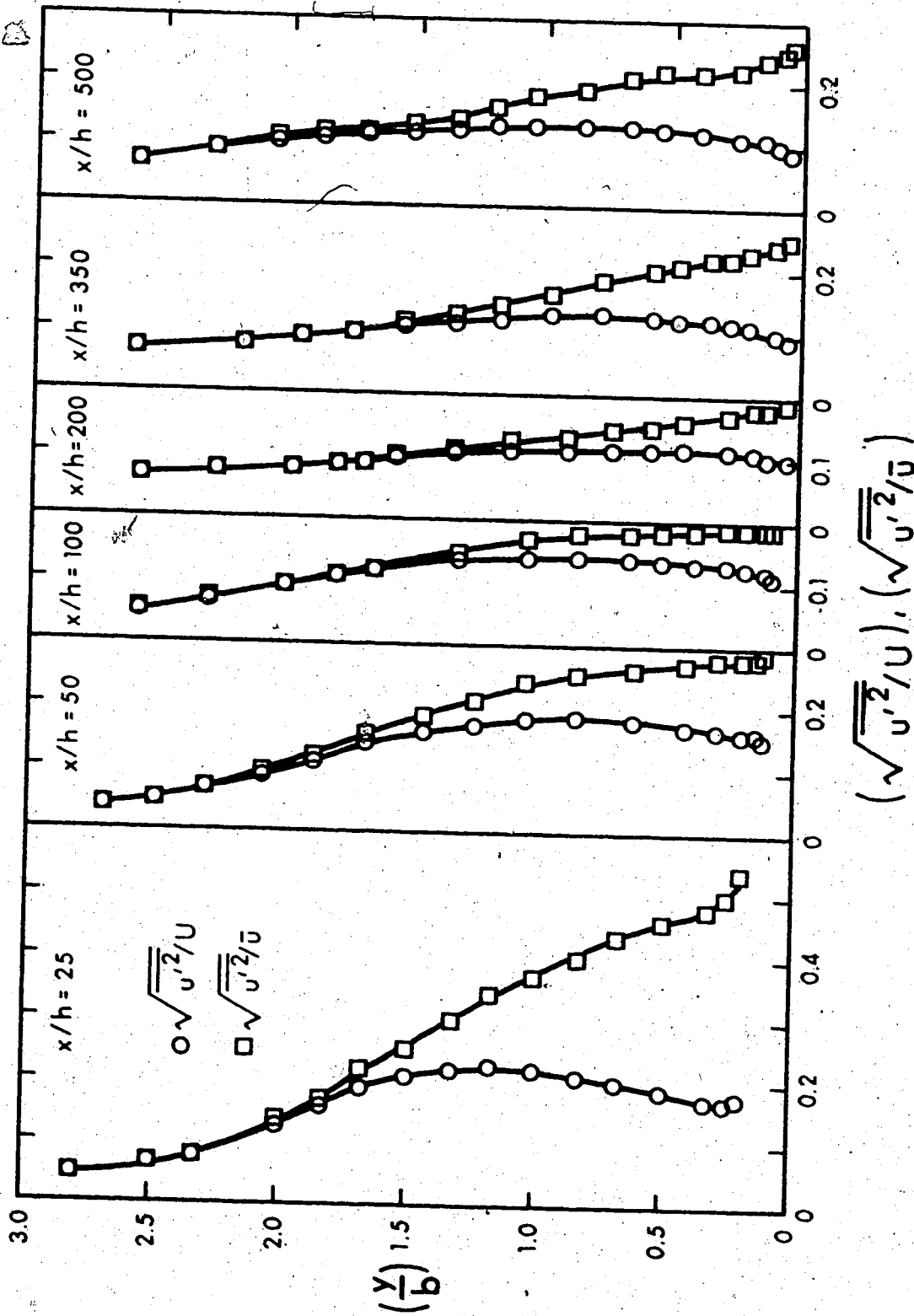


FIGURE 5.11 LONGITUDINAL COMPONENT OF RELATIVE TURBULENCE INTENSITY FOR RUN NUMBER 9

CHAPTER VI

SUMMARY AND CONCLUSIONS

6.1 SUMMARY

In hydraulic engineering, wall-wakes are often encountered, and more often than not, they are three-dimensional in nature. Therefore, study of two-dimensional wall-wakes is necessary for understanding the complex behaviour of the three-dimensional ones. This study is the first step in understanding the mechanics of the three-dimensional wall-wake. At first, an investigation of two-dimensional wall-wakes with zero pressure gradients was carried out. The influence of wall roughness was examined for one case. The study was then extended to wall-wakes with adverse pressure gradients. The measurement of a few of the turbulence characteristics, for cases with and without adverse pressure gradients, comprised the last part of the study. The significant conclusions drawn from the present investigation are given below.

6.2 ZERO PRESSURE GRADIENT FLOWS

From a similarity analysis of the boundary layer types of equations, the decay of the maximum velocity defect and the growth of the length scales, in the far-wake region, were given by the following expressions:

$$u_{lm} \propto x^{-1/2}$$

$$b \propto x^{1/2}$$

Expressions for u_{lm} and b were also derived for the near-wake region.

Experimental observations (Chapter IV) showed that the flow field of the wall-wake was divided into an inner and an outer-region. The outer region was essentially similar to that of a plane-wake, and the inner region to that of a boundary layer. Different shapes and sizes of obstacles showed that the velocity profiles in the outer and inner regions satisfied similarity beyond $x/h \approx 25$. The logarithmic 'law of the wall' was found to be valid in the inner region. A power law distribution of velocity, as a function of half-wake-width, b , and u_* , was also found to be valid in the inner region. The characteristic length scales for the inner and outer layers (b and v/u_*) were found to be proportional

to $x^{1/2}$. The point of interaction between the inner and outer layer profiles gave the indication of having a constant-ratio with the length scale, b . A similar constant ratio expression was obtained analytically.

Prandtl's mixing length hypothesis was found to give good results for the shear stress distribution across the flow. Similarity in the profiles of shear stress and turbulence fluctuations was found beyond $x/h = 100$. The coefficient of skin friction was found to vary only slightly in the downstream direction of the flow.

The effects of wall roughness and the free-stream Reynolds' number were not noticed in the outer layer. A thickening of the inner layer, because of the roughness, was observed.

6.3 ADVERSE PRESSURE GRADIENT FLOWS

On the basis of similarity, expressions for the length and velocity scales were obtained. Expressions for flow parameters were derived in simple forms, in terms of the exponent m . Gartshore's (1965) expression for eddy viscosity was found to give satisfactory results for moderately strong adverse pressure gradient flows.

The only case of weak adverse pressure gradient tested was found to give interesting results. Variations of the wake-width and velocity defect were found to occur in a manner similar to those for strong adverse pressure

gradient. However, a large discrepancy was found between the values predicted by the semi-empirical equations and the ones experimentally observed. There is an indication that the skin friction influences the diffusive behaviour of the outer region of the wall-wake, for weak adverse pressure gradient flow. However, the limited amount of experimental evidence in this regard prohibits any generalizing of the above statement.

Adverse pressure gradient was found to reduce the inner layer (the wake was found to grow). The interaction of the inner and the outer layers ($\delta w/b$) was predicted to decrease, in proportion to $x^{-2/3(m+1)}$, in the downstream direction. The characteristic length scales for the inner and outer layers were found to have a constant ratio. The skin friction was found to vary in proportion to $x^{-2(m+1)}$, or with the characteristic Reynolds number, $(u_{1m} b/\nu)$. A semi-logarithmic velocity profile, in terms of $\lambda (= y/b)$, was found to be valid in the inner region.

Turbulence fluctuations and shear stress were found to satisfy similarity in the far-wake region. A simple expression, derived on the basis of the expression for $R_e = \frac{u_{1m} b}{\epsilon}$, proposed by Gartshore, was found for shear stress distribution across the flow.

It is hoped that this study will serve to provide some understanding of the complex nature of the flow.

associated with turbulent wall-wakes. However, it should be noted that more measurements of turbulence characteristics are necessary before a full understanding of the subject can be achieved.

LIST OF REFERENCES

1. Abramovich, G.N. (1963): "The Theory of Turbulent Jets", The M.I.T. Press, Cambridge, Mass., 1963 (English Translation).
2. Anderson, O.K. (1966): "Time Resolution Power in Correlation Measurements with DISA type 55D01 Hot-Wire and Hot-Film Anemometer". DISA Information No. 4, Dec. 4, 1966. Published by DISA, Herlev, Denmark.
3. Arie, M. and Rouse, H. (1956): "Experiments on Two-Dimensional Flow over a Normal Wall". Jol. of Fluid Mech., Vol. 1, pt. 2, 1956.
4. Bradbury, L.J.S. (1963): "An Investigation into the Structure of a Turbulent Plane Jet". Ph.D. Thesis, University of London, 1963.
5. Bradshaw, P. (1971): "An Introduction to Turbulence and its Measurement". Pergamon Press Ltd., Headington Hill Hall, Oxford, 1971.
6. Clauser, F.H. (1956): "The Turbulent Boundary Layer". Advances in Applied Mechanics, Vol. IV, Academic Press, New York, 1956.

7. Collis, D.C. and Williams, M.J. (1959): "Two Dimensional Convection from Heated Wires at Low Reynolds' Number". Jol. of Fluid Mech., Vol. 6, 1959.
8. Gartshore, I.S. (1965): "The Stream wise Development of Two-Dimensional Wall-Jets and Other Two-Dimensional Turbulent Shear Flows". Mech. Engg. Ph.D. Thesis, McGill University, Canada, 1965.
9. Good, M.C. and Joubert, P.N. (1968): "The Form Drag of Two-Dimensional Bluff-Plates Immersed in Turbulent Boundary Layers". Jol. of Fluid Mech., Vol. 31, pt. 3, 1968.
10. Gorlin, S.M. and Slezinger, I.I. (1966): "Wind Tunnels and Their Instrumentation". Edited by Israel Program for Scientific Translations Ltd., Jerusalem, 1966 (English Translation).
11. Hama, F.R. (1954): "Boundary Layer Characteristics for Smooth and Rough Surfaces". Trans. of the Soc. of Naval Architect and Marine Engineers, Vol. 62, 1954.
12. Hill, P.G.; Schaub, U.W. and Senoo, Y. (1963): "Turbulent Wakes in Pressure Gradients". Jol. of Appl. Mech., Trans. ASME, paper No. 63-WA-5, 1963.

13. Hinze, J.O. (1959): "Turbulence, An Introduction to Its Mechanism and Theory". McGraw-Hill Book Co., Ltd., New York, 1959.
14. Hoerner, S.F. (1965): "Fluid-Dynamics Drag". Published by the Author, 1965.
15. Hollingshead, A.B. (1972): "Boundary Shear Distribution in Open Channel Flow". Ph.D. Thesis, Dept. of Civil Engg., Univ. of Alberta, Canada, 1972.
16. Hwang, L.S. and Laursen, E.M. (1963): "Shear Measurement Technique for Rough Surfaces". Jol. of the Hyd. Div., Proc. ASCE, March 1963.
17. Kennelly, A.E.; Wright, C.A. and Bylevelt, J.S. (1909) "The Convection of Heat from Copper Wires". Trans. AIEE, Vol. 28, 1909.
18. King, L.V. (1914): "On the Convection of Heat from Small Cylinders in a Stream of Fluid". Phil. Trans., Roy. Soc., London, 1914.
19. Klatt, F. (1969): "The X Hot-Wire Probe in a Plane Flow Field". DISA Information No. 8, July 1969; DISA, Herlev, Denmark.
20. Klebanoff, P.S. (1954): "Characteristics of Turbulence in a Boundary Layer with Zero Pressure Gradient". NACA Tech. Notes 3178, 1954.

21. Liepmann, H.W. and Fila, G.H. (1947): "Investigations of Effects of Surface Temperature and Single Roughness Elements on Boundary Layer Transition". NACA Rep. 390, 1947.
22. Liu, C.K.; Kline, S.J. and Johnston, J.P. (1966): "An Experimental Study of Turbulent Boundary Layer on Rough Walls". Report MD-15, Thermodynamics Div., Dept. of Mech. Engg., Stanford University, Stanford, Calif., 1966.
23. Ludwig, H. and Tillman, W. (1950): "Investigations of the Wall Shear Stress in Turbulent Boundary Layers". Trans. NACA, Wash., Tec. Memo. No. 1285, 1950.
24. Mickley, H.S. and Davis, R.S. (1957): "Momentum Transfer for Flow over a Flat Plate with Blowing". NACA TN. 4017, Nov. 1957.
25. Moore, W.F. (1951): "An Experimental Investigation of the Boundary Layer Development Along a Rough Surface". Ph.D. Dissertation, State Univ. of Iowa, 1951.
26. Newman, B.G. (1967): "Turbulent Jets and Wakes in Pressure Gradients". Fluid Mech. of Internal Flow. Edited by G. Sovran, Elsevier Publishing Co., Amsterdam, 1967.

27. Patel, R. and Newman, B.G. (1961): "Self-Preserving, Two Dimensional Turbulent Jets and Wall-Jets in a Moving Stream". McGill University, Mech. Engg. Rep. No. Ae5, 1961.
28. Patel, V.C. (1965): "Calibration of Preston Tube and Limitations on its Use in Pressure Gradients". Jol. of Fluid Mech., Vol. 23, pt. 1, 1965.
29. Preston, J.H. (1954): "The Determination of Turbulent Skin Friction by Means of Pitot Tubes". Jol. of Aero. Sc., vol. 58, 1954.
30. Roshko, A. (1954): "On the Drag and Shedding Frequency of Two-Dimensional Bluff Bodies". NACA TN 3169, July 1954.
31. Roshko, A. (1955): "On the Wake and Drag of Bluff Bodies". Jol. of Aero. Sc., Vol. 22, No. 2, 1955.
32. Rotta, J. (1953): "On the Theory of Turbulent Boundary Layer". NACA TM. 1344, Feb. 1953.
33. Runstadler, P.W.; Kline, S.T. and Reynolds, W.C. (1963): "An Experimental Investigation of the Flow Structure of the Turbulent Boundary Layer". Report MD-8, Dept. of Mech. Engg., Stanford University, Stanford, Calif., 1963.

34. Schlichting, H. (1930): "Über das ebene Windschattenproblem", Ingr.-Arch., Vol. 5, 1930.
35. Schlichting, H. (1968): "Boundary Layer Theory", McGraw Hill Book Co., 1968 (Sixth Edition).
36. Scottron, V.E. (1967): "Turbulent Boundary Layer Characteristics Over a Rough Surface in An Adverse Pressure Gradient". Hydromechanics Laboratory Research and Development Report No. 2659, Wash., 1967.
37. Sforza, P.M. and Mons, R.F. (1969): "The Wall-Wake: Flow Behind An Obstacle on a Flat Surface". AIAA Paper 69-747, Ottawa, Canada, 1969.
38. Sforza, P.M. and Mons, R.F. (1970): "Wall-Wake: Flow Behind a Leading Edge Obstacle". AIAA Journal, Vol. 8, pt. 2, 1970.
39. Tani, I. and Hama, F.R. (1953): "Some Experiments on the Effect of Single Roughness Element on Boundary Layer Transition". Jol. Aero. Sc., Vol. 20, 1953.
40. Tani, I. (1961): "Effects of Two-Dimensional and Isolated Roughness on Laminar Flow". Boundary Layer Flow Control, Vol. 2, Pergamon Press, New York, 1961.

41. Tollmien, W. (1933): "Die von Kármánsche Ähnlichkeitshypothese in der Turbulenz-Theorie und das ebene Windschattenproblem". Ing.-Arch., Vol. 4, 1933.
42. Torrence, M.G. (1967): "Concentration Measurements of an Injected Gas in a Supersonic Stream". NASA Tech. Note D-3860, April 1967.
43. Townsend, A.A. (1949): "Local Isotropy in the Turbulent Wake of a Cylinder". Australian Jol. Sc. Research, Vol. 2A, 1949.
44. Townsend, A.A. (1956-a): "The Structure of Turbulent Shear Flow". Cambridge University Press, 1956.
45. Townsend, A.A. (1956-b): "The Properties of Equilibrium Boundary Layers". Jol. of Fluid Mech., Vol. 1, 1956.
46. Wieghardt, K.E.G. (1953): "On the Resistance of Screens". Aero. Quart., Vol. 4, pt. II, 1953.
47. Wagnanski, I. and Fiedler, H.E. (1968): "Jets and Wakes in Tailored Pressure Gradient". The Physics of Fluids, Vol. 11, No. 12, 1968.

ADDITIONAL REFERENCES

1. Carmody, T. (1964): "Establishment of a Wake Behind a Disk". Jol. of Basic Engg., ASME, 1964.
2. Chevroy, R. (1968): "The Turbulent Wake of a Body of Revolution". Jol. of Basic Engg., Trans. ASME, 1968.
3. Gartshore, I.S. (1967): "Two Dimensional Turbulent Wakes". Jol. of Fluid Mech., Vol. 30, pt. 3, 1967.
4. Hwang, N.H.C. and Baldwin, L.V. (1966): "Decay of Turbulence in axisymmetric wakes". Jol. of Basic Engg., ASME., Series D, 1966.
5. Kuo, Y.H. and Baldwin, L.V. (1967): "The Formation of Elliptic Wakes". Jol. of Fluid Mech., Vol. 27, pt. 2, 1967.
6. Steiger, M.H. and Bloom, M.H. (1962): "Three Dimensional Viscous Wakes". Jol. of Fluid Mech., Vol. 14, 1962.
7. Swain, L.M. (1929): "On the Turbulent Wake Behind a Body of Revolution". Proc. Roy. Soc., (London), A., 135, 799, 1929.

A P P E N D I X - A

MEASURED MEAN FLOW CHARACTERISTICS

TABLE A.1

MEASURED MEAN-VELOCITY DISTRIBUTIONS

RUN NUMBER 1: $h = 0.25$ in., $U_o = 40.0$ fps, $R_e = 5,200$

$x = 5.0$ in		$x = 7.5$ in		$x = 10.0$ in		$x = 15.0$ in	
y ft	u fps	y ft	u fps	y ft	u fps	y ft	u fps
0.006	21.8	0.006	26.0	0.006	27.0	0.006	27.9
0.008	22.5	0.008	26.8	0.008	28.2	0.008	29.7
0.010	23.2	0.010	27.6	0.010	29.0	0.010	30.6
0.012	24.0	0.012	28.1	0.012	29.5	0.012	31.2
0.014	24.5	0.014	28.5	0.014	29.9	0.014	31.8
0.016	25.1	0.016	28.8	0.016	30.2	0.016	32.5
0.021	26.3	0.021	29.4	0.021	30.6	0.021	33.0
0.026	28.3	0.026	29.9	0.026	31.1	0.026	33.4
0.036	31.2	0.036	31.8	0.036	32.0	0.036	34.2
0.046	34.3	0.046	33.9	0.046	33.5	0.046	34.8
0.056	37.1	0.056	35.2	0.056	34.8	0.056	35.3
0.066	38.4	0.066	37.0	0.066	36.0	0.066	36.0
0.076	39.4	0.076	38.3	0.076	36.9	0.076	36.7
0.086	39.8	0.086	39.3	0.086	38.0	0.086	37.3
0.096	40.0	0.096	39.7	0.096	39.0	0.096	37.9
		0.106	39.9	0.106	39.6	0.106	38.5
		0.126	40.0	0.116	39.9	0.116	38.9
				0.126	40.0	0.126	39.3
						0.136	39.6
						0.146	39.8
						0.156	39.9
						0.176	40.0

TABLE A.1 (CONTINUED)

x = 20.0 in		x = 25.0 in		x = 50.0 in		x = 100.0 in	
y ft	u fps	y ft	u fps	y ft	u fps	y ft	u fps
0.006	29.4	0.006	29.7	0.006	29.6	0.006	29.0
0.008	30.2	0.008	30.6	0.008	30.0	0.008	29.5
0.010	31.0	0.010	31.3	0.010	30.7	0.010	30.6
0.012	31.5	0.012	31.8	0.012	31.3	0.012	31.3
0.014	32.1	0.014	32.3	0.014	32.0	0.014	31.9
0.016	32.6	0.016	32.6	0.016	32.4	0.016	32.4
0.021	33.2	0.021	33.4	0.021	33.5	0.021	33.8
0.026	33.8	0.026	34.0	0.026	34.5	0.026	34.7
0.036	34.3	0.036	34.6	0.036	36.0	0.036	36.3
0.046	35.5	0.046	35.3	0.046	37.0	0.046	37.3
0.056	35.9	0.056	35.8	0.056	37.3	0.056	37.7
0.066	36.4	0.066	36.4	0.066	37.8	0.066	38.0
0.076	36.8	0.076	36.8	0.076	38.0	0.086	38.5
0.086	37.2	0.086	37.2	0.086	38.2	0.106	38.8
0.096	37.6	0.096	37.6	0.106	38.6	0.126	39.0
0.106	38.0	0.106	38.0	0.126	38.8	0.146	39.2
0.116	38.4	0.116	38.4	0.146	39.0	0.166	39.3
0.126	38.8	0.126	38.8	0.166	39.3	0.196	39.4
0.136	39.0	0.136	39.0	0.196	39.7	0.226	39.6
0.146	39.4	0.146	39.2	0.226	39.9	0.256	39.8
0.156	39.6	0.166	39.5				
0.166	39.8	0.176	39.7				
0.176	39.9	0.196	39.9				
0.176	40.0						

TABLE A.2

MEASURED MEAN-VELOCITY DISTRIBUTIONS

RUN NUMBER 2: $h = 0.25$ in., $U_o = 96.0$ fps, $R_e = 12,500$

$x = 6.25$ in $x = 12.5$ in $x = 25.0$ in $x = 50.0$ in

y ft	u fps	y ft	u fps	y ft	u fps	y ft	u fps
0.001	34.0	0.001	43.5	0.001	45.5	0.001	41.6
0.002	43.5	0.002	50.4	0.002	51.8	0.002	52.4
0.004	50.4	0.004	61.6	0.004	62.0	0.004	60.0
0.006	55.6	0.006	66.4	0.006	68.0	0.006	63.5
0.008	57.5	0.008	67.6	0.008	69.0	0.008	64.5
0.010	58.5	0.010	68.0	0.010	70.5	0.010	67.2
0.015	60.0	0.015	70.5	0.015	73.0	0.015	72.0
0.020	61.2	0.020	73.0	0.020	75.0	0.020	75.0
0.025	61.2	0.030	73.5	0.030	77.2	0.030	82.0
0.030	64.0	0.040	74.5	0.040	80.0	0.040	84.4
0.040	66.6	0.050	76.5	0.050	80.8	0.050	85.0
0.050	73.5	0.060	80.0	0.060	82.0	0.060	85.5
0.060	77.0	0.080	82.0	0.080	84.0	0.080	86.5
0.080	84.0	0.100	86.0	0.100	86.0	0.100	88.0
0.100	90.0	0.150	93.0	0.150	90.0	0.150	90.5
0.200	93.5	0.200	96.0	0.200	93.5	0.200	92.0
0.300	95.0	0.300	96.0	0.300	95.0	0.300	93.7
0.400	95.0	0.400	96.0	0.400	96.0	0.400	94.8
						0.600	96.0

TABLE A.2 (CONTINUED)

x = 65.0 in x = 85.0 in x = 105.0 in x = 125.0 in

y ft	u fps	y ft	u fps	y ft	u fps	y ft	u fps
0.001	42.0	0.001	46.0	0.001	46.0	0.001	41.6
0.002	52.4	0.002	53.5	0.002	53.5	0.002	54.0
0.004	60.0	0.004	60.0	0.004	58.8	0.004	58.8
0.006	66.0	0.006	68.0	0.006	68.0	0.006	64.5
0.008	72.0	0.008	69.0	0.008	69.0	0.008	66.6
0.010	73.0	0.010	73.0	0.010	73.0	0.010	68.0
0.015	76.2	0.015	77.0	0.015	76.0	0.015	70.4
0.020	77.5	0.020	80.0	0.020	77.0	0.020	74.0
0.030	84.4	0.030	86.0	0.030	83.5	0.030	77.0
0.040	86.0	0.040	87.0	0.040	87.0	0.040	82.8
0.050	88.0	0.050	88.2	0.050	87.6	0.050	88.0
0.060	88.4	0.060	89.0	0.060	88.0	0.060	88.5
0.080	89.0	0.080	89.7	0.080	90.6	0.080	90.0
0.100	89.5	0.100	90.3	0.100	91.0	0.100	91.5
0.150	90.8	0.200	91.5	0.200	92.2	0.150	92.0
0.200	91.8	0.400	94.3	0.300	93.2	0.200	92.3
0.400	93.5	0.600	95.4	0.500	94.5	0.300	93.0
0.600	96.0	0.700	95.8	0.600	95.0	0.400	93.7
				0.700	95.6	0.500	94.2
						0.600	94.6
						0.700	95.2

TABLE A.3

MEASURED MEAN-VELOCITY DISTRIBUTIONS

RUN NUMBER 3: $h = 0.25$ in., $U_0 = 96.0$ fps, $R_e = 12,500$

$x = 6.25$ in $x = 12.5$ in $x = 18.75$ in $x = 25.0$ in

y ft	u fps	y ft	u fps	y ft	u fps	y ft	u fps
0.001	15.0	0.001	37.0	0.001	43.0	0.001	42.0
0.002	28.0	0.002	48.0	0.002	55.0	0.002	51.0
0.003	34.8	0.004	57.5	0.004	61.5	0.004	60.0
0.005	38.4	0.006	60.0	0.006	65.6	0.006	64.0
0.007	40.0	0.008	61.5	0.008	67.0	0.008	67.0
0.010	43.0	0.010	62.4	0.010	68.5	0.010	67.0
0.015	44.0	0.015	64.0	0.015	70.0	0.020	71.0
0.020	46.0	0.020	65.6	0.020	71.0	0.030	73.0
0.025	48.0	0.030	67.0	0.030	71.5	0.040	75.3
0.030	51.0	0.040	68.5	0.040	73.0	0.050	77.5
0.035	54.0	0.060	70.0	0.060	75.0	0.060	78.0
0.040	58.0	0.080	75.3	0.080	77.5	0.080	80.0
0.050	62.0	0.100	80.0	0.100	80.0	0.100	81.0
0.060	66.4	0.120	83.0	0.120	82.0	0.150	84.0
0.070	71.0	0.150	88.0	0.150	86.0	0.200	88.0
0.080	77.5	0.200	93.0	0.200	89.5	0.300	92.5
0.090	84.0	0.250	94.5	0.300	93.5	0.400	94.0
0.100	88.0	0.350	96.0	0.400	94.0	0.500	94.8
0.120	90.8	0.450	96.5	0.500	95.0	0.700	96.0
0.150	92.0			0.600	95.8		
0.200	94.0						
0.300	96.6						
0.400	97.5						

TABLE A.3 (CONTINUED)

$x = 37.5$ in		$x = 50.0$ in		$x = 65.0$	
y ft	u fps	y ft	u fps	y ft	u fps
0.001	40.0	0.001	43.0	0.001	45.5
0.002	50.0	0.002	52.5	0.002	55.0
0.004	60.0	0.004	63.0	0.004	63.0
0.006	63.5	0.006	65.6	0.006	66.0
0.008	65.6	0.008	67.0	0.008	67.0
0.010	67.0	0.010	68.5	0.010	70.0
0.015	71.5	0.015	74.0	0.015	71.0
0.020	71.5	0.020	75.3	0.020	76.5
0.030	76.4	0.030	80.0	0.030	80.5
0.040	78.0	0.040	81.0	0.040	83.0
0.060	80.0	0.060	84.0	0.060	86.0
0.080	81.0	0.080	86.0	0.080	87.0
0.100	83.0	0.100	86.5	0.100	89.3
0.150	85.5	0.150	88.1	0.150	90.1
0.200	88.5	0.200	89.8	0.200	91.0
0.300	92.0	0.300	92.0	0.300	92.2
0.400	93.5	0.400	93.3	0.400	93.3
0.600	95.3	0.600	95.2	0.500	94.0
0.700	96.0	0.800	96.3	0.700	95.8

TABLE A.3 (CONTINUED)

x = 85.0 in		x = 105.0 in		x = 125.0 in	
y ft	u fps	y ft	u fps	y ft	u fps
0.001	43.0	0.001	43.0	0.001	40.0
0.002	59.0	0.002	59.0	0.002	52.0
0.004	62.0	0.004	60.5	0.004	57.6
0.006	63.5	0.006	64.0	0.006	64.0
0.008	67.0	0.008	65.6	0.008	65.6
0.010	67.0	0.010	68.5	0.010	66.5
0.015	70.0	0.015	70.0	0.015	72.0
0.020	74.0	0.020	74.5	0.020	75.3
0.030	77.5	0.030	80.0	0.030	78.0
0.040	81.0	0.040	82.0	0.040	81.0
0.050	86.0	0.050	86.0	0.060	89.5
0.060	88.0	0.060	88.0	0.080	90.0
0.080	88.8	0.080	89.5	0.100	91.0
0.100	89.5	0.100	90.8	0.200	92.4
0.150	91.3	0.150	91.5	0.300	93.3
0.200	91.8	0.250	92.6	0.400	94.0
0.300	92.7	0.400	93.8	0.500	94.5
0.450	93.8	0.550	94.4	0.600	95.2
0.600	94.7	0.800	95.7	0.800	95.7
0.800	95.8				

TABLE A.4 (CONTINUED)

$x = 65.0$ in		$x = 85.0$ in		$x = 105.0$ in		$x = 125.0$ in	
y ft	u fps	y ft	u fps	y ft	u fps	y ft	u fps
0.001	48.0	0.001	48.0	0.001	49.0	0.001	50.0
0.002	58.0	0.002	60.5	0.002	59.0	0.002	60.0
0.003	62.8	0.003	63.5	0.003	62.4	0.003	65.0
0.004	64.0	0.004	64.0	0.004	63.6	0.004	66.0
0.005	64.5	0.006	65.6	0.006	66.4	0.006	69.2
0.007	65.0	0.008	67.2	0.008	70.8	0.008	71.4
0.010	69.2	0.010	68.4	0.010	71.4	0.010	73.0
0.015	71.6	0.015	71.5	0.015	76.0	0.015	74.0
0.020	74.0	0.020	73.6	0.020	77.4	0.020	79.2
0.030	75.4	0.025	75.4	0.030	80.5	0.030	80.5
0.040	77.2	0.030	76.8	0.040	83.6	0.040	83.6
0.050	84.0	0.040	80.0	0.060	87.5	0.060	87.0
0.060	86.2	0.050	82.8	0.080	89.2	0.080	88.4
0.080	87.4	0.060	84.4	0.100	89.8	0.100	89.6
0.100	88.1	0.080	86.0	0.150	90.4	0.150	90.6
0.150	88.8	0.100	89.0	0.200	91.0	0.200	91.0
0.200	89.5	0.150	89.5	0.300	91.8	0.300	91.8
0.300	91.2	0.200	90.2	0.400	92.7	0.400	92.7
0.400	93.2	0.300	91.5	0.500	93.6	0.500	93.5
0.500	94.8	0.400	93.0	0.600	94.4	0.650	94.4
0.600	96.4	0.500	94.0	0.800	95.8	0.800	95.4
		0.600	94.8				
		0.800	96.0				

TABLE A.5
MEASURED MEAN-VELOCITY DISTRIBUTIONS

RUN NUMBER 5: $h = 0.75$ in., $U_0 = 96.0$ fps, $R_e = 37,500$

$x = 18.75$ in $x = 30.0$ in $x = 45.0$ in $x = 60.0$ in

y ft	u fps	y ft	u fps	y ft	u fps	y ft	u fps
0.001	37.5	0.001	44.0	0.001	44.0	0.001	44.0
0.002	48.0	0.003	55.0	0.003	58.0	0.003	59.5
0.003	51.5	0.005	60.0	0.005	62.5	0.005	65.0
0.004	53.2	0.010	65.0	0.010	69.0	0.010	70.5
0.005	54.0	0.015	68.1	0.015	73.0	0.015	74.5
0.007	56.0	0.020	69.2	0.020	76.0	0.020	77.5
0.010	56.5	0.030	71.5	0.030	79.0	0.030	80.0
0.015	58.0	0.040	74.0	0.040	81.0	0.040	82.0
0.020	59.5	0.050	75.0	0.050	82.0	0.050	84.0
0.030	60.5	0.060	76.0	0.060	82.5	0.060	85.0
0.040	62.0	0.080	77.0	0.080	83.0	0.080	86.4
0.050	63.0	0.100	78.5	0.110	84.2	0.100	87.5
0.060	64.0	0.120	80.0	0.140	85.5	0.120	88.3
0.080	66.0	0.140	81.5	0.180	87.0	0.150	89.3
0.100	69.0	0.160	83.0	0.230	88.5	0.200	90.1
0.120	71.7	0.180	84.2	0.290	90.0	0.250	90.6
0.140	75.5	0.220	87.0	0.350	91.0	0.300	91.1
0.160	79.0	0.260	88.5	0.450	92.5	0.400	93.0
0.185	83.0	0.300	90.0	0.550	94.0	0.500	94.3
0.210	86.3	0.370	92.0	0.700	95.2	0.600	95.0
0.250	89.0	0.450	93.5			0.700	95.2
0.300	92.0	0.550	95.0				
0.400	94.0						
0.500	95.0						
0.600	95.0						

TABLE A.5 (CONTINUED)

x = 75.0 in x = 90.0 in x = 105.0 in x = 136.0 in

y ft	u fps	y ft	u fps	y ft	u fps	y ft	u fps
0.001	42.0	0.001	44.0	0.001	44.0	0.001	42.0
0.003	53.3	0.003	59.5	0.003	56.5	0.003	55.0
0.005	62.5	0.005	65.0	0.005	64.0	0.005	61.0
0.010	68.0	0.010	70.0	0.010	68.0	0.010	65.3
0.015	74.0	0.015	74.0	0.015	73.0	0.015	70.5
0.020	76.5	0.020	77.0	0.020	75.3	0.025	77.5
0.030	80.5	0.030	81.0	0.030	80.0	0.035	79.0
0.040	83.0	0.040	83.7	0.050	84.5	0.045	82.0
0.050	85.3	0.050	86.2	0.070	88.5	0.065	84.5
0.060	86.7	0.060	87.5	0.110	90.5	0.085	88.0
0.080	88.3	0.080	88.5	0.150	92.0	0.105	89.5
0.100	89.5	0.100	90.0	0.250	92.7	0.125	90.7
0.150	90.4	0.150	91.3	0.350	93.5	0.150	92.3
0.200	91.0	0.200	91.8	0.450	94.1	0.200	93.0
0.250	91.5	0.300	92.5	0.550	94.6	0.300	94.0
0.350	92.4	0.400	93.3	0.700	95.0	0.500	94.5
0.450	93.3	0.500	94.0	0.850	95.2	0.700	95.0
0.600	94.5	0.600	94.6				
0.750	95.3	0.800	95.2				

TABLE A.6

MEASURED MEAN-VELOCITY DISTRIBUTION

RUN NUMBER 6: $h = 0.50$ in., $U_o = 96.0$ fps, $R_e = 25,000$
(ROUGH WALL)

$x = 10.0$ in $x = 20.0$ in $x = 25.0$ in $x = 37.5$ in

y ft	u fps	y ft	u fps	y ft	u fps	y ft	u fps
0.001	24.8	0.001	33.0	0.001	33.0	0.001	32.5
0.002	26.6	0.002	34.5	0.002	35.2	0.002	33.0
0.004	28.2	0.004	40.0	0.004	41.0	0.004	37.5
0.006	29.8	0.006	44.0	0.006	44.0	0.006	42.5
0.008	31.2	0.008	47.0	0.008	47.0	0.008	46.2
0.010	31.2	0.010	49.5	0.010	49.8	0.010	49.0
0.015	32.5	0.015	53.2	0.015	54.0	0.015	53.2
0.020	32.5	0.020	55.7	0.020	57.3	0.020	57.2
0.030	34.0	0.030	58.7	0.030	60.3	0.030	61.8
0.040	36.5	0.040	61.0	0.040	63.2	0.040	65.0
0.050	38.8	0.050	62.5	0.050	64.5	0.050	67.2
0.060	42.0	0.060	63.2	0.060	66.0	0.060	68.5
0.070	46.0	0.070	64.0	0.070	66.5	0.070	70.0
0.080	52.3	0.080	65.0	0.080	68.0	0.080	70.7
0.100	62.7	0.100	70.7	0.100	71.5	0.090	71.7
0.120	71.6	0.120	73.0	0.150	76.0	0.100	73.0
0.140	79.5	0.140	75.7	0.200	80.5	0.120	74.7
0.160	85.0	0.160	78.6	0.250	86.0	0.140	76.2
0.180	89.0	0.180	82.5	0.300	88.7	0.160	77.8
0.200	90.5	0.200	85.0	0.400	91.5	0.180	79.0
0.220	92.0	0.220	87.5	0.500	93.8	0.200	80.7
0.250	93.2	0.250	91.3	0.600	95.0	0.250	84.2
0.300	94.0	0.300	93.3	0.700	96.0	0.300	88.0
0.350	94.7	0.400	94.2			0.400	90.7
0.400	95.4	0.500	95.0			0.500	93.0
0.500	96.2	0.600	96.0			0.600	94.6
						0.700	95.8

TABLE A.6 (CONTINUED)

x = 50.0 in x = 75.0 in x = 100.0 in x = 125.0 in

y ft	u fps	y ft	u fps	y ft	u fps	y ft	u fps
0.001	33.0	0.001	32.5	0.001	31.2	0.001	31.2
0.002	35.2	0.002	35.2	0.003	34.0	0.002	34.0
0.004	40.5	0.004	40.0	0.005	38.0	0.004	40.0
0.006	44.0	0.006	43.2	0.007	42.0	0.006	43.2
0.008	47.0	0.008	46.2	0.010	46.0	0.008	45.2
0.010	49.8	0.010	49.0	0.015	49.7	0.010	47.0
0.015	54.0	0.015	52.5	0.020	53.3	0.015	50.7
0.020	56.5	0.020	55.7	0.030	57.3	0.020	53.3
0.030	62.5	0.030	60.3	0.040	61.0	0.030	57.3
0.040	65.2	0.040	64.0	0.050	63.8	0.040	60.2
0.050	67.2	0.050	66.0	0.060	65.2	0.050	62.5
0.060	68.5	0.060	68.5	0.070	67.2	0.060	64.0
0.070	70.5	0.070	70.0	0.080	69.0	0.080	66.5
0.080	71.7	0.080	71.7	0.100	73.0	0.100	69.0
0.100	75.0	0.100	74.0	0.120	75.0	0.120	72.8
0.120	76.8	0.120	77.0	0.140	77.5	0.140	75.8
0.140	78.0	0.140	79.0	0.160	79.5	0.160	78.0
0.160	79.5	0.160	80.0	0.180	80.3	0.180	79.5
0.180	80.7	0.180	81.2	0.200	81.3	0.200	81.0
0.200	81.5	0.200	83.0	0.220	82.7	0.250	83.3
0.220	83.2	0.220	84.0	0.250	83.6	0.300	85.5
0.250	84.8	0.250	85.3	0.300	86.3	0.375	87.7
0.300	87.0	0.300	87.2	0.350	88.5	0.450	89.5
0.350	90.0	0.350	89.5	0.400	89.5	0.525	91.7
0.400	91.5	0.400	91.0	0.500	91.0	0.600	92.5
0.500	93.7	0.500	93.0	0.600	92.8	0.700	93.8
0.600	95.0	0.600	94.8	0.700	94.5	0.800	94.5
0.700	95.8	0.700	95.5	0.800	95.6	0.900	95.2
		0.800	95.8				

TABLE A.7

MEASURED MEAN VELOCITY DISTRIBUTIONS

RUN NUMBER 9 (APG-III): $h = 0.25$ in, $u_0 = 145$ fps

x y ft	5.0 in u fps	7.5 in u fps	10.0 in u fps	12.5 in u fps	18.75 in u fps	25.0 in u fps
0.001	29.0	43.0	50.0	46.0	44.0	40.0
0.005	33.1	62.1	67.8	62.0	61.4	60.1
0.01	38.2	71.6	74.0	70.1	68.4	63.5
0.02	47.0	77.5	78.1	75.7	73.6	68.5
0.03	55.8	82.3	84.0	79.0	75.7	71.6
0.04	72.4	87.4	87.3	82.0	78.7	74.5
0.05	90.0	94.6	91.0	85.0	81.0	76.0
0.06	107.6	100.6	94.0	88.5	83.0	77.0
0.07	117.0	107.3	98.3	91.0	84.1	79.0
0.08	125.0	113.0	102.0	94.4	86.6	80.2
0.09	130.7	117.5	106.5	97.0	87.2	81.5
0.10	135.0	122.0	110.2	100.5	90.4	83.0
0.11	136.5	124.5	114.0	104.0	92.0	84.2
0.12	137.0	127.5	117.0	106.5	94.4	85.8
0.13	138.0	129.5	119.5	110.1	96.2	87.2
0.15	139.0	131.0	122.6	114.0	100.7	90.0
0.17	139.5	131.8	125.0	117.8	105.0	97.2
0.20	140.3	132.2	125.7	121.3	109.5	104.0
0.25	143.0	133.0	127.0	122.8	115.0	108.0
0.30	143.0	133.0	127.0	122.7	115.0	108.0

TABLE A.7 (CONTINUED)

x y (ft)	37.5 in u fps	50.0 in u fps	62.5 in u fps	81.25 in u fps	100.0 in u fps	125.0 in u fps
0.001	35.0	29.5	23.0	19.0	14.2	10.0
0.005	51.1	40.6	34.2	27.2	20.0	17.0
0.01	54.0	46.0	37.5	31.0	24.0	19.0
0.02	58.0	50.4	42.0	32.6	26.0	21.0
0.03	61.0	53.0	45.0	35.3	26.7	22.7
0.04	63.5	54.8	46.3	36.5	28.0	23.0
0.05	65.0	56.6	47.0	37.5	29.0	24.0
0.06	66.7	58.0	47.7	37.0	29.6	24.5
0.08	69.4	59.5	50.6	38.8	31.2	26.0
0.10	71.5	61.7	52.5	41.5	33.0	26.7
0.12	73.5	63.7	55.0	43.0	34.5	27.0
0.14	75.4	66.1	57.4	44.2	35.7	28.6
0.16	77.5	67.8	58.8	46.4	37.7	30.2
0.18	80.0	69.5	61.2	48.5	39.0	31.0
0.20	82.0	71.5	63.0	50.0	40.3	33.0
0.22	84.2	73.3	64.8	53.0	43.4	35.2
0.25	87.0	76.0	67.7	58.0	47.5	38.0
0.30	92.0	80.5	72.5	62.8	51.7	43.2
0.35	95.8	84.0	76.7	63.7	58.3	49.2
0.40	97.7	88.2	79.5	71.0	64.5	56.0
0.45	97.6	89.5	82.0	74.6	70.2	63.8
0.50	98.0	90.0	83.8	78.0	73.8	70.7
0.55	98.0	90.0	83.8	79.2	74.1	72.2
0.60	98.0	90.0	83.8	79.2	74.0	72.2

TABLE A.8

FLOW PARAMETERS FOR ZERO PRESSURE GRADIENT FLOWS

RUN NUMBER 1				RUN NUMBER 2			
x ft	b ft	u_{1m} fps	u_* fps	x ft	b ft	u_{1m} fps	u_* fps
0.416	0.038	12.4	1.47	0.333	0.035	43.0	---
0.625	0.044	10.0	1.90	0.416	0.042	33.5	3.0
0.833	0.047	7.6	1.70	0.520	0.048	27.0	3.5
1.250	0.065	6.4	1.80	1.040	0.063	16.3	3.9
1.660	0.079	5.2	1.90	1.560	0.083	13.5	4.2
2.080	0.089	4.6	1.95	2.080	0.094	12.0	4.1
4.160	0.125	3.5	1.90	3.120	0.110	9.6	4.0
8.330	0.167	2.4	1.85	4.160	0.130	8.8	4.1
				5.400	0.137	7.1	4.0
				7.100	0.160	6.1	4.0
				8.750	0.177	5.6	4.0
				10.400	0.190	5.1	4.2
RUN NUMBER 3				RUN NUMBER 4			
0.333	0.051	69.0	---	0.625	0.096	71.0	---
0.416	0.058	51.0	---	0.833	0.110	56.0	---
0.520	0.065	40.0	---	1.040	0.137	36.5	3.4
1.040	0.085	21.0	3.85	2.000	0.175	20.0	3.95
1.560	0.098	16.0	3.90	3.120	0.200	16.0	3.80
2.080	0.106	15.0	4.25	4.160	0.217	13.5	3.90
3.120	0.130	12.5	4.20	5.400	0.240	11.5	3.90
4.160	0.154	10.0	4.00	7.100	0.268	10.5	3.90
5.400	0.170	9.0	4.15	8.750	0.300	9.4	3.95
7.100	0.195	7.9	4.00	10.400	0.333	8.6	3.90
8.750	0.230	7.1	4.00				
10.400	0.250	6.3	3.90				

TABLE A.8 (CONTINUED)

RUN NUMBER 5				RUN NUMBER 6			
x ft	b ft	u_{lm} fps	u_* fps	x ft	b ft	u_{lm} fps	u_* fps
1.00	0.125	57.5	---	0.66	0.090	73.0	---
1.25	0.156	42.0	---	0.83	0.104	53.0	---
1.56	0.187	32.5	---	1.25	0.125	30.0	3.26
2.50	0.230	21.0	1.95	1.67	0.150	22.5	4.40
3.75	0.260	18.8	3.55	2.08	0.160	19.0	4.35
5.00	0.290	15.0	3.20	3.12	0.190	15.3	4.45
6.25	0.320	13.0	3.50	4.16	0.215	14.5	4.50
7.80	0.360	12.0	3.60	6.25	0.260	12.5	5.00
8.75	0.390	10.5	3.60	8.33	0.290	10.5	4.40
9.40	0.390	10.3	3.90	10.40	0.345	9.5	4.40
10.00	0.400	10.0	4.13				
11.25	0.420	9.5	4.05				

TABLE A.9

FLOW PARAMETERS FOR ADVERSE PRESSURE GRADIENT FLOWSRUN NUMBER 7 (APG I): $h = 0.50$ in., $U_0 = 107.0$ fps

x ft	b ft	U fps	u_{1m} fps	u_* fps
0	---	107.0	---	---
0.45	---	107.0	---	---
0.63	0.108	104.0	42.5	---
1.00	0.115	103.0	32.0	---
2.07	0.140	99.0	17.8	3.70
3.12	0.175	93.0	14.0	3.08
4.15	0.188	89.0	9.8	3.27
6.25	0.195	85.5	9.0	3.02
8.35	0.190	82.5	8.3	2.95
10.40	0.201	80.2	6.4	2.90

RUN NUMBER 8 (APG II): $h = 0.50$ in., $U_0 = 121.0$ fps

x ft	b ft	U fps	u_{1m} fps	u_* fps
0	---	121.0	---	---
0.55	---	121.0	---	---
0.80	---	120.0	---	---
1.00	0.108	117.0	69.0	---
2.07	0.198	105.0	42.5	3.40
3.12	0.202	98.0	34.8	2.45
4.15	0.238	92.0	32.2	2.15
6.25	0.260	84.6	30.7	2.12
8.35	0.282	77.5	28.7	1.73
10.40	0.318	73.8	24.8	1.61

TABLE A.9 (CONTINUED)

 RUN NUMBER 9 (APG III): $h = 0.25$ in., $U_0 = 145.0$ fps

x ft	b ft	U fps	u_{1m} fps	u_* fps
0	---	145.0	---	---
0.25	---	144.5	---	---
0.55	0.058	138.0	55.3	6.75
0.80	0.080	127.6	49.8	5.85
1.05	0.095	122.0	43.3	4.55
1.55	0.125	114.5	35.4	3.44
2.10	0.150	107.3	29.5	3.12
3.12	0.195	97.0	27.2	2.55
4.15	0.222	90.0	26.1	2.34
5.20	0.232	84.0	25.2	2.06
6.75	0.252	79.7	22.8	1.91
8.20	0.270	74.0	20.7	1.65
10.40	0.295	72.5	22.0	1.62

A P P E N D I X - B

MEASURED TURBULENCE CHARACTERISTICS

TABLE B1

TURBULENCE CHARACTERISTICS FOR RUN NUMBER 2

$x = 6.25$ in., $h = 0.25$ in., $U_0 = 96.0$ fps

y (ft)	(u'/U_0)	(v'/U_0)	(w'/U_0)	$(-\overline{u'v'}/U_0^2) \cdot 10^3$
0.012	0.139	0.104	0.085	3.19
0.015	0.143	0.108	0.086	3.58
0.020	0.150	0.117	0.088	5.39
0.030	0.162	0.125	0.094	7.89
0.040	0.170	0.132	0.098	10.11
0.050	0.173	0.134	0.100	11.31
0.060	0.162	0.123	0.093	9.30
0.070	0.148	0.112	0.083	7.16
0.080	0.128	0.098	0.073	4.45
0.090	0.103	0.080	0.057	2.46
0.100	0.078	0.062	0.040	1.54
0.110	0.060	0.049	0.027	0.73
0.120	0.047	0.040	0.021	0.33
0.130	0.039	0.033	0.017	0.08
0.150	0.029	0.024	0.012	0.03
0.200	0.019	0.016	0.009	0.03

$x = 12.50$ in.

0.012	0.098	0.071	0.058	2.15
0.015	0.100	0.073	0.059	2.36
0.020	0.100	0.071	0.060	--
0.030	0.110	0.083	0.062	4.60
0.040	0.113	0.087	0.064	6.25
0.050	0.115	0.088	0.068	6.50
0.060	0.117	0.089	0.064	7.10
0.070	0.116	0.088	0.064	6.80
0.080	0.115	0.088	0.062	7.00
0.100	0.105	0.080	0.051	5.80
0.120	0.090	0.070	0.043	4.45
0.150	0.055	0.045	0.023	0.90
0.200	0.023	0.020	0.007	0.12
0.250	0.014	0.012	0.003	0.02
0.300	0.009	0.008	0.002	0.01

NOTE: u' , v' and w' are the root-mean square values of the velocity fluctuations

TABLE B.1 (CONTINUED)

x = 25.0 in.

y(ft)	(u'/U ₀)	(v'/U ₀)	(w'/U ₀)	(-u'v'/U ₀ ²) .10 ³
0.012	0.080	0.058	0.048	2.50
0.015	0.080	0.059	0.047	2.65
0.020	0.080	0.059	0.046	2.60
0.030	0.078	0.059	0.044	2.80
0.040	0.077	0.059	0.043	2.90
0.060	0.077	0.060	0.042	3.00
0.080	0.077	0.061	0.042	3.40
0.100	0.077	0.060	0.042	3.50
0.120	0.077	0.060	0.041	3.80
0.150	0.074	0.059	0.038	3.60
0.200	0.047	0.038	0.022	1.55
0.250	0.022	0.019	0.009	0.14
0.300	0.011	0.009	0.004	0.06
0.350	0.007	0.006	0.003	----

x = 50. in.

0.012	0.077	0.056	0.046	1.90
0.015	0.075	0.054	0.045	2.08
0.020	0.074	0.053	0.044	2.28
0.030	0.070	0.051	0.041	2.26
0.040	0.067	0.049	0.037	2.20
0.060	0.061	0.046	0.033	1.76
0.080	0.057	0.043	0.031	1.50
0.100	0.055	0.042	0.030	1.45
0.150	0.053	0.041	0.027	1.45
0.200	0.051	0.039	0.026	1.40
0.250	0.043	0.033	0.023	0.92
0.300	0.027	0.022	0.013	0.38
0.350	0.020	0.015	0.005	0.16
0.400	0.010	0.009	0.004	0.02

TABLE B.1 (CONTINUED)

x = 87.5 in.

y (ft)	(u'/U ₀)	(v'/U ₀)	(w'/U ₀)	(-u'v'/U ₀ ²) · 10 ³
0.012	0.072	0.052	0.044	2.00
0.015	0.072	0.052	0.044	2.00
0.020	0.071	0.051	0.043	2.20
0.030	0.067	0.048	0.041	1.90
0.040	0.064	0.047	0.038	2.00
0.060	0.060	0.044	0.032	1.85
0.100	0.052	0.039	0.030	1.55
0.150	0.046	0.034	0.024	1.12
0.200	0.041	0.031	0.022	0.80
0.250	0.038	0.029	0.021	0.80
0.300	0.036	0.027	0.019	0.62
0.350	0.030	0.023	0.015	0.56
0.400	0.020	0.016	0.009	0.22
0.500	0.012	0.011	0.009	0.04

x = 125.0 in.

0.012	0.069	0.051	0.042	1.73
0.015	0.069	0.051	0.042	1.75
0.020	0.068	0.049	0.042	1.71
0.030	0.066	0.048	0.039	1.65
0.040	0.064	0.047	0.037	1.58
0.050	0.062	0.046	0.036	1.48
0.070	0.058	0.043	0.033	1.25
0.090	0.055	0.041	0.032	1.14
0.110	0.052	0.039	0.030	0.90
0.150	0.048	0.036	0.026	0.71
0.200	0.043	0.032	0.023	0.16
0.250	0.038	0.029	0.020	0.10
0.300	0.033	0.025	0.018	0.10
0.400	0.027	0.021	0.014	0.05
0.500	0.022	0.018	0.010	0.02
0.600	0.018	0.016	0.008	-----

TABLE B.2

TURBULENCE CHARACTERISTICS FOR RUN NUMBER 4

$x = 12.5$ in., $h = 0.50$ in., $U_0 = 96.0$ fps

y (ft)	(u'/U_0)	(v'/U_0)	(w'/U_0)	$(-\overline{u'v'}/U_0^2) \cdot 10^3$
0.012	0.159	0.115	0.085	1.46
0.015	0.162	0.118	0.085	1.92
0.020	0.166	0.123	0.086	3.26
0.030	0.170	0.130	0.086	4.95
0.040	0.171	0.132	0.087	6.96
0.050	0.177	0.138	0.090	7.84
0.060	0.182	0.141	0.092	9.30
0.070	0.187	0.146	0.096	11.00
0.080	0.190	0.148	0.098	11.80
0.090	0.193	0.151	0.099	12.85
0.100	0.197	0.153	0.100	14.20
0.120	0.198	0.153	0.102	14.50
0.140	0.192	0.150	0.097	14.40
0.160	0.176	0.136	0.083	11.70
0.180	0.154	0.120	0.073	9.13
0.200	0.126	0.100	0.062	6.00
0.250	0.061	0.052	0.042	0.80
0.300	0.031	0.026	0.036	0.04
0.400	0.011	0.010	0.031	----

$x = 25.0$ in.

0.012	0.097	0.070	0.053	0.64
0.015	0.099	0.071	0.055	0.77
0.020	0.102	0.074	0.055	1.20
0.030	0.104	0.077	0.055	1.34
0.040	0.107	0.081	0.056	1.34
0.060	0.110	0.085	0.056	1.97
0.080	0.113	0.089	0.056	3.23
0.100	0.116	0.090	0.057	4.12
0.120	0.119	0.094	0.060	4.80
0.150	0.123	0.097	0.062	6.10
0.200	0.121	0.093	0.062	6.15
0.250	0.103	0.080	0.056	3.87
0.300	0.075	0.062	0.042	0.56
0.350	0.048	0.041	0.032	0.06
0.400	0.033	0.030	0.028	0.05
0.500	0.023	0.022	0.026	

TABLE B.2 (CONTINUED)

 x = 50.0 in.

y(ft)	(u'/U ₀)	(v'/U ₀)	(w'/U ₀)	(-u'v'/U ₀ ²) · 10 ³
0.012	0.076	0.055	0.039	1.82
0.015	0.076	0.055	0.039	2.11
0.020	0.072	0.052	0.039	2.08
0.030	0.069	0.051	0.038	1.80
0.040	0.068	0.051	0.037	1.73
0.060	0.066	0.050	0.036	1.57
0.080	0.064	0.049	0.035	1.40
0.100	0.064	0.050	0.035	1.31
0.150	0.063	0.050	0.036	1.52
0.200	0.063	0.050	0.037	1.68
0.250	0.062	0.049	0.037	1.60
0.300	0.058	0.046	0.036	1.60
0.350	0.052	0.041	0.033	1.00
0.400	0.043	0.035	0.027	0.16
0.500	0.025	0.021	0.023	0.02
0.600	0.013	0.010	0.021	0.01

 x = 75.0 in.

0.012	0.073	0.053	0.041	1.82
0.020	0.071	0.052	0.039	1.80
0.030	0.067	0.049	0.038	1.68
0.040	0.060	0.045	0.040	1.68
0.060	0.058	0.042	0.041	1.36
0.080	0.055	0.041	0.037	1.18
0.100	0.053	0.040	0.032	1.04
0.150	0.050	0.038	0.031	1.00
0.200	0.048	0.037	0.032	0.87
0.250	0.047	0.036	0.032	0.80
0.300	0.045	0.035	0.032	0.72
0.350	0.042	0.035	0.031	0.64
0.400	0.038	0.030	0.026	0.51
0.500	0.030	0.026	0.027	0.25
0.600	0.020	0.017	0.027	0.10
0.700	0.011	0.009	0.026	0.03

TABLE B.2 (CONTINUED)

 $x = 100.0$ in.

y (ft)	(u'/U_0)	(v'/U_0)	(w'/U_0)	$(-u'v'/U_0^2) \cdot 10^3$
0.012	0.076	0.055	0.040	1.65
0.020	0.073	0.052	0.037	1.68
0.030	0.070	0.051	0.036	1.68
0.040	0.066	0.048	0.036	1.65
0.060	0.062	0.046	0.033	1.67
0.080	0.057	0.042	0.032	1.44
0.100	0.053	0.039	0.030	1.14
0.150	0.054	0.039	0.029	0.80
0.200	0.044	0.033	0.029	0.55
0.250	0.042	0.032	0.029	0.45
0.300	0.040	0.031	0.029	0.40
0.350	0.039	0.030	0.028	0.44
0.400	0.036	0.028	0.027	0.37
0.500	0.029	0.024	0.023	0.13
0.600	0.022	0.019	0.022	0.02

 $x = 125.0$ in.

0.012	0.073	0.052	0.038	1.55
0.020	0.071	0.051	0.038	1.55
0.030	0.069	0.050	0.037	1.50
0.040	0.068	0.050	0.036	1.40
0.060	0.063	0.047	0.034	1.25
0.080	0.058	0.042	0.031	1.00
0.100	0.055	0.041	0.029	0.68
0.150	0.047	0.036	0.029	0.62
0.200	0.042	0.033	0.030	0.60
0.250	0.039	0.030	0.029	0.57
0.300	0.038	0.029	0.029	0.50
0.350	0.036	0.028	0.029	0.43
0.400	0.034	0.027	0.029	0.32
0.500	0.029	0.023	0.027	0.16
0.600	0.023	0.019	0.026	0.04
0.700	0.017	0.014	0.023	0.04
0.800	0.013	0.010	0.017	---
0.900	0.011	0.009	0.011	---

TABLE B.3

TURBULENCE CHARACTERISTICS FOR RUN NUMBER 6 (ROU|| WALL)

$x = 12.5$ in., $h = 0.50$ in., $U_0 = 96.0$ fps

y (ft)	(u'/U_0)	(v'/U_0)	(w'/U_0)	$(-\overline{u'v'}/U_0^2) \cdot 10^3$
0.012	0.190	0.161	0.130	2.15
0.014	0.187	0.158	0.130	1.50
0.016	0.189	0.161	0.132	1.65
0.020	0.191	0.164	0.134	2.00
0.025	0.197	0.169	0.134	2.70
0.030	0.202	0.174	0.135	3.10
0.040	0.210	0.184	0.138	4.40
0.050	0.217	0.191	0.140	5.60
0.060	0.221	0.195	0.144	7.60
0.080	0.236	0.208	0.150	10.30
0.100	0.243	0.213	0.153	11.75
0.120	0.244	0.215	0.158	13.30
0.150	0.228	0.201	0.138	12.30
0.180	0.170	0.147	0.105	6.05
0.210	0.116	0.102	0.076	2.40
0.250	0.058	0.050	0.026	0.20
0.300	0.032	0.030	0.014	0.05

$x = 25.0$ in.

0.012	0.139	0.114	0.092	2.92
0.017	0.138	0.112	0.090	2.85
0.022	0.135	0.109	0.086	2.75
0.032	0.133	0.105	0.079	2.45
0.042	0.132	0.104	0.076	2.25
0.062	0.131	0.108	0.071	2.30
0.082	0.133	0.111	0.069	2.50
0.102	0.135	0.113	0.070	2.87
0.152	0.141	0.118	0.075	3.75
0.202	0.143	0.121	0.073	4.25
0.252	0.117	0.100	0.062	3.62
0.302	0.080	0.070	0.039	1.45
0.352	0.040	0.036	0.016	0.40
0.402	0.022	0.020	0.011	0.04

TABLE B.3 (CONTINUED)

$x = 50.0$ in.				
y (ft)	(u'/U_0)	(v'/U_0)	(w'/U_0)	$(-\overline{u'v'}/U_0^2) \cdot 10^3$
0.012	0.130	0.106	0.085	3.12
0.022	0.129	0.100	0.078	3.00
0.032	0.121	0.096	0.071	2.65
0.042	0.114	0.091	0.066	2.50
0.062	0.101	0.080	0.060	1.85
0.082	0.096	0.076	0.051	1.60
0.102	0.089	0.071	0.047	1.40
0.132	0.083	0.067	0.043	1.15
0.162	0.080	0.064	0.040	1.00
0.202	0.077	0.062	0.040	0.90
0.252	0.075	0.060	0.039	0.88
0.302	0.069	0.054	0.037	0.75
0.402	0.055	0.048	0.027	0.58
0.502	0.031	0.028	0.016	0.05
$x = 75.0$ in.				
0.012	0.116	0.094	0.086	2.00
0.020	0.115	0.092	0.081	1.90
0.030	0.110	0.088	0.074	1.75
0.040	0.103	0.081	0.069	1.42
0.050	0.098	0.077	0.065	1.45
0.070	0.089	0.070	0.058	1.15
0.100	0.080	0.062	0.050	0.95
0.130	0.071	0.055	0.042	0.75
0.160	0.065	0.052	0.040	0.58
0.200	0.064	0.053	0.040	0.48
0.250	0.062	0.053	0.038	0.62
0.300	0.056	0.049	0.035	0.50
0.400	0.047	0.040	0.028	0.36
0.600	0.022	0.022	0.012	0.01

TABLE B.3 (CONTINUED)

 x = 100.0 in.

y(ft)	(u'/U ₀)	(v'/U ₀)	(w'/U ₀)	(-u'v'/U ₀ ²) · 10 ³
0.012	0.110	0.089	0.082	2.00
0.022	0.109	0.086	0.075	1.90
0.032	0.102	0.080	0.070	1.68
0.042	0.097	0.075	0.067	1.50
0.062	0.090	0.069	0.061	1.40
0.082	0.085	0.065	0.057	1.20
0.102	0.079	0.062	0.051	1.10
0.132	0.071	0.054	0.046	0.80
0.162	0.063	0.049	0.042	0.63
0.202	0.057	0.044	0.036	0.40
0.252	0.051	0.041	0.032	0.33
0.302	0.045	0.036	0.029	0.27
0.402	0.037	0.030	0.025	0.18
0.502	0.030	0.025	0.024	0.10
0.602	0.024	0.021	0.017	0.03
0.702	0.021	0.019	0.013	0.01

 x = 125.0 in.

0.012	0.100	0.079	0.076	2.00
0.022	0.100	0.081	0.070	2.05
0.032	0.097	0.076	0.064	2.00
0.042	0.094	0.073	0.061	1.96
0.062	0.087	0.067	0.058	1.87
0.082	0.083	0.065	0.055	1.77
0.102	0.081	0.063	0.049	1.60
0.132	0.076	0.059	0.044	1.35
0.162	0.071	0.056	0.040	0.84
0.202	0.065	0.054	0.040	0.70
0.252	0.056	0.047	0.036	0.63
0.302	0.046	0.038	0.030	0.50
0.408	0.036	0.029	0.022	0.25
0.502	0.031	0.026	0.017	0.15
0.602	0.028	0.025	0.016	0.13
0.702	0.021	0.019	0.012	0.02

TABLE B.4

TURBULENCE CHARACTERISTICS FOR RUN NUMBER 8 (APG II)

$x = 12.5 \text{ in.}, h = 0.50 \text{ in.}, U = 117.0 \text{ fps}$

$y(\text{ft})$	(u'/U)	(v'/U)	(w'/U)	$(-u'v'/U^2) \cdot 10^3$
0.012	0.170	0.121	0.101	1.06
0.015	0.170	0.122	0.104	1.55
0.020	0.172	0.126	0.105	2.87
0.030	0.177	0.122	0.107	4.95
0.040	0.182	0.127	0.114	7.13
0.060	0.192	0.146	0.121	10.43
0.100	0.210	0.160	0.128	15.62
0.120	0.213	0.166	0.133	18.11
0.160	0.202	0.158	0.117	18.05
0.200	0.158	0.127	0.085	9.80
0.260	0.068	0.056	0.043	1.26
0.300	0.038	0.032	0.019	0.09
0.350	0.038	0.032	0.011	0.09

$x = 25.0 \text{ in.}, U = 105.0 \text{ fps}$

0.012	0.120	0.086	0.072	2.18
0.015	0.122	0.092	0.075	2.64
0.020	0.125	0.095	0.074	2.93
0.030	0.131	0.100	0.075	3.22
0.040	0.134	0.104	0.075	3.32
0.060	0.140	0.110	0.077	4.50
0.080	0.144	0.115	0.077	5.37
0.110	0.147	0.117	0.078	6.40
0.150	0.147	0.116	0.080	6.50
0.200	0.145	0.115	0.079	6.45
2.250	0.134	0.106	0.073	5.80
0.300	0.107	0.086	0.055	3.25
0.350	0.075	0.062	0.041	1.56
0.400	0.048	0.042	0.022	0.80
0.450	0.030	0.026	0.014	0.22

TABLE B.4 (CONTINUED)

$x = 50.0$ in., $U = 92.0$ fps

y (ft)	(u'/U)	(v'/U)	(w'/U)	$(-\overline{u'v'}/U^2) \cdot 10^3$
0.012	0.088	0.062	0.055	2.70
0.015	0.089	0.063	0.055	2.76
0.020	0.090	0.065	0.055	3.00
0.030	0.093	0.067	0.056	3.30
0.040	0.094	0.069	0.056	3.48
0.060	0.095	0.071	0.056	3.67
0.080	0.097	0.073	0.056	4.00
0.110	0.098	0.076	0.056	4.15
0.150	0.098	0.076	0.057	4.50
0.200	0.097	0.076	0.054	4.87
0.250	0.095	0.075	0.053	4.70
0.300	0.090	0.071	0.052	4.10
0.350	0.082	0.066	0.046	3.30
0.400	0.075	0.060	0.041	2.44
0.450	0.060	0.050	0.035	1.83
0.500	0.052	0.042	0.028	1.22
0.550	0.045	0.036	0.023	0.26

$x = 75.0$ in., $U = 84.6$ fps

0.012	0.086	0.062	0.053	2.65
0.015	0.087	0.062	0.054	2.63
0.020	0.088	0.063	0.054	2.91
0.030	0.089	0.064	0.055	3.00
0.040	0.090	0.065	0.056	3.12
0.060	0.091	0.067	0.056	3.50
0.080	0.091	0.068	0.055	3.80
0.110	0.093	0.071	0.055	4.10
0.150	0.093	0.070	0.055	4.28
0.200	0.093	0.071	0.053	4.77
0.250	0.090	0.070	0.052	4.61
0.300	0.085	0.067	0.048	4.28
0.400	0.075	0.060	0.042	2.97
0.450	0.067	0.052	0.037	2.32
0.500	0.061	0.047	0.033	1.47
0.550	0.055	0.042	0.029	0.80
0.600	0.050	0.040	0.026	0.22

TABLE B.4 (CONTINUED)

 x = 100.0 in., U = 77.5 fps

y(ft)	(u'/U)	(v'/U)	(w'/U)	$(-u'v'/U^2) \cdot 10^3$
0.012	0.082	0.058	0.051	2.00
0.015	0.083	0.060	0.051	2.12
0.020	0.085	0.061	0.052	2.20
0.030	0.087	0.062	0.053	2.32
0.040	0.089	0.064	0.053	2.60
0.060	0.092	0.067	0.054	3.10
0.080	0.093	0.068	0.056	3.63
0.110	0.096	0.071	0.056	3.80
0.150	0.096	0.072	0.056	4.08
0.200	0.096	0.072	0.055	4.71
0.250	0.095	0.072	0.054	4.63
0.300	0.091	0.070	0.051	4.45
0.350	0.084	0.064	0.045	3.90
0.400	0.079	0.061	0.043	3.29
0.450	0.075	0.058	0.040	2.56
0.500	0.070	0.054	0.038	1.83
0.550	0.066	0.052	0.036	0.85
0.600	0.062	0.048	0.033	0.15

 x = 25.0 in., U = 73.8 fps

0.015	0.083	0.059	0.053	1.22
0.020	0.086	0.061	0.053	1.83
0.040	0.090	0.064	0.054	1.95
0.070	0.094	0.069	0.057	3.06
0.100	0.097	0.073	0.060	3.42
0.150	0.100	0.076	0.060	4.03
0.200	0.100	0.076	0.060	4.60
0.250	0.104	0.080	0.059	4.90
0.300	0.097	0.073	0.060	4.64
0.350	0.093	0.071	0.056	4.22
0.400	0.088	0.067	0.050	3.80
0.450	0.084	0.066	0.050	3.17
0.500	0.081	0.063	0.044	2.81
0.550	0.080	0.062	0.043	2.04
0.600	0.078	0.061	0.042	1.40
0.650	0.077	0.061	0.042	0.85

TABLE B.5

TURBULENCE CHARACTERISTICS FOR RUN NUMBER 9 (APG III)

$x = 6.25$ in., $h = 0.25$ in., $U = 136.0$ fps

y (ft)	(u'/U)	(v'/U)	(w'/U)	$(-\overline{u'v'}/U^2) \cdot 10^3$
0.012	0.176	0.130	0.096	3.8
0.015	0.168	0.119	0.098	---
0.020	0.175	0.126	0.104	---
0.030	0.188	0.137	0.116	4.95
0.040	0.201	0.148	0.125	7.58
0.050	0.213	0.160	0.136	9.72
0.060	0.220	0.166	0.143	11.93
0.070	0.226	0.173	0.146	14.34
0.080	0.223	0.173	0.142	15.95
0.090	0.207	0.161	0.129	13.50
0.100	0.188	0.149	0.111	11.27
0.110	0.158	0.125	0.091	8.22
0.120	0.132	0.106	0.069	5.35
0.130	0.109	0.088	0.054	3.40
0.140	0.078	0.077	0.040	1.72
0.150	0.068	0.057	0.033	0.94
0.170	0.047	0.040	0.021	0.22

$x = 12.5$ in., $U = 122.0$ fps

0.012	0.152	0.108	0.078	3.75
0.015	0.155	0.111	0.078	4.37
0.020	0.159	0.116	0.080	4.68
0.030	0.166	0.123	0.082	6.23
0.040	0.170	0.130	0.081	7.81
0.060	0.177	0.136	0.084	9.83
0.080	0.184	0.141	0.085	11.83
0.100	0.183	0.142	0.084	12.86
0.120	0.170	---	0.080	---
0.140	0.161	0.123	0.073	10.00
0.160	0.142	0.109	0.065	7.60
0.180	0.115	0.089	0.051	4.60
0.200	0.091	0.073	0.038	3.04
0.220	0.067	0.055	0.028	1.50
0.240	0.047	0.039	0.020	0.80
0.260	0.041	0.032	0.017	0.38

TABLE B.5 (CONTINUED)

 $x = 25.0 \text{ in.}, U = 107.3 \text{ fps}$

$y(\text{ft})$	(u'/U)	(v'/U)	(w'/U)	$(-u'v'/U^2) \cdot 10^3$
0.012	0.113	0.080	0.068	1.38
0.015	0.115	0.083	0.070	1.41
0.020	0.120	0.087	0.071	1.50
0.030	0.125	0.092	0.070	1.62
0.040	0.128	0.096	0.072	1.70
0.060	0.132	0.099	0.073	2.06
0.080	0.137	0.104	0.073	2.27
0.100	0.139	0.107	0.073	2.50
0.130	0.141	0.104	0.074	2.90
0.160	0.140	0.111	0.074	2.92
0.200	0.137	0.105	0.072	2.40
0.250	0.117	0.090	0.064	1.21
0.270	0.107	0.083	0.058	0.90
0.300	0.095	0.075	0.050	0.32

 $x = 50.0 \text{ in.}, U = 90.0 \text{ fps}$

0.012	0.098	0.068	0.060	1.00
0.015	0.100	0.070	0.061	1.00
0.020	0.102	0.073	0.062	1.12
0.030	0.106	0.077	0.065	1.21
0.040	0.110	0.080	0.064	1.38
0.060	0.113	0.085	0.063	1.62
0.080	0.114	0.086	0.063	1.75
0.100	0.115	0.087	0.063	1.94
0.130	0.116	0.088	0.063	2.23
0.160	0.114	0.087	0.064	2.50
0.200	0.112	0.086	0.064	2.76
0.250	0.109	0.084	0.062	2.70
0.300	0.106	0.081	0.057	2.10
0.350	0.100	0.077	0.054	1.54
0.380	0.094	0.073	0.051	1.20
0.400	0.090	0.069	0.048	0.97

TABLE B.5 (CONTINUED)

$x = 87.50$ in., $U = 77.2$ fps

y (ft)	(u'/U)	(v'/U)	(w'/U)	$(-u'v'/U^2) \cdot 10^3$
0.012	0.092	0.065	0.059	0.73
0.015	0.095	0.067	0.059	0.72
0.020	0.099	0.071	0.060	0.85
0.030	0.103	0.075	0.062	0.97
0.050	0.109	0.081	0.066	1.37
0.070	0.115	0.084	0.067	1.58
0.090	0.118	0.088	0.068	1.80
0.120	0.121	0.090	0.069	2.00
0.150	0.126	0.094	0.069	2.26
0.200	0.129	0.096	0.069	2.60
0.250	0.127	0.095	0.069	2.70
0.300	0.121	0.089	0.069	2.43
0.350	0.114	0.086	0.063	2.00
0.400	0.108	0.084	0.059	1.62
0.450	0.099	0.077	0.053	0.90
0.500	0.094	0.073	0.048	0.36

$x = 125.0$ in., $U = 72.5$ fps

0.012	0.092	0.066	0.058	0.56
0.015	0.092	0.065	0.058	0.53
0.020	0.096	0.069	0.060	0.62
0.030	0.101	0.074	0.062	0.81
0.050	0.105	0.078	0.063	0.93
0.070	0.110	0.081	0.065	1.45
0.090	0.114	0.086	0.067	1.62
0.120	0.120	0.091	0.068	1.81
0.160	0.124	0.094	0.071	2.17
0.200	0.131	0.100	0.073	2.40
0.250	0.133	0.101	0.077	2.72
0.300	0.132	0.101	0.077	2.70
0.350	0.132	0.100	0.077	2.35
0.400	0.126	0.099	0.074	2.10
0.450	0.123	0.096	0.068	1.60
0.500	0.114	0.091	0.064	1.10
0.550	0.109	0.086	0.061	0.41
0.600	0.105	0.084	0.051	0.08